Doctoral theses at NTNU, 2022:66

Hanne-Line Rabben

Translational Research on Gastric Cancer - Pharmacological Validations of Metabolism-Based Treatments

Doctoral thesis

NTNU
Norwegian University of Science and Technology
Thesis for the Degree of
Philosophiae Doctor
Faculty of Medicine and Health Sciences
Department of Clinical and Molecular Medicine

NTNU
Norwegian University of
Science and Technology

Hanne-Line Rabben

Translational Research on Gastric Cancer - Pharmacological Validations of Metabolism-Based Treatments

Thesis for the Degree of Philosophiae Doctor

Trondheim, March 2022

Norwegian University of Science and Technology
Faculty of Medicine and Health Sciences
Department of Clinical and Molecular Medicine

NTNU
Norwegian University of
Science and Technology

NTNU
Norwegian University of Science and Technology

Thesis for the Degree of Philosophiae Doctor

Faculty of Medicine and Health Sciences
Department of Clinical and Molecular Medicine

ISBN 978-82-326-6859-5 (printed ver.)
ISBN 978-82-326-6537-2 (electronic ver.)
ISSN 1503-8181 (printed ver.)
ISSN 2703-8084 (online ver.)

Doctoral theses at NTNU, 2022:66

Printed by NTNU Grafisk senter

Norsk sammendrag

Bakgrunn/mål: Metabolsk reprogrammering er et kjennetegn for kreft og et lovende område for nyutvikling av kreftbehandling. Magekreft er den femte mest vanlige kreftformen på verdensbasis, og er den tredje dødeligste blant krefttypene. Den femårige overlevelsesraten for magekreft er 10-30%. I forkant av arbeidet som er gjort i denne avhandlingen har vi demonstrert at denervering reduserte kreftforekomsten i magekreft. Kreftsvulster består av kreftceller og immun/inflammasjonsceller i tumorens mikromiljø. Målene i denne avhandlingen var i) å studere nervesignalenes rolle i kreftsvulstens metabolske uttrykk og ii) å utvikle metabolske behandlingsregimer som forhindrer og/eller behandler tumorigenesen og øker overlevelsen.

Materialer og Metoder: Totalt ble 22 pasienter, 471 mus (inkludert transgene INS-GAS mus og kjemisk-induserte mus) og 7 cellelinjer studert i denne avhandlingen. Eksperimentell kirurgi som ensidig vagotomi, farmakologiske valideringer både *in vitro*, *in vivo* og *in silico* samt kliniske evalueringer og studier ble gjort. Omics-teknologi ble brukt og inkluderte komparativ transkriptomics, multi-omics og identifikasjon av beregningsbaserte nye målrettede terapier ved hjelp av bioinformatiske verktøy.

Resultater: INS-GAS musene hadde lignende metabolsk profil og metabolsk reprogrammering som magekreftpasientene. Glutaminolysen var felles metabolsk signatur. Vagotomi reverserte den metabolske reprogrammering, hvor metabolismen skiftet fra glutaminolyse til OXPHOS og/eller glykolyse og vi så en normalisering i energimetabolismen i kreftcellene og tumormikromiljøet. WNT-mTOR var viktig i dette skiftet. Et metabolsk behandlingsregime ble utarbeidet for å målrettet behandle SNAP25, mTOR, PDP1/ α-KGDH og glutaminolysen. Effekten av målrettet nervemetabolsk behandling som inkluderte lokalinjeksjon med BoNT-A; systemisk behandling med RAD001 og CPI-613 men uten cytostatika ble påvist i INS-GAS musene. Lokalinjeksjoner med BoNT-A ble testet i kreftpasienter med langtkommen magekreft og erklært som trygg prosedyre. Genuttrykk og bioinformatiske analyser av signalspor avslørte videre at ivermectin var assosiert med WNT/β-catenin sporet og proliferasjon. Effekten av ivermectin ble påvist *in silico*, *in vitro* og *in vivo*. Kjemopreventiv effekt av phenetyl isothiocyanate (PEITC) ble påvist *in vitro* og *in vivo*, og synergistisk antiproliferativ effekt av PEITC og Cisplatin ble funnet *in vitro*. PEITC tømte glutation-lagrene og induserte cellesyklus-arrest i G2/M fase i magekreftcellene.

Konklusjoner: Denne avhandlingen har benyttet translasjonsforskning til å finne nye behandlingsmetoder for magekreft. Resultatene som er presentert i avhandlingen viser at magekreft er glutamin-avhengig og har en reprogrammert metabolsk profil. Dette har sammenheng med og er påvirkbart av nerveforsyningen til kreftsvulsten. SNAP25, WNT/β-catenin, mTOR, PDP1/α-KGDH, glutaminolysen og glutation er mulige mål for behandling i magekreft. Disse resultatene viser til viktigheten av nerveforsyning til svulsten som modulerer den metabolske reprogrammeringen som samlet gir et rasjonale for klinisk translasjonspotensial av anti-metabolittbehandling i magekreft.

Hanne-Line Rabben
Institutt for Klinisk og Molekylær Medisin (IKOM)
Veiledere: Chun-Mei Zhao og Duan Chen
Finansiert av Samarbeidsorganet (samarbeid mellom Helse Midt-Norge RHF og NTNU)
Ovennevnte avhandling er funnet verdig til å forsvares offentlig for graden philosophiae doctor i medisin. Digital disputas finner sted fredag 04. mars kl. 12.15.

Table of Contents

Acknowledgements

This thesis was carried out at the Research Group of Experimental Pharmacology and Surgery, Department of Clinical and Molecular Medicine, Faculty of Medicine and Health Sciences, Norwegian University of Science and Technology between January 2016 and September 2021.

The PhD fellowship that has led to this thesis was awarded by The Liaison Committee for Education, Research and Innovation in Central Norway (Samarbeidsorganet). The work in this thesis has been founded by The Liaison Committee for Education, Research and Innovation in Central Norway (Samarbeidsorganet).

Thanks to my main supervisor Dr. **Chun-Mei Zhao** for making this thesis possible. You invited me into the group as a Master student and provided me a PhD position. Thanks for supervising me and taking care of me both at work and outside of work. At work, your rigorous scientific training and hands-on supervision led me to being more and more independent at the late stage of my PhD program. For instance, you always kept me staying on top of literature when I was drowning in experiments. You trained me in every practical and writing skills from my Master thesis to PhD thesis and meanwhile you always provided me space to think independently, build new ideas, and design and perform new experiments. I enjoyed almost-daily-scientific discussions and laboratory work with you. Without you, none of this work would be possible. Furthermore, thanks for supporting me to travel between continents, dining with Nobel laureates and presenting our work in the largest GI conference in the world. I am forever grateful. Outside of work, you have kindly invited me for so many delicious meals prepared with dedication and love. You have a unique way of maintaining the work-life balance, which I admire very much.

Thanks to my co-supervisor Prof. **Duan Chen** for training my critical thinking, challenging my academic mindset and for your unconditional encouragement in science. Thanks for always being available. Thanks for numerous discussions on research and life in general, and for believing that anything is possible. Where others see challenge, you see possibilities.

Thanks to my good friend and mentor Dr. **Anders Øverby** for introducing me to Duan and Chun-Mei's research group. Without your dedication and engagement, I would never pursue the journey into becoming a researcher. I want to thank you for inviting me to Japan during my Masters' study to work on your Postdoc projects and for always allowing me space to perform experiments in Japan, which resulted in paper III in this thesis. I am forever grateful for that. Thanks for giving me enough challenges to grow, enough confidence to try and for being there with a good advice. I also want to thank Prof. **Masahiko Nakamura**, Prof. **Hidenori Matsui** and Dr. **Tetsufumi Takahashi** at Kitasato University for unconditional support and friendship in Japan.

Thanks to my good friend Dr. **Magnus Kringstad Olsen** for being a great colleague during my stay in the research group. Thanks for always having the technical solutions, and for all the hours we spent in the animal house. Your logical thinking and quick problem solving has saved me numerous times and I am forever thankful.

I want to thank my co-authors **Aleksandr Ianevski**, Dr. **Gøran Troseth Andersen** and profs. **Timothy C. Wang, Steinar Lundgren, Jon Erik Grønbech, Denis Kainov and Atle Magnar Bones** for great scientific collaborations.

I also want to thank my friends Dr**. Helene Johannessen** and Dr. **Yosuke Kodama** for sharing data and for good conversations about research. I admire your work capacity and strength.

Thanks to previous colleague Dr. **Xing Cai** for collaboration on early animal experiments and training in the cell lab. Also, thanks to **Sophie Rovers**, Dr. **Benedict Man Hung Choi**, **Therese Stork Høiem**, **Jeanette Ulvestad**, **Simon Geithus** and **Mathilde Resell**.

I especially want to thank **Anne Åm**, **Trine Skoglund**, **Knut Grøn**, **Mona Gaustad**, **Venke-Lill Nygård**, **Erling Wold** and **Nils Hagen** at the Unit of Comparative Medicine, St. Olavs Hospital for follow up on animal experiments and breeding of mice. My gratefulness also goes to **Nina Beate Liabakk** for help and assistance on the FACS-machine, **Arn-Sigurd Halmøy** and **Karin Solvang-Garten** at ISB for lending me the PreCellys machine; to Dr. **Vidar Beisvåg**, **Arnar Flatberg**, **Sten Even Erlandsen** and **Tom Wheeler** at the Genomic Core Facility for cooperation, good discussions and technical work regarding RNA sequencing; to **Toril Rolfseng** for good discussion on RNA isolation; to Dr. **Davi de Miranda Fonseca, Lars Hagen** and **Animesh Sharma** at PROMEC for collaboration on proteomics; to Dr. **Toril Holien** for assistance in lentiviral transfection and *in vivo* imaging; to Dr. **Wei Wang** and **Ping Ji** for assistance and advice on *in vitro* experiments; to Dr. **Per Arne Aas** for always being available for lab-technical questions and to Dr. **Caroline Hild Pettersen** and Dr. **Helle Samdal** for great company and fun in the cell lab.

I also want to thank my family in Frøya; my sister Dr. **Charlotte Rabben**, my father **Christoffer Rabben**, my mother **Ulrikke Wedø Rabben** and my boyfriend **Stian Hassum** for unconditional support during my years of study in Trondheim. Thanks to **Ole Magnar Sørgård Espnes**. I appreciate all your love and support. Thanks to my friend and mentor Dr. **Edith Rian**; my friends **Katja S. Engebråten, Ellen Marie Meinhardt**, **Nana Anderaa, Marthe Grønbech Hafskjold** and **Hjørdis Sørensen** for all the fun we had at Gløshaugen and our annual attendance at Forsker Grand Prix, social and scientific events we participated in and for good support during my years of study in Trondheim.

List of papers

This thesis is based on the following original research papers, which are referred to by their Roman numerals in the text.

I. **Hanne-Line Rabben**, Gøran Troseth Andersen, Magnus Kringstad Olsen, Anders Øverby, Aleksandr Ianevski, Denis Kainov, Timothy C. Wang, Steinar Lundgren, Jon Erik Grønbech, Duan Chen, Chun-Mei Zhao. **Neural signaling modulates metabolism of gastric cancer.** *iScience* 2021;24(2):102091. Doi: 10.1016/j.isci.2021.102091. PMID: 33598644; PMCID: PMC7869004.

II. **Hanne-Line Rabben**, Gøran Troseth Andersen, Aleksandr Ianevski, Magnus Kringstad Olsen, Denis Kainov, Jon Erik Grønbech, Timothy Cragin Wang, Duan Chen, Chun-Mei Zhao**. Computational Drug Repositioning and Experimental Validation of Ivermectin in Treatment of Gastric Cancer**. *Frontiers in Pharmacology* 2021;12:625991. Doi: https://doi.org/10.3389/fphar.2021.625991. PMID: 33867984; PMCID: PMC8044519.

III. **Hanne-Line Rabben**, Yosuke Kodama, Masahiko Nakamura, Atle Magnar Bones, Timothy Cragin Wang, Duan Chen, Chun-Mei Zhao, Anders Øverby. **Chemopreventive effect of dietary isothiocyanates in animal models of gastric cancer and synergistic anticancer effect with cisplatin in human gastric cancer cells.** *Frontiers in Pharmacology* 2021;12:613458. Doi: https://doi.org/10.3389/fphar.2021.613458. PMID: 33897415; PMCID: PMC8060630.

Abbreviations

α-KG	alpha-ketoglutarate
ATP	adenosine triphosphate
BoNT-A	Botulinum toxin type A
C-at	cis-aconitate
CPI-613	6,8-Bis(benzylthio)-octanoic acid, devimistat
DALY	cancer-related disability-adjusted life-years
dMMR	mismatch repair deficiency
F6P	fructose-6-phosphate
FU	5-fluorouracil
G6P	glucose-6-phosphate
GC	gastric cancer
GCO	global cancer observatory
GC/MS	gas chromatography/mass spectrometry
GDH	glu dehydrogenase
Glc	glucose
GLOBOCAN	Global Cancer Incidence, Mortality and Prevalence
Gln	L-glutamine
Glu	L-glutamate
Gly	glycine
GSH	glutathione, reduced
GSSG	glutathione, oxidized
HPLC	high performance liquid chromatography
H.p.	*Helicobacter pylori*
IARC	International Agency for Research
i.p.	intraperitoneally
ILMN	illumina identifiers
INS-GAS	insulin-gastrin transgenic mice
IPA	Ingenuity Pathway Analysis
KGDH	alpha-ketoglutarate dehydrogenase
KRAS	kirsten rat sarcoma viral oncogene

LC/GC-MS	liquid/gas chromatography mass spectrometry
LGR5+	leucine-rich repeat containing G protein–coupled receptor 5- positive
M3R	muscarinic acetylcholine receptor 3
MS	median survival
MS	mass spectrometry
MSI	microsatellite instability
mTOR	mammalian/mechanistic target of rapamycin
NCCN	National Comprehensive Cancer Network
NGF	nerve growth factor
NMR	nuclear magnetic resonance
OGDH	oxoglutarate dehydrogenase
OS	overall survival
OX	oxaliplatin
Oxo	5-oxoproline
OXPHOS	oxidative phosphorylation
PDH	pyruvate dehydrogenase
PDAC	pancreatic ductal adenocarcinoma
qRT-PCR	quantitative real-time polymerase chain reaction
RIN	RNA integrity number
RNA	ribonucleic acid
SEM	standard error of the mean
SNAP-25	synaptosomal nerve-associated protein 25
TCA	tricarboxylic acid cycle/Krebs cycle/citric acid cycle
Thr	threonine
TME	tumor microenvironment
UVT	unilateral anterior truncal vagotomy
VEGF	vascular endothelial growth factor
WHO	world health organization
WT	wild-type

Abstract

Background/aims: Metabolic reprogramming is a hallmark of cancer and a promising target for developing new anti-cancer treatments. Gastric cancer (GC) is the 5th most common malignant disease worldwide with the 3rd highest incidence and mortality rate among all types of cancers. The 5-year overall survival rate of GC is 10-30%. Prior to this thesis, it has been demonstrated that denervation suppressed GC tumorigenesis. The tumors comprise cancer cells and the associated stromal and immune/inflammatory cells, i.e., tumor microenvironment (TME). The aims of this thesis were *i)* to study the neural singling in modulating metabolism of GC and *ii)* to develop metabolism-based treatments that prevent and/or inhibit the tumorigenesis and improve the overall survival.

Materials and Methods: A total of 22 GC patients, 471 mice (including transgenic INS-GAS model and chemically-induced model) and 7 human GC cell lines were studied in the thesis. Experimental surgery, i.e., unilateral vagotomy, pharmacological validations *in vitro*, *in vivo*, *in silico*, clinical evaluation and pilot clinical trial were performed. Omics technology including comparative transcriptomics, multi-omics, drug-target interaction prediction, computational drug repositioning and bioinformatics were applied.

Results: The INS-GAS mice mimicked GC patients in terms of metabolic reprogramming characterized by glutaminolysis as a metabolic signature. Vagotomy reversed the metabolic reprogramming, reflected by metabolic switch from glutaminolysis to OXPHOS/glycolysis and normalization of the energy metabolism in cancer cells and TME via WNT-mTOR signaling pathway. Metabolism-based treatment was developed to pharmacologically target SNAP25, mTOR, PDP1/α-KGDH and glutaminolysis. The efficacy of nerve-cancer metabolism treatment by intratumoral injection of BoNT-A (SNAP25 inhibitor) with systemic administration of RAD001 and CPI-613 but not cytotoxic drugs was approved *in vivo,* and the feasibility was tested in patients. GC gene expression signature and data/pathway mining revealed 9 molecular targets of ivermectin in both human and mouse GC associated with WNT/β-catenin signaling as well as cell proliferation pathways. The efficacy of ivermectin in inhibiting GC was approved *in silico*, *in vitro* and *in vivo*. Chemopreventive effect of dietary phenethyl isothiocyanate (PEITC) was approved *in vitro* and *in vivo* and synergistic anticancer effect of PEUTC and cisplatin was founded *in vitro*. PEITC depleted glutathione and induced G2/M cell cycle arrest in GC cells.

Conclusions: The nature of this thesis was translational in order to develop new treatments through drug repositioning for GC. The results of this thesis suggested that GC was glutamine dependent with altered neuronal and metabolic signaling pathways and that SNAP25, WNT/β-catenin, mTOR, PDP1/α-KGDH, glutaminolysis, and glutathione were potential drug-targets for treatment of GC. These findings point to the importance of neural signaling in modulating the tumor metabolism and provide a rational basis for clinical translation of the potential anti-metabolism therapies for GC in the future.

1. Introduction

1.1 Translational research

Translational research has been defined as "a bidirectional process that involves multidisciplinary integration among basic, clinical, practice, population, and policy-based research" [1-3]. The overall goal can be highlighted as following: to speed up scientific discovery into patient and community benefit. Successful integration of evidence-based interventions is an essential part of translational research. A significant proportion of the evidence-based interventions involve novel drugs that are to be tested in pre-clinical and clinical trials. However, 80% of all novel drugs fail safety criteria during phase I trials or have unacceptable side effects or lack of efficacy in phase II or III trials [4]. Another approach uses existing and approved drugs for treatment of new diseases, known as drug repositioning or drug repurposing [5]. The latter approach is extremely time saving, given that the average amount of time from novel discovery of a drug to implementation in clinical use, i.e., "from bench to bedside" is at least 10 years. In this thesis, we performed translational research and drug repositioning.

1.2 Background on cancer

1.2.1 Cancer incidence and mortality

In 2018, eighteen million new cases of cancer and over nine million cancer-related deaths were registered according to the GLOBOCAN database. This ranks cancer as one of the top deadliest diseases in the world in 2019, among ischemic heart disease, stroke and lifestyle diseases such as diabetes mellitus, and Alzheimer's disease. Cancer is a multifaced disease, where prognosis varies with cancer type and depend on genetic, environmental and epigenetic or geographical/demographic factors. However, all cancers can be characterized by at least one of six hallmarks that enable cancer to survive, proliferate, and disseminate. Hanahan and Weinberg described the following attributes of cancer cells: 1) sustaining proliferative signaling, 2) evading growth suppressors, 3) activating invasion and metastasis, 4) enabling replicative immortality, 5) inducing angiogenesis and 6) resisting cell death [6]. These hallmarks have been described and extensively investigated during the last decades. Additionally, emerging hallmarks include 7) avoiding immune destruction and 8) deregulating cellular energetics, which involve the capability to modify, or reprogram cellular metabolism [6]. While no. 7) is now being extensively investigated using immune therapies, the mechanisms underlying metabolic reprogramming in different types of cancer are still unclear. In this thesis, we elaborated further on metabolic reprogramming in gastric cancer and further extend the understanding of neoplastic progression at the cellular and molecular levels.

1.2.2 Gastric cancer and current treatment strategies

With a 10-30% 5-year overall survival rate, gastric cancer (GC) is the 5th most common malignant disease worldwide with the 3rd highest incidence and mortality rate among all cancers [7]. According to GLOBOCAN, over one million new cases were registered in 2020, comprising 5.6% of all new cases (Fig. 1) [8]. Although GC remains as one of the most common cancers, incidence and mortality trends decreases. This is most likely due to eradication strategy of *H. pylori* during the latest decades.

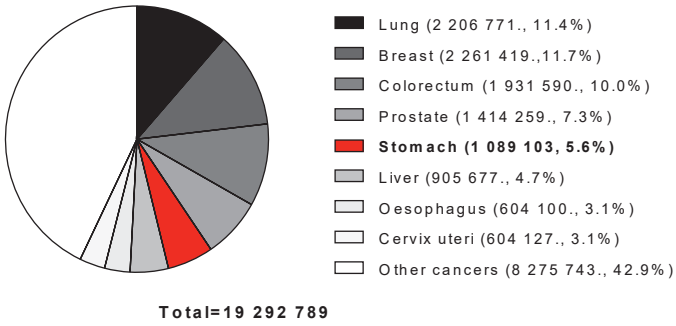

Fig.1. Estimated new cancer cases in 2020 by cancer type. Numbers from GCO/GLOBOCAN database available at https://gco.iarc.fr/today/data/factsheets/cancers/39-All-cancers-fact-sheet.pdf. Made in GraphPad Prism v.6.

Most GC are gastric adenocarcinomas (as opposed to gastric neuroendocrine tumors, gNETs), which are malignant epithelial neoplasms. GC is a heterogeneous disease, both genetically and phenotypically which progresses via different pathways of carcinogenesis. *H. pylori* infection in the stomach is known to increase the risk of developing GC; likewise, the eradication of *H. pylori* is known to prevent progression of hypergastrinemic-induced GC [9-11]. Human GC usually comprises of intestinal-, diffuse-, or mixed types (Laurens classification). Intestinal GC usually develops through the Correa cascade, initiating from gastritis to atrophy, intestinal metaplasia (IM), dysplasia and neoplasia (cancer)(Fig. 2).

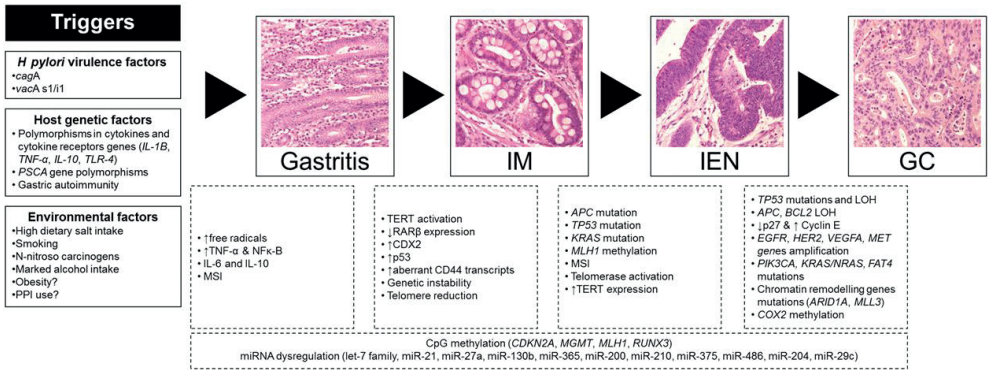

Fig. 2. Gastric cancer tumorigenesis involves an inflammation-associated cascade from gastritis, intestinal metaplasia (IM) and intraepithelial neoplasia (IEN) towards cancer [12]. Reprinted from Gastric Cancer as Preventable Disease, Clinical Gastroenterology and Hepatology, Vol. 25, issue 12, pages 1833-1843, Massimo Rugge, Robert M. Genta, Francesco Di Mario, Emad M. El-Omar, Hashem B. El-Serag, Matteo Fassan, Richard H. Hunt, Ernst J. Kuipers, Peter Malfertheiner, Kentaro Sugano, David Y. Graham with permission from Elsevier (https://ars.els-cdn.com/content/image/1-s2.0-S154235651730602X-gr3.jpg).

Diffuse adenocarcinomas in the stomach lack distinct differentiation. The current common treatments for gastric adenocarcinomas involve surgery in patients at stage I, surgery combined with systemic chemotherapy at stage II, and chemotherapy plus targeted therapies at stages III and IV (Table 1) [13]. The staging is based on the invasiveness of the tumor, from non-invasive (stage 0) to metastatic disease (stage 4). The chemotherapy regimens recommended by the National Comprehensive Cancer Network (NCCN) are 1) fluorouracil and oxaliplatin, 2) fluorouracil and cisplatin, or 3) a fluoropyrimidine (fluorouracil or capecitabine) and paclitaxel [14], although 13 drugs (both neoadjuvant and targeted therapies) are approved according to NIH (https://www.cancer.gov/about-cancer/treatment/drugs/stomach#1). The recommendations are based upon the fact that the most common activating mutations in GC driver genes affect ERBB2 (also known as HER2), VEGF and more recently PD-L1. If patients overexpress ERBB2/HER2, the recommended targeted therapy is Trastuzumab (also known as Herceptin®). Ramucirumab (also known as CYRAMZA®) has been successful against the vascular endothelial growth factor receptor 2 (VEGFR2). Patients with stage 3 or 4 gastric cancer that overexpress PD-L1 or has microsatellite instability (MSI) or mismatch repair deficiency (dMMR) are recommended Pembrolizumab (KEYTRUDA®).

Other commonly mutated genes are KRAS, PI3K, and the receptor tyrosine kinases FGFR2, EGFR, MET and related signaling molecules and downstream pathways [15]. Onartuzumab has been tested in a phase III study without significant effects on MET-positive/HER2-negative GC patients [16].

Table 1. Current recommended and approved treatment strategies in gastric cancer. Source; NCCN.

Stage	Treatment	Biomarkers that influence targeted therapy decision	Targeted therapies	Reference
Stage 0, non-invasive	Surgery	-	-	[14]
Stage 1(A,B), early GC	Surgery Chemotherapy	-	-	[14]
Stage 2 (A,B)	Surgery Chemotherapy, Radiation Targeted treatments	ERBB2/HER2, PD-L1, VEGFR2	Pembrolizumab Trastuzumab Ramucirumab	[14, 16-18]
Stage 3 (A,B,C)	Surgery Chemotherapy Radiation Targeted treatments	ERBB2/HER2, PD-L1, VEGFR2	Pembrolizumab Trastuzumab Ramucirumab	[14, 16-18]
Stage 4, advanced/non-resectable GC with/without metastasis	Surgery (if possible) Chemotherapy, Radiation Targeted treatments	ERBB2/HER2, PD-L1, VEGFR2	Pembrolizumab Trastuzumab Ramucirumab	[13, 15-17]

Drug combination regimens include FU-LV (Fluorouracil + Leucovorin Calcium), and TPF (Docetaxel + Cisplatin + Fluorouracil) or XELIRI (Capecitabine + Irinotecan hydrochloride) for advanced or metastasized GC [19-21]. Current recommendations are use of targeted therapies *only* when locoregional resection of stomach cannot be

performed, the cancer is recurrent after previous treatment or *after* metastatic cancer lesions are detected. Although combinations of drugs increase success of treatment, it remains a tremendous challenge to identify *efficient* combinations of drugs for use in GC, both due to large number of drugs and huge numbers of tumor variants. GC is usually diagnosed at later stages and affecting the older population, raising several important concerns. In this thesis, we performed drug prediction and repurposing based on omics-data from pre-clinical and clinical samples of gastric cancer.

1.2.3 The mouse model of gastric cancer

Commonly used animal models to study GC include *i*) chemically-induced GC using carcinogens (e.g. N-methyl-N-nitrosourea (MNU)), *ii*) transgenic mice, i.e. the INS-GAS mice, *iii*) knockout mice (loss of function), i*v*) knock-in models (gain of function), *v*) xenograft models of GC and *vi*) *H.p*. infected mouse models of GC. Transgenic, chemically induced, *H.p.* – infected, and gene knock-out models were previously used by our research group in demonstrating the nerve-cancer crosstalk in GC [22]. The transgenic insulin – gastrin (INS-GAS) mouse is a well-established model that develop spontaneous GC at the age of 10-12 months [22-24]. The background strain, FVB/N, obtained from Taconic Farms Inc. (Germantown, NY), is an inbred mouse strain preferable for transgenic analyses. INS-GAS mice were developed by recombinant DNA technology, placing the human gastrin gene under control of the rat insulin 1 promoter [25, 26]. Hypergastrinemia in INS-GAS mice is associated with carcinogenesis in the stomach through the induction of apoptosis in gastric epithelial cells [27, 28]. Persistent gastrin expression will cause pathological changes in the INS-GAS mouse stomach wall, inducing acute and subsequent chronic gastritis, which further develops into atrophic gastritis and intestinal metaplasia. In this respect, the GC of INS-GAS mouse is representative of human intestinal GC. The process of tumor development in INS-GAS mice mimics the tumorigenesis in humans, making the INS-GAS mice a good model of human GC. However, it is important to acknowledge some anatomical differences in the rodent and human stomachs. INS-GAS mice develop cancer in the glandular area in corpus/fundus, also known as the body of stomach, leaving the forestomach; rumen, and lower part: antrum, cancer-free. Corpus/fundus in rodents corresponds to corpus alone in the human stomach, which do not include fundus [29].

The human stomach is divided into four parts which display different histological characteristics: (*i*) cardia, (*ii*) fundus, (*iii*) corpus (or body), and (*iv*) antrum/pylorus. Mice lack cardia but have two different glandular domains (the body and the antrum). Despite anatomical inequalities in GI anatomy between human and rodents, the pathogenesis of GC is usually the same, especially for the intestinal type of GC that follows the Correa pathway from gastritis to cancer. Various experimental models to study GC pathogenesis have been developed. However, "humanized" versions of mouse models will more closely approximate human GC pathogenesis. Although it is often difficult to identify the site of the original cancer in humans, GC is thought to arise in three major sites, the antrum, corpus, and cardia.

1.3 Tumor microenvironment

It is recognized that cancer progression is largely influenced by the tumor microenvironment (TME). In recent decades, cancer research has expanded exponentially

beyond the study of rapidly dividing cells to include complex and extensive interactions between cancer and non-cancer cells that constitute the TME. As an integral part of the tumor, the TME is an active player in cell adaptation and resistance to anti-cancer therapies, which is not only composed of proliferating cancer cells but also of stromal cells, cancer-associated fibroblasts (CAFs), blood vessels and endothelial cells, infiltrating immune cells, a variety of associated tissue cells and nerve. The dogma has been that the TME is created by, and at all times shaped and dominated by the tumor, which orchestrates molecular and cellular events taking place in surrounding tissues. In addition, stress introduced in different formats and in different locations within the TME including oxidative stress or hypoxia plays a key role in cancer progression, metastasis, and resistance to therapies [30]. Therefore, tumor cells rewire their metabolic properties to shape hypoxic stress, resist anti-cancer therapies, and escape the immune system. Adaptations can appear autonomously or through interactions with other cells in the TME. In this regard, it has become clear that anti-cancer therapies can be more effective in combination with agents that target key factors in the TME in order to suppress resistance mechanisms associated with the complexity of the TME. Elaborating such combination therapies remains challenging, since it relies on more knowledge of the interaction between cancer cells and their TME. More recently, there are accumulating evidence of a bidirectional crosstalk between the tumor cells and the nerves that infiltrate the tumor and TME [31]. Our understanding of the impact of the TME on tumor development and metabolic adaptation should include strategies that can be considered to overcome a hostile TME and elaborate a more favorable TME to support anti-cancer therapies.

1.4 Role of the nervous system in cancer

1.4.1 Nerves and cancer

Neurons release neurotransmitters, neuroligins, chemokines or soluble growth factors in the TME that drive their own survival and spread. On the other hand, tumors express nerve-specific growth factors and microRNAs that support local neurons and guide neuronal growth into tumors [32-39]. The vagus nerve, which is the 10^{th} cranial nerve, innervates vital organs including the stomach and pancreas in the abdomen. In the abdomen, the vagus nerve is the main parasympathetic outflow to the gastro-intestinal organs including both stomach and pancreas, and conveys information between the gastrointestinal tract and the central nervous system, often referred to as the gut-brain-axis [40]. Both efferent and afferent nerve fibers innervate the stomach, providing a bidirectional “communication” between the stomach and the brain.

Although many cancers including stomach, pancreas, prostate and colon show increased nerve density [22, 41-44], the overall significance of tumor-associated neural plasticity and perineural invasion remains uncertain [41, 45, 46]. However, we have demonstrated that innervated tumors are more aggressive than less densely innervated tumors [22, 43, 47]. Nerves accompany blood vessels, and a link between adrenergic nerve signaling and angiogenesis within the TME has been described [48]. The role of the autonomic nervous system in cancer formation was under-recognized before gaining increased attention during the last decade [32, 33, 35, 36, 38, 39, 43, 49-52]. These studies showed that nerves were active participants in the disease progression, as opposed to previous belief that

nerves were passive bystanders. One question that arises is *why.* Cancer cells release neurotrophic factors to attract nerves, thereby initiating their own innervation to optimize growth conditions [53]. On the other hand, neurotransmitters or neuropeptides secreted from the nerves stimulate the tumor cell proliferation, migration, invasion and survival, leading to tumor development, progression and metastasis [49-51, 54-56] (Fig. 3). Previously, our research group demonstrated the important role of nerve-cancer crosstalk in GC, adding new knowledge to the interrelationship between different cell types in the TME and the nervous system [22]. Most importantly, acetylcholine was found to induce WNT signaling in gastric stem cells through the muscarinic 3 receptor.

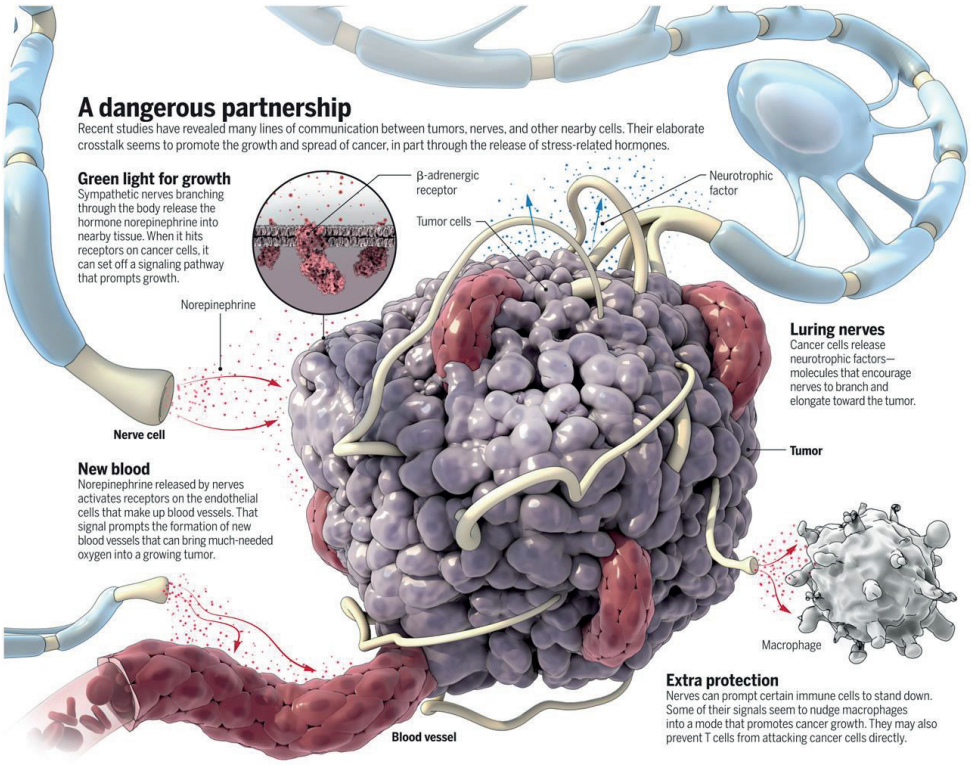

Fig. 3. Innervation of tumor by nerves and blood vessels. The autonomic innervation of the stomach is largely parasympathetic, and the vagal nerve fibers are distributed along the greater and lesser curvature of the stomach where gastric cancer is frequently found. Acetylcholine is released by nerves and act on muscarinic 3 receptors on cells in the tumor microenvironment. From Servick *et al.* 2019 [53]. Reprinted with permission from AAAS.

1.4.2 Vagotomy and gastric tumorigenesis

The role of the vagus nerve in the control of gastric acid secretion was shown in 1814 by Benjamin Brodie and later elaborated on by Ivan Pavlov [57]. Vagotomy is the surgical resection of the vagus nerve that innervates the stomach. Vagotomy procedures include truncal, selective and highly selective vagotomies, depending on where the branch is cut. Unilateral truncal vagotomy involves cutting only one branch that innervates one side of the stomach, leaving the other side innervated and thus does not impair the overall functional capacity of the stomach, leaving gastric acid output, circulating gastrin levels and motility unchanged. Vagotomy has historically been used as a surgical treatment for peptic ulcers because it reduces gastric acid secretion. Surgical treatment such as partial gastrectomy or vagotomy have traditionally been thought to be associated with an increased risk of GC due to the secondary hypochlorhydric conditions in the stomach, but a 20+ year follow-up study after vagotomy showed no increased risk of developing GC [57-59].

1.4.3 Botulinum Toxin type A

Botulinum toxin (BoNT) is created by the anaerobic gram-positive bacterium C. *botulinum*, existing in eight antigenically distinguishable exotoxins (A, B, C1, C2, D, E, F and G)[60]. BoNT-A was FDA approved in 1989 for therapeutic use, and for cosmetic use such as reduction of wrinkles in 2002 [61]. BoNT cleaves synaptosomal-associated protein 25 (SNAP-25), a member of the soluble N-ethylmaleimide-sensitive factor attachment receptor (SNARE) family, known to be involved in vesicle fusion [62, 63]. Thus, the mechanism of action by BoNT is to prevent the fusion of neurotransmitter-containing vesicles with the plasma membrane, stopping the release of the neurotransmitter [63].

1.5 Metabolism in general and cancer metabolism in particular

1.5.1 Cellular homeostasis

All cells, whether quiescent, replicating, or activated, need to produce ATP and synthesize macromolecules to maintain their basic cellular functions. Metabolic precursors such as acetyl-CoA, amino acids, purines and pyrimidines are synthesized from nutrients to form more complex structures such as proteins, lipids and nucleotides [64]. These processes require ATP. Proliferating cells need ATP in larger quantities. In an evolutionary perspective, cells have been equipped with several mechanisms to obtain energy, especially ATP. Cells of normally differentiated tissues maintain homeostasis and obtain energy through the oxygen-dependent pathway of oxidative phosphorylation (OXPHOS) as well as through the oxygen-independent pathway of glycolysis. Since OXPHOS is more efficient in generating ATP than glycolysis, it is recognized that the presence of oxygen results in the activation of OXPHOS and the inhibition of glycolysis (the so-called Pasteur effect).

1.5.2 Cancer metabolism

Although cancer is generally considered a genetic disease, emerging evidence suggests that cancer should also be recognized as a metabolic disease, as the metabolic

reprogramming is one of the hallmarks of cancer [6, 65, 66]. Cells in the TME are usually different from “normal” cells, and thus, the “cancer metabolic reprogramming” is reflected by cancer cell metabolic profiles as well as the microenvironment of tumors which has important implications for tumorigenesis, progression, prognosis and metastasis [65-67]. The current knowledge on cancer metabolic reprogramming includes the following six attributes: (1) deregulated uptake of glucose and amino acids, (2) use of opportunistic modes of nutrient acquisition, (3) use of glycolysis/tricarboxylic acid (TCA) cycle intermediates for biosynthesis and nicotinamide adenine dinucleotide phosphate (NADPH) production, (4) increased demand for nitrogen, (5) alterations in metabolite-driven gene regulation, and (6) metabolic interactions with the microenvironment [68, 69].

1) Deregulated uptake of glucose and amino acids

Glucose and amino acid uptake are usually increased in growth factor-stimulated cells. Growth factors, such as insulin, epidermal growth factor (EGF), fibroblast growth factor (FGF), erythropoietin (ePo), platelet-derived growth factor (PDGF), transforming growth factors (TGFs) and cytokines, promote cell growth, proliferation or differentiation through different signaling pathways that link to metabolic pathways. Thus, the growth factors are highly capable of altering metabolite programs and metabolite levels endogenously. Another trait of growth-factor stimulated cells is the enhanced ability to take up nutrients from outside of the cell.

2) Use of opportunistic modes of nutrient acquisition

Cells can adjust gene expression to activate different mechanisms to take up extracellular nutrients to deal with depleted nutrient status, includes macropinocytosis, entosis of living cells, uptake of lipid, and phagocytosis of apoptotic bodies.

3) Cell can use glycolysis/tricarboxylic acid (TCA) cycle intermediates for biosynthesis and nicotinamide adenine dinucleotide phosphate (NADPH) production (Fig. 4).

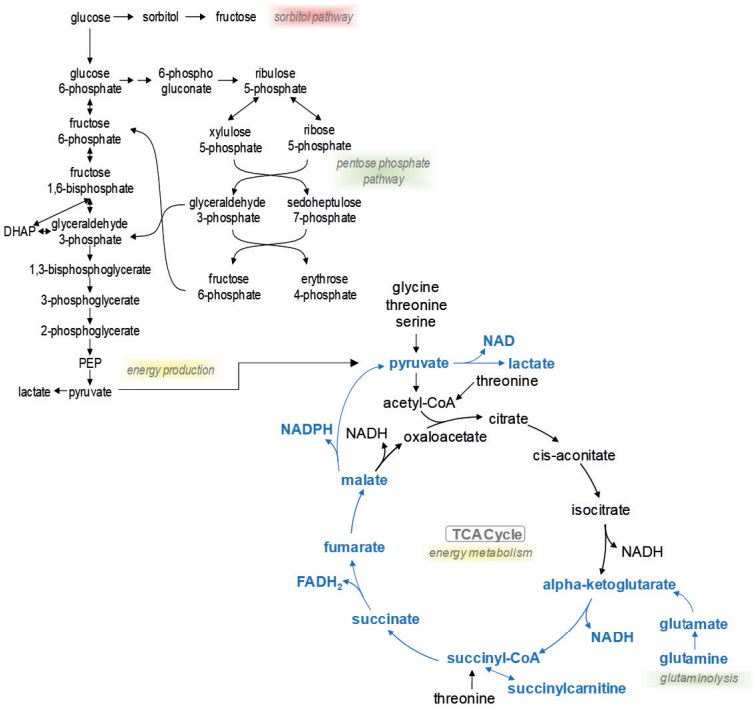

Fig.4. Metabolic pathways of glycolysis/energy metabolism including the TCA cycle are used for production of NADPH and ATP.

4) Increased demand of glutamine as nitrogen source

Glutamine is an excellent source for *de novo* production of nitrogen-containing nucleotides. The production of uracil and thymine requires one glutamine molecule, whereas cytosine and adenine each require two, and building a guanine base requires three molecules of glutamine. Glutaminolysis activates Rag-mTOR signaling, providing an explanation for glutamine addiction in the TME [70]. mTORC1 can be activated by glutamine via gutaminolysis and α-ketoglutarate production upstream of Rag. The mTORC1/S6K1 pathway regulates glutamine metabolism through the elF4B-dependent control of c-Myc translation. Moreover, mTORC1 activation stimulates uptake of glutamine while Myc stimulates glutamine catabolism and increases the expression of cellular transporters of glutamine [70, 71].

5) Alterations in metabolite-driven gene regulation

The removal of acetyl and methyl marks is guided by the cellular metabolic state. Sirtuins, a class of deacetylases known to be dysregulated in cancer, catalyzes the removal of acetyl marks from histone and nonhistone proteins, and utilizes NAD+ as a cofactor, while FAD serves as a cofactor for a lysine-specific demethylase LSD1. These enzymes are sensitive to changes in NAD+ and FAD to orchestrate global posttranslational and epigenetic changes that promote energy conservation. Certain metabolites, like Acetyl-CoA and crotonyl-CoA, also directly influence gene expression.

6) Metabolic interactions with the microenvironment

The reprogramming of the TME utilizes several strategies and affects numerous cell types. Examples of deregulating factors include intrinsic features like genetic programs within cancer cells or extrinsic factors like oxygen levels, nutrient availability, blood supply, pH, cell-cell interactions and paracrine signaling [72].

1.5.3 Metabolic reprogramming in gastric cancer

Cancer cells (and some non-malignant proliferating cells) can activate glycolysis in the presence of adequate oxygen levels in the mitochondria (aerobic glycolysis or Warburg effect) [69, 73]. Cancer cells do not exclusively depend on aerobic glycolysis to satisfy bioenergetical needs [74]. The dogma has been that metabolic reprogramming in GC mainly involves changes or disturbance in the glycolysis/Warburg effect. Crucial within the metabolic reprogramming are the enzymes hexokinase II, pyruvate kinase M2, pyruvate dehydrogenase kinase, enolase, GLUTs, lactate dehydrogenase. Additionally, metabolic reprogramming often involves changes in mitochondrial proteins including Mitochondrial topoisomerase I and SIRT3 and noncoding RNAs or proteins that regulates these factors. Besides metabolic pathways, metabolic reprogramming also heavily involves lipid metabolism and additional regulators like Snail, HIF-1α, Thymidine phosphorylase, p53 and monocarboxylic acid transporters [75]. Accordingly, numerous attempts to develop metabolism-based therapies to the patients have not yet succeeded and need to be exploited for development of treatments [73, 76-79].

However, the implications of mitochondrial metabolism and the dynamic reprogramming of cellular energetics go beyond the Warburg effect and also involve deregulated amino acid uptake and utilization [74]. During tumorigenesis, oncogenic mutations in growth-factor-responsive signaling proteins such as PIK3CA, Akt, and KRAS induce high levels of glucose uptake, the majority of which is excreted as lactate. This shift drives the accumulation of metabolic intermediates that are required for anabolic cell growth, including ribose sugars, fatty acids, and reducing equivalents. In this thesis, we provided evidence that GC is glutamine dependent rather than glucose dependent and has enhanced glutamine metabolism and amino acid utilization. This was in line with a recent report that the TME was dynamic in the sense that glucose was preferentially consumed by immune cells over cancer cells, and in fact the TME myeloid cells took up more glucose than the cancer cells [80].

1.6 Drugs that target cancer metabolism

Drugs that target cancer metabolism include antimetabolites which are developed to target different mechanisms, including inhibition of enzyme activity involved in nucleotide base synthesis and incorporation into DNA, thus affecting both nucleotide biosynthesis and DNA replication [81]. Among antimetabolites are chemotherapeutic drugs, like 5-FU, oxaliplatin and cisplatin.

Recently, ivermectin has been repurposed as a new anti-cancer drug although the mechanism is debated. Ivermectin was first used to treat River Blindness disease [82]. Since then, ivermectin has been repositioned as a broad-spectrum antiviral, antimicrobial and anti-cancer agent [82-86]. Ivermectin has shown to inhibit the WNT-TCF pathway in

cancer, through repressing the levels of C-terminal β-CATENIN and of CYCLIN D1 in an okadaic acid-sensitive manner, indicating its action involves protein phosphatases [82]. This provided a rational for testing ivermectin as therapeutics in cancers that display activated WNT-signaling, such as GC.

Another class of small molecule drugs to target energy metabolism are the anti-carcinogenic isothiocyanates (ITCs). ITCs are found in vegetables and have been intensively investigated as anti-cancer agents in breast and other cancers [87-95]. In this thesis, we tested the potentiating effect of ITCs together with chemotherapeutic drugs in GC.

2. Aim/objectives of thesis

2.1 Principal aim

The overriding aim of this thesis was to develop metabolism-based new treatments for GC through translational research and drug repositioning.

2.2 Specific objectives

2.2.1 To characterize the metabolic signature of GC as potential therapeutic targets in patients (Paper I)

2.2.2 To investigate the effects of anti-nerve-cancer metabolism therapy using multi-omics approaches in animal models of GC (Papers I and II)

2.2.3 To identify drug combinations using drug repositioning approach with special focus on energy metabolism of GC (Papers I and II)

2.2.4 To investigate glutathione-depleting agents targeting energy metabolism for GC (Paper III)

2.2.5 To evaluate the safety of local BoNT-A injections in elderly patients diagnosed with GC (Paper I)

3. Materials and methods

3.1 Project design

The work in this thesis has followed the workflow as illustrated in Fig. 5. Transcriptomics and metabolomics were performed on gastric tumor and healthy samples from mice and humans with advanced GC. Computational drug repurposing was applied to identify candidate drugs and experimental validation followed in preclinical studies using mice.

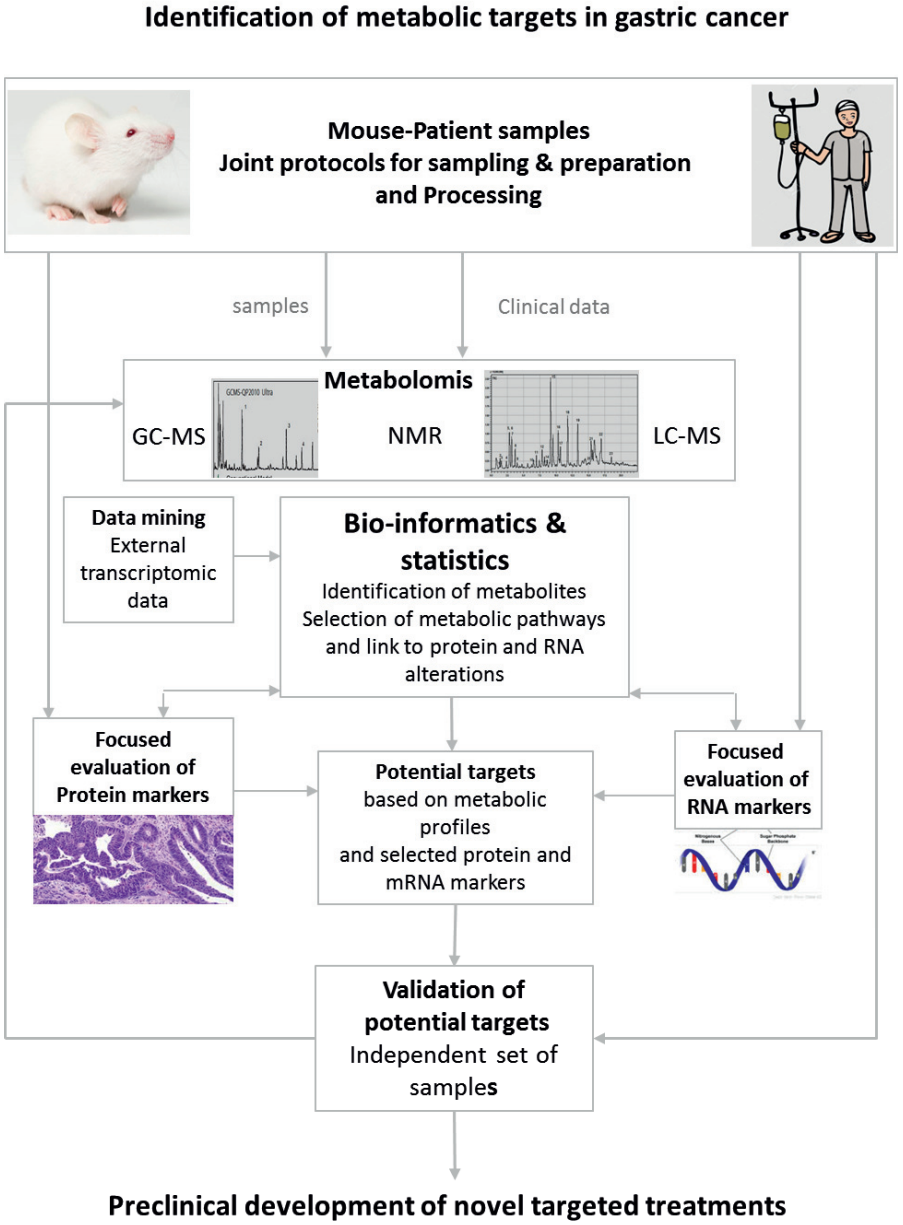

Fig. 5. Workflow of identification of metabolic targets from mouse and patient samples to validation of selected targets.

3.2 Animals

In this thesis, four-hundred-seventy-one mice were used. In paper I, three hundred-twenty-four mice were used and some of the mice were followed- up for more than one year to measure the overall survival rate. In paper II, fifty-seven mice were used. In paper III, ninety mice were used. The mouse GC model was the transgenic INS-GAS mice which spontaneously develop GC at our own institute [22, 26] and its wild-type (WT) mice (FVB strain) (papers I and II) or MNU-induced GC (FVB)(Paper III). The mice included in each study in this thesis were randomly assigned to the experimental groups using a random number table. After randomization, the groups were gender adjusted. Mice were housed ~5 mice per cage on wood chip bedding with a 12-hour light/dark cycle in a specific pathogen free environment with room temperature of 22°C and 40-60% relative humidity.

3.3 Experimental designs

The work conducted in this thesis is summarized in Fig. 6.

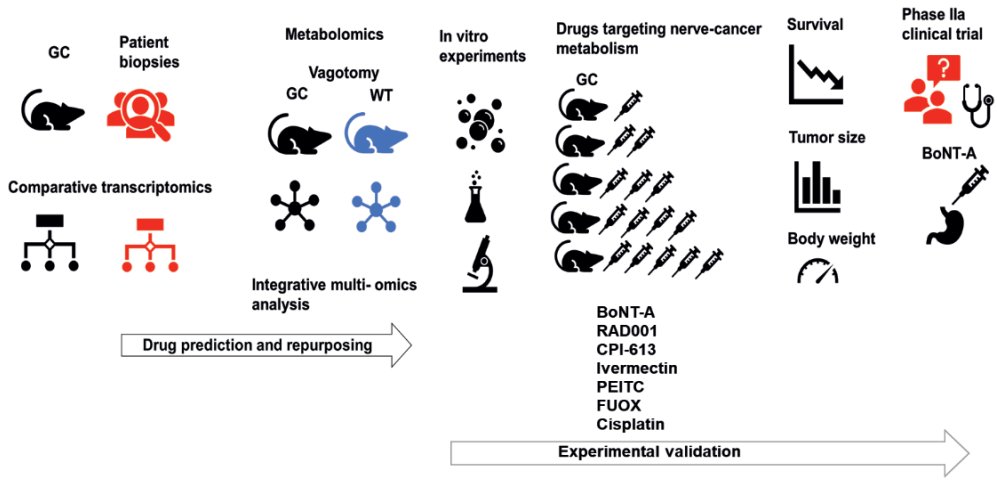

Fig. 6. Flow chart of methods used in the thesis (Papers I-III).

3.3.1 Experimental design (Paper I)

In the 1st experiment, stomach biopsies were taken from patients (N=16) diagnosed with gastric adenocarcinoma. Transcriptomics were performed on cancer biopsies and healthy stomach control tissue. Patients were followed-up for 5+ years.

In the 2nd experiment, stomach biopsies were taken from INS-GAS mice at 12 months of age (N=3) with GC and from healthy stomachs of FVB mice (N=3). Transcriptomic comparison was performed.

In the 3rd experiment, INS-GAS mice (N=6) or wild-type (WT) FVB mice (N=10) at 6 months of age underwent unilateral vagotomy or sham operation into anterior side of the stomach. After 6 months post vagotomy, samples were taken for metabolomics and transcriptomics analyses.

In the 4th experiment, INS-GAS mice (N=41) underwent unilateral vagotomy (UVT) and FUOX treatment as previously described [22].

In the 5th experiment, INS-GAS mice (N=86) at 12-14 months of age underwent BoNT-A treatment and FUOX treatment as previously described [22].

In the 6th experiment, INS-GAS mice (N=181) underwent BoNT-A treatment (anterior side of stomach). Mice were treated with RAD001 (1.5 mg/kg/day for 3 weeks, i.p.), CPI-613 (20 mg/kg/week, once weekly for 3 weeks, i.p.), or combination of RAD001 and CPI-613. Saline injection intraperiotoneally (i.p.) was used as control. The mice were allowed one week rest after the first cycle of treatment, and then the treatment cycle was repeated once, yielding a total treatment window of 8 weeks.

3.3.2 Experimental design (Paper II)

Thirty-one INS-GAS mice were randomly divided into age-and gender balanced experimental groups: ivermectin treatment (12 females and nine males at age of 10 months) and controls (no treatment, six females and four males at age of 10 months). Ivermectin was administered at a dose of 10 mg/kg once per day for 5 days, followed by no treatment for 5 days and then injection once per day for 10 days. This regimen was repeated 10 days later. The total duration of treatment was 2 months (2 × 30 days). 10 WT FVB mice were included as controls.

3.3.3 Experimental design (Paper III)

Ninety mice were randomly divided into age-and gender balanced experimental groups: FVB mice, FVB mice + MNU, FVB mice + MNU + prePEITC, FVB mice + MNU + postPEITC, INS-GAS mice and INS-GAS mice + PEITC.

All animal experiments in papers I-III were designed strictly according to 3Rs (the guideline for human use of animals; Replace, Refine, Reduce) [96].

3.4 Gastric cancer patients

3.4.1 Patients

In paper I, twenty-two patients (17 men aged 49-87 years and 5 women aged 51-83 years) were included. In the first study, human stomach specimens (both tumors and the adjacent non-tumor tissues) were taken immediately after total/subtotal or distal gastrectomy from 16 patients with intestinal or diffuse GC. Patients were followed-up for 5 years since 2012 at St. Olavs Hospital, Trondheim, Norway. The data from the 16 patients were included in papers I and II. The study was approved by the Regional Committees for Medical and Health Research Ethics Central Norway (REK 2012-1029). In the second study, six patients were enrolled into a pilot phase II study according to inclusion criteria and written consent (Extended Data Clinical Trial Protocol). Inclusion criteria are listed in Transparent Methods in Paper I. The study was approved by the Regional Committees for Medical and Health Research Ethics Central Norway (REK 2012-1031).

3.4.2 Pathological evaluation of patient biopsies

Total, subtotal or distal gastrectomy was performed on 16 patients diagnosed with GC (REK 2012-1029). Biopsies from 4 pre-determined positions in corpus (major and minor

curvature), cardia and antrum were collected. Biopsies from adjacent, normal tissue was taken 5-10 cm from the tumor site. TNM status was defined, and samples were classified according to Lauren's classification, (Intestinal, diffuse or mixed/combined type), WHO classification (tubular, papillary, mucinous and poorly cohesive), WHO grading (well, moderately or poorly differentiated), and were reviewed according to the Japanese pathological classification. Samples were assigned gastric histopathology scoring including inflammation, epithelial defects, oxynthic atrophy, epithelial hyperplasia and dysplasia and an overall GHAI score.

3.4.3 RNA sequencing

In order to characterize GC in the mouse model (Papers I and II), total RNA was extracted from harvested stomachs of INS-GAS or FVB mice. Mechanical disruption of tissue was performed using Precellys 24 homogenizer (Bertin technologies, France) and NucleoSpin® RNA according to manufacturer's instruction that uses Silica-membrane technology and mini-spin columns (Nacalai-Tesque, Japan). Lysis buffer containing reducing agent beta-mercaptoethanol was added to the frozen tissue in appropriate screw-cap tubes and run on Precellys 24 using Zirconium oxide beads (1.4 mm and 2.8 mm) until complete dissolved tissue and clear lysate was obtained (30s x2, 5000 rpm). RNA quality and quantity were obtained using NanoDrop One (Thermo Scientific, Norway). RNA integrity (RIN) score was assessed on an Agilent 2100 bioanalyzer and found satisfactory (i.e., RIN score above 8.0) before a cDNA library was prepared using Illumina TruSeq Stranded mRNA Library Prep kit. Transcripts were obtained using Illumina HiSeqNS500 instrument (NextSeq 500) at 75 bp with paired-end (PE) reads using NS500H flowcells with 25 M reads/sample. Paired end forward read length (R1): 81, reverse read length (R2): 81.

3.5 Experimental surgery

In paper I, UVT was performed (Fig. 7) under isoflurane anesthesia as described previously [22]. The success of UVT was confirmed by reduced thickness of gastric mucosa and reduced tissue-levels of metabolites that are involved in DNA/protein synthesis in the denervated side in comparison with the innervated side of the stomach.

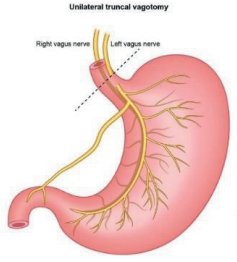

Fig. 7. Drawing of unilateral vagotomy in the stomach. The anterior branch of the vagus nerve is cut. Made by author.

3.6 Sample collection and preparation

In Papers I-III, mouse tissue samples were collected under isoflurane inhalation anesthesia (1.75-2.0 %), and the anterior and posterior parts of stomachs were collected. Stomachs were opened along the greater curvature and fixed on silicone-boards. Pictures were taken before anterior and posterior parts were cut and fixed in formalin for histopathological analysis or cryotubes in liquid N_2 for cryopreservation. In paper I, transcriptomics of mouse GC in which mice underwent UVT at 6 months of age and the stomachs were collected 6 months afterwards, the data from our previous study was re-analyzed (according to 3Rs principle). For metabolomics, GC and WT mice at 6 months of age underwent the same UVT or sham operation and the stomachs were collected as described previously [22]. Six months after UVT, animals were terminated for sampling, and tissue samples from the denervated anterior stomach and tissue samples from the posterior stomach with intact innervation were analyzed with liquid chromatography/mass spectrometry and gas chromatography/mass spectrometry. For RNA sequencing in papers I and II, mouse stomach samples were collected upon completing treatment regimens.

3.7 Microarray and qRT-PCR

In paper I, total RNA was extracted from harvested stomachs of mice or surgical biopsies of patients. The collected mouse stomachs after vagotomy and human stomach samples were kept frozen at -80°C until further processing. Total RNA from the frozen stomach samples was isolated and purified using an Ultra-Turrax rotating-knife homogenizer and the mirVana miRNA Isolation Kit (AM1560, Ambion) according to the manufacturer's instructions. Concentration and purity of total RNA were assessed using a NanoDrop (NanoDrop Technologies, Inc., Wilmington, DE) photometer. The A260/280 ratios were 2.05±0.01 for mouse samples and 1.96±0.10 for human samples (mean ± SEM). RNA integrity was assessed using a Bioanalyzer (Agilent Technologies, Palo Alto, CA) and found satisfactory with RIN values 9.1±0.1 for mouse samples, and 8.7±0.9 for human samples (means ± SEM). The microarray gene expression analysis followed standard protocols, analyzing 300 ng total RNA per sample with the Illumina MouseWG-6 and HumanHT-12 Expression BeadChips (Illumina, San Diego, CA). Microarray data were confirmed by qRT-PCR array (RT2 Profiler PCR Array, SABiosciences, Qiagen, MD) (StepOnePlusTM, Applied Biosystem, Foster City, CA). Mouse WNT pathway RT2 profiler PCR array was used (StepOnePlusTM, Applied Biosystems), which targeted key genes involved in the canonical and non-canonical WNT pathways and endogenous genes for reaction control (89 genes and 7 controls). The reaction was performed according to the manufacturer's instructions (SABiosciences Corporation, QIAGEN Norway). Mouse microarray data were deposited in the Gene Expression Omnibus (GEO accession no. GSE30295), and human data in ArrayExpress (accession no. E-MTAB-1338).

3.8 Metabolomics (paper I)

Metabolomics of mouse stomach samples was performed using a platform that incorporates two separate ultrahigh-performance liquid chromatography/tandem mass spectrometry (UHPLC/MS/MS2) injections and one gas chromatography/mass spectrometry (GC/MS) injection per sample by Metabolon (USA). Identification, relative

quantification, data-reduction and quality-assurance components of the process were included in the analysis platform. 343 metabolites were identified. The informatics system consisted of four major components, the Laboratory Information Management System (LIMS), the data extraction and peak-identification software, data processing tools for QC and compound identification, and a collection of information interpretation and visualization tools for use by data analysts. The hardware and software foundations for these informatics components were the LAN backbone, and a database server running Oracle 10.2.0.1 Enterprise Edition. Liquid chromatography/Mass Spectrometry (LC/MS, LC/MS2): The LC/MS portion of the platform was based on a Waters ACQUITY UPLC and a Thermo-Finnigan LTQ mass spectrometer, which consisted of an electrospray ionization (ESI) source and linear ion-trap (LIT) mass analyzer. The sample extract was split into two aliquots, dried, and then reconstituted in acidic or basic LC-compatible solvents, each of which contained 11 or more injection standards at fixed concentrations. One aliquot was analyzed using acidic positive ion optimized conditions and the other using basic negative ion optimized conditions in two independent injections using separate dedicated columns. Extracts reconstituted in acidic conditions were gradient eluted using water and methanol both containing 0.1% Formic acid, while the basic extracts, which also used water/methanol, contained 6.5 mM Ammonium Bicarbonate. The MS analysis alternated between MS and data-dependent MS2 scans using dynamic exclusion. The samples destined for gas chromatography/mass spectrometry (GC/MS) analysis were re-dried under vacuum desiccation for a minimum of 24 hours prior to being derivatized under dried nitrogen using bistrimethyl-silyl-triflouroacetamide (BSTFA). The GC column was 5% phenyl and the temperature ramp was from 40° to 300° C in a 16-minute period. Samples were analyzed on a Thermo-Finnigan Trace DSQ fast-scanning single-quadrupole mass spectrometer using electron impact ionization. The instrument was tuned and calibrated for mass resolution and mass accuracy on a daily basis. The information output from the raw data files was automatically extracted. Metabolon QC samples and standards were MTRX in which large pool of human plasma was maintained by Metabolon that has been characterized extensively.

3.9 Chemicals and reagents

Reagents in this thesis included Dulbecco's Modified Eagle's Medium (DMEM) (cat. no 08456-65, Nacalai tesque, Japan) with 1.0 g/l D-glucose (10 mM), L-Glutamine (584.00 mg/L, 4.0 mM) and Sodium Pyruvate (110.00 mg/L, 1.0 mM) (Nacalai tesque, Japan), DMEM (cat.no. D6046, Sigma Aldrich, Norway) with 1.0 g/l D-glucose (10 mM), L-Gln (584 mg/L, 4.0 mM) and Sodium Pyruvate (110.00 mg/L, 1.0 mM), DMEM (no glucose, no glutamine, no pyruvate, no phenol red) (cat.no: A1443001, Gibco, ThermoFisher Scientific, Grand Island, NY), RPMI-1640 medium (Sigma Aldrich, Cat. no. R8758) with L-Gln (0.3 g/L, 2.0 mM), Fetal Bovine Serum (cat. no. F7524 Sigma Aldrich, Norway), Sodium Pyruvate (110.00 mg/L, 1.0 mM, Nacalai tesque, Japan), L-Gln (cat. no. G7513-100ML, Sigma Aldrich), Penicillin/Streptomycin cocktail (cat. no. P4333-100ML, Sigma Aldrich, Norway), Recombinant human β-Nerve Growth factor (NGF, cat. no. 450-01, Peprotech), RNase A (cat. no R4875-100MG, Sigma Aldrich, Norway), Propidium Iodide (cat. no. P4170, 10 mg, ≥94.0% (HPLC), Sigma Aldrich, Norway), Triton-X (cat. no. T9284, Sigma Aldrich, Norway), sodium acetate buffer (10 mM, CH3COONa, MW: 82.03, pH 5.2), Tris-HCl (1 M, NH2C(CH2OH)3; MW: 121.14, pH 8,0). Trypsin-EDTA

solution (cat. no. T4049-100ML, Sigma Aldrich). 2 mM L-glutamine (cat. no. G6275), 1 mM L-glutamate (cat. no. G6150), glutamic dehydrogenase (L-GLDH, cat. no. G5900), NAD (cat. no. N9268), 0.5 M acetate buffer, pH 5 (cat. no. A4433), 100 mM adenosine 5'-Diphosphate, 1 ml (ADP, cat No. A4558), glutaminase (cat. no. G8880), hydrazine hydrate (cat. no. H0883, 3ml), tris-EDTA buffer (cat. no. T3161), dimethylsulfoxide (DMSO, cat. no D8418, Sigma Aldrich), collagen type I (4 mg/mL, Sigma-Aldrich, Norway). The drugs used included BoNT-A (Botox ® 100 U, Botox Allergan Inc.), RAD001 (mTORC1 inhibitor, Everolimus, InvivoGen, San Diego, CA), CPI-613 (targeting PDP1/KGDH, Sigma Aldrich, Norway), ivermectin (Sigma-Aldrich, Oslo, Norway), AITC (cat. no. 377430, Sigma Aldrich, Germany), BITC (cat. no. 252492, Sigma Aldrich, Poland), PEITC (cat. no. 253731, Sigma Aldrich, United States), and cisplatin (Wako Pure Chemical Industries Ltd., Osaka, Japan, cat. no. 033-20091, Lot. SAQ1693 or TOCRIS Bioscience, Abingdon, United Kingdom, cat. no. 2251). Kits used included NucleoSpin® RNA (Macherey Nagel, June 2015, Rev. 17), Glutamine/glutamate determination kit, Sigma, Saint Louis, Missouri), total GSH determination kit (Sigma, United States), illumina TruSeq Stranded mRNA Library Prep kit, Cell Count Reagent SF (Nacalai tesque, Japan, cat.no 07553-44), Cell counting Kit-8 (CCK-8) reagent (Sigma, cat. no. 96992).

3.10 Cells and cultivation

Cell lines used in this thesis included AGS, MKN74 (human gastric cancer adenocarcinoma, intestinal type), MKN45 and KATO-III (human gastric cancer adenocarcinoma, diffuse type). AGS cells were kindly provided by Prof. Sasakawa, Tokyo University, Japan, MKN45 cells were kindly provided by Prof. Kamiya, Kyorin University, Japan, MKN74 cells were kindly provided by Prof. T.C Wang and KATO-III cells were purchased from the LGC group. AGS and MKN45 cells were maintained in Dulbecco's Modified Eagle's Medium (DMEM (1.0 g/l Glucose, 10 mM) with L-Gln (584.00 mg/L, 4.0 mM) and Sodium Pyruvate (110.00 mg/L, 1.0 mM) (Nacalai tesque, Japan) supplemented with 10% fetal bovine serum (FBS; ThermoFisher Scientific, Grand Island, NY) and antibiotic-antimycotic solution (1%) containing penicillin, streptomycin and amphotericin B (Nacalai tesque, Japan). MKN74 and KATO-III cells were maintained in RPMI-1640 medium (Sigma Aldrich, Norway) supplemented with fetal bovine serum (10%, FBS), Sodium pyruvate and penicillin streptomycin solution (1%) in a humidified incubator holding 5% CO_2 and 37°C.

3.11 *In vitro* experiments

3.11.1 Drug screen of BRC+FUOX (Paper I)

Cells (1.5-2.5x10^3) were plated (24h) and subjected to individual dose-response drug screens and sequential combination treatment during 3 days in culture. First, cells were treated with either serum-free medium or BoNT-A without serum at 0.25 U BoNT-A/well and incubated for 24 hrs. CPI-613 and RAD001 were dissolved in DMSO at highest solubility before diluted in the medium. The cells were treated with RAD001, CPI-613, combination of these or vehicle (DMSO) control and incubated for 24 hrs. A combination of 5-FU and oxaliplatin or medium control was added to the cells for 24 hrs. To assess whether the drug combinations acted synergistically, we calculated Bliss synergy scores for RAD001 + CPI-613 combinations using the SynergyFinder web-application [97].

Synergy scores were quantified as an average excess over expected drug combination effect given by the Bliss reference model, which is one of the most popular synergy scoring models [98].

3.11.2 Drug screen of ivermectin (Paper II)

For proliferation assay, MKN74 and KATO-III were seeded in 96-well plates ($2.5x10^3$ cells/well and $3.0x10^3$ cells/well, respectively) and incubated overnight. Ivermectin (MW: 875.09 g/mol) was dissolved in DMSO (100%) to 50 mM stock solution. Cells were treated with ivermectin (0–50 µM) or vehicle control (0.45% v/v DMSO) for 24, 48, and 72 h. Proliferation was measured using a commercial CCK-8 Kit (Sigma Aldrich, Oslo, Norway) with absorbance read at 450 nm.

3.11.3 Drug screen of ITCs (Paper III)

For proliferation assay, $1.5x10^3$ cells of AGS, $2.5x10^3$ of MKN45 or MKN74 or $3.0x10^3$ cells of KATO-III were seeded in 96-well plates before incubated overnight allowing cells to reach confluence. Treatments were accompanied by vehicle controls (n=12) on each plate (0.05% DMSO). Cells were treated with AITC (Sigma Aldrich, Germany), BITC (Sigma Aldrich, Poland), PEITC (Sigma Aldrich, United States), cisplatin (Wako Pure Chemical Industries Ltd., Japan) or (Tocris, Norway) and 5-fluorouracil (Sigma Aldrich, China) as indicated in the text. Following treatment, Cell Count Reagent SF (Nacalai tesque, Japan) was added according to providers' instructions to each well before mixing and incubating for 1.0 - 1.5 h. Proliferation was determined by measuring absorbance at 450 nm using a well plate reader.

3.11.4 Gln/pyr depletion (Paper III)

In paper III, cells ($1.0x10^4$) were plated and allowed to reach confluency (24h) before treated with 0-2.0 mM L-glutamine and 1.0 mM pyruvate in DMEM supplemented with dialyzed bovine serum (10%) and glucose at 25 mM. In depletion testing, either glutamine or pyruvate was omitted from the medium. Proliferation was assessed using Cell Count Reagent SF or Cell counting Kit-8 reagent was calculated relative to controls. Determination of endogenous L-glutamine and L-glutamate was performed after 1, 6 and 24 h in culture using a detection kit (Glutamine/glutamate determination kit, Sigma, Saint Louis, Missouri).

3.11.5 Total GSH determination (Paper III)

Total cellular glutathione level was determined in PEITC, AITC or BSO-treated AGS cells. Cells were seeded in T25 flasks ($1.5x10^5$ cells per flask) and incubated overnight prior to treatment. The cultures were treated with either 10–20 µM PEITC, 50–100 µM AITC, or 0–100 µM BSO or vehicle control (0.1% DMSO) for 3 or 6 h. The doses were based on IC_{50}-range and previous literature. Each treatment was performed in quadruples. Cells were harvested and centrifuged (1,500 rpm, 5 min) before determination of total cellular glutathione using a commercial glutathione assay kit (Sigma, United States) according to manufacturers' instructions. Briefly, cell pellets were deproteinized in 5-sulfosalicylic acid (SSA) solution (5%), vortexed and snap-freezed (3 times in total)

before centrifugation (1,500 rpm, 5 min). Supernatants were transferred to clean tubes and stored on ice until analysis. 10 µl from each sample was applied to a 96-well plate in separate wells in duplicates and mixed together with 150 µl reaction mixture containing 95mM potassium phosphate buffer (pH 7), 0.95 mM EDTA, 0.031 mg/ml DTNB, 0.115 units/ml glutathione reductase and 0.24% 5-sulfosalicylic acid. 50 µl of NADPH solution (0.16 mg/ml, resulting in final concentration of 0.038 mg/ml (48 µM) NADPH) was added to each well and mixed. Immediately after mixing, a kinetic read was performed in 1 min intervals for 5 min at 412 nm using a spectrophotometric plate reader to detect the formation of the yellow product 5-thio-2-nitrobenzoic acid (TNB).

3.11.6 Glutamate/glutamine determination upon ITC treatment (Paper III)

AGS cells were seeded in 24-well plates (1.0x10^4 cells per well) and incubated over night to attain confluency. The cultures were then treated with PEITC (10–30 µM) and AITC (50–200 µM) for 2–24 h in defined DMEM (4.5 g/L glucose, 2 mM glutamine or 0.2 mM glutamine and 1 mM sodium pyruvate) supplemented with dialyzed FBS before samples were collected and analyzed for glutamate and glutamine content. Determination of glutamate/glutamine was performed using a detection kit (Sigma, United States) following the manufacturers' instructions. Briefly, from each sample to be analyzed, one sample was prepared for estimating endogenous glutamate, and one sample was prepared for estimating endogenous glutamate and glutamate converted from glutamine based on an initial deamination reaction catalyzed by glutaminase of the samples. All samples were then mixed with glutamic dehydrogenase which generates α-ketoglutarate and converts NAD+ to NADH which was detected spectrophotometrically at 340 nm. Glutamate content was then calculated using a standard curve, whereas glutamine content was calculated by subtracting the endogenous glutamate concentration from the total concentration of endogenous glutamate and glutamine-derived glutamate.

3.11.7 Cell cycle analysis (BRC+FUOX) (Paper I)

$0.15x10^6$ MKN74 cells were seeded in 6-well plates and incubated overnight prior to treatment. Cells were treated with 2.5 U BoNT-A/well for 24 h. The medium was changed, and cells treated with RAD001 (15 µM), CPI-613 (200 µM), a combination (15 µM RAD001 + 200 µM CPI-613) or DMSO control (0.25 %) for 24 h. The next day, medium was changed, and cells washed in PBS before treatment with 5-FU (50 µM) + Oxaliplatin (10 µM) or medium control. Following 24 h chemotherapy-treatment, cells were harvested by trypsin, washed twice in room tempered PBS, resuspended in ice cold ethanol (70 %) and kept at -20°C for minimum 15 min. Cells were then washed twice in cold PBS and centrifuged (1500 rpm, 5 min, 4°C), and resuspended in freshly prepared PI staining solution (0.25 % Triton- X-100, 50 µg/ml propidium iodide (PI) and 200 µg/ml RNase A) for minimum 30 min. Cell cycle distribution was analyzed using a fluorescence-activated cell sorter (FACS). Single cells were gated to exclude doublets and clustered cells (Supplementary material 2) and data were analyzed using Microsoft Excel 2010. $2.0x10^4$ cells were counted per sample, and percentage cell distribution was derived from obtained histograms in FACSDiva.

3.11.8 Cell Cycle Analysis (PEITC +/- Cisplatin) (Paper III)

KATO-III were seeded as $2.5x10^5$ cells in 6-well plates and incubated over two nights before treated with 0, 5 or 10 μM PEITC for 12 and 24 h or PEITC (0, 5, 10 μM) together with cisplatin (25 or 50 μM) for 24 h. Cells were harvested, resuspended in PBS and fixated in chilled ethanol (−20°C, 70%) for minimum 15 min. Cells were then pelleted and resuspended in freshly prepared propidium iodide (PI) staining solution (0.25% Triton- X-100, 50 μg/ml PI and 200 μg/ml RNase A) for 30 min. Cell cycle distribution was analyzed using a FACS Canto flow cytometer counting $2.0x10^4$ cells per sample in triplicates. Cell cycle distribution was acquired from the obtained histograms using FACS Diva software.

3.12 Drug treatments in mouse models of gastric cancer

3.12.1 Drug treatments (Paper I)

BoNT-A was dissolved in saline (0.9% NaCl) containing methylene blue (1.0 %) to visualize the injection. The achieved concentration of BoNT-A was 0.25 U of BoNT-A/mL. The abdominal cavity was accessed through a midline incision (laparotomy) under isoflurane inhalation anesthesia (1.75-2.0%) and the BoNT-A solution was injected unilaterally into the serosa along the lesser and greater curvature in the anterior side of the corpus (i.e. tumor area) of the stomach (Fig. 8). Depending on size of the stomach, a volume between 0.3 – 0.8 mL was injected into the stomach. Thus, for a mouse receiving 0.4 mL BoNT-A (0.25 U/mL) the dose corresponded to 0.10 U. The injection needle size was 30 G.

Fig. 8. BoNT-A injection in the INS-GAS mouse stomach. Photo by Chun-Mei Zhao.

RAD001 stock aliquots were prepared in10 mM concentrations (522 μL DMSO to 5 mg RAD001) and stored at – 80 °C in appropriate volumes. For *in vivo* experiments, RAD001 was given at a dose of 1.5 mg/kg by intraperitoneal (i.p.) injections. A daily working solution of 1.0 mg/mL was prepared from stock using saline (0.9 %) and injected with 50 mg/mL glucose solution (room tempered) in a total volume of 0.2 mL. The injection needle size was 27 G.

CPI-613 was dissolved in DMSO and prepared as stock solutions of 15 mg/mL. For *in vitro* experiments, CPI-613 was prepared as 75 mg/mL stock solutions. The aliquots were stored at – 80 °C in appropriate volumes. At the day of injection, a working solution of 5 mg/mL was freshly prepared by adding saline (0.9 % NaCl). CPI-613 was given at a dose

of 20 mg/kg in glucose solution (50 mg/mL) in a total volume of 0.2 mL by intraperitoneal (i.p.) injections. The injection needle size was 27 G.

5-Fluorouracil was given at a dose of 25 mg/kg, diluted with glucose solution (50 mg/mL) or saline (0.9% NaCl) in a volume of 0.5 mL. **Oxaliplatin** was given at the dose of 5 mg/kg, diluted with glucose (50 mg/mL) or saline (0.9% NaCl) in a volume of 0.5 mL. Both drugs were injected separately but simultaneously. The injection needle size was 27 G.

3.12.2 Drug treatment (Paper II)

Ivermectin was reconstituted from lyophilized powder in DMSO to 50mM solution and then diluted in saline (0.5 ml) before intraperitoneal injection at a dose of 10 mg/kg with 27G needle.

3.12.3 Drug treatment (Paper III)

PEITC was administered through an AIN-76A diet (3–5 μmol PEITC/g diet) for 10 weeks in FVB mice either during or following administration of MNU. PEITC was administered through an AIN-76A diet (3–5 μmol PEITC/g diet) for 10 weeks in INS-GAS mice at the age of 9 months.

3.13 Measurement of survival rate, body weight and tumor size (Papers I-III)

Animals were followed up by daily inspection with scoring sheet, weighing and euthanized according to primary human endpoints. Scoring parameters included severe body weight loss (>25%), stress behavior, abdominal pain or reduced physical activity and was followed in collaboration with the responsible veterinarian at the animal facility. Body weight was measured daily (during treatment) or weekly (during follow up). Tumor volume density (% of glandular area of the stomach occupied by tumor) was measured using a point count method described earlier[14]. Animals that received less than one cycle of treatment or died due to human error were censored.

3.14 Data processing and visualization

R/Bioconductor environment was used to process omics-data before differential expression analysis. Microarray data were $\log_2$ transformed and quantile normalized. Gene expression profiles from both microarray and qRT-PCR were analyzed independently by a paired robust *t*-test for mouse samples or a paired *t*-test for human samples. Illumina microarray data was analyzed using Lumi on the log2 scale and was analyzed using the empirical Bayesian method implemented in Limma. Paired *t*-statistics were computed by fitting a linear robust or non-robust regression to the anterior and posterior stomach samples within each mouse or to the cancer and the adjacent non-cancerous tissue samples within each patient. False discovery rate adjusted *p*-values less than 0.05 were defined as differentially expressed. RNA sequencing data processing included process data normalization, graphical exploration of raw and normalized data, test for differential expression for each feature between the conditions, raw *p*-value adjustments and export of lists of features having a significant differential expression between the conditions. The analysis was performed using the R software (R Core Team 2017), Bioconductor [85] packages including DESeq2 [86, 87] and the SARTools package developed at PF2 - Institut Pasteur. Normalization and differential analysis are

carried out according to the DESeq2 model and package. Graphical data visualization and data analyses were carried out using GraphPad Prism software 6.0 (GraphPad Software, U.S), Excel 2016 (Microsoft), IPA (Qiagen, Aarhus, Denmark) and RStudio version 3.5.2 (2018-12-20). Diagram plots were created with JavaScript library D3.js v.4. SPSS v.23-25 was used to perform test statistics including *t*-tests and non-parametric tests, one-way ANOVA, and correlation/linear regression analyses. Heatmaps were encoded in RStudio using heatmap.2. A connectivity Map (cMap) was used to link genes, drugs, and disease states to human gastric cancer gene expression signature.

3.15 Ingenuity Pathway Analysis (IPA)

In papers I and II, transcriptomics and metabolomics datasets were analyzed using IPA (QIAGEN, Hilden, Germany) which has sophisticated algorithms and criteria to calculate predicted functional activation/inhibition of canonical pathways, diseases and functions, transcription regulators and regulators based on their downstream molecule expressions (QIAGEN Inc., https://www.qiagenbioinformatics.com/products/ingenuitypathway-analysis). Analyses included pathway enrichment and mapping of diseases and functions. Regulatory z-scores for canonical pathways that overlapped with our experimental data were calculated using the formula described previously [99]. To generate the network of up- or down-regulated genes, custom-made molecular networks were developed based on information contained in the IPAs knowledge base. Networks of these genes were then algorithmically generated based on their interrelationships. Filtering of datasets included species, *p*-value cut-off and/or *q*-value cut-offs. Molecular networks and canonical pathways were algorithmically constructed based on known connectivity and relationships among metabolites and genes/proteins using Ingenuity knowledge base. The significance of the association between the dataset molecules and the canonical pathways was measured by Fischer's exact test that was used to calculate a *p*-value determining the probability that the association between the genes in the dataset and the canonical pathway by chance alone. Z-scores were calculated in IPA based on the dataset's correlation with the activated state. Negative z-scores indicate a decrease in activity, positive z-scores indicate an increase in activity. Canonical pathways were identified using statistical cut-offs at $p<0.05$ and/or $q<0.05$.

3.16 Ethics

The studies including human patients were approved by the Regional Committees for Medical and Health Research Ethics Central Norway (REK 2012-1029 and REK 2012-1031). The studies were conducted in accordance with the guidelines for GCP (Good Clinical Practice) and it was also approved the Norwegian Medicines Agency (2012-002493-31). All animal experiments were performed according to the 3Rs principle (Reduce, Reuse and Refine) and approved by The Norwegian Food Safety Authority (Mattilsynet; FOTS numbers 3985, 4594, 5242 and 6860).

3.17 Statistics

Statistical comparisons of experimental conditions were performed to test the H_0 hypothesis that there was no difference between the experimental and control groups. The H_0 hypothesis was rejected if *p*-value was <0.05, meaning that there is significant

difference between the groups. Comparisons between experimental groups, between anterior and posterior sides of the stomachs and between different location sites of patients were performed using independent *t*-test, paired *t*-test, ANOVA followed by Dunnett's or Tukey's post hoc test. Survival curves were obtained using Kaplan-Meier curves with log-rank test. Values are expressed as means with SEM or SD and statistical methods are shown in the specific figure legends.

4. Results

Most results are presented in the original papers (Papers I-III) and additional results that were important in the context of this thesis are presented below (Figs 9-16).

4.1 Human gastric cancer (Papers I and II)

Current understanding of the molecular signaling in tumor development of GC includes dysregulation in signaling pathways of WNT, Notch, HIPPO, Sonic hedgehog as well as epithelial-mesenchymal transition (EMT), cell cycle, matrix metalloproteinases and growth factor signaling of EGF, VEGF, TGF-β and HER2. In order to test our hypothesis of a nerve-cancer metabolism axis in paper I, we performed transcriptomics analysis of tumor specimens collected from human patients who have been followed up for 5+ years after surgery. Microarray analysis was performed on groups of samples from the cardia, antrum and corpus (major and minor curvature). Global transcription profiles were made for contrasts between cancer (all sites) *vs.* normal adjacent tissue (all sites) and intestinal metaplasia (all sites) *vs.* normal adjacent tissue (all sites)(Paper I; Figs. 8J,K).

We next focused on the neoplasia profiling. Human GC samples comprised of intestinal, diffuse and mixed type adenocarcinoma. Pathway enrichment analysis across all types of adenocarcinomas showed a total of 634 signaling pathways that were activated or inhibited (Paper I; Fig. 1A). Many of the pathways that were highly activated (positive z-score) are involved in cell proliferation (PI3K/Akt, ERK/MAPK and mTOR), inflammation and cytokine production (TREM1 signaling and chemokine signaling), nucleotide repair (NER pathway and DNA damage response), cell signaling (cyclins and cell cycle regulation), or development (WNT). Additionally, considering both inhibited and activated pathways, we found that metabolic pathways had a central role in GC (Paper I; Figs. 1A and 2A). Differently expressed genes in cancer *vs.* normal adjacent tissue affected major biofunctions involved in cancer, organismal injury and abnormalities and gastrointestinal disease (Fig. 9).

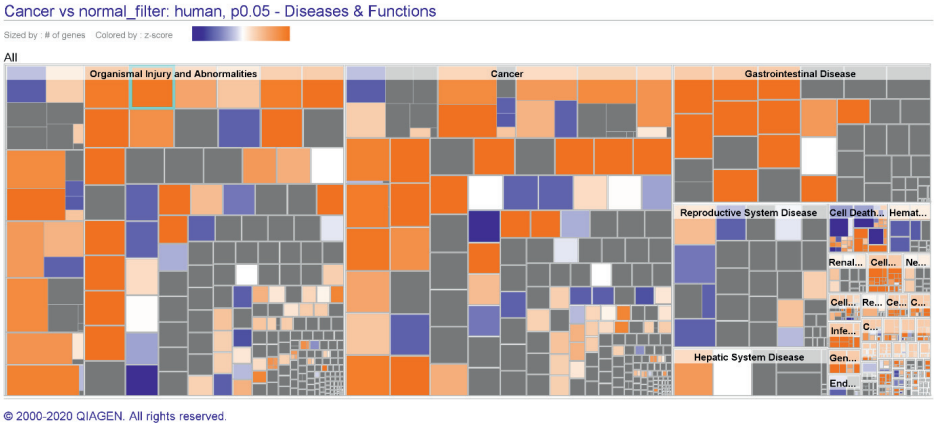

Fig. 9. Functional tissue morphology obtained in Ingenuity Pathway Analysis (IPA) in patients diagnosed with gastric cancer *vs.* normal adjacent tissue. Size of square reflect number of genes; color reflect direction. Orange: activation, blue: inhibition; grey: status not obtained; white: no difference in overall activity.

Next, we identified major regulators in the dataset with predicted activation. MYC and β-catenin (also known as CTNNB1) were predicted activated with z-scores of +2.757 (p<0.05) and +2.440 (p<0.05), respectively, based on downstream gene expression. Previous studies have shown that GC was mediated in part by acetylcholinergic-induced WNT signaling [22, 100]. Since both MYC and β-catenin are involved with the WNT signaling, we took a closer look at the pathway and found that an activated WNT-signaling pathway displayed accumulated levels of β-catenin, given that GSK3β levels were decreased (Fig. 10).

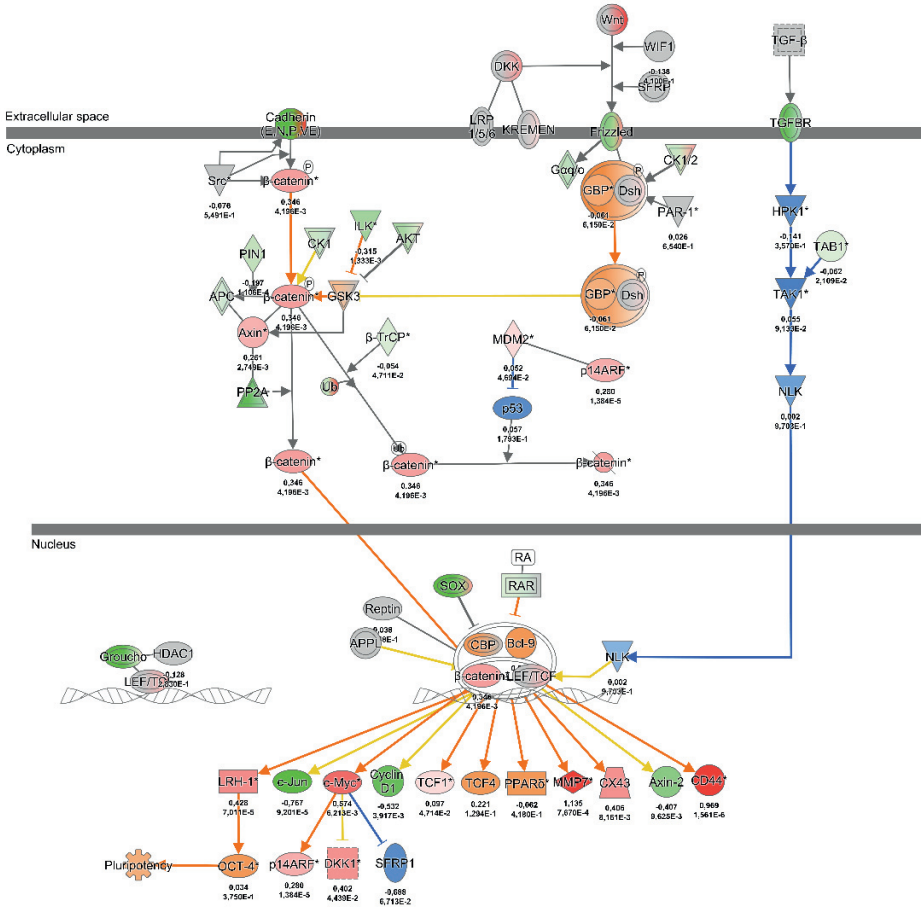

Fig. 10. Wnt/β-catenin signaling was activated in human gastric cancer via the frizzled receptor (shown in orange). Target genes were also affected. Orange: predicted activated; Blue: predicted inhibition; Green: downregulated; Red: upregulated; Grey: did not pass p-value cut-off (0.05). Annotated with $\log_2$-fold change, p-value, and z-scores. Created in IPA.

To identify potential drug candidates among differentially expressed genes in human GC, we created a connectivity Map (cMap) (Paper II; Fig 2A-B). The cMap was built upon a large-scale compendium of functional perturbations in cancer cell lines coupled to the human GC gene expression signature based on the L1000 assay [101]. A diverse range of drugs were repurposed based on the cMap scoring, including mTOR inhibitors, acetylcholine inhibitors/agonists and GABA receptor agonist. We next created a t-SNE plot using single-cell data released by the study of premalignant lesions and GC [102]. The panel of 34 metabolic genes found to be differentially expressed in GC were expressed across several cell types in the TME (Paper I; Fig. 3).

4.2 The transgenic INS-GAS mouse as a model of gastric cancer (Papers I-III)

Translational research requires animal models for pre-clinical testing. The transgenic INS-GAS mice develop intestinal type GC at 10 months of age with progression from initiation to advanced cancer (usually seen from 12-18 months). Transcriptomics analysis of gastric tumor samples *vs*. WT mice revealed activation in crucial biofunctions related to development, immune system and cell signaling (Fig. 11).

Fig. 11. Functional tissue morphology of the transgenic mouse model of gastric cancer *vs*. WT mice (FVB) revealed activation (orange) in biofunctions of cellular movement, organismal development, organismal injury, cancer, immune cell trafficking, inflammatory response and others. Square size by significance, color by activation status. Orange: predicted activated; blue: predicted inhibition; grey: did not pass p-value cut-off (0.05). Created in IPA.

When we compared transcriptomics profiles of the human GC *vs.* normal tissue in the same stomach and the mouse GC *vs.* normal tissue of wild-type (WT) FVB mice, we found a strong correlation among canonical pathway activation (Paper I; Figs. 1A,B,D). Up-regulated signaling pathways in both human and mouse GC included WNT/β-catenin, mTOR, PI3K/Akt, neuroinflammation, ERK/MAPK, HIPPO and the CCK/gastrin-mediated pathway (which is specific for the stomach), and the down-regulated signaling pathways included AMPK signaling which is associated with OXPHOS, glycolysis, and fatty acid β-oxidation (Paper I; Figs. 1A,B).

4.3 Metabolic reprogramming in gastric cancer

4.3.1 Metabolic reprogramming in gastric cancer is evident at both transcriptomic and metabolic levels (Paper I)

We next constructed a "GC metabolic gene expression profile" consisting of 140 genes involved in OXPHOS, fatty acid β-oxidation, carbohydrate metabolism, and energy metabolism including the TCA cycle and glutaminolysis (Paper I; Fig. 2). The GC metabolic gene expression profile was characterized by dysregulations of glutaminolysis and associated transporters of amino acids, the TCA cycle, carbohydrate metabolism and fatty acid β-oxidation, and displayed a positive correlation between human and mouse gastric cancer. These results suggested that the mouse model of GC used in this thesis

would be useful for studying the molecular mechanisms of human GC metabolic reprogramming.

Metabolomics has been extensively used to mechanically understand disease development and progression. After confirming the correlation of metabolic profiles in human and mouse GC (Paper I; Fig. 2D), we sought to determine whether the changes in metabolic reprogramming transcriptomic profile were reflected in metabolite levels in GC. GC and WT mice at 12 months of age were screened. To validate the transcriptomics analysis and further characterize the metabolic reprogramming, we quantified a total of 343 metabolites using LC/MS and GC/MS. 152 metabolites were altered between mouse GC and WT (p<0.05), whereof 53 metabolites were up-regulated and 99 metabolites were downregulated (Fig.12). The metabolites were grouped into amino acids, carbohydrates, cofactors and vitamins, energy metabolism including the TCA cycle, lipid metabolism, nucleotide metabolism, peptides and xenobiotics (Fig. 12)

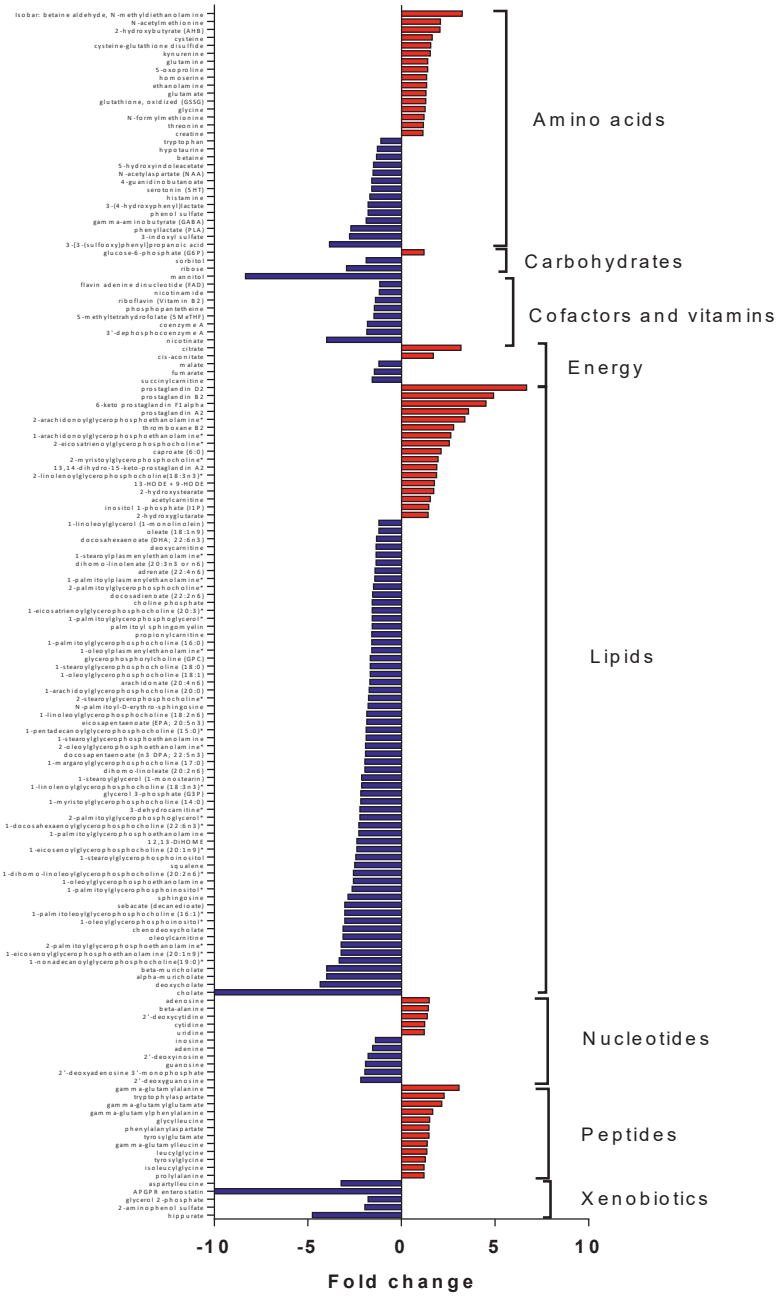

Fig. 12. Differentially altered metabolites in mouse GC *vs.* WT (p<0.05).

Some metabolites such as prostaglandin E2, methionine, and glycine, are known to be abundant in GC [90-93]. In comparison with WT mice, GC mice displayed an increased carbon flux through the TCA cycle, which was reflected by higher levels of glycine, oxidized glutathione (GSSG), citrate, 5-oxoproline, cis-aconitate, L-glutamate, L-glutamine and threonine, but not glycolysis (represented by glucose, fructose-6-phosphate and lactate) (Paper I; Fig. 4). Given the elevated levels of glutamine and glutamate, we suggested that the increased carbon flux through the TCA cycle was mediated through glutaminolytic anaplerosis rather than through pyruvate. The levels of coenzyme A (CoA), which is needed to convert pyruvate to Acetyl-CoA, were low in the tumor samples thus supporting this notion (Fig. 13) [103]. In fact, most coenzymes were deprived in GC, including nicotinate, nicotinamide, riboflavin, flavin adenine dinucleotide (FAD), phosphopantetheine, 3'-dephosphocoenzyme A (Fig. 13). Moreover, the results of both transcriptomics and metabolomics data indicated a metabolic reprogramming in GC.

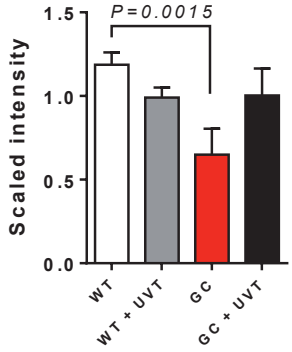

Fig. 13. Relative levels of Coenzyme A in WT and GC mice with and without vagotomy. A substantial decrease in coenzyme A was found in GC, which might have implications for energy metabolism and metabolic reprogramming. Error bars: SEM; *p*-value: One-way ANOVA between groups.

4.3.2 Energy metabolism and the glutamine, glutamate and glutathione pool (Paper III)

Next, to investigate the relationship between energy metabolism and proliferation, we determined total glutathione levels, glutamine and glutamate levels in AGS and MKN45 cells after treatment with aromatic phenetyl isothiocyanate (PEITC) or alkalic allyl isothiocyanate (AITC) (Paper III, Figs. 3A,B). ITCs are glutathione-depleting agents, thus introducing oxidative stress responses upon entry of a cell [104, 105]. PEITC was previously shown by our group to induce gastric cancer cell growth by disintegration of microtubules [93]. Indeed, a decrease in intracellular glutathione was observed in the human GC cell lines, while an increase in glutamine levels were seen after 5 or 10 μM of PEITC as well as G2/M-phase arrest (Paper III; Figs.4A and 7A). Thus, energy metabolism is sensitive to perturbations and shifts and these perturbations affect the growth and proliferative potential of the cancer cells.

4.3.3 Vagotomy and prolonged anti nerve-cancer therapy reverses the metabolic reprogramming of gastric cancer (Paper I)

Vagal innervation is known to regulate epithelial cell proliferation in the stomach and has recently been implicated in GC development and progression [22, 34, 39, 100]. UVT takes advantage of the fact that each (anterior or posterior) vagal trunk innervates only one-half of the stomach, and consequently, UVT does not impair the overall function of the stomach. In a previous study, we showed that vagotomy during the preneoplastic stage of tumorigenesis diminished tumor incidence and size, and attenuated tumor cell proliferation specifically in the denervated portion of the stomach, suggesting that the vagus nerve promotes gastric cancer growth [22]. Consistent with this idea, pharmacologic denervation via local injection of BoNT-A into the gastric wall similarly impaired preneoplastic growth. In this thesis, we further examined the effect of UVT and BoNT-A on the metabolic reprogramming of GC. In a comparison between the innervated and denervated stomach of GC mice, signaling pathways had reversed activation pattern after vagotomy (Paper I; Fig. 1C) and metabolic genes were reversed after vagotomy and displayed negative correlations between the two sides of stomach after UVT (Paper I; Fig. 2E). Furthermore, metabolomics comparison between mouse GC and WT with and without UVT found that 48 of the 152 metabolites identified altered in GC were reversed after UVT (Paper I, Fig. 4A). The metabolic signature of GC reflects the changes in both cancer cells and the TME rather than specific mutations of oncogenes (i.e."oncometabolites"). It should be noted that the effects of vagotomy on the metabolites were different between WT and GC mice (Paper 1, Fig 4), suggesting a different response of denervation on normal tissue compared to tumor tissue. These results correspond well to changes in the metabolic gene expression profile, suggesting that vagotomy reversed the metabolic reprogramming of GC at both transcript and metabolite levels. Vagotomy had distinct effects in GC *vs*. WT. After vagotomy, the energy metabolism reflected by glutaminolysis but not glycolysis intermediates were reduced in GC mice (Paper I, Fig. 4). Comparison of GC after vagotomy *vs.* WT without vagotomy revealed no difference in the energy metabolism, suggesting that vagotomy in GC mice led to a normalization of the energy metabolism (Paper I, Fig. 4). However, WT mice responded to vagotomy differently compared to GC mice, namely having reduced glutaminolysis as well as glycolysis. Additional differential changes induced by vagotomy in control and tumor tissue included altered levels of the potent tripeptide antioxidant glutathione and other metabolites related to gastrointestinal physiology. In control tissue, vagotomy was associated with decreases in both reduced (GSH) and oxidized (GSSG) glutathione, whereas reduced levels of GSSG but increased GSH levels were observed in post-vagotomy tumor tissue. These changes may be suggestive of a less oxidative environment following vagotomy in GC attributable to increased GSH availability.

Alterations in energy metabolite levels including glutamate, glutathione and glycine after vagotomy also affected the activation pattern of excitation of neurons, stimulation of neurons, response and firing of neurons were active in gastric cancer but inhibited after vagotomy (Fig. 14)

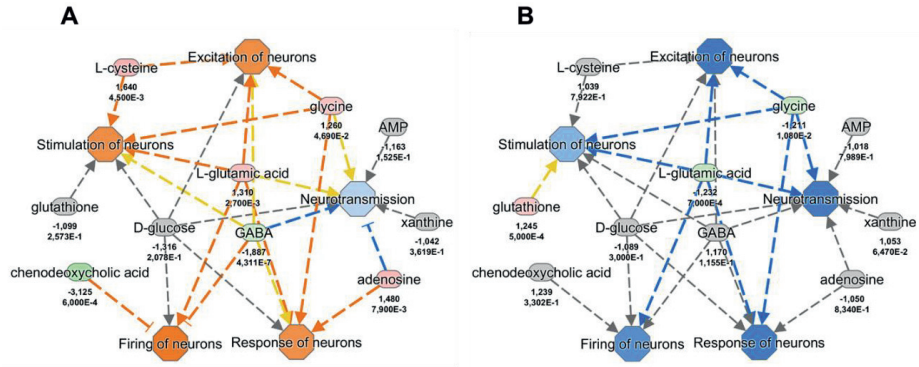

Fig. 14. Alterations in metabolite levels led to changes in neuronal functions after vagotomy. Activated functions (**A**) in GC vs. healthy mice; inhibited functions in GC after vagotomy *vs.* GC (**B**). Green: decreased level; red: increased level; Orange: predicted activated; blue: predicted inhibited; grey: did not pass p-value cut-off (0.05).

4.3.4 Metabolic reprogramming and signaling pathway activation (Paper I)

The pathway statistics by IPA was made based on the number of molecules in the designated pathway that overlapped with the dataset molecules. This created a ratio to determine the overlap significance that a certain pathway was present in the dataset. The direction of the expressed molecules was taken into consideration when calculating the z-score of activation/inhibition. IPA classified a pathway as confident activated with a z-score >2.

Analysis of mouse GC using IPA revealed activation of GP6 signaling pathway, leukocyte extravasation signaling, osteoarthritis pathway, STAT3 pathway, integrin signaling, ILK signaling, colorectal cancer metastasis signaling, Th2 pathway, neuroinflammation signaling pathway, cardiac β-adrenergic signaling, apelin liver signaling pathway, signaling by Rho family GTPases, dendritic cell maturation, production of nitric oxide and reactive oxygen species in macrophages, synaptogenesis signaling pathway, leukotriene biosynthesis, eNOS signaling, IL-8 signaling, actin cytoskeleton signaling, acute phase response signaling, role of NFAT in cardiac hypertrophy, adrenomedullin signaling pathway, ERK/MAPK signaling and synaptic long term depression signaling ($p<0.05$, z-score>2). Recent studies have been linking glutaminolysis to increased proliferative potential of cancer cells due to its modulation of STAT3 and glutathione signaling [106].

Furthermore, pathways such as paxillin signaling, the complement system, LPS/IL-1 mediated inhibition of RXR function, basal cell carcinoma signaling, relaxin signaling, macropinocytosis signaling, Fcγ receptor-mediated phagocytosis in macrophages and monocytes, iCOS-iCOSL signaling in T helper cells, endothelin-1 signaling, role of NFAT in regulation of the immune response, calcium-induced T lymphocyte apoptosis, phospholipases, glioblastoma multiforme signaling, corticotropin releasing hormone signaling, coagulation system, calcium signaling, VEGF signaling, regulation of actin-

based motility by Rho and cardiac hypertrophy signaling were also activated ($p<0.05$, z-score>1).

Strongly activated but with less significant p-values were TREM1 signaling, IL-6 signaling, sonic hedgehog signaling, agrin interactions at neuromuscular junction, p38 MAPK signaling, p70S6K signaling, GPCR-mediated nutrient sensing in enteroendocrine cells, Tec kinase signaling, Cdc42 signaling, interferon signaling, toll-like receptor signaling, HIPPO signaling and glutamate receptor signaling (z-score>2)

Other pathways that were activated although less prominent included inhibition of angiogenesis by TSP1, nitric oxide signaling in the cardiovascular system, phospholipase C signaling, γ-glutamyl cycle, RhoA signaling, glioma invasiveness signaling, choline biosynthesis III, telomerase signaling, tRNA splicing, eicosanoid signaling, dermatan sulfate biosynthesis, prostanoid biosynthesis, ephrin receptor signaling, CDK5 signaling, mouse embryonic stem cell pluripotency, PI3K/AKT signaling, cholecystokinin/gastrin-mediated signaling, chondroitin sulfate biosynthesis, and FAT10 cancer signaling pathway ($p<0.05$, $0<$z-score<1) and Wnt/β-catenin signaling, HMGB1 signaling, death receptor signaling, NF-κB activation by viruses, α-adrenergic signaling, G Beta Gamma Signaling, IL-7 Signaling Pathway, Chemokine Signaling, mTOR Signaling, Androgen signaling (z-score >1, variant p-values).

We next performed integrative multi-omics of transcriptomics and metabolomics to find the common essential signaling pathways. Forty-two signaling pathways appeared in both transcriptomics and metabolomics datasets of mouse GC (Paper I, Fig. 5A). Not surprisingly, the identified pathways were heavily involved in metabolism, but also nerve-related pathways such as neuroinflammation and serotonin-signaling appeared to be crucial.

4.4 Identification of drug-targets in the nerve-cancer metabolism axis (Papers I and II)

The rational design for therapies that directly target components of signaling or metabolic pathways calls for a systems approach. We performed drug-target interaction prediction and computational drug repositioning of approved and investigational drugs/compounds (e.g., existing at www.clinicaltrial.gov) in GC mice and GC patients using IPA. We identified the network nodes (i.e., drug targets) at the levels of proteins, mRNAs, microRNA, lncRNAs and metabolites with special focus on the following four targets with potential drugs: SNAP25 with BoNT-A, mTOR with RAD001, PDP1/α-KGDH with CPI-613 and GLS with DON, 968, CB839 or BPTES in both GC mice and patients. In our previous study, we have demonstrated that either local vagotomy or local injection of BoNT-A suppresses gastric cancer [47]. This was most likely because BoNT-A binds selectively to synaptosomal nerve-associated protein 25 (SNAP25), which is an integral protein required for docking and release of acetylcholine from vesicles situated in the vagal nerve endings [107, 108]. RAD001 is a rapamycin analog that specifically inhibits the mTORC1 complex by binding to FKBP12 [109]. The enzymes pyruvate dehydrogenase (PDH/PDP1) and α-ketoglutarate dehydrogenase (α-KGDH) controls acetyl-CoA/pyruvate and glutamine/glutamate anaplerotic steps to the TCA cycle, respectively. The lipoate analog CPI-613 (6,8-Bis[(phenylmethyl)thio-octanoic acid) inhibits both enzymes [110-114]. Glutaminase inhibitors, such as CB-839, BPTES, DON

and 968, have been tested in a variety of cancers [115] but have limited efficacy and considerable adverse effects (Paper I, Fig. 6).

In paper II, the cMap showed associated differentially expressed genes with drug candidates like ivermectin. The interaction network of ivermectin was linked to the WNT/β-catenin pathway and proliferation (Paper II; Fig. 3), which we explored further in paper II.

4.5 Experimental validations

4.5.1 *In vitro* and pre-clinical testing of metabolomics-based targeted therapies (Papers I and II)

Next, we performed *in vitro* and *in vivo* experiments to validate the efficacies of the potential metabolic targeted therapies. In order to develop a therapeutic strategy, we first performed a panel of combination treatments *in vitro* and found that treatment of human GC cells with either RAD001 or CPI-613 reduced cell proliferation in dose-dependent manners (Paper I; Figs. 7A-D). Combination of RAD001 and CPI-613 at IC_{50} doses for either 24 h or 48 h resulted in synergistic inhibition which led us to test a combination of the inhibitors *in vivo* (Paper I; Figs. 7E-G). When we tested ivermectin *in vitro*, we found that ivermectin inhibited cell proliferation in time-and concentration-dependent manners (Paper II; Figs. 5A,B). Cell cycle arrest was also observed, but the underlying mechanism needed to be further explored.

4.5.2 Synergistic anti-proliferative effects of ITCs and cisplatin (Paper III)

To investigate the potential effects of glutathione-depleting ITCs, AGS and MKN45 cells were treated with PEITC, AITC and BITC to find the IC_{50} (Paper III; Figs. 2B-E). Upon drug screening, cells were pre-treated with PEITC, BITC or AITC for 1, 3 or 24 h followed by cisplatin or 5-FU treatment for 48 h (Paper III; Fig. 5). Increased inhibition of proliferation was found upon pre-treatment compared to cisplatin treatment alone (Paper III; Fig 5).

4.6 Therapeutic effects of prolonged anti-nerve-cancer therapy targeting the WNT/β-catenin pathway *in vivo* (Paper I)

GC mice that received BoNT-A with a combination of RAD001 and CPI-613 injections weekly had longer survival than both control mice and mice receiving BRC+FUOX. OS and MS were 33% and 148 days, respectively, in GC mice without any treatment (age-matched controls, AMC), 40% and 40 days in GC mice that received either FUOX or BRC + FUOX, but 90% and 249 days in GC mice that received BRC in comparisons with AMC (Paper I; Fig. 7)

Within the treatment period of 2 months, neither 5-FU and oxaliplatin given either alone or as FUOX nor RAD001 and CPI-613 given either alone or in combination reduced the tumor size, whereas BoNT-A alone reduced the tumor size and had synergic effects when given together with FUOX or as BRC+FUOX. There was no difference between FUOX and BRC+FUOX. These results suggested that BoNT-A had no cytotoxic effect and that BRC (BoNT-A+RAD001+CPI-613 without 5-FU and/or oxaliplatin) increased OS and

MS without reducing the tumor size in GC mice (Paper I, Figs. 6I-K). Thus, BRC could be a potential cytotoxic chemo-free therapy for GC.

We next measured the body weight during or after treatment and compared the endpoint -assessed body weight of each mouse towards the survival days. Body weight distribution were different between BRC and BRC+FUOX (Paper I; Fig. 7J). Importantly, percentage body weight loss among mice receiving BRC were less than BRC+FUOX.

Effects of prolonged treatment of combination therapies were assessed by taking a closer look at the global profiles. Mouse GC without treatment displayed activation in all categories associated with tumor morphology, cellular movement, cancer and cell-to-cell signaling. However, after prolonged BRC treatment, these activations were either less prominent or reversed and decreased (Fig. 15).

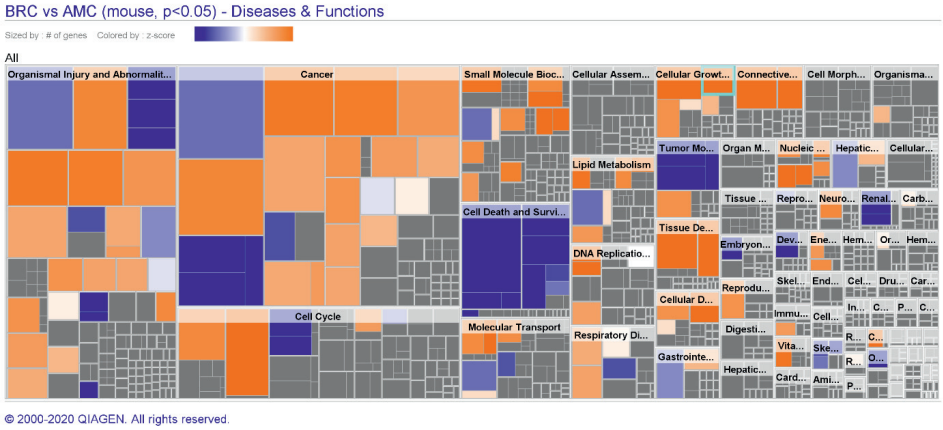

Fig. 15. Functional tissue morphology after BRC treatment for 2 months. Blue: decreased activity; orange: increased activity. Grey; NA.

To further investigate the underlying potential mechanisms of survival and tumor size reductions in mice, we compared the transcriptomic profiles of mouse GC before and after RC, BRC, FUOX, and BRC+FUOX. 156 canonical pathways were identified post RC treatment in mouse GC (Paper I, Fig. S5) and there was a negative correlation in pathway activity before and after treatment, while no significant correlation was found between the 175 matching pathways in mouse GC with and without FUOX (Paper I, Fig. S5).

In order to re-verify the mechanism of action upon treatment, we performed transcriptomics with focusing on the gene expression profile of glutaminolysis-WNT-mTOR-c-MYC and synaptogenesis signaling pathways as presented in Paper I; Fig. 8A. We found that BRC reversed the gene expression profile as same as vagotomy, supporting that BRC was a nerve-cancer metabolism therapy for GC. Prolonged treatment with the combination for 2 months resulted in a down-regulation of glutaminolysis-WNT-mTOR-c-MYC signaling pathway as vagotomy, suggesting a possible mechanism of “nerve-

cancer metabolism therapy" (Fig. 16). As WNT-signaling induces activation of mTORC1 signaling [116], these results further confirmed that vagotomy induced the metabolic switch from glycolysis to glutaminolysis via WNT-mTOR signaling, which is known to be associated with reduced thickness of mucosa in WT mice and suppressed tumorigenesis in GC mice.

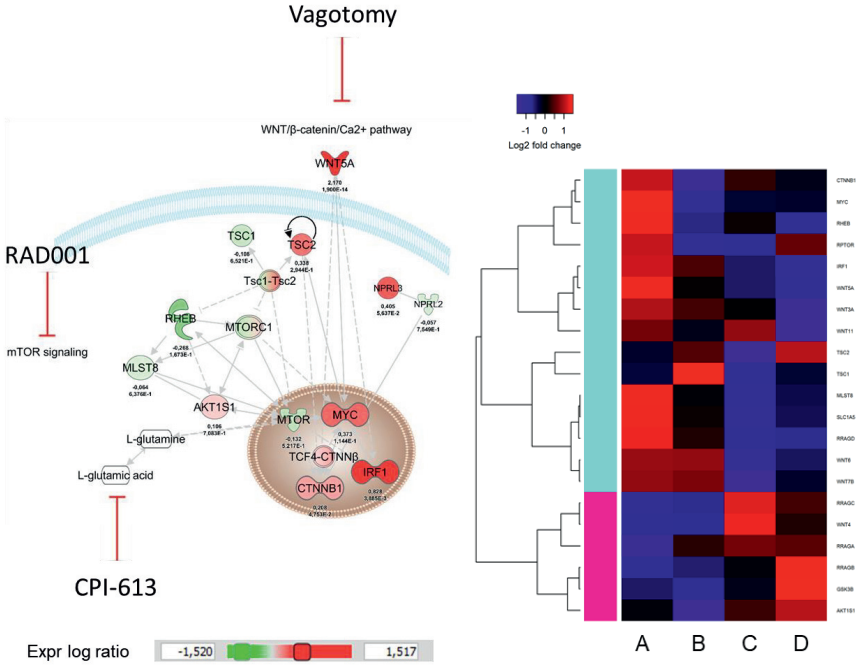

Fig. 16. Key genes in WNT-mTOR-cMYC pathways in GC (A), GC after vagotomy (B), GC after RC (C) and GC after BRC (D). *GC: gastric cancer; RC: RAD001 + CPI-613; BRC: BonT-A + RAD001 + CPI-613*

In silico experimentation on nodes in the WNT/β-catenin signaling-mTOR network showed that inhibition of nodes in the WNT cluster inhibited the mTOR cluster but not *vice versa* (Paper I; Figs. 8E,F).

Recent literature has highlighted the implications of the interplay between the unique metabolism of tumors and the metabolism of suppressive immune cells [117, 118]. Ivermectin also inhibited proliferation of the gastric tumor mass (Paper II; Fig. 6).

In this thesis we have followed up 16 patients who underwent subtotal or total gastrectomy with radical lymph node dissection, adjuvant chemoradiotherapy or perioperative chemotherapy for five years. We found that patients with high scores of gastric histology activation index (GHAI) had shorter MS than those with low scores (Paper I; Fig. 8G) and there was positive correlation between upregulated gene expression and GHAI score (Paper I; Fig. 8H) and negative correlation between upregulated gene expression profile and OS (Paper 1; Fig. 8I). Furthermore, we found distinct expression

profiles in signaling pathways in general and the metabolic gene expression profiles in particular between metaplasia and neoplasia, suggesting that the two pathological phenotypes harbor distinct metabolic profiles and that the network of the metabolic genes within the neoplasia could be the potential target. These results supported the rationale of BRC clinical trial.

4.7 Pilot phase II clinical trial with local BoNT-A injection (Paper I)

Injections of BoNT-A directly into the tumor were associated with a small amount of bleeding from the injection sites, but the bleeding was self-limited and none of the patients required surgical or endoscopic intervention or blood transfusions. All patients were without any adverse effects or complications and discharged from hospital the first day after the procedure. Thus, the procedure with BoNT-A injections was well tolerated, without any immediate surgical complications or adverse effects in patients with advanced GC. Due to aggressive progression at advanced late-stage disease, four out of six patients did not survive until eight weeks after the BoNT-A injection. Two out of six patients were followed for eight weeks and one patient was followed for 20 weeks after receiving BoNT-A treatment. We found that the tumor size was reduced during the first eight weeks and the tumor growth was stabilized afterwards in one of three patients. These results suggested that endoscopic injection of BoNT-A is safe and BRC can be further tested in GC patients that failed 2nd line chemotherapy (Paper I; Fig. 8L).

5. Discussion

The overarching objective of the work presented in this thesis was to develop new treatment options through drug repositioning approach with the new concept of "nerve-cancer metabolism axis" for GC. In paper I, we investigated the nerve signaling implications in metabolism of cancer cells as well as the TME. In paper II, we validated ivermectin in treating advanced GC, while in paper III, we utilized glutathione-depleting dietary isothiocyanates to perturb the energy metabolism and thus inhibit the proliferation potential in GC.

5.1 The nerve-cancer metabolism axis

In paper I, we found that the mouse GC model was well representative of human GC, particularly regarding the metabolic reprogramming. Common to both human and mouse GC was the innervation of nerves in the stomach tumors. After extensive metabolic and transcriptomic evaluation, the lack of dysregulated Warburg effect was prominent in GC. By comparisons between WT *vs.* GC mice, which also included a comparison of the innervated side *vs* denervated sides of the same stomach of WT or GC mice, we found that inhibition of glutaminolysis and restoration of OXPHOS/glycolysis after vagotomy were the likely mechanisms underlying vagotomy-induced suppression of GC tumorigenesis. Thus, the lack of glycolytic metabolite elevations, along with a notable increase of glutaminolytic metabolites and inactivated AMPK signaling in the mouse GC

model, led us to suggest that GC is glutamine dependent rather than glucose dependent (Fig. 17).

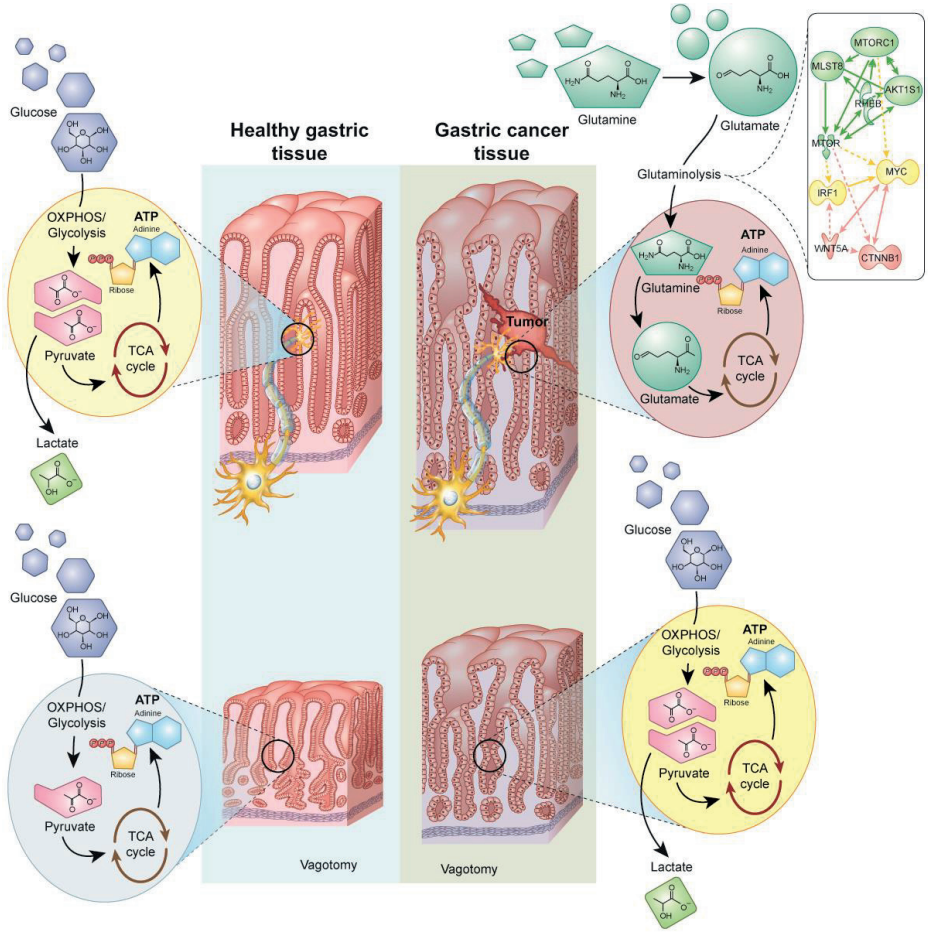

Fig. 17. Vagotomy induces metabolic reprogramming in healthy gastric tissue (marked in light blue rectangle) and gastric cancer tissue (light grey rectangle). Glucose is normally metabolized through oxidative phosphorylation (OXPHOS)/glycolysis and tricarboxylic acid (TCA) cycle to produce ATP and lactate in healthy cells. Glutaminolysis (via WNT-mTOR-cMYC pathway) and TCA cycle take place in cancer cells. Vagotomy reduces lactate generation in healthy cells and induces a normalization of ATP production in cancer cells.

5.2 Applications of systems biology and computational drug repositioning (Papers I and II)

Traditionally, cancer research focusses on the "one gene-one treatment" approach. In this thesis we aimed to investigate the new concept of a "nerve-cancer metabolism axis" by employing a systems biology approach. Systems biology has been defined in numerous ways since its introduction two decades ago. Systems biology is a multidisciplinary field that aim to explore and explain complex cellular and physiological phenomena in organisms in a mechanistic way at cellular and molecular level [119, 120]. One of the first definitions was given in 1949 by Max Delbrück, who claimed that "*any living cell carries with it the experiences of a billion of years of experimentation by its ancestors*"[121]. Systems biology has in recent years changed how we understand huge amounts of biological data, and in 2003, systems biology was defined as "*the computational integration of data generated by the suite of genetic, transcriptomic, proteomic and metabonomic platforms to understand function through different levels of biomolecular organization*" [122]. Cornerstones of systems biology require prior knowledge available from a wide variety of sources, including databases such as Reactome, KEGG and TCGA.

Current treatments of GC involve diagnosis, such as genetic risk assessments, pathological assessment and biomarker screening, and treatments, such as chemotherapy and surgery. Along with aforementioned aspects, systemic therapies are chosen in the context of performance status, medical co-morbidities and toxicity profile. Given the heterogeneity of GC and the multifactorial disease picture, such traditional approaches might fall short in providing effective treatment and may fail to work efficiently for the individual patient. These challenges call for a systems approach, using sophisticated algorithms in understanding of the genetic, metabolomic and phenomics characteristics of GC. Therefore, the work in this thesis has performed multi-omics analysis, computational drug repurposing and *in silico* experiments to answer our research questions. We used the Ingenuity Knowledge Base to identify a metabolic profile for advanced GC in both patients and mice, that has led to provide therapeutic effect of proposed drug regimens of BoNT-A, RAD001 and CPI-613 treatments or ivermectin in GC mice.

In papers I and II, we used network representation to perform *in silico experiments* to predict the effects on one pathway or disease function on another or the effect of a drug on a network. Network biology can be understood as a representation of objects or entities in a system, referred to as "nodes" and "edges" [127]. In biology, a node can range from a molecule, protein, gene or ligand to a cell or a person. The edges represent true interaction or contacts between the defined nodes, or, as in the case of metabolomics, the biochemical process from one molecule to the next [127]. So why do we need network representation in biology? The clearest answer relies on the opportunity to retrieve a global picture of drug-disease-host interaction or the complex picture of a disease, which is not possible by the study of single genes or proteins alone [127]. In this thesis we have actively used the systems biology approach to identify aberrant regulated genes and metabolites to gain insight into disease mechanisms and for development of metabolomics-based targeted therapies.

Through the last two decades, next generation sequencing has revolutionized the way we have learned and understood cancer as a disease. Multi-omics is a new approach to the same research questions. Omics data typically provides a list of differentially expressed entities associated with a disease. These data are useful as markers of the disease process and might give insight to which biological pathways or processes are different between the disease and control groups. However, analysis of only one data type has some limitations. Traditionally, genomics, transcriptomics, proteomics and metabolomics have been applied separately. More recently, multi-omics approaches have been applied to a wide range of biological problems and diseases using network representation [120]. Integration of different omics data types is often used to elucidate potential causative changes that lead to disease, or the treatment targets, that can then be tested in further molecular studies [120, 123]. The most known drawback of integration of omics data is the risk of lack of correlation between the different omics. In this thesis, we presented a new methodology to show interactions of metabolites and gene expression and their link to canonical signaling pathways (Paper I; Fig. 5). The Eye diagrams were made in Seurat and used the Ingenuity Knowledge Base to map common pathways. In paper II, we also used the cMAP to show associations between a large-scale compendium of functional perturbations in cancer cell lines coupled to the human GC gene expression signature based on the L1000 assay [101]. Furthermore, in papers I and II we used a new approach of *in silico* experimentation where nodes in a network were manipulated to predict the effect on other nodes, total network scores or pathway status. Advantages of the *in silico* approach to predicting drug effects are the study of hypothetical compounds. Not only did it provide predictions on drug effects, but also directionality that one would need mechanistic studies to investigate otherwise. *In silico* experimentation has low cost and are much faster than typical wet lab experimentation. Additionally, *in silico* experiments using the Ingenuity Knowledge Base were based on both human and mouse data [124].

In the research conducted in this thesis, the transgenic insulin-gastrin (INS-GAS) mouse model was used to investigate molecular gene expression and metabolic signature of GC. The process of tumor development in INS-GAS mice mimic the tumorigenesis in humans, making the INS-GAS mice a good model of human GC. Notably, both gene expression and signaling pathway activity correlated well between human patients' biopsies and the INS-GAS mice (Paper I).

5.3 Key findings (Papers I-III)

In this thesis, we investigated the effects of denervation and characterized the metabolic signature of mouse GC. We chose to use multi-omics and computational drug repositioning to describe and investigate potential new therapies for GC. The work in this thesis, using mouse models of GC and GC biopsies from patients, has shown a nerve-cancer metabolism axis in the TME. This axis was investigated by three different approaches, namely *i)* surgical denervation, *ii)* pharmacological denervation and *iii)* systemic therapy. In papers I and II, we utilized all three approaches either alone or in combinations, while in paper III, which was built upon the knowledge of energy metabolism as a target in GC, we used only systemic therapy.

In paper I, pharmacological denervation therapy (BoBT-A) together with targeted therapies (RAD001 and CPI-613) reduced tumor size and increased overall survival in

mice with GC. In paper II, ivermectin, which is usually used to treat river-blindness disease or other infectious conditions, was tested in mice with gastric cancer and found that it reduced tumor size and inhibited WNT signaling. In paper III, energy metabolism was investigated by glutathione-depleting PEITC and was found to be effective in prevention (but not treatment at the given dose) of gastric cancer.

5.3.1 Metabolic reprogramming

There are still knowledge gaps in human health and disease regarding cancer metabolism and the nerve-cancer axis [125]. In this thesis, we have addressed these knowledge gaps using denervation strategies followed by multi-omics to characterize the gastric cancer profile and effects of denervation. We questioned the current dogmas of metabolic reprogramming that takes place in the TME to gain mechanistic insight by applying both metabolomics and transcriptomics. How cancer cells reprogram their microenvironment to assist tumor growth is an area of intense investigation. The current knowledge of reprogramming encompasses multiple strategies, including metabolic switch, secreted growth factors and alterations to the extracellular matrix and cell-to-cell interactions and signaling. It should be stressed that "tumor metabolism" is not synonymous with the metabolism of cell proliferation. Tumors require proliferation to grow, but many factors within the TME can influence cellular energetics and metabolism. Proliferating cells are constantly encountering metabolic stresses, as they exceed the available oxygen and nutrient supply to support growth and survival. In paper I, we investigated the metabolic reprogramming profiles of both metaplastic and neoplastic lesions from patients. Overexpressed canonical pathways in metaplastic lesions were mainly metabolic pathways, including superpathway of melatonin degradation, serotonin degradation, citrulline metabolism, nicotine degradation I and II, fatty acid β-oxidation, cholesterol biosynthesis and energy-related pathways such as TCA cycle and acyl-CoA hydrolysis. Overall, the activation of metabolic pathways in pre-neoplastic lesions could indicate that metabolic reprogramming not only active in cancer but is actually a driver in tumor progression. Indeed, neoplastic lesions had more aberrantly regulated metabolic genes than metaplastic lesions.

In paper I, we applied metabolomics to identify relevant metabolites involved in molecular mechanisms in gastric cancer. The detected metabolites grouped into carbohydrates, amino acids, lipids, nucleotides, xenobiotics, co-factors and vitamins. In paper I, we focused mostly on metabolites related to amino acids, glycolysis and energy metabolism.

5.3.2 Anaerobic glycolysis/Warburg effect/lactate

Many cancers display increased glucose influx and concurrent upregulated glycolytic enzymes facilitating the multistep utilization of glucose for energy. Usually, this cue is instructed by upstream growth factor signaling. When rapidly proliferating cells in a nutrient-rich environment continue to take up and metabolize glucose in excess of their anabolic requirements (known as aerobic glycolysis or "the Warburg effect"), excess glycolytic intermediates are diverted into other pathways. These pathways support the production of non-essential amino acids, nucleotides or lipids required for cell growth. Alternatively, excess intermediates are dealt with by converting pyruvate into lactate and secreting lactate back into the extracellular environment. It has been a dogma that

oncogenic c-MYC coordinately increases the expression of PDK1, LDHA and MCT1 which facilitate the efflux of lactate from the cytosol back into the extracellular space. Additionally, the stabilization of HIF1α by hypoxia or in various oncogenic contexts also triggers coordinated transcriptional upregulation of LDHA and PDK1. Both c-MYC and HIF1α activate overlapping sets of glycolytic genes including lactate dehydrogenase [126]. If so, we would hypothesize that PDK1-mediated inhibition of the TCA cycle would result in increased glycolysis and ATP levels by shunting pyruvate towards lactate production. However, both metabolic and transcriptomics analyses revealed that intermediates and enzymes of the glycolytic pathway including lactate were *not* elevated in the gastric cancer. However, we found inhibition in specific steps of the TCA cycle with increased activity in other steps particularly towards glutamine anaplerosis. Gene expression of LDHA and PDK1 were not significantly altered in gastric cancer mice whereas the glutamine transporter SLC1A5 was upregulated, further supporting that gastric cancer was not glucose-driven but rather glutamine-driven [69]. Several metabolites of carbohydrate and energy metabolism have been previously associated with gastric cancer, including lactate, glucose, citrate, alpha-ketoglutarate and fumarate although the results were not consistent across studies [127].

5.3.3 Metabolic reprogramming in the immune niche of TME: the role of glutamine

It is known that mTORC1 enhances glutaminolysis by activating MYC-GLS and GLUD1, establishing a loop accounting for high consumption of glutamine in the TME. Not only did we identify increased levels of glutamine and glutamate in the gastric cancer samples; we also found changes in inflammatory pathways and biofunctions and aberrantly regulated glutaminolytic genes not only restricted to cancer cells but also in other cells in the gastric TME. More recently, studies have revealed that the metabolic pathways of oxidative metabolism, glycolysis, and glutaminolysis preferentially fuel the cell fate decisions and effector functions of immune cells [128], which was supportive of the observations in paper I.

5.3.4 Cutting the nerve-cancer crosstalk by vagotomy or BoNT-A

Vagotomy was employed as a surgical treatment for peptic ulcer due to its inhibitory effects on gastric acid secretion in 70s-80s [59]. The vagus nerve is in a key position to bidirectionally link several peripheral metabolic organs with the brain, including the stomach. Therefore, the vagus nerve is increasingly targeted for neuromodulation therapy. Epidemiological, animal and clinical studies have shown that vagotomy reduces the risk of gastric cancer and suppresses gastric tumorigenesis [22, 58, 100, 129]. In previous studies, we showed that vagotomy suppressed gastric tumorigenesis which was probably through muscarinic cholinergic/acetylcholine receptor 3 (M3R)-mediated WNT signaling, proposing a possible nerve-cancer crosstalk [22, 34, 59] (Fig. 18).

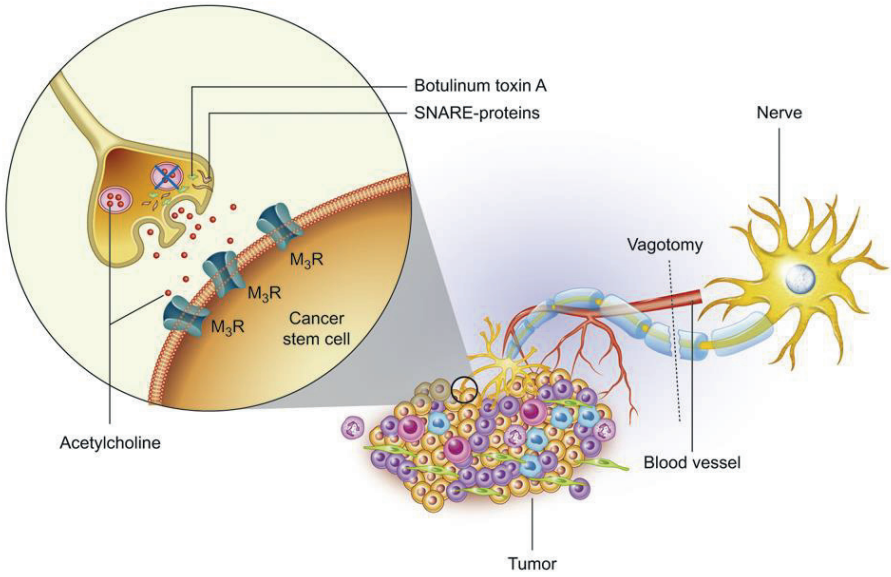

Fig. 18. The crosstalk between nerves and cancer seem to promote the growth and spread of cancer. Zhao *et al.* 2014, Rabben *et. al.* 2016.

5.3.5 Signaling pathways underlying the metabolic reprogramming

Current available methods to evaluate molecular pathology of gastric cancer involve assessment of oncogenes, overexpression of growth factors/receptors, inactivation/point mutations of tumor suppressor genes, DNA repair genes, microsatellite instability, copy number variations, microRNA expression, DNA methylation, proteomics, cell adhesion molecules, loss of heterogeneity, silencing of tumor suppressors by CpG island methylation, and Epstein-Bar virus status [130-132]. Molecular pathology aids clinical evaluation for early diagnosis, tumor classification and therapeutic intervention. The applications of molecular testing such as the testing of CDH1 gene for hereditary diffuse gastric carcinoma (HDGC) and of ERBB2 (also known as HER2) expression in gastric cancers have had significant impact on treatment guidelines and are becoming standard patient care [130]. In paper I, we have shown the shared metabolic signature in gene profiles between human cancer biopsies and the transgenic INS-GAS model of gastric cancer. In our previous study, we showed that vagotomy during the preneoplastic stage of tumorigenesis diminished tumor incidence and size and attenuated tumor cell proliferation specifically in the denervated portion of the stomach, and that this effect was mediated in part by inhibition of WNT signaling [21]. For instance, vagotomy reduced the expression of WNT-regulated stem cell markers and decreased the expansion of leucine-rich repeat containing G protein–coupled receptor 5 –positive (LGR5+) stem cells in the gastric mucosa via activation of the muscarinic acetylcholine receptor 3 (M3R) in LGR5+ stem cells. M3R signaling stimulated ligand independent WNT activation and enhanced the growth of gastric organoids *in vitro*, whereas deletion of M3R or treatment with an M3R inhibitor in combination with chemotherapy suppressed WNT signaling and

reduced gastric tumor formation in mice. Importantly, in patients with gastric cancer, WNT signaling was associated with neural pathways and neuronal density was correlated with tumors. These findings allowed us to suggest nerves as important regulators of gastric stem cell expansion and tumor progression signaling [21]. As expected, in paper I we found that the gene expression of WNT5A and β-catenin, mTOR, c-MYC was up-regulated in GC and inhibited by vagotomy. WNT/Ca^{2+} signaling has been suggested to play a role in metabolic reprogramming [133]. MIR17HG has been reported to be involved in interferon regulatory factor 1 (IRF-1)-mediated WNT- β-catenin signaling [131]. Signaling pathways that have known roles in tumorigenesis of the stomach include developmental pathways such as WNT, Notch, Hedgehog, AKT/PI3K and mTOR. WNT signaling has been implicated in cancer metabolism, especially through the associated mTOR and c-MYC pathways [71, 134-137]. Amino acid metabolism is coupled with mTOR signaling and linked through c-MYC to glutamine metabolism and the mTOR pathway[70, 138, 139]. mTORC1 is a major regulator of proliferation and senses cytosolic concentrations of amino acids that serve as an indicator of the nutritional status in the cell [140]. mTORC1 also promotes α-KG production by activating Glu dehydrogenase (GDH)[141]. As α-KG is a key intermediate of the TCA cycle, mTORC1 may stimulate ATP production through activation of GDH. WNT5A, a ligand that binds to multiple frizzled receptors, is a regulator of metabolic reprogramming in dendritic cells in the context of tumor immune surveillance [142]. Activation of β-catenin signaling results in the up-regulation of genes involved in glutamine metabolism [137]. In this thesis, further exploration of the connection of the WNT signaling and metabolic reprogramming in GC led to new drug treatment strategies to inhibit these pathways at the same time.

The traditional way to screen anti-cancer drugs is to use cell lines as representative models for cancer [143]. The first immortalized cell lines were created around 1968. The American Type Culture Collection currently holds over 4,000 cell lines from over 150 different species. Benefits of immortalized cell lines are that drug testing is relatively cheap, fast and feasible and particularly relevant are cultured cells which represent a disease state model and those which demonstrate abnormalities (e.g. genetically or biochemically) including alterations in receptors, enzymes, ion channels, and receptor signaling pathways [143]. In paper I, we chose to evaluate BRC therapy in two different cell lines of human gastric adenocarcinoma, representing both diffuse and intestinal type GC.

Drug repurposing involves identifying new uses for approved or investigational drugs and provides substantial shorter timelines compared to novel drugs [5] and can be performed *in silico* prior to drug screening. It is becoming generally accepted that precision oncology must be guided by predictive treatment responses, achieved by extensive characterization of transcriptomic, proteomic, and/or metabolic profile. While drug combination effects have been studied for well over a century, repurposing of low-risk existing drugs are a newer approach to improve treatment response. Current approaches to drug repositioning include computational approaches (data-driven) and experimental approaches [4]. The approaches are applied individually or in combination to systematically analyze big data to obtain meaningful interpretations for drug repositioning hypotheses. Challenges to these approaches include evolving gap between the availability (i.e., the generation of big data) *vs.* ability to interpret, analyze and integrate the data for useful strategies. Another

layer of complexity is added due to the fact that much of the data obtained are unstructured or non-standardized. Publicly available databases for transcriptomics data are becoming well known, (e.g., TCGA, Reactome and KEGG), but are rarer for other omics-data or clinical trial data, and there is especially need for greater access to data from industry-sponsored clinical trials phase II–IV. Barriers to drug repositioning beyond data interpretation, drug safety or effect measures include patent considerations, regulatory considerations and organizational hurdles [4]. Based on multi-omic data analysis performed on our pre-clinical and patients' samples, we identified SNAP25, mTOR and PDP1/α-KGDH as drug targets for the nerve-cancer metabolism axis in paper I. BoNT-A is selectively targeting SNAP25, while RAD001 is approved as an mTORC1 inhibitor by the FDA. The lipoate analog CPI-613 are being investigated against a range of cancers in over hundred phase I studies, twentysix phase II studies and three phase III studies, including refractory or relapsed acute myeloid leukemia, T-cell non-Hodgkin lymphoma, high-grade B-cell lymphoma, myeloid sarcoma, PDAC, Burkitt lymphoma and a range of other lymphomas, small cell lung cancer (https://reports.ingenuity.com/rs/nodeview/nodeview.jsp?did=ING:5c865&analysisid=-1&exportId=&sourceName=RS&speciesType=&shownvf=1#p). Additionally, glutaminase inhibitors, such as CB-839, BPTES, DON and 968, have been tested in a variety of cancers [107] but usually has limited efficacy or side effects.

The BLISS synergy model is widely used to analyze drug combination data when screening for candidate drug combinations. The method compares the observed combination response with the predicted combination response. The assumption is that there is no effect from any drug-drug interaction, and typically the combination effect is declared synergistic if observed response is greater than predicted response. In addition to CPI-613 and RAD001 used in paper I, these glutaminase inhibitors could be worthwhile to test in the future.

Research has an increased focus on the development of new minimally invasive treatments in general. Since majority of elderly GC patients has either poor ECOG status or inoperable gastric tumors, utilizing BoNT-A to achieve pharmacological denervation introduces a less invasive, more rapid procedure to obtain blockade in nerve-cancer crosstalk. The purpose of the initial clinical trial in paper I was to obtain data needed to calculate sample size in a larger controlled trial in the future.

5.3.6 Metabolic reprogramming reversed by vagotomy in gastric cancer

In general, metabolic reprogramming in cancer includes *i)* deregulated uptake of glucose and amino acids; *ii)* use of opportunistic modes of nutrient acquisition, *iii)* use of glycolysis/tricarboxylic acid (TCA) cycle intermediates for biosynthesis and nicotinamide adenine dinucleotide phosphate (NADPH) production; *iv)* increased demand for nitrogen; *v)* alterations in metabolite-driven gene regulation, and *vi)* metabolic interactions with the microenvironment. Metabolic reprogramming was a general phenomenon that took place in both human and mouse gastric cancer, but not in human metaplasia (pre-cancerous lesions). Metabolic reprogramming that took place in neoplasia affected the whole tumor microenvironment, rather than the specific cell types. In paper I, we found that the metabolic reprogramming could be reversible upon denervation, thus serving as a potential therapeutic target. We also showed that prolonged anti-nerve-cancer therapy reduced the tumor size, prolonged survival and increased

quality of life in GC mice. Our data has challenged the dogma that cancers are glucose-dependent, proving that glycolysis/Warburg was not crucial for tumor growth nor was it a target for treatment of GC. Patients with densely innervated tumors had more aggressive profile and/or poor clinical outcome. If nerves were only microenvironmental bystanders, innervated organs would not differ in local areas with tumor occurrence.

The TME presents physical, immunologic, and metabolic barriers to durable immunotherapy responses. Recent findings in immunometabolism have shown that the effects of cancer cells and cancer cell metabolism on the TME may directly modulate essential T cell metabolic pathways and activities. The immunotherapy in GC is limited by the lack of gastric-specific tumor microenvironment [144]. The results in paper I showed that GC was glutamine-dependent, suggesting a potential targeted treatment strategy. A recent study suggested a "metabolic checkpoint" for tumor immunotherapy, which effector T cells responded to glutamine antagonism by markedly upregulating oxidative metabolism and adopting a long-lived, highly activated phenotype [118]. Thus, we might suggest that the therapeutic strategy proposed in paper I can enhance the robustness of GC immunotherapeutic approaches, although future studies should characterize the intrinsic immune escape mechanisms, adopted specifically by GC. Taken together, combination of nerve-cancer metabolism-based therapy and immunotherapy may drive the future of GC as this indication begins to move away from chemotherapy and towards targeted and personalized therapy, leading to the best possible outcome in GC treatment, particularly for elderly.

In addition to GC, nerve-cancer crosstalk and metabolic reprogramming take place in other types of cancer, e.g., prostate cancer, colorectal cancer, pancreatic cancer and breast cancer [48, 145-149]. More studies are needed to investigate the underlying mechanisms, along with the metabolic reprogramming and restoration and immunometabolism within the TME.

5.3.7 Gastric cancer subtypes, pathogenesis and the implications of heterogeneity

Gastric carcinogenesis is a multistep process connected with several pathological stages. Gastric adenocarcinomas may be subjected to several classification systems, including Lauren classification for histological subgroups (e.g. diffuse *vs.* intestinal or mixed type), WHO grading, Japanese classification and TNM staging [130, 150]. However, due to the high level of molecular heterogeneity in GC, there has been an emerging interest and need for further classifying GC based on patterns of molecular alterations and their correlation with disease progression and prognosis. The incidence distribution of different types of GC and their associated risk factors such as conventional GC (80%), early-onset GC (10%), gastric stump cancers (7%) and hereditary diffuse GC (3%), should also be considered. In paper I, we investigated the molecular profiles and metabolic reprogramming in patients with both metaplasia and neoplasia and found a correlation between gene expression of metabolic genes and clinical parameters such as GHAI and survival in patients diagnosed with cancer (neoplasia). Notably, metabolic genes were less significantly dysregulated in the pathological state of metaplasia, suggesting that metabolic reprogramming took place at later stages in the multistep progression of GC. Thus, determining the underlying mechanisms for each molecular subtype of GC is important to further understand the gastric tumorigenesis. Studies have shown that healthy samples taken from the same organ or tissue, so-called "normal adjacent tissue"

were morphologically normal but displayed a molecularly altered pre-neoplastic state and these changes were evident up to 1 cm from the margins of the tumor [151, 152]. Therefore, when we harvested samples from our GC patients, we applied minimum 5 cm between the different sites (i.e., tumor, metaplasia and control) for comparison.

5.4 Translational potential

The work in this thesis has explored computational drug repositioning to organize our current knowledge, to predict potential responses using novel combinations of drugs (paper I), and repositioning drugs with already approved use in other diseases (papers I-II) for GC. Chemoprevention was explored in paper III. A systems approach to cancer treatment can contribute to *i)* increased putative treatment options, *ii)* personalized treatment options based on, but not restricted to, metabolic profile and biomarkers, i.e., "correct drug for the correct patients at the right time" and *iii)* less overtreatment which is a huge economic burden but also leads to increased death rate among cancer patients. In addition to its high incidence and mortality, GC accounts for the 3rd highest cancer-related disability-adjusted life-years (DALYs) after lung and liver cancers [153]. The remarkable aging of the population will be likely associated with the increased incidence of the elderly diagnosed with GC. Thus, well-tolerative and best-suited therapy should be developed for the elderly patients. The results of paper I indicated that endoscopic submucosal/intratumoral injection of BoNT-A combined with non-cytotoxic chemotherapy could be an ideal therapy for elderly. In paper I, we choose the non-cytotoxic drugs, namely RAD001 (also known as everolimus) and CPI-613 (devimistat), as they have been well tested in clinical trials for other types of cancer [154-158].

5.5 Limitations

The so-called "metabolic escape" has been suggested as a mechanism by cancer cells to avoid cell death in response to inhibited glutaminolysis. Thus, it has been proposed that tumors that suffer from glucose/glutamine starvation could activate fatty acid catabolism for survival. In Paper I, the results might suggest that the metabolic escape took place after vagotomy, leading to an activation of Acetyl-CoA with increased levels of lysolipids and polyunsaturated fatty acids. Furthermore, acyl carnitine oleoylcarnitine, a long-chain acyl carnitine that accumulates during certain metabolic conditions, such as fasting and nutrient deficiency was increased after vagotomy along with its transporter SLC25A20, probably supporting the notion that acyl carnitines serve to deliver fatty acids to the mitochondria for β-oxidation to produce Acetyl-CoA. Monoacylglycerol 1-stearoylglycerol (1-monostearin) was increased after vagotomy in GC but not in WT, probably further suggesting that vagotomy-induced suppression of tumorigenesis was mediated in part through accelerated degradation of diacyl - or triacylglyserols, as well deoxycarnitine, succinylcarnitine and 3-dehydrocarnitine. These assumptions need to be further investigated.

Another limitation to preclinical trials includes optimization of doses and duration of treatments. Also, different windows for chemoprevention and therapeutic effects during the tumorigenesis from initiation, promotion and progression exist and need to be better mapped in each individual study. More and specific biomarkers for cell proliferation and apoptosis, particularly in papers II-III could be included in the future.

6. Conclusions

The results of the thesis showed the characterization of metabolic signature of GC and the potential of targeting metabolism with drug repositioning strategy. Metabolic reprogramming took place in GC cells and the TME. SNAP25, mTOR, PDP1/α-KGDH, and glutaminolysis were potential drug targets in GC. Combination treatment of denervation therapy, metabolic- and checkpoint-therapy using BoNT-A, RAD001, and CPI-613 reduced tumor size and increased overall survival. Ivermectin reduced the tumor size in GC mice which was associated with inactivation of WNT/β-catenin signaling and dysregulation of cell proliferation/apoptosis pathways. PEITC showed chemopreventive effect and synergistic anti-cancer effect. Taken together, a new therapeutic approach targeting nerve-cancer-metabolic axis in GC was proposed in this thesis (Fig. 19).

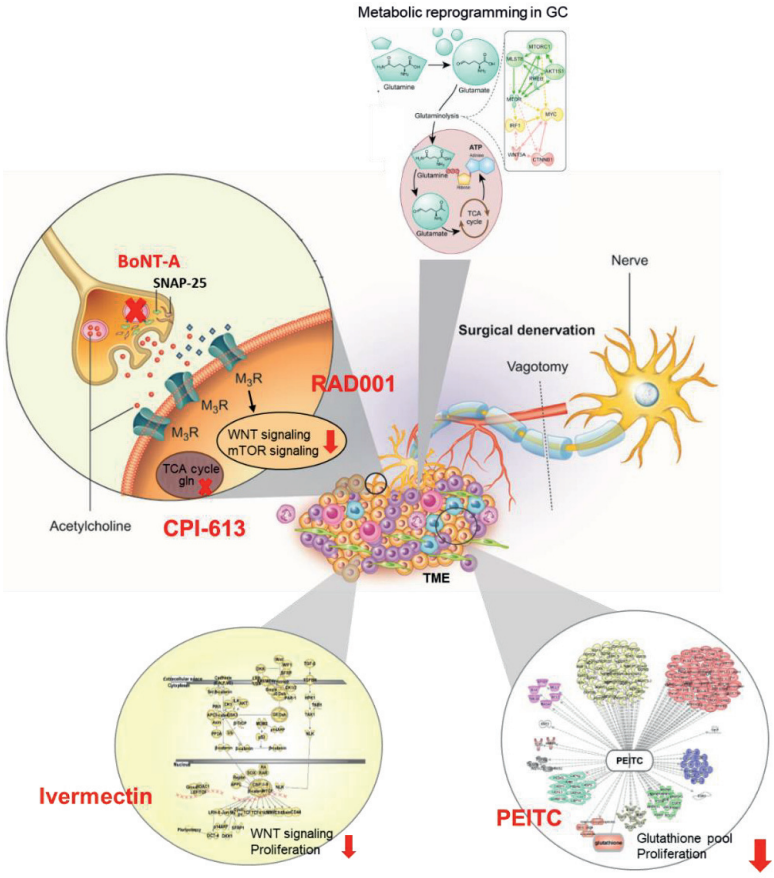

Fig. 19. Metabolic reprogramming of GC and metabolism-based treatments with drug repositioning towards the WNT/β-catenin-mTOR signaling pathways (Papers I and II), proliferation (Papers I-III) and metabolic signature (Papers I and III).

7. Future Perspectives

Translational research presented in this thesis can be accelerated using the approach of systems biology and drug repositioning. All drugs applied in this thesis have been used in humans for other indications (but not gastric cancer yet) and/or clinical trials for other types of cancer than GC. Thus, it would be feasible to design clinical trials (phase II) based on the results of papers I-III.

In considering future perspectives in the field of oncology, personalized or precision medicine targeting metabolic reprogramming is promising based on the metabolic profiling of cancer cells as well as TME (Fig. 20).

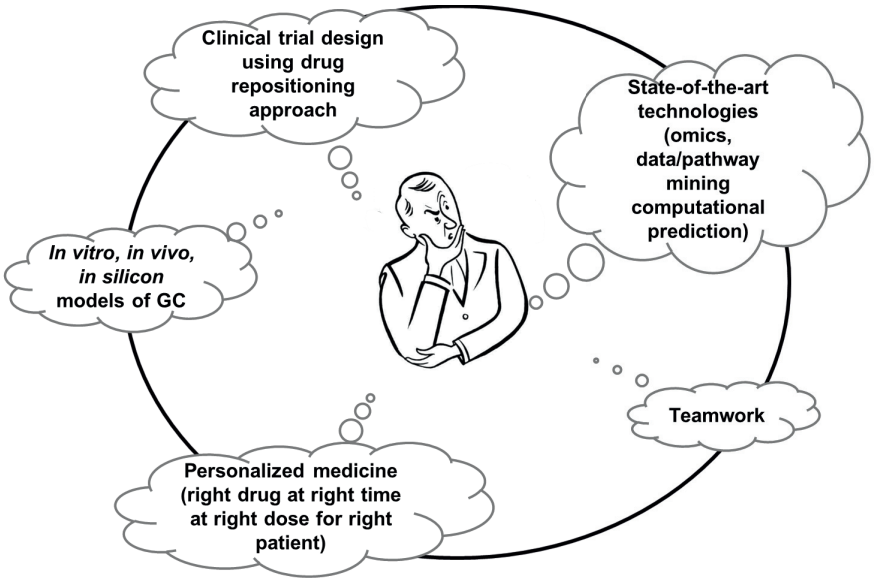

Fig. 20. Thinking about translational research on metabolism-based treatments for GC in the future. Modified from Duan Chen and Chun-Mei Zhao [3].

References

1. Drolet, B.C. and N.M. Lorenzi, *Translational research: understanding the continuum from bench to bedside.* Transl Res, 2011. **157**(1): p. 1-5.
2. Zoellner, J.M. and K.J. Porter, *Chapter 6 - Translational Research: Concepts and Methods in Dissemination and Implementation Research*, in *Nutrition in the Prevention and Treatment of Disease (Fourth Edition)*, A.M. Coulston, et al., Editors. 2017, Academic Press. p. 125-143.
3. Filaretova LP, T.K.e., *Cell/Tissue Injury and Cytoprotection/Organoprotection in the Gastrointestinal Tract: Mechanisms, Prevention and Treatment.* . Front Gastrointest Res. Vol. Basel, Karger, 2012, vol 30, pp 24–31. .
4. Kelloff, G.J. and C.C. Sigman, *New science-based endpoints to accelerate oncology drug development.* Eur J Cancer, 2005. **41**(4): p. 491-501.
5. Pushpakom, S., et al., *Drug repurposing: progress, challenges and recommendations.* Nature Reviews Drug Discovery, 2019. **18**(1): p. 41-58.
6. Hanahan, D. and R.A. Weinberg, *Hallmarks of cancer: the next generation.* Cell, 2011. **144**(5): p. 646-74.
7. Rawla, P. and A. Barsouk, *Epidemiology of gastric cancer: global trends, risk factors and prevention.* Prz Gastroenterol, 2019. **14**(1): p. 26-38.
8. Parkin, D.M., et al., *Global Cancer Statistics, 2002.* CA: A Cancer Journal for Clinicians, 2005. **55**(2): p. 74-108.
9. Lee, C.W., et al., *Combination of sulindac and antimicrobial eradication of Helicobacter pylori prevents progression of gastric cancer in hypergastrinemic INS-GAS mice*, in *Cancer Res*. 2009: United States. p. 8166-74.
10. Chen, D., et al., *Does Helicobacter pylori infection per se cause gastric cancer or duodenal ulcer? Inadequate evidence in Mongolian gerbils and inbred mice.* FEMS Immunol. Med. Microbiol., 2007. **50**(2): p. 184-9.
11. Parsonnet, J., et al., *Helicobacter pylori Infection and the Risk of Gastric Carcinoma.* New England Journal of Medicine, 1991. **325**(16): p. 1127-1131.
12. Rugge, M., et al., *Gastric Cancer as Preventable Disease.* Clin Gastroenterol Hepatol, 2017. **15**(12): p. 1833-1843.
13. Qiu, H. and Z. Zhou, *[Updates and interpretation on NCCN clinical practice guidelines for gastric cancer 2017 version 5].* Zhonghua Wei Chang Wai Ke Za Zhi, 2018. **21**(2): p. 160-164.
14. *National Comprehensive Cancer Network. Gastric Cancer:* . 2019 [cited 2020 12.05.2020]; Version 2.2019.:[Available from: https://www.nccn.org/patients/guidelines/content/PDF/stomach-patient.pdf.
15. Deng, N., et al., *A comprehensive survey of genomic alterations in gastric cancer reveals systematic patterns of molecular exclusivity and co-occurrence among distinct therapeutic targets.* Gut, 2012. **61**(5): p. 673-84.
16. Digklia, A. and A.D. Wagner, *Advanced gastric cancer: Current treatment landscape and future perspectives.* World J Gastroenterol, 2016. **22**(8): p. 2403-14.
17. Doi, T., et al., *Safety, pharmacokinetics, and antitumour activity of trastuzumab deruxtecan (DS-8201), a HER2-targeting antibody-drug conjugate, in patients with advanced breast and gastric or gastro-oesophageal tumours: a phase 1 dose-escalation study.* Lancet Oncol, 2017. **18**(11): p. 1512-1522.
18. Fuchs, C.S., et al., *Safety and Efficacy of Pembrolizumab Monotherapy in Patients With Previously Treated Advanced Gastric and Gastroesophageal Junction Cancer: Phase 2 Clinical KEYNOTE-059 Trial.* JAMA Oncol, 2018. **4**(5): p. e180013.

19. Sasaki, T., et al., *[Combination chemotherapy for gastric cancer including LV/5-FU].* Gan To Kagaku Ryoho, 2004. **31**(12): p. 1952-6.
20. Ghi, M.G., et al., *Induction TPF followed by concomitant treatment versus concomitant treatment alone in locally advanced head and neck cancer. A phase II-III trial.* Ann Oncol, 2017. **28**(9): p. 2206-2212.
21. Luo, H.Y., et al., *Phase 2 study of capecitabine and irinotecan combination chemotherapy (modified XELIRI regimen) in patients with advanced gastric cancer.* Am J Clin Oncol, 2011. **34**(6): p. 555-60.
22. Zhao, C.M., et al., *Denervation suppresses gastric tumorigenesis.* Sci Transl Med, 2014. **6**(250): p. 250ra115.
23. Wang, T.C., et al., *Synergistic interaction between hypergastrinemia and Helicobacter infection in a mouse model of gastric cancer.* Gastroenterology, 2000. **118**(1): p. 36-47.
24. Wang, T.C. and S.J. Brand, *Function and regulation of gastrin in transgenic mice: a review.* Yale J Biol Med, 1992. **65**(6): p. 705-13; discussion 737-40.
25. Wang, T.C., et al., *Pancreatic gastrin stimulates islet differentiation of transforming growth factor alpha-induced ductular precursor cells.* J Clin Invest, 1993. **92**(3): p. 1349-56.
26. Wang, T.C., et al., *Processing and proliferative effects of human progastrin in transgenic mice.* J Clin Invest, 1996. **98**(8): p. 1918-29.
27. Cui, G., et al., *Gastrin-induced apoptosis contributes to carcinogenesis in the stomach.* Lab Invest, 2006. **86**(10): p. 1037-51.
28. Przemeck, S.M., et al., *Hypergastrinemia increases gastric epithelial susceptibility to apoptosis.* Regul Pept, 2008. **146**(1-3): p. 147-56.
29. DeSesso, J.M. and C.F. Jacobson, *Anatomical and physiological parameters affecting gastrointestinal absorption in humans and rats.* Food and Chemical Toxicology, 2001. **39**(3): p. 209-228.
30. Noman, M.Z., et al., *Improving Cancer Immunotherapy by Targeting the Hypoxic Tumor Microenvironment: New Opportunities and Challenges.* Cells, 2019. **8**(9).
31. Pundavela, J., et al., *Nerve fibers infiltrate the tumor microenvironment and are associated with nerve growth factor production and lymph node invasion in breast cancer.* Mol Oncol, 2015. **9**(8): p. 1626-35.
32. Boilly, B., et al., *Nerve Dependence: From Regeneration to Cancer.* Cancer Cell, 2017. **31**(3): p. 342-354.
33. Faulkner, S., et al., *Tumor Neurobiology and the War of Nerves in Cancer.* Cancer Discov, 2019. **9**(6): p. 702-710.
34. Hayakawa, Y., et al., *Nerve Growth Factor Promotes Gastric Tumorigenesis through Aberrant Cholinergic Signaling.* Cancer Cell, 2017. **31**(1): p. 21-34.
35. Jobling, P., et al., *Nerve-Cancer Cell Cross-talk: A Novel Promoter of Tumor Progression.* Cancer Res, 2015. **75**(9): p. 1777-81.
36. Li, X., et al., *Neuroproteins in Cancer: Assumed Bystanders Become Culprits.* Proteomics, 2018: p. e1800049.
37. Monje, M., et al., *Roadmap for the Emerging Field of Cancer Neuroscience.* Cell, 2020. **181**(2): p. 219-222.
38. Wang, K., et al., *Nervous system and gastric cancer.* Biochimica et Biophysica Acta (BBA) - Reviews on Cancer, 2019: p. 188313.
39. Zahalka, A.H. and P.S. Frenette, *Nerves in cancer.* Nat Rev Cancer, 2020. **20**(3): p. 143-157.

40. Skandalakis, L.J., S.W. Gray, and J.E. Skandalakis, *The history and surgical anatomy of the vagus nerve.* Surg. Gynecol. Obstet., 1986. **162**(1): p. 75-85.
41. Drapiewski, J.F., *Carcinoma of the Pancreas: A Study of Neoplastic Invasion of Nerves and its Possible Clinical Significance.* American Journal of Clinical Pathology, 1944. **14**(11): p. 549-556.
42. Liebig, C., et al., *Perineural invasion is an independent predictor of outcome in colorectal cancer.* Journal of clinical oncology : official journal of the American Society of Clinical Oncology, 2009. **27**(31): p. 5131-5137.
43. Magnon, C., et al., *Autonomic nerve development contributes to prostate cancer progression.* Science, 2013. **341**(6142): p. 1236361.
44. Liebl, F., et al., *The impact of neural invasion severity in gastrointestinal malignancies: a clinicopathological study.* Ann Surg, 2014. **260**(5): p. 900-7; discussion 907-8.
45. Gasparini, G., et al., *Nerves and Pancreatic Cancer: New Insights into a Dangerous Relationship.* Cancers (Basel), 2019. **11**(7).
46. Stopczynski, R.E., et al., *Neuroplastic changes occur early in the development of pancreatic ductal adenocarcinoma.* Cancer Res, 2014. **74**(6): p. 1718-27.
47. Seifert, P. and M. Spitznas, *Axons in human choroidal melanoma suggest the participation of nerves in the control of these tumors.* Am J Ophthalmol, 2002. **133**(5): p. 711-3.
48. Chen, D. and G.E. Ayala, *Innervating Prostate Cancer.* N Engl J Med, 2018. **378**(7): p. 675-677.
49. Ayala, G.E., et al., *Cancer-related axonogenesis and neurogenesis in prostate cancer.* Clin Cancer Res, 2008. **14**(23): p. 7593-603.
50. Mancino, M., et al., *The neuronal influence on tumor progression.* Biochim Biophys Acta, 2011. **1816**(2): p. 105-18.
51. Arese, M., et al., *Tumor progression: the neuronal input.* Ann Transl Med, 2018. **6**(5): p. 89.
52. Seifert, P. and M. Spitznas, *Tumours may be innervated.* Virchows Arch, 2001. **438**(3): p. 228-31.
53. Servick, K., *War of nerves.* Science, 2019. **365**(6458): p. 1071-1073.
54. Entschladen, F., et al., *Neoneurogenesis: tumors may initiate their own innervation by the release of neurotrophic factors in analogy to lymphangiogenesis and neoangiogenesis.* Med Hypotheses, 2006. **67**(1): p. 33-5.
55. Entschladen, F., et al., *The cancer's nervous tooth: Considering the neuronal crosstalk within tumors.* Semin Cancer Biol, 2008. **18**(3): p. 171-5.
56. Entschladen, F., et al., *Tumour-cell migration, invasion, and metastasis: navigation by neurotransmitters.* Lancet Oncol, 2004. **5**(4): p. 254-8.
57. Woodward, E.R., *The history of vagotomy.* Am J Surg, 1987. **153**(1): p. 9-17.
58. Lundegardh, G., et al., *Gastric cancer risk after vagotomy.* Gut, 1994. **35**(7): p. 946-9.
59. Rabben, H.L., et al., *Vagotomy and Gastric Tumorigenesis.* Curr Neuropharmacol, 2016. **14**(8): p. 967-972.
60. Nigam, P.K. and A. Nigam, *BOTULINUM TOXIN.* Indian Journal of Dermatology, 2010. **55**(1): p. 8-14.
61. Lang, A., *History and uses of BOTOX (botulinum toxin type A).* Lippincotts Case Manag, 2004. **9**(2): p. 109-12.
62. Peng, L., et al., *Cytotoxicity of botulinum neurotoxins reveals a direct role of syntaxin 1 and SNAP-25 in neuron survival.* Nat Commun, 2013. **4**: p. 1472.

63. Blasi, J., et al., *Botulinum neurotoxin A selectively cleaves the synaptic protein SNAP-25.* Nature, 1993. **365**(6442): p. 160-3.
64. Vazquez, A., et al., *Cancer metabolism at a glance.* J Cell Sci, 2016. **129**(18): p. 3367-73.
65. Yoshida, G.J., *Metabolic reprogramming: the emerging concept and associated therapeutic strategies.* J Exp Clin Cancer Res, 2015. **34**: p. 111.
66. Vander Heiden, M.G. and R.J. DeBerardinis, *Understanding the Intersections between Metabolism and Cancer Biology.* Cell, 2017. **168**(4): p. 657-669.
67. Loponte, S., et al., *The Many Facets of Tumor Heterogeneity: Is Metabolism Lagging Behind?* Cancers (Basel), 2019. **11**(10).
68. Pavlova, N.N. and C.B. Thompson, *The Emerging Hallmarks of Cancer Metabolism.* Cell metabolism, 2016. **23**(1): p. 27-47.
69. Zhu, J. and C.B. Thompson, *Metabolic regulation of cell growth and proliferation.* Nat Rev Mol Cell Biol, 2019. **20**(7): p. 436-450.
70. Csibi, A., et al., *The mTORC1/S6K1 pathway regulates glutamine metabolism through the eIF4B-dependent control of c-Myc translation.* Curr Biol, 2014. **24**(19): p. 2274-80.
71. Villar, V.H., et al., *Glutaminolysis and autophagy in cancer.* Autophagy, 2015. **11**(8): p. 1198-208.
72. Lyssiotis, C.A. and A.C. Kimmelman, *Metabolic Interactions in the Tumor Microenvironment.* Trends Cell Biol, 2017. **27**(11): p. 863-875.
73. Liberti, M.V. and J.W. Locasale, *The Warburg Effect: How Does it Benefit Cancer Cells?* Trends Biochem Sci, 2016. **41**(3): p. 211-218.
74. Cassim, S., et al., *Warburg and Beyond: The Power of Mitochondrial Metabolism to Collaborate or Replace Fermentative Glycolysis in Cancer.* Cancers (Basel), 2020. **12**(5).
75. Liu, Y., et al., *Metabolic reprogramming results in abnormal glycolysis in gastric cancer: a review.* Onco Targets Ther, 2019. **12**: p. 1195-1204.
76. Schulze, A. and A.L. Harris, *How cancer metabolism is tuned for proliferation and vulnerable to disruption.* Nature, 2012. **491**(7424): p. 364-73.
77. Coller, H.A., *Is cancer a metabolic disease?* Am J Pathol, 2014. **184**(1): p. 4-17.
78. Wishart, D.S., *Is Cancer a Genetic Disease or a Metabolic Disease?* EBioMedicine, 2015. **2**(6): p. 478-9.
79. Seyfried, T.N., et al., *Cancer as a metabolic disease: implications for novel therapeutics.* Carcinogenesis, 2014. **35**(3): p. 515-27.
80. Reinfeld, B.I., et al., *Cell-programmed nutrient partitioning in the tumour microenvironment.* Nature, 2021. **593**(7858): p. 282-288.
81. Luengo, A., D.Y. Gui, and M.G. Vander Heiden, *Targeting Metabolism for Cancer Therapy.* Cell chemical biology, 2017. **24**(9): p. 1161-1180.
82. Melotti, A., et al., *The river blindness drug Ivermectin and related macrocyclic lactones inhibit WNT-TCF pathway responses in human cancer.* EMBO Mol Med, 2014. **6**(10): p. 1263-78.
83. Juarez, M., A. Schcolnik-Cabrera, and A. Dueñas-Gonzalez, *The multitargeted drug ivermectin: from an antiparasitic agent to a repositioned cancer drug.* American journal of cancer research, 2018. **8**(2): p. 317-331.
84. Drinyaev, V.A., et al., *Antitumor effect of avermectins.* Eur J Pharmacol, 2004. **501**(1-3): p. 19-23.
85. Dou, Q., et al., *Ivermectin Induces Cytostatic Autophagy by Blocking the PAK1/Akt Axis in Breast Cancer.* Cancer Res, 2016.
86. Crump, A., *Ivermectin: enigmatic multifaceted 'wonder' drug continues to surprise and exceed expectations.* J Antibiot (Tokyo), 2017. **70**(5): p. 495-505.

87. Wu, X., Q.H. Zhou, and K. Xu, *Are isothiocyanates potential anti-cancer drugs?* Acta Pharmacol Sin, 2009. **30**(5): p. 501-12.
88. Yang, M.D., et al., *Phenethyl isothiocyanate inhibits migration and invasion of human gastric cancer AGS cells through suppressing MAPK and NF-kappaB signal pathways.* Anticancer Res, 2010. **30**(6): p. 2135-43.
89. Ho, C.C., et al., *Benzyl isothiocyanate (BITC) inhibits migration and invasion of human gastric cancer AGS cells via suppressing ERK signal pathways.* Hum Exp Toxicol, 2011. **30**(4): p. 296-306.
90. Li, Y. and T. Zhang, *Targeting cancer stem cells with sulforaphane, a dietary component from broccoli and broccoli sprouts.* Future Oncol, 2013. **9**(8): p. 1097-103.
91. Tang, T., et al., *PEITC reverse multi-drug resistance of human gastric cancer SGC7901/DDP cell line.* Cell Biol Int, 2014. **38**(4): p. 502-10.
92. Minarini, A., et al., *Exploring the effects of isothiocyanates on chemotherapeutic drugs.* Expert Opin Drug Metab Toxicol, 2014. **10**(1): p. 25-38.
93. Øverby, A., et al., *Naturally occurring phenethyl isothiocyanate-induced inhibition of gastric cancer cell growth by disruption of microtubules.* J Gastroenterol Hepatol, 2014. **29 Suppl 4**: p. 99-106.
94. Ling, X., et al., *Synergistic effect of allyl isothiocyanate (AITC) on cisplatin efficacy in vitro and in vivo.* Am J Cancer Res, 2015. **5**(8): p. 2516-30.
95. Lawson, A.P., et al., *Naturally Occurring Isothiocyanates Exert Anticancer Effects by Inhibiting Deubiquitinating Enzymes.* Cancer Res, 2015. **75**(23): p. 5130-42.
96. *The Principles of Humane Experimental Technique.* Medical Journal of Australia, 1960. **1**(13): p. 500-500.
97. Ianevski, A., et al., *SynergyFinder: a web application for analyzing drug combination dose–response matrix data.* Bioinformatics, 2017. **33**(15): p. 2413-2415.
98. Ianevski, A., et al., *Prediction of drug combination effects with a minimal set of experiments.* Nature Machine Intelligence, 2019. **1**(12): p. 568-577.
99. Krämer, A., et al., *Causal analysis approaches in Ingenuity Pathway Analysis.* Bioinformatics (Oxford, England), 2014. **30**(4): p. 523-530.
100. Wang, L., et al., *Muscarinic acetylcholine receptor 3 mediates vagus nerve-induced gastric cancer.* Oncogenesis, 2018. **7**(11): p. 88-88.
101. Subramanian, A., et al., *A Next Generation Connectivity Map: L1000 Platform and the First 1,000,000 Profiles.* Cell, 2017. **171**(6): p. 1437-1452.e17.
102. Zhang, P., et al., *Dissecting the Single-Cell Transcriptome Network Underlying Gastric Premalignant Lesions and Early Gastric Cancer.* Cell Rep, 2020. **30**(12): p. 4317.
103. DeBerardinis, R.J., et al., *The Biology of Cancer: Metabolic Reprogramming Fuels Cell Growth and Proliferation.* Cell Metabolism, 2008. **7**(1): p. 11-20.
104. Gupta, P., et al., *Phenethyl isothiocyanate: a comprehensive review of anti-cancer mechanisms.* Biochim Biophys Acta, 2014. **1846**(2): p. 405-24.
105. Trachootham, D., et al., *Selective killing of oncogenically transformed cells through a ROS-mediated mechanism by beta-phenylethyl isothiocyanate.* Cancer Cell, 2006. **10**(3): p. 241-52.
106. Sun, N., et al., *Glutamine affects T24 bladder cancer cell proliferation by activating STAT3 through ROS and glutaminolysis.* Int J Mol Med, 2019. **44**(6): p. 2189-2200.
107. Naumann, M. and J. Jankovic, *Safety of botulinum toxin type A: a systematic review and meta-analysis.* Curr Med Res Opin, 2004. **20**(7): p. 981-90.
108. Dressler, D., F.A. Saberi, and E.R. Barbosa, *Botulinum toxin: mechanisms of action.* Arq Neuropsiquiatr, 2005. **63**(1): p. 180-5.

109. Faivre, S., G. Kroemer, and E. Raymond, *Current development of mTOR inhibitors as anticancer agents.* Nat Rev Drug Discov, 2006. **5**(8): p. 671-88.
110. Dorsam, B. and J. Fahrer, *The disulfide compound alpha-lipoic acid and its derivatives: A novel class of anticancer agents targeting mitochondria.* Cancer Lett, 2016. **371**(1): p. 12-9.
111. Lee, K.C., et al., *Translational assessment of mitochondrial dysfunction of pancreatic cancer from in vitro gene microarray and animal efficacy studies, to early clinical studies, via the novel tumor-specific anti-mitochondrial agent, CPI-613.* Ann Transl Med, 2014. **2**(9): p. 91.
112. Pardee, T.S., et al., *A phase I study of the first-in-class antimitochondrial metabolism agent, CPI-613, in patients with advanced hematologic malignancies.* Clin Cancer Res, 2014. **20**(20): p. 5255-64.
113. Stuart, S.D., et al., *A strategically designed small molecule attacks alpha-ketoglutarate dehydrogenase in tumor cells through a redox process.* Cancer Metab, 2014. **2**(1): p. 4.
114. Zachar, Z., et al., *Non-redox-active lipoate derivates disrupt cancer cell mitochondrial metabolism and are potent anticancer agents in vivo.* J Mol Med (Berl), 2011. **89**(11): p. 1137-48.
115. Fung, M.K.L. and G.C.-F. Chan, *Drug-induced amino acid deprivation as strategy for cancer therapy.* Journal of hematology & oncology, 2017. **10**(1): p. 144-144.
116. Shimobayashi, M. and M.N. Hall, *Making new contacts: the mTOR network in metabolism and signalling crosstalk.* Nat Rev Mol Cell Biol, 2014. **15**(3): p. 155-62.
117. Oh, M.H., et al., *Targeting glutamine metabolism enhances tumor specific immunity by modulating suppressive myeloid cells.* J Clin Invest, 2020.
118. Leone, R.D., et al., *Glutamine blockade induces divergent metabolic programs to overcome tumor immune evasion.* Science, 2019. **366**(6468): p. 1013-1021.
119. Karahalil, B., *Overview of Systems Biology and Omics Technologies.* Curr Med Chem, 2016. **23**(37): p. 4221-4230.
120. Hasin, Y., M. Seldin, and A. Lusis, *Multi-omics approaches to disease.* Genome Biol, 2017. **18**(1): p. 83.
121. *Max Delbruck Quotes*. 1949; Available from: https://www.azquotes.com/author/23590-Max_Delbruck.
122. Nicholson, J.K. and I.D. Wilson, *Opinion: understanding 'global' systems biology: metabonomics and the continuum of metabolism.* Nat Rev Drug Discov, 2003. **2**(8): p. 668-76.
123. Jinawath, N., et al., *Bridging the gap between clinicians and systems biologists: from network biology to translational biomedical research.* J Transl Med, 2016. **14**(1): p. 324.
124. Ekins, S., J. Mestres, and B. Testa, *In silico pharmacology for drug discovery: applications to targets and beyond.* British journal of pharmacology, 2007. **152**(1): p. 21-37.
125. Olswang, L.B. and P.A. Prelock, *Bridging the Gap Between Research and Practice: Implementation Science.* J Speech Lang Hear Res, 2015. **58**(6): p. S1818-26.
126. Kim, J.W., et al., *HIF-1-mediated expression of pyruvate dehydrogenase kinase: a metabolic switch required for cellular adaptation to hypoxia.* Cell Metab, 2006. **3**(3): p. 177-85.
127. Huang, S., et al., *A systematic review of metabolomic profiling of gastric cancer and esophageal cancer.* Cancer biology & medicine, 2020. **17**(1): p. 181-198.
128. Ganeshan, K. and A. Chawla, *Metabolic Regulation of Immune Responses.* Annual Review of Immunology, 2014. **32**(1): p. 609-634.

129. Berthoud, H.R. and W.L. Neuhuber, *Vagal mechanisms as neuromodulatory targets for the treatment of metabolic disease.* Ann N Y Acad Sci, 2019. **1454**(1): p. 42-55.
130. Hu, B., et al., *Gastric cancer: Classification, histology and application of molecular pathology.* Journal of gastrointestinal oncology, 2012. **3**(3): p. 251-261.
131. Yun, S., et al., *Clinical significance of overexpression of NRG1 and its receptors, HER3 and HER4, in gastric cancer patients.* Gastric Cancer, 2018. **21**(2): p. 225-236.
132. *Comprehensive molecular characterization of gastric adenocarcinoma.* Nature, 2014. **513**(7517): p. 202-9.
133. Asem, M.S., et al., *Wnt5a Signaling in Cancer.* Cancers, 2016. **8**(9): p. 79.
134. Karner, C.M., et al., *Increased glutamine catabolism mediates bone anabolism in response to WNT signaling.* J Clin Invest, 2015. **125**(2): p. 551-62.
135. Sethi, J.K. and A. Vidal-Puig, *Wnt signalling and the control of cellular metabolism.* Biochem J, 2010. **427**(1): p. 1-17.
136. Sherwood, V., et al., *WNT5A-mediated beta-catenin-independent signalling is a novel regulator of cancer cell metabolism.* Carcinogenesis, 2014. **35**(4): p. 784-94.
137. Cadoret, A., et al., *New targets of beta-catenin signaling in the liver are involved in the glutamine metabolism.* Oncogene, 2002. **21**(54): p. 8293-301.
138. Wise, D.R., et al., *Myc regulates a transcriptional program that stimulates mitochondrial glutaminolysis and leads to glutamine addiction.* Proc Natl Acad Sci U S A, 2008. **105**(48): p. 18782-7.
139. Xu, X., et al., *Tumor suppressor NDRG2 inhibits glycolysis and glutaminolysis in colorectal cancer cells by repressing c-Myc expression.* Oncotarget, 2015. **6**(28): p. 26161-76.
140. Howell, J.J. and B.D. Manning, *mTOR couples cellular nutrient sensing to organismal metabolic homeostasis.* Trends Endocrinol Metab, 2011. **22**(3): p. 94-102.
141. Csibi, A., et al., *The mTORC1 pathway stimulates glutamine metabolism and cell proliferation by repressing SIRT4.* Cell, 2013. **153**(4): p. 840-54.
142. Zhao, F., et al., *Paracrine Wnt5a-beta-Catenin Signaling Triggers a Metabolic Program that Drives Dendritic Cell Tolerization.* Immunity, 2018. **48**(1): p. 147-160.e7.
143. Allen, D.D., et al., *Cell lines as in vitro models for drug screening and toxicity studies.* Drug Dev Ind Pharm, 2005. **31**(8): p. 757-68.
144. Subhash, V.V., et al., *Strategies and Advancements in Harnessing the Immune System for Gastric Cancer Immunotherapy.* J Immunol Res, 2015. **2015**: p. 308574.
145. Zahalka, A.H., et al., *Adrenergic nerves activate an angio-metabolic switch in prostate cancer.* Science, 2017. **358**(6361): p. 321-326.
146. Renz, B.W., et al., *beta2 Adrenergic-Neurotrophin Feedforward Loop Promotes Pancreatic Cancer.* Cancer Cell, 2018. **33**(1): p. 75-90.e7.
147. Dubeykovskaya, Z., et al., *Neural innervation stimulates splenic TFF2 to arrest myeloid cell expansion and cancer.* Nat Commun, 2016. **7**: p. 10517.
148. Kamiya, A., et al., *Genetic manipulation of autonomic nerve fiber innervation and activity and its effect on breast cancer progression.* Nat Neurosci, 2019. **22**(8): p. 1289-1305.
149. Mauffrey, P., et al., *Progenitors from the central nervous system drive neurogenesis in cancer.* Nature, 2019. **569**(7758): p. 672-678.
150. *Japanese classification of gastric carcinoma: 3rd English edition.* Gastric Cancer, 2011. **14**(2): p. 101-12.
151. Russi, S., et al., *Gastric Normal Adjacent Mucosa Versus Healthy and Cancer Tissues: Distinctive Transcriptomic Profiles and Biological Features.* Cancers (Basel), 2019. **11**(9).
152. Aran, D., et al., *Comprehensive analysis of normal adjacent to tumor transcriptomes.* Nat Commun, 2017. **8**(1): p. 1077.

153. *The global, regional, and national burden of stomach cancer in 195 countries, 1990-2017: a systematic analysis for the Global Burden of Disease study 2017.* Lancet Gastroenterol Hepatol, 2020. **5**(1): p. 42-54.
154. Kim, S.T., et al., *Prospective phase II trial of everolimus in PIK3CA amplification/mutation and/or PTEN loss patients with advanced solid tumors refractory to standard therapy.* BMC Cancer, 2017. **17**(1): p. 211.
155. Kim, H.S., et al., *Phase 1b study of pasireotide, everolimus, and selective internal radioembolization therapy for unresectable neuroendocrine tumors with hepatic metastases.* Cancer, 2018. **124**(9): p. 1992-2000.
156. Chung, V., et al., *Phase Ib Trial of mFOLFOX6 and Everolimus (NSC-733504) in Patients with Metastatic Gastroesophageal Adenocarcinoma.* Oncology, 2016. **90**(6): p. 307-12.
157. Pardee, T.S., et al., *A Phase I Study of CPI-613 in Combination with High-Dose Cytarabine and Mitoxantrone for Relapsed or Refractory Acute Myeloid Leukemia.* Clin Cancer Res, 2018. **24**(9): p. 2060-2073.
158. Alistar, A., et al., *Safety and tolerability of the first-in-class agent CPI-613 in combination with modified FOLFIRINOX in patients with metastatic pancreatic cancer: a single-centre, open-label, dose-escalation, phase 1 trial.* Lancet Oncol, 2017. **18**(6): p. 770-778.

Paper I

iScience

CellPress
OPEN ACCESS

Article

Neural signaling modulates metabolism of gastric cancer

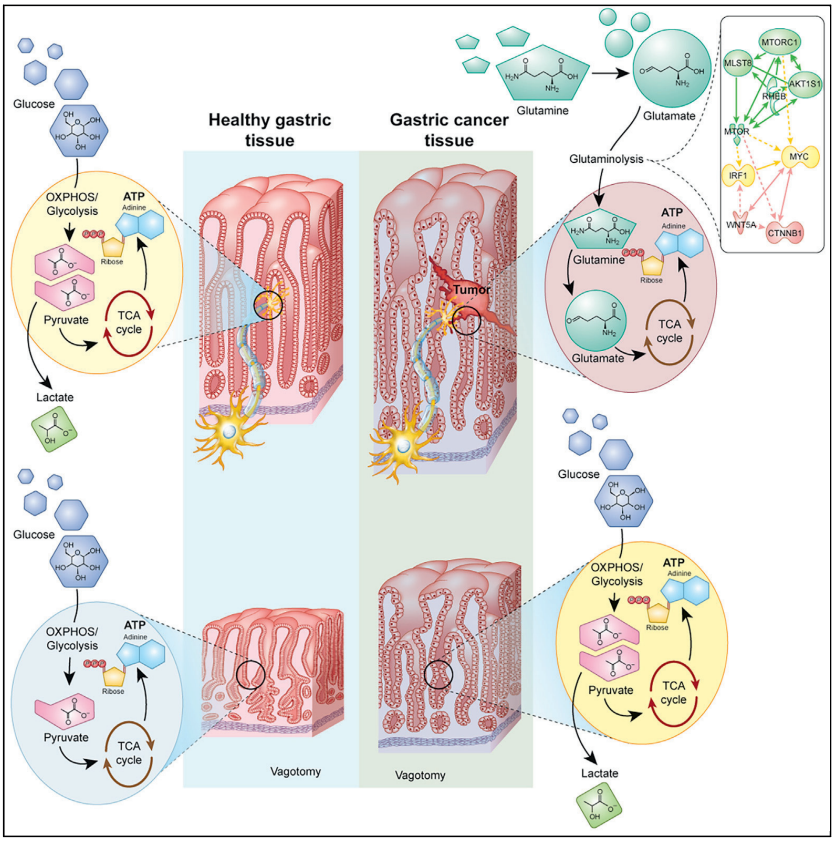

Hanne-Line Rabben, Gøran Troseth Andersen, Magnus Kringstad Olsen, ..., Jon Erik Grønbech, Duan Chen, Chun-Mei Zhao

chun-mei.zhao@ntnu.no

HIGHLIGHTS

Metabolic reprogramming in gastric cancer cells and tumor microenvironment

SNAP25, mTOR, PDP1/ α-KGDH, and glutaminolysis as potential drug targets

Combination of botulinum toxin type A, RAD001, and CPI-613 as a potential treatment

Rabben et al., iScience 24, 102091
February 19, 2021
https://doi.org/10.1016/j.isci.2021.102091

iScience

CellPress
OPEN ACCESS

Article

Neural signaling modulates metabolism of gastric cancer

Hanne-Line Rabben,[1,2,6] Gøran Troseth Andersen,[1,6] Magnus Kringstad Olsen,[1] Anders Øverby,[1] Aleksandr Ianevski,[1] Denis Kainov,[1] Timothy Cragin Wang,[1,3] Steinar Lundgren,[1,4] Jon Erik Grønbech,[1,5] Duan Chen,[1] and Chun-Mei Zhao[1,2,7,*]

SUMMARY

Tumors comprise cancer cells and the associated stromal and immune/inflammatory cells, i.e., tumor microenvironment (TME). Here, we identify a metabolic signature of human and mouse model of gastric cancer and show that vagotomy in the mouse model reverses the metabolic reprogramming, reflected by metabolic switch from glutaminolysis to OXPHOS/glycolysis and normalization of the energy metabolism in cancer cells and TME. We next identify and validate SNAP25, mTOR, PDP1/α-KGDH, and glutaminolysis as drug targets and accordingly propose a therapeutic strategy to target the nerve-cancer metabolism. We demonstrate the efficacy of nerve-cancer metabolism therapy by intratumoral injection of BoNT-A (SNAP25 inhibitor) with systemic administration of RAD001 and CPI-613 but not cytotoxic drugs on overall survival in mice and show the feasibility in patients. These findings point to the importance of neural signaling in modulating the tumor metabolism and provide a rational basis for clinical translation of the potential strategy for gastric cancer.

INTRODUCTION

Cancer is considered a genetic disease with tumor characteristics and metabolic reprogramming (Hanahan and Weinberg, 2011; Wishart, 2015; Whiteside, 2008). The tumor mass consists of primary tumor (i.e. cancer cells) and the associated stromal cells and immune/inflammatory cells, i.e. tumor microenvironment (TME) that usually is different from normal stroma. As cancer cells continue proliferation, the tumor increases in size with an associated remodeling of the TME that determines whether the primary tumor is eradicated, metastasizes, or establishes dormant micrometastases (Loponte et al., 2019; Yoshida, 2015; Vander Heiden and Deberardinis, 2017). The cancer metabolic reprogramming is reflected by alterations in the metabolic profiles of both cancer cells as well as TME. Cancer cells can activate glycolysis in the presence of adequate oxygen levels (aerobic glycolysis or the so-called Warburg effect) within TME, whereas cells of normally differentiated tissues obtain energy through the oxygen-dependent pathway of oxidative phosphorylation (OXPHOS) as well as through the oxygen-independent pathway of glycolysis (Liberti and Locasale, 2016). Emerging evidence suggests that the cancer metabolic reprogramming exhibits the following hallmarks: (1) deregulated uptake of glucose and amino acids, (2) use of opportunistic modes of nutrient acquisition, (3) use of glycolysis/tricarboxylic acid (TCA) cycle intermediates for biosynthesis and nicotinamide adenine dinucleotide phosphate (NADPH) production, (4) increased demand for nitrogen, (5) alterations in metabolite-driven gene regulation, and (6) metabolic interactions between cancer cells and the TME (Pavlova and Thompson, 2016). However, development of treatment targeting the cancer metabolic reprogramming has not yet been successful due to the large differences between tumor types and TME, thus this area is ripe for the strategic development of future targeted treatments for individual cancer types (Schulze and Harris, 2012; Coller, 2014; Liberti and Locasale, 2016; Wishart, 2015; Seyfried et al., 2014).

Gastric cancer (GC) is the fifth most common malignant disease worldwide with the third highest incidence and mortality rate among all cancers (Rawla and Barsouk, 2019). The 5-year overall survival rate for gastric cancer is 10%–30% except for Japan (50%–70%) (Parkin et al., 2005; Matsuda and Saika, 2013). Previously, we and others have demonstrated that vagotomy suppressed gastric tumorigenesis, suggesting a "nerve-cancer cell crosstalk" (Zhao et al., 2014; Hayakawa et al., 2017; Jobling et al., 2015; Wang et al., 2018). In the present study, we used the approaches of *in vitro*, *in vivo*, *in silico*, clinical evaluation, and pilot clinical trial,

[1]Department of Clinical and Molecular Medicine, Norwegian University of Science and Technology (NTNU), 7491 Trondheim, Norway

[2]The Central Norway Regional Health Authority, Norway

[3]Division of Digestive and Liver Diseases, Columbia University College of Physicians and Surgeons, New York, NY 10032-3802, USA

[4]Cancer Clinic, St. Olavs Hospital, Trondheim University Hospital, 7006 Trondheim, Norway

[5]Surgical Clinic, St. Olavs Hospital, Trondheim University Hospital, 7006 Trondheim, Norway

[6]These authors contributed equally

[7]Lead contact

*Correspondence: chun-mei.zhao@ntnu.no

https://doi.org/10.1016/j.isci.2021.102091

and employed the omics technology including comparative transcriptomics (human versus mouse), t-SNE, multi-omics (transcriptomics versus metabolomics), drug-target interaction prediction, and computational drug repositioning (Figure S1). We showed that the animal model we used mimicked GC patients in terms of tumor characteristics and metabolic reprogramming. We found that GC exhibited a metabolic reprogramming, i.e., the use of glutaminolysis for biosynthesis, that differed from other cancer types (Hanahan and Weinberg, 2011; Schulze and Harris, 2012) and that vagotomy reversed the metabolic reprogramming from glutaminolysis to OXPHOS/glycolysis in cancer cells as well as TME of the GC mice. We also identified the metabolic signature and validated the drug-target signaling interactions targeting nerve-cancer metabolism in human cancer cell lines and GC mice and developed a therapeutic strategy using a combination of denervation and cytotoxic free chemotherapy. This treatment appeared effective, particularly with regard to overall survival rate in aged GC mice, and showed potential in a pilot clinical trial in aged GC patients, suggesting a possible "metabolism-based" approach for GC (Figure S1. Study design, Related to Figure 1).

RESULTS

Human and mouse GC display similar metabolic reprogramming profile

Many studies on cancer metabolic reprogramming have been performed primarily in cancer cell lines to link "oncometabolites" to specific mutations of oncogenes. However, there has been a paucity of mechanistic studies in animal models of cancer investigating metabolic reprogramming, particularly any studies that have been closely linked with human studies or clinical trials (Deberardinis and Chandel, 2016). In the present study, we performed comparative transcriptomics using surgical biopsies of patients diagnosed with gastric adenocarcinoma and stomach samples from GC mice, i.e., the transgenic INS-GAS mice, which is a well-known model of spontaneous GC (Wang et al., 1996; Zhao et al., 2014; Fox and Wang, 2007). Human GC samples comprised of intestinal, diffuse, and mixed type adenocarcinoma, whereas mouse GC were predominantly of intestinal type. We compared transcriptomics profiles of the human GC tumor versus benign tissue in the same stomach and the mouse GC tumor versus normal tissue of wild-type (WT) mice. We found that the expression profile of signaling pathways was similar between human and mouse GC (Figures 1A, 1B, and 1D; Data S1. Canonical pathways in gastric cancer, Related to Figure 1). It should be noticed that the upregulated signaling pathways in both human and mouse GC included WNT/β-catenin; mTOR, PI3K/Akt, neuroinflammation, ERK/MAPK, HIPPO, and the CCK/gastrin-mediated pathway (which is specific for the stomach), and the downregulated signaling pathways included AMPK signaling, which is associated with OXPHOS, glycolysis, and fatty acid β-oxidation (Data S1). The expression profile of signaling pathways was confirmed by real-time PCR in which 89 genes related to WNT signaling pathway were measured (Table S1. Gene detected by real-time PCR and RNAseq, Related to Figure 1).

We then constructed a "GC metabolic gene expression profile" consisting of 140 genes that are involved in OXPHOS (37 genes), fatty acid β-oxidation (8 genes), carbohydrate metabolism (62 genes), and energy metabolism including the TCA cycle and glutaminolysis (34 genes). The GC metabolic gene expression profile was characterized by dysregulations of glutaminolysis and associated transporters of amino acids, the TCA cycle, carbohydrate metabolism, and fatty acid β-oxidation and displayed a positive correlation between human and mouse GC (Figures 2A, 2B, and 2D; Data S2. Metabolic genes in gastric cancer, Related to Figures 2 and 3). These results suggested that the mouse model of GC used in the present study would be useful for studying the molecular mechanisms of human GC metabolic reprogramming. Upstream regulator analysis of mouse RNA sequencing data from neoplastic lesions versus normal/healthy tissue revealed 144 regulators with increased activation whereof 8 regulators within the WNT/β-catenin signaling pathway—Tgf beta, WNT1, CD44, JUN, TGFB1, TGFBR1, TGFB2, and CTNNB1 (z-scores>2, $p < 0.05$)—were activated upstream of the mTOR pathway intermediates EIF3C, MRAS, PDPK1, RHOB, PPP2CA, PRKCG, and RHOA (Figure 2F; Table S2. Upstream regulators in mouse GC, Related to Figure 2F).

A single-cell atlas of gastric antral premalignant and early malignant mucosa has been recently constructed using single-cell mRNA sequencing data and visualized with t-distributed stochastic neighbor embedding (t-SNE) algorithm (Zhang et al., 2019). We performed t-SNE utilizing the gene expression data that are deposited at GEO (accession number GSE134520) (Zhang et al., 2019) and found that TCA cycle and glutaminolysis-dependent gene expression profile, particularly MDH1, MDH2, GLUL, IDH3B, DLD, SDHB, SLC17A5, SLC12A8, and OGDH, overlaid on the single-cell atlas of both cancer cells and TME (such as other proliferative cells, neck-like cells, pit mucous cells, enteroendocrine cells, T cells, and fibroblasts) (Figures 3A and 3B).

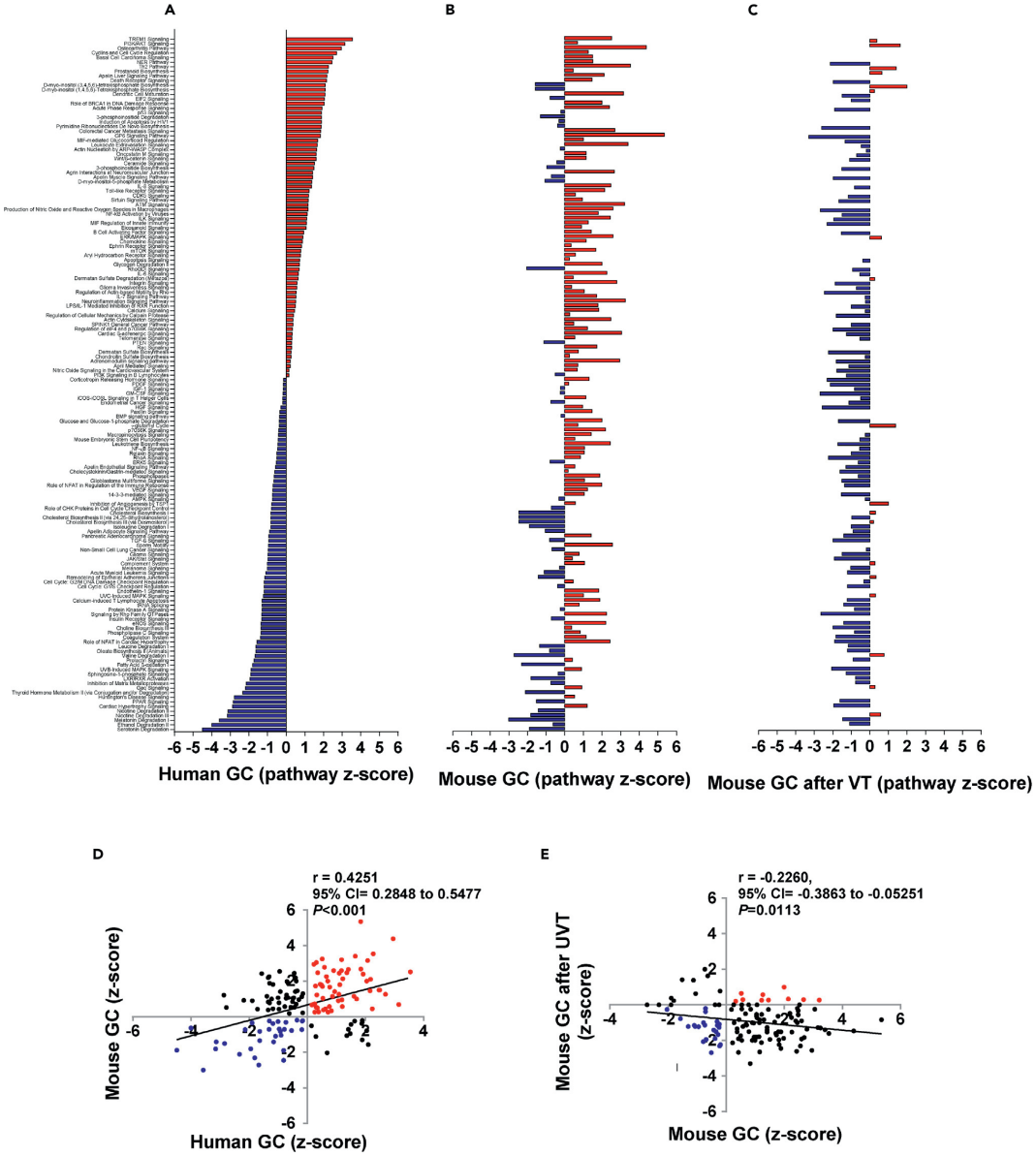

Figure 1. Signaling pathways in gastric cancer (GC)

Waterfall diagrams showing signaling pathways that were differentially activated (marked in red) and inhibited (blue) in human gastric cancer (GC) versus normal adjacent tissue (A) and mouse GC versus WT (B) or after vagotomy (C). Note: names of signaling pathways are listed in the same order in A–C. For detailed information, see Data S1.

Correlation between human and mouse GC (D) and mouse GC after vagotomy (E) in terms of Z-score. Z-scores were generated in IPA using datasets with differently expressed genes ($p < 0.05$). Pearson's test was used for correlation, and a linear regression line was drawn using GraphPad Prism v6. UVT in E: unilateral vagotomy (which results in innervated and denervated sides within the same stomach).

For study groups, see Table S12 (Study groups, Related to Figures 7K and 8G–8L).

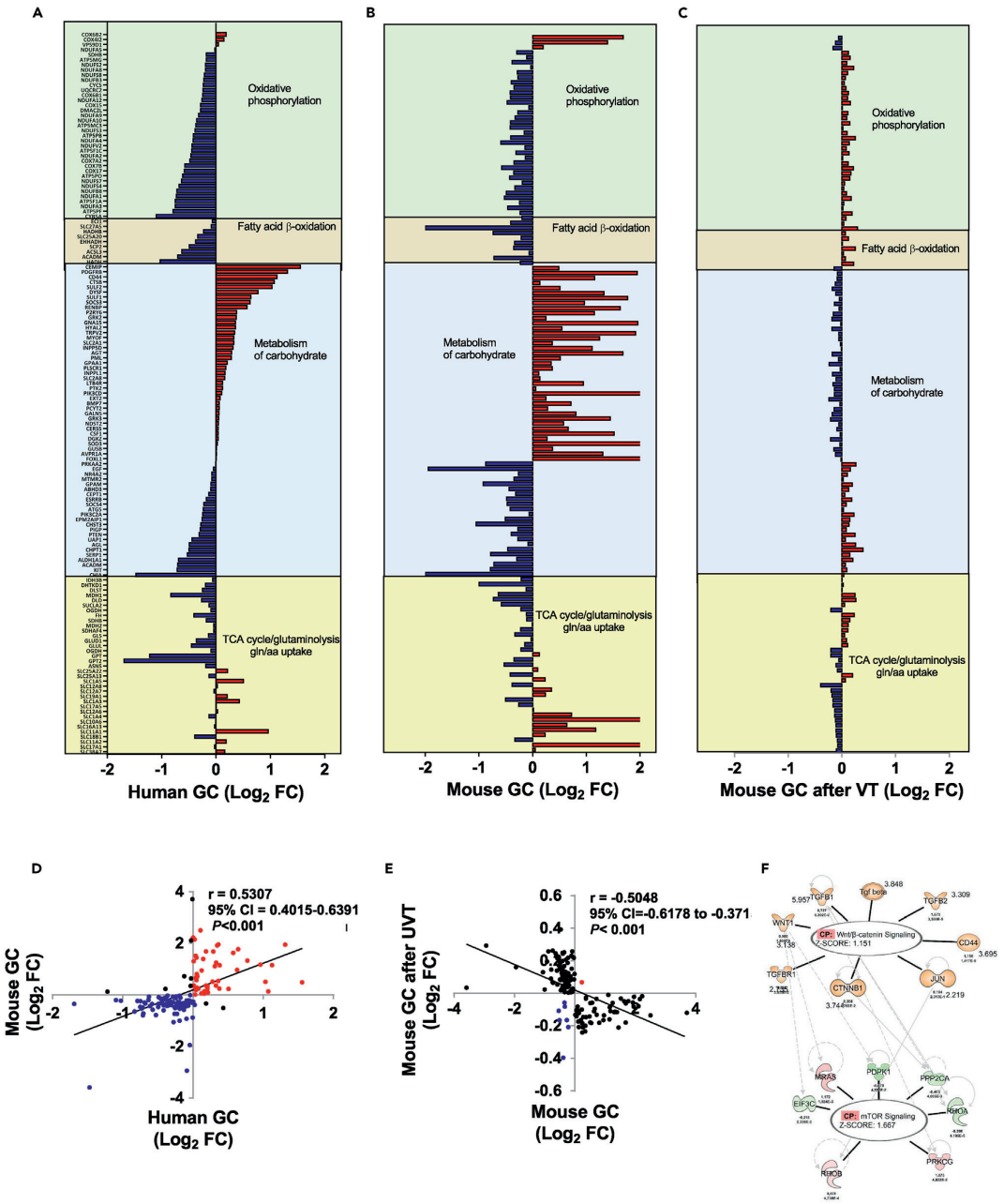

Figure 2. Metabolic gene expression profiles in gastric cancer (GC)

Waterfall diagrams showing metabolic gene expression profiles of human gastric cancer (GC)(A), mouse GC (B), and mouse GC (6 months after vagotomy (VT)(C). Note: names of genes are listed in the same order in A–C and differentially expressed genes in upregulation (marked in red) and downregulation

Figure 2. *Continued*

(blue). For detailed information, see Data S2. Pearson's test was used for correlation, and a linear regression line was drawn using GraphPad Prism v6. UVT in E: unilateral vagotomy (which results in innervated and denervated sides within the same stomach). Upstream regulator analysis of mouse GC transcriptomics performed in IPA revealed regulators of the WNT/β-catenin signaling pathway being upstream of mTOR signaling (F).
Orange: predicted activated; Blue: predicted inhibition; Green: downregulated; Red: upregulated; Gray: did not pass p value cut-off. Annotated with $\log_2$ fold change, p value, and z-scores, see Table S2.

Vagotomy reverses the metabolic reprogramming of GC

Vagal innervation is known to regulate epithelial cell proliferation in the stomach and has recently been implicated in GC development and progression (Hayakawa et al., 2017; Wang et al., 2018; Zhao et al., 2014; Zahalka and Frenette, 2020). Vagal denervation can be achieved surgically, pharmacologically, or genetically. The surgery includes bilateral truncal vagotomy or unilateral truncal vagotomy (UVT). UVT takes advantage of the fact that each (anterior or posterior) vagal trunk innervates only one-half of the stomach, and consequently, UVT does not impair the overall function of the stomach. In a previous study, we showed that vagotomy during the pre-neoplastic stage of tumorigenesis diminished tumor incidence and size, and attenuated tumor cell proliferation specifically in the denervated portion of the stomach, suggesting that the vagus nerve promotes gastric cancer growth. Consistent with this idea, pharmacologic denervation via local injection of botulinum toxin A (BoNT-A) into the gastric wall similarly impaired pre-neoplastic growth. Furthermore, vagotomy or BoNT-A treatment at later stages of tumorigenesis suppressed GC progression and augmented the antitumor effect of cytotoxic chemotherapy in tumor-bearing mice, resulting in prolonged survival (Zhao et al., 2014). In the present study, we further examined the effect of vagotomy on the metabolic reprogramming of GC. In a comparison between the innervated and denervated GC mouse stomachs after UVT, the expression profiles of signaling pathways as well as the metabolic genes were reversed after vagotomy activities and displayed negative correlations between the two sides of stomach after UVT (Figure 1B versus 1C; 2B versus 2C; 1E, 2E; Data S1 and S2).

We then performed metabolomics analysis of gastric tissues in GC and WT mice that underwent UVT. By comparison of GC between innervated tumors and denervated tumors, we identified 48 dysregulated metabolites representing a "metabolic signature" of GC, and furthermore we found that the levels of metabolites, regardless of the direction of change in individual metabolites, were reversed after vagotomy to the normal levels of WT mice (Figure 4A; Table S3. Metabolite signature, Related to Figure 4; Table S13. Metabolite involved with DNA/protein syntheses, Related to Figure 4). We suggest that the metabolic signature of GC reflects the changes in both cancer cells and TME rather than specific mutations of oncogenes (i.e. "oncometabolites"). Among the metabolites in the metabolic signature of GC, some metabolites such as prostaglandin E2, methionine, and glycine are known to be abundant in GC (Uefuji et al., 2000; Wang and Dubois, 2018; Sanderson et al., 2019; Hirayama et al., 2009). Of note, the effects of vagotomy on the metabolites were different between WT and GC mice, suggesting a different response of denervation on normal tissue compared with tumor tissue (Figure 4A; Table S3; Data S3. Metabolites measured by LC/MS and GC/MS by Metabolon, Related to Figures 4 and S2A–S2D). These results corresponded well to changes in the metabolic gene expression profile, suggesting that vagotomy reversed the metabolic reprogramming of GC at both transcript and metabolite levels.

We next focused on the effects of vagotomy on tumor energy metabolism encompassing the OXPHOS/glycolysis (including the Warburg effect), glutaminolysis, and the TCA cycle (Figures 4B–4N; Table S4. Energy metabolites, Related to Figures 4B–4N). Metabolic flexibility of the tumor involves anaplerotic steps in energy metabolism (Smith et al., 2018). In comparison with WT mice, GC mice displayed an increased glutaminolytic flux through the TCA cycle, which was reflected by higher levels of glycine, oxidized glutathione (GSSG), citrate, 5-oxoproline, cis-aconitate, L-glutamate, L-glutamine, and threonine (Figures 4B, 4C, 4E, 4F, 4I, 4J, 4K, and 4N) but not the glycolysis (represented by glucose, lactate, and fructose-6-phosphate) (Figures 4G, 4L, and 4M). After vagotomy, the glutaminolysis, but not glycolysis, intermediates were reduced in GC mice (Figure 4). Comparison of GC after vagotomy versus WT without vagotomy revealed no difference in the energy metabolism (Figures 4B–4N and S2A–S2D), suggesting that vagotomy in GC mice led to a normalization of the energy metabolism. However, WT mice responded to vagotomy differently compared with GC mice, namely having reduced glutaminolysis as well as glycolysis (Figures 4B–4N and S2A–S2D. Gastric cancer is glutamine-dependent, Related to Figure 4; Table S4).

To confirm that GC was dependent on glutamine and/or pyruvate, we measured endogenous L-glutamine and L-glutamate levels in human gastric adenocarcinoma cell line (AGS cells). We found stable levels of

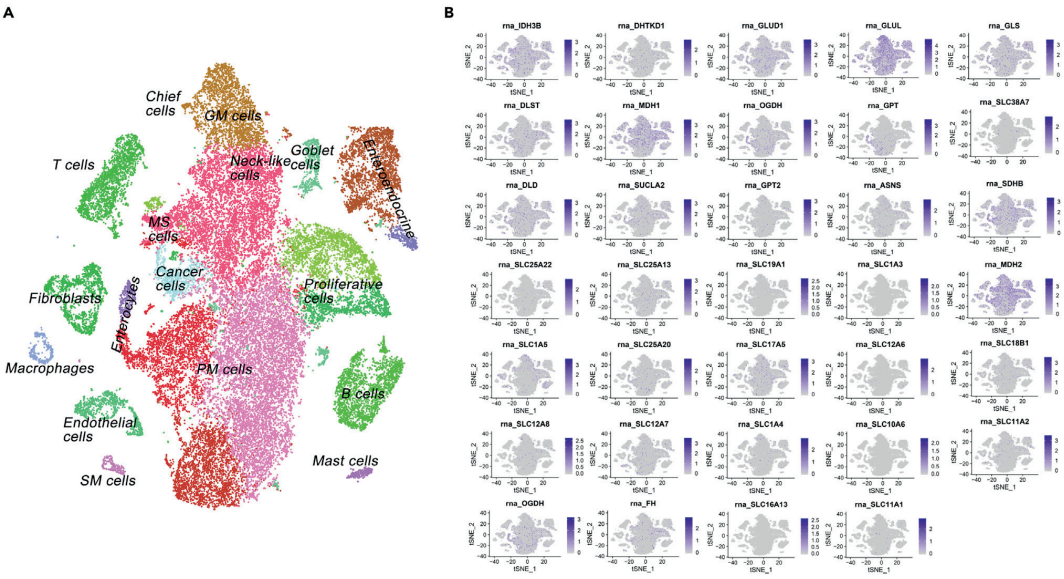

Figure 3. Glutamine-dependent gene expression profile of gastric cancer (GC) according to the single-cell atlas

tSNE plot of single-cell data released by the study of premalignant lesions and gastric cancer (Zhang et al., 2019) (A). The expression patterns of 34 TCA/glutaminolysis/gln uptake genes according to Figure 2 (B). Single-cell data were processed using Seurat v3 (https://doi.org/10.1016/j.cell.2019.05.031). Data was normalized for each of the 13 samples independently, followed by the functions FindIntegrationAnchors, IntegrateData, ScaleData, and RunPCA with default parameters. As in the original study, cells with number of expressed genes lower than 400 or larger than 7,000 were removed, and 20% or more of UMIs were mapped to mitochondrial or ribosomal genes. 50 PCs were utilized to visualize the single-cell atlas with a tSNE plot.

L-glutamine and L-glutamate during a culture period of 1–24 h (Figure S2E). We further performed *in vitro* experiments in AGS and MKN45 cells (both human gastric adenocarcinoma cell lines). The proliferation rates of both cells were time and concentration dependent on glutamine (Figures S2, S2F, and S2G). Moreover, the cell proliferation was reduced and eventually stopped 24–72 h after depletion of glutamine but not pyruvate (Figures S2, S2H, and S2I). These results confirmed that GC cells were glutamine dependent.

Vagotomy alters neuronal, metabolic, and WNT-mTOR signaling pathways in GC

To explore the signaling pathways by which vagotomy reverses metabolic reprogramming in GC mice, we performed integrative omics (multi-omics) of transcriptomics versus metabolomics and found the signaling pathways associated with metabolism, such as synaptogenesis signaling pathway, endocannabinoid neuronal synapse pathway, role of MAPK signaling, neuroinflammation signaling pathway, glutamate receptor signaling, glutathione biosynthesis, glutamate degradation II, and UDP-N-acetyl-D-glucosamine biosynthesis II (Figure 5A; Table S5. Signaling pathways involved in mouse gastric cancer, Related to Figure 5A). We also found that metabolite-related signaling pathways, such as synaptic long-term depression, triacylglycerol biosynthesis, and CDP-diacylglycerol biosynthesis I were attenuated after vagotomy, whereas antioxidant action of vitamin C and purine nucleotides *de novo* biosynthesis II were activated, suggesting compensatory responses after vagotomy (Figure 5B; Table S6. Signaling pathways involved in mouse gastric cancer after vagotomy, Related to Figure 5B). Furthermore, vagotomy in GC mice reversed or restored the signaling pathways of "WT" phenotype, including TCA cycle II (eukaryotic), protein kinase A signaling, calcium signaling, gap junction signaling, and phospholipases (Figure 5C; Table S7. Signaling pathways involved in mouse gastric cancer with and without vagotomy, Related to Figure 5C). The results were in line with the signaling pathways revealed by transcriptomics showing that WNT/β-catenin signaling and mTOR signaling were inhibited after vagotomy (Data S1) and in agreement with our previous study showing that vagotomy reduced the expression of WNT-regulated stem cell markers and decreased the expansion of leucine-rich repeat containing G-protein-coupled receptor 5-positive ($LGR5^+$) stem cells in the gastric mucosa (Zhao et al., 2014). Other reports showed that mTORC1/2 activity was associated

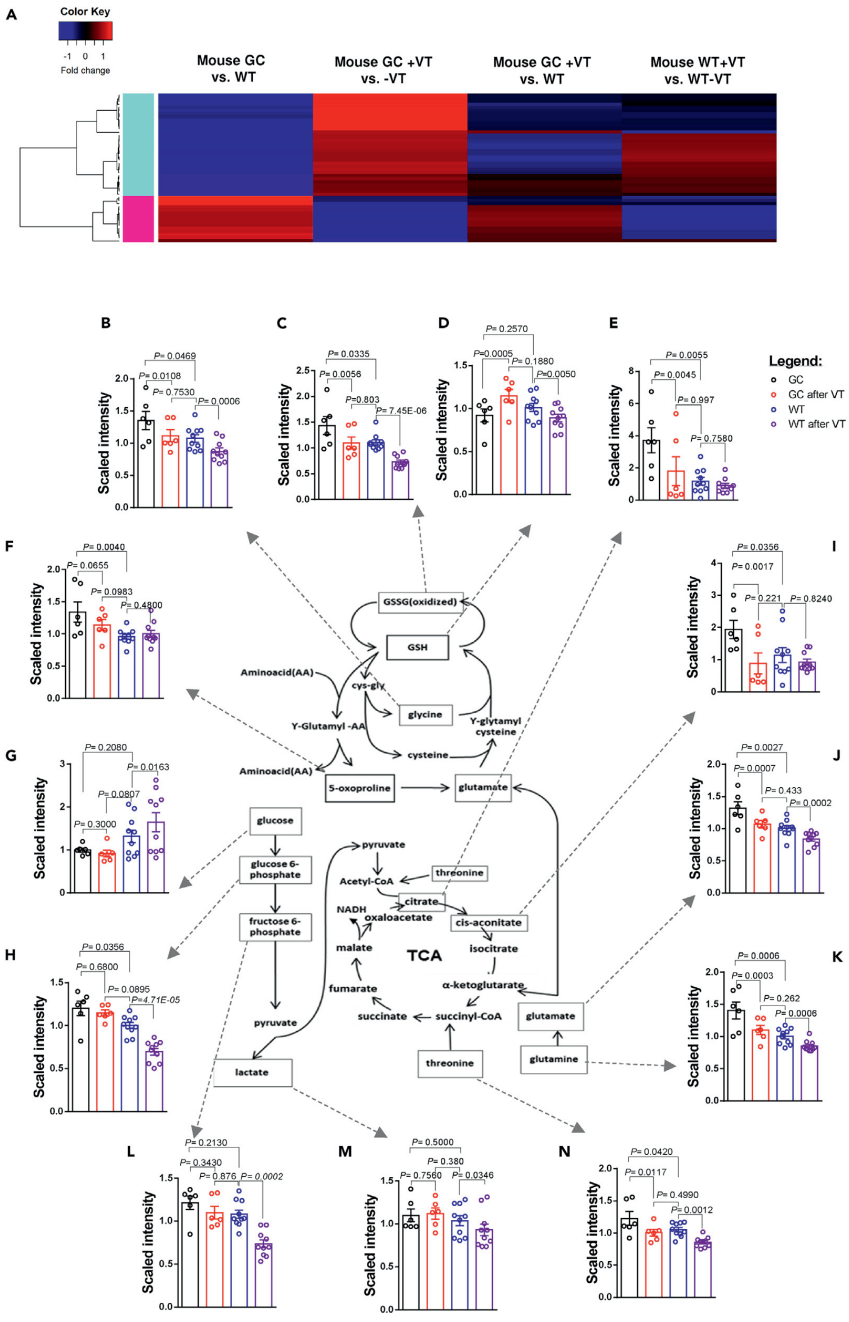
A
Color Key
-1 0 1
Fold change
Mouse GC vs. WT
Mouse GC +VT vs. -VT
Mouse GC +VT vs. WT
Mouse WT+VT vs. WT-VT
B
C
D
E
Legend:
GC
GC after VT
WT
WT after VT
Scaled intensity
F
G
H
I
J
K
L
M
N
GSSG(oxidized)
GSH
Aminoacid(AA)
cys-gly
glycine
Y-Glutamyl -AA
Y-glytamyl cysteine
cysteine
5-oxoproline
glutamate
glucose
glucose 6-phosphate
fructose 6-phosphate
pyruvate
lactate
Acetyl-CoA
threonine
citrate
NADH
oxaloacetate
cis-aconitate
malate
TCA
isocitrate
fumarate
α-ketoglutarate
succinate
succinyl-CoA
glutamine

Figure 4. Effects of vagotomy on metabolite levels in wild-type (WT) and gastric cancer (GC) mice

Heatmap showing metabolite fold changes of mouse gastric cancer (GC) versus wild-type (WT), mouse GC after unilateral vagotomy (VT), i.e. innervated versus denervated sides within the same stomach, mouse GC after VT versus WT mice, and mouse WT after VT, i.e. innervated versus denervated sides within the same stomach (A). Color key shows fold change in red (increase) or blue (decrease), generated using differently expressed metabolites ($p < 0.05$) in mouse GC versus WT (1) and mouse GC after VT (2) with the heatmap.2 function in RStudio version 3.5.2. For detailed information, see Table S3 and Data S3. Energy metabolism after VT (B–N): levels of metabolites in energy metabolism encompassing OXPHOS/glycolysis/Warburg effect, glutaminolysis, and TCA (B-N). Metabolites in mouse gastric cancer (GC) (marked in black), wild-type WT (blue), GC after VT (red), and WT after VT (purple). Glu: L-glutamate; Gln: L-glutamine; GSH: reduced glutathione; GSSG: oxidized glutathione; Gly: glycine; Thr: threonine; Oxo: 5-oxoproline; C-at: cis-aconitate; Glc: glucose; G6P: glucose-6-phosphate; F6P: fructose-6-phosphate.

Bars represent means of n = 6 (GC) or n = 10 (WT) relative scaled intensities with SEM and one-way ANOVA p values. For detailed information, see Table S4 and Figures S2A–S2D.

with glutamine-dependent anaplerosis (Liao et al., 2019; Duran et al., 2012). Taken together, the results suggested that glutaminolysis, neuronal signaling, WNT/β-catenin signaling, and mTOR signaling of GC were altered by vagotomy, and thus might represent potential therapeutic targets.

Drug-target interaction prediction shows SNAP25, mTOR, PDP1/α-KGDH, and glutaminolysis as drug targets

We next performed drug-target interaction prediction and computational drug repositioning of approved and investigational drugs/compounds (e.g. existing at the website of ClinicalTrials.gov) in GC mice and patients. We identified the network nodes (i.e. drug targets) at the levels of proteins, mRNAs, microRNA, and metabolites with special focus on the following four targets with potential drugs: SNAP25 with BoNT-A, mTOR with RAD001 (also known as Everolimus), PDP1/α-KGDH with CPI-613, and GLS with DON, 968, CB839, or BPTES in both GC mice and patients (Figures 6 and S3. Drug target prediction, Related to Figure 6). In our previous study, we have demonstrated that either local vagotomy or local injection of BoNT-A suppresses GC (Zhao et al., 2014). This was most likely because BoNT-A binds selectively to synaptosomal nerve-associated protein 25 (SNAP25), which is an integral protein required for docking and release of acetylcholine from vesicles situated in the vagal nerve endings (Naumann and Jankovic, 2004; Dressler et al., 2005). RAD001 is a rapamycin analog that specifically inhibits the mTORC1 complex by binding to FKBP12 (Faivre et al., 2006). The enzymes pyruvate dehydrogenase (PDH/PDP1) and α-ketoglutarate dehydrogenase (α-KGDH) control acetyl-CoA/pyruvate and glutamine/glutamate anaplerotic steps to the TCA cycle, respectively. The lipoate analog CPI-613 (6,8-Bis[(phenylmethyl)thio-octanoic acid) inhibits both enzymes (Dorsam and Fahrer, 2016; Lee et al., 2014; Pardee et al., 2014; Stuart et al., 2014; Zachar et al., 2011). Glutaminase inhibitors, such as CB-839, BPTES, DON, and 968, have been tested in a variety of cancers (Fung and Chan, 2017) but have limited efficacy and considerable adverse effects. It should also be noticed that the WNT signaling pathway did not appear as drug-target *per se*, as there are no drugs yet developed (Kahn, 2014). Thus, we tested neither the glutaminase inhibitors nor any inhibitors of the WNT signaling pathway in the present study. Next, we performed *in vitro* experiments to validate the efficacies of these potential metabolic-targeted therapies. Treatment of human GC cells with either RAD001 or CPI-613 reduced cell proliferation in dose-dependent manners (Figures 7A–7D). Combination of both inhibitors at IC_{50} doses for either 24 or 48 h resulted in synergistic inhibition (Figures 7E–7G). We found that BoNT-A alone was without any significant concentration-dependent inhibition on cell proliferation and did not enhance the inhibitory effects of neither 5-FU and/or oxaliplatin nor RAD001 and/or CPI-613 in any range of concentration responses (Figure S4. *In vitro* drug screening, Related to Figure 7), suggesting that the cytotoxic effect of BoNT-A on the cells does not take place *in vitro*. We also found that combination of RAD001 and CPI-613 had similar inhibitory effect with or without adding 5-FU and/or oxaliplatin (Figure S4).

Preclinical trial shows therapeutic effects of nerve-cancer metabolism therapy for GC

Previously, we demonstrated that gastric denervation by either vagotomy or local BoNT-A injection had similar anti-tumor effects (Zhao et al., 2014). Vagotomy can be performed at open surgery (laparotomy) or using minimally invasive surgery (laparoscopy), whereas pharmacological denervation by BoNT-A injection into the gastric wall can be achieved through gastroscopy, which is much less invasive in comparison with laparoscopic vagotomy.

Many GC patients are elderly who have poor tolerance to the current therapeutic options including subtotal or total gastrectomy with radical lymph node dissection, adjuvant chemoradiotherapy, or perioperative chemotherapy. Systemical use of cytotoxic drug treatment in elderly patients is usually associated with concerns regarding quality of life and overall survival (OS). Thus, the therapeutic strategy should be focused on

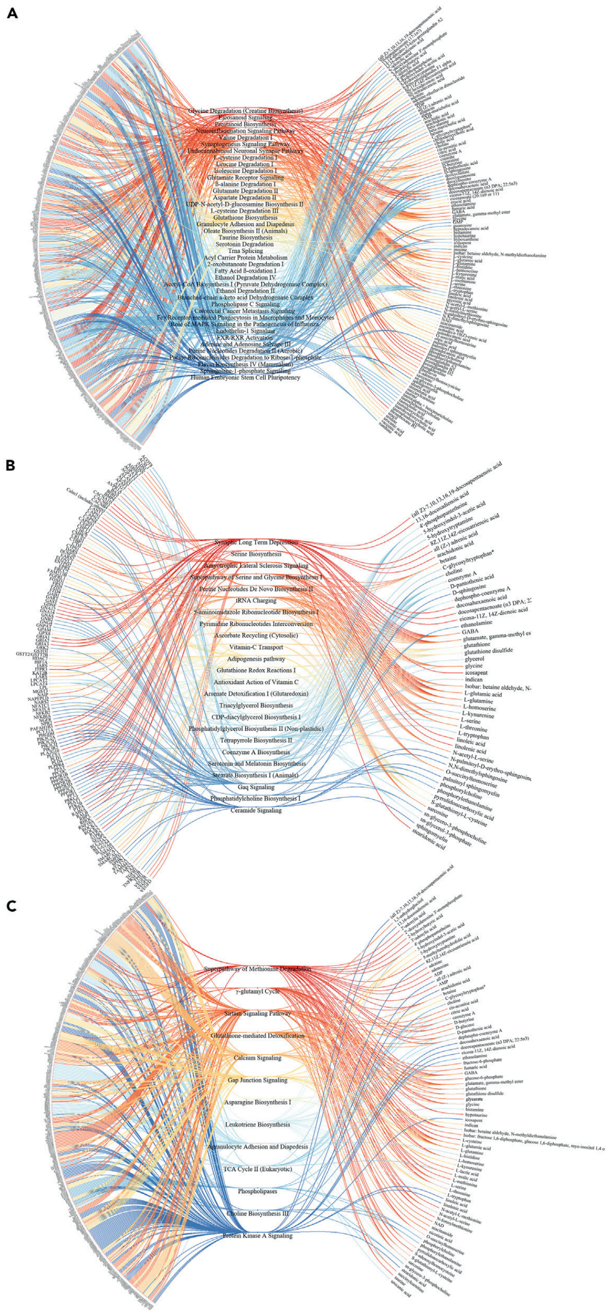
A
Glycine Degradation (Creatine Biosynthesis)
Eicosanoid Signaling
Estanoid Biosynthesis
Neuroinflammation Signaling Pathway
Valine Degradation I
Synaptogenesis Signaling Pathway
Endocannabinoid Neuronal Synapse Pathway
L-cysteine Degradation I
Leucine Degradation I
Isoleucine Degradation I
Glutamate Receptor Signaling
β-alanine Degradation I
Glutamate Degradation II
Aspartate Degradation II
UDP-N-acetyl-D-glucosamine Biosynthesis II
L-cysteine Degradation III
Glutathione Biosynthesis
Granulocyte Adhesion and Diapedesis
Oleate Biosynthesis II (Animals)
Taurine Biosynthesis
Serotonin Degradation
Trna Splicing
Acyl Carrier Protein Metabolism
2-oxobutanoate Degradation I
Fatty Acid β-oxidation I
Ethanol Degradation IV
Acetyl-CoA Biosynthesis I (Pyruvate Dehydrogenase Complex)
Ethanol Degradation II
Branched-chain a-keto acid Dehydrogenase Complex
Phospholipase C Signaling
Colorectal Cancer Metastasis Signaling
Fcγ Receptor-mediated Phagocytosis in Macrophages and Monocytes
Role of MAPK Signaling in the Pathogenesis of Influenza
Endothelin-1 Signaling
FXR/RXR Activation
Adenine and Adenosine Salvage III
Purine Nucleotides Degradation II (Aerobic)
Purine Ribonucleosides Degradation to Ribose-1-phosphate
Flavin Biosynthesis IV (Mammalian)
Sphingosine-1-phosphate Signaling
Human Embryonic Stem Cell Pluripotency
B
Synaptic Long Term Depression
Serine Biosynthesis
Amyotrophic Lateral Sclerosis Signaling
Superpathway of Serine and Glycine Biosynthesis I
Purine Nucleotides De Novo Biosynthesis II
tRNA Charging
5-aminoimidazole Ribonucleotide Biosynthesis I
Pyrimidine Ribonucleotides Interconversion
Ascorbate Recycling (Cytosolic)
Vitamin-C Transport
Adipogenesis pathway
Glutathione Redox Reactions I
Antioxidant Action of Vitamin C
Arsenate Detoxification I (Glutaredoxin)
Triacylglycerol Biosynthesis
CDP-diacylglycerol Biosynthesis I
Phosphatidylglycerol Biosynthesis II (Non-plastidic)
Tetrapyrrole Biosynthesis II
Coenzyme A Biosynthesis
Serotonin and Melatonin Biosynthesis
Stearate Biosynthesis I (Animals)
Gαq Signaling
Phosphatidylcholine Biosynthesis I
Ceramide Signaling
C
Superpathway of Methionine Degradation
γ-glutamyl Cycle
Sirtuin Signaling Pathway
Glutathione-mediated Detoxification
Calcium Signaling
Gap Junction Signaling
Asparagine Biosynthesis I
Leukotriene Biosynthesis
Granulocyte Adhesion and Diapedesis
TCA Cycle II (Eukaryotic)
Phospholipases
Choline Biosynthesis III
Protein Kinase A Signaling

Figure 5. Multi-omics in gastric cancer (GC)

"Butterfly" diagrams showing signaling pathways (in center) that overlap with a significant Fisher's test ($p < 0.05$) between transcriptomics (left panel) and metabolomics datasets (right panel) in comparison between mouse gastric cancer (GC) versus wild-type (A), GC with versus without innervation (after VT) (B), and both GC versus WT and GC after VT (C). Diagram plots were created with JavaScript library D3.js v4. For detailed information, see Tables S5–S7.

the clinical endpoints, including OS and quality of life and, to lesser extent, tumor size. Thus, we performed different treatments of GC mice at 9–15 months of age and followed-up as long as the mice lived (maximal 14 months after starting treatment). Treatments included 5-FU plus oxaliplatin (named FUOX) and combinations of gastric injection of BoNT-A, RAD001, and CPI-613 (named BRC) with or without FUOX for 2 months (Figure 7H), and mice were followed-up by measuring OS, median survival (MS) time, body weight changes, and tumor size. We found that OS and MS were 33% and 148 days, respectively, in GC mice without any treatment (age-matched controls, AMC), 40% and 40 days in GC mice that received either FUOX or BRC + FUOX, but 90% and 249 days in GC mice that received BRC in comparisons with AMC (Figure 7I). Of note, the survival rates in mice with cytotoxic drugs *per se* (i.e. FUOX) or in combination with BRC were worse than mice without any treatment. Quality of life in mice can be measured by body weight change. FUOX induced body weight loss to the human endpoint (i.e. 25% of initial weight or less than 25% but with poor physical appearance) during the treatment period. BRC induced about 10% weight loss during the treatment and attenuated the weight loss by FUOX (Figure 7J). Within the treatment period of 2 months, 5-FU and oxaliplatin given either alone or as FUOX did not reduce the tumor size, RAD001 and CPI-613 given either alone or in combination also did not reduce the tumor size, whereas BoNT-A alone reduced the tumor size and had synergic effects when given together with FUOX or as BRC + FUOX (Figure 7K). There was no difference in tumor size between FUOX and BRC + FUOX (Figure 7K). Thus, these results suggested that BoNT-A *per se* had no cytotoxic effect *in vivo* and that BRC (BoNT-A + RAD001+-CPI-613 without 5-FU and/or oxaliplatin) increased OS and MS, suggesting a potential cytotoxic chemo-free therapy for GC.

In order to verify the mechanism of action, we performed transcriptomic profiling with focus on the gene expression profile of glutaminolysis-WNT-mTOR-c-MYC signaling pathways and found that vagotomy and treatment with metabolic inhibitors with or without pharmacological denervation, i.e., RC or BRC, in GC mice for 2 months reversed the gene expression profile of glutaminolysis-WNT-mTOR-c-MYC signaling pathway, suggesting a possible mechanism of "nerve-cancer metabolism therapy" (Figures 8 and S5A–S5D. Nerve-cancer metabolism in gastric cancer, Related to Figure 8A), supporting that BRC is a nerve-cancer metabolism therapy for GC. We further analyzed the gene expression pattern of glutaminolysis-WNT-mTOR-c-MYC signaling pathway in GC mice based on the single-cell transcriptome atlas of (human) stomach (Zhang et al., 2019) and found that the upregulated gene expression was reversed after vagotomy, RC or BRC in both cancer cells and TME (e.g. T cells, B cells, macrophages, fibroblast, mast cells, and endothelial cells) (Figure 8B), suggesting that the nerve-cancer metabolism therapy acts on both cancer cells and TME in GC. Furthermore, computational network modeling revealed intensive connections across the genes within the cell type and with the genes involved in glutaminolysis (Figures 8C, 8D, and S6A–S6E. Single-cell atlas and glutamine pathways, Related to Figures 8C and 8D).

WNT-signaling induces activation of mTORC1 signaling through the inhibition of GSK3β (Shimobayashi and Hall, 2014) or through induction of MYC in a CTNNB1-dependent manner (Zhang et al., 2012; Grigoryan et al., 2013). We next performed an *in silico* experiment to predict the effects of inhibition of nodes/genes in WNT/β-catenin network on mTOR network and *vice versa*, which are based on both experimental data, the Ingenuity Knowledge Base, and peer-reviewed literature. We first constructed two functional cluster networks of WNT/β-catenin and mTOR signaling based on the gene expression profile of GC mice (Figure 8E), and the *in silico* testing by inhibition of β-catenin (CTNNB1), c-MYC (MYC), or WNT7B either alone or in combination with other genes/nodes within the cluster showed that the inhibition of WNT/β-catenin network led to inhibition of the mTOR cluster, whereas inhibition of the mTOR kinase or mTORC1 complex either alone or in combination with other genes/nodes within the cluster was without inhibition on the WNT/β-catenin cluster (Figures 8F and S7A. *In silico* modeling, Related to Figure 8), probably suggesting a downstream signal flow in WNT-mTOR signaling pathways. Of note, inhibition of either Frizzled, GSK3β, or DVL nodes alone was without effect on mTOR cluster. As expected, functional cluster networks of both WNT/β-catenin and mTOR as predicted through *in silico* testing were inhibited 2 months after RC in GC mice (Figure S7B. *In silico* modeling, Related to Figure 8).

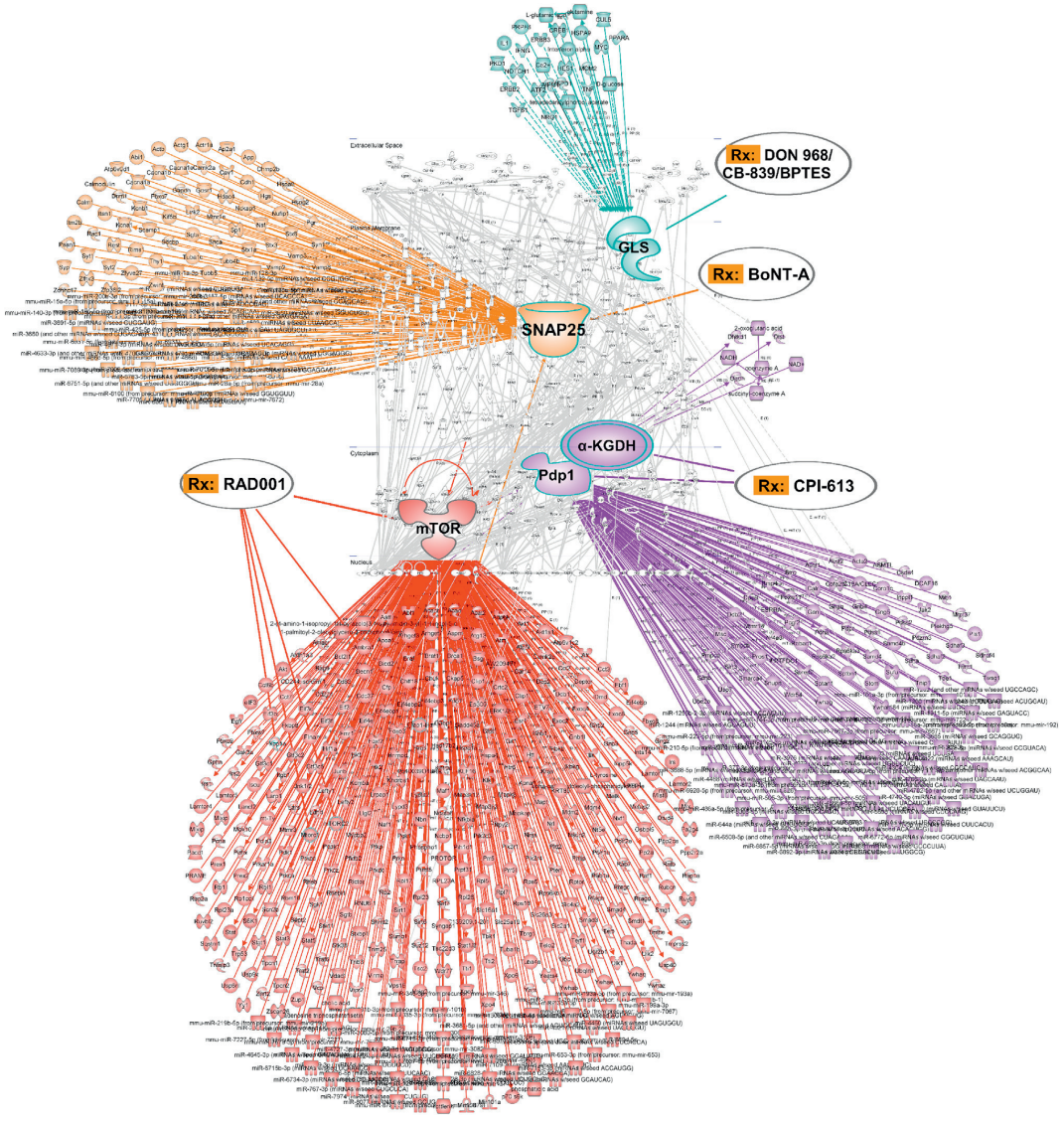

Figure 6. Drug target prediction and repurposing

"Waterdrop" diagrams showing drug-target. Interaction prediction and computational drug repositioning from transcriptomics data in mouse GC created in Ingenuity Pathway Analysis (IPA). Note: nodes of RAD001-targeted mTOR (marked in red), CPI-613-targeted PDP1 and/or α-KGDH (purple), BoNT-A-targeted SNAP25 (yellow), and DON/968/CB-839/BPTES-targeted GLS (light blue). Lines represent biological relationships between molecules that include proteins, genes, mRNAs, microRNAs, and metabolites, generated from differentially expressed drug target genes (only drug targets differentially expressed between mouse GC versus WT at $p < 0.05$, $q < 0.05$ are shown, light gray). Molecule nodes are fetched from RNA sequencing data in mouse GC versus WT, and edges are generated based on causal information in the Ingenuity Knowledge Base. The overlay-tool in IPA is used to predict drugs for indicated nodes.

See also Figure S3.

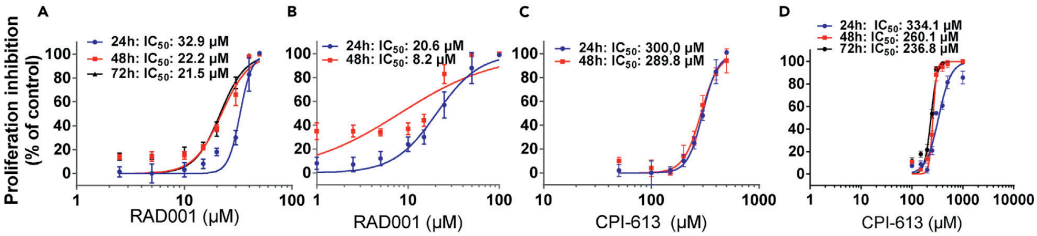

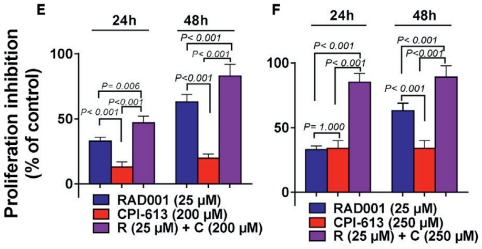

G

BLISS synergy score	5.29	0.83	29.22	13.42
CPI-613 (μM)	200	200	250	250
RAD001 (μM)	25	25	25	25
Duration (h)	24	48	24	48

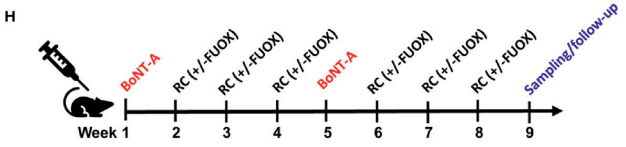

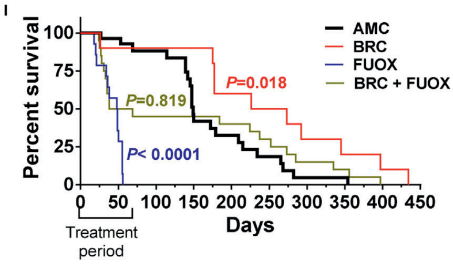

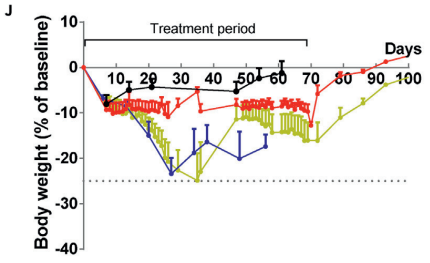

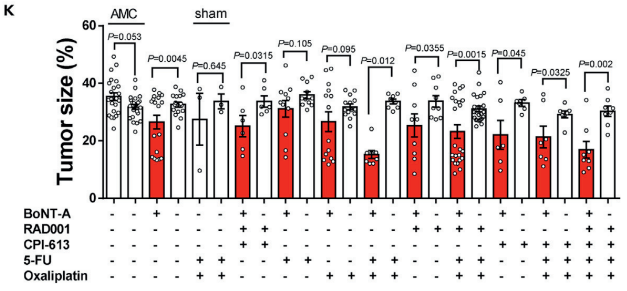

Figure 7. Validation of BRC treatment *in vitro* and *in vivo*

Dose- and time-dependent inhibition of proliferation in response to RAD001 and CPI-613 in MKN74 (A, C) and KATO-III cells (B, D).

Proliferation inhibition of MKN74 cells in response to either RAD001 (25 μM), CPI-613 (200 μM or 250 μM), or combinations at 24–48 h (E-F) with BLISS synergy score for each combination (G).

BLISS score >10 indicates synergistic effect. Mean of n = 3–12 replicates/treatment with SD. Two-way ANOVA between treatments (time x dose).

Proliferation was measured using CCK-8 kit at 450 nm. See also Figures S2 and S4. Timeline for *in vivo* treatment of BoNT-A, RAD001, CPI-613 with and without FUOX over a period of two months (H).

Kaplan-Meier survival curves (I) and body weight change (J) in mouse GC (age 9–15 months) that received more than 1 cycle of treatments of BoNT-A (0.1 U/month) + RAD001 (1.5 mg/kg/day) + CPI-613 (20 mg/kg/week) (BRC), 5-fluorouracil (5 mg/kg/week) + Oxaliplatin (25 mg/kg/week) (FUOX), or BRC + FUOX or no treatment (age-matched control, AMC). Log rank (Mantel-Cox) post hoc test between groups (two-tailed). GraphPad Prism v6.

Tumor size (expressed as volume density in % of glandular area of stomach occupied by tumor) of mouse GC after 2 months treatment with indicated drugs (K). Mean ± SEM with paired t test (AMC: two-tailed, treatments: one-tailed) between anterior (denervated) and posterior (innervated) side of the stomach or non-parametric test as appropriate. Sham: Laparotomy procedure without denervation surgery.

Metabolic gene expression profile in neoplasia is a target site for BRC in clinical trial

Pathogenesis of GC is believed to involve the following cascade: gastritis, atrophy, intestinal metaplasia, dysplasia, and ultimately malignant neoplasms, known as the Correa pathway (Correa, 1992). However, it remains unclear whether metaplasia is a direct precursor of GC, and if so, it should be taken together with neoplasia as targets for treatment of GC (Kinoshita et al., 2017). We have followed-up 17 patients who underwent subtotal or total gastrectomy with radical lymph node dissection, adjuvant chemoradiotherapy, or perioperative chemotherapy for 5 years. We found that patients with high scores of gastric histology activation index (GHAI) had shorter MS than those with low scores, and there was positive correlation between upregulated gene expression and GHAI score and negative correlation between upregulated gene expression profile and OS (Figures 8G–8I). Furthermore, we found distinct expression profiles in signaling pathways in general and the metabolic gene expression profiles in particular between metaplasia and neoplasia (Figures 8J and 8K), suggesting that the two pathological phenotypes harbored distinct metabolic profiles and that the network of the metabolic genes within the neoplasia should be the potential target. These results supported the rationale of BRC clinical trial.

We next carried out a pilot phase II clinical trial (https://clinicaltrials.gov/ct2/show/NCT01822210?term=BoNT-A+and+gastric+cancer&draw=2&rank=1) in which BoNT-A injection was performed through gastroscopy (without systemic administration of RAD001 plus CPI-613). The purpose of this initial clinical trial was to obtain data needed to calculate sample size in a larger controlled trial. Six enrolled patients were diagnosed as gastric adenocarcinomas with locally non-resectable and/or with distant metastasis and lack of response or non-tolerance to second-line chemotherapy (Table S8. Baseline patient data, Related to Figure 8L). We found that the procedure with BoNT-A injections was well tolerated, without any immediate surgical complications or adverse effects. Injections directly into the tumor were associated with a small amount of bleeding from the injection sites, but the bleeding was self-limited and none of the patients required surgical or endoscopic intervention or blood transfusions. We found that the tumor size was reduced during the first 8 weeks and the tumor growth was stabilized afterward in one of three patients (Figure 8L; Table S9. Primary outcome measures, Related to Figure 8L). All patients were without adverse effects or complications and discharged from hospital the first day after the procedure (Tables S10. Secondary outcome measures (short term), Related to Figure 8L; Table S11. Secondary outcome measures (long-term), Related to Figure 8L). Due to aggressive progression at advanced late-stage disease, four out of six patients did not survive until eight weeks after the BoNT-A injection. Two out of six patients were followed for eight weeks and one patient was followed for 20 weeks after receiving BoNT-A treatment. These results suggested that endoscopic injection of BoNT-A could be safe and BRC can be further tested in GC patients that failed second-line chemotherapy.

DISCUSSION

Vagotomy was used extensively in 70s–80s as a surgical treatment for peptic ulcer, due to its inhibitory effects on gastric acid secretion (Rabben et al., 2016). Inhibition of cholinergic signaling has proved to be a possible therapeutic modality (Magnon et al., 2013) and epidemiological, animal, and clinical studies have shown that vagotomy reduces the risk of GC and suppresses gastric tumorigenesis, most likely through muscarinic cholinergic/acetylcholine receptor 3 (M3R)-mediated WNT signaling, proposed as a nerve-cancer crosstalk (Zhao et al., 2014; Hayakawa et al., 2017; Wang et al., 2018).

Cancer cells exhibit a high rate of glycolysis even in the presence of oxygen, the so-called Warburg effect, which has been well recognized as a form of metabolic reprogramming (Hanahan and Weinberg, 2011; Liberti

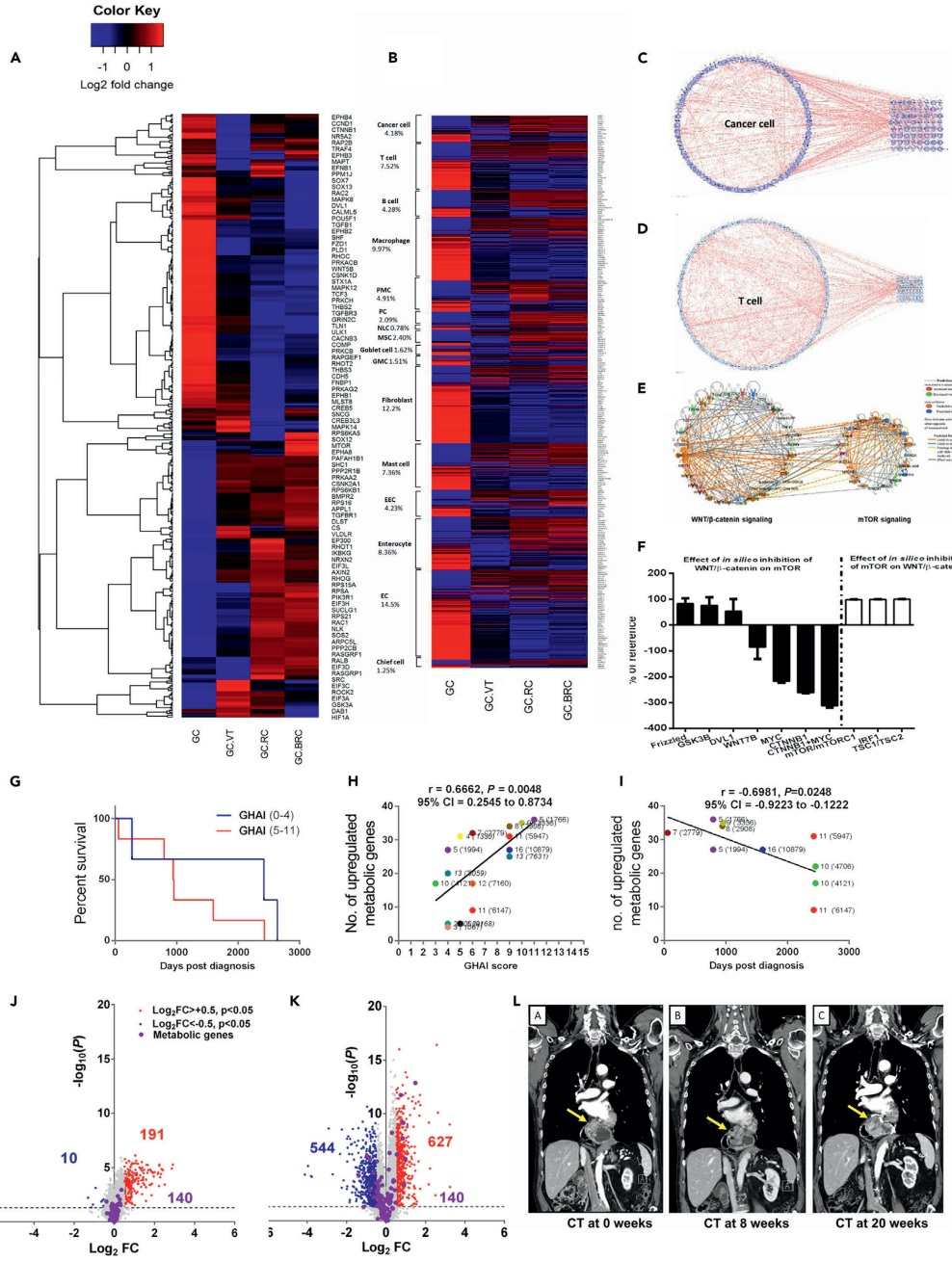
A
Color Key
-1 0 1
Log2 fold change
GC
GC.VT
GC.RC
GC.BRC
B
Cancer cell 4.18%
T cell 7.52%
B cell 4.28%
Macrophage 9.97%
PMC 4.91%
PC 2.09%
NLC 0.78%
MSC 2.40%
Goblet cell 1.62%
GMC 1.51%
Fibroblast 12.2%
Mast cell 7.36%
EEC 4.23%
Enterocyte 8.36%
EC 14.5%
Chief cell 1.25%
C
Cancer cell
D
T cell
E
WNT/β-catenin signaling
mTOR signaling
F
Effect of in silico inhibition of WNT/β-catenin on mTOR
Effect of in silico inhibition of mTOR on WNT/β-catenin
% of reference
Frizzled
GSK3B
DVL1
WNT7B
MYC
CTNNB1
mTORC1
IRF1
TSC1/TSC2
G
GHAI (0-4)
GHAI (5-11)
Percent survival
Days post diagnosis
H
r = 0.6662, P = 0.0048
95% CI = 0.2545 to 0.8734
No. of upregulated metabolic genes
GHAI score
I
r = -0.6981, P=0.0248
95% CI = -0.9223 to -0.1222
no. of upregulated metabolic genes
Days post diagnosis
J
Log2FC>+0.5, p<0.05
Log2FC<-0.5, p<0.05
Metabolic genes
-log10(P)
191
10
140
Log2 FC
K
-log10(P)
544
627
140
Log2 FC
L
A
B
C
CT at 0 weeks
CT at 8 weeks
CT at 20 weeks

Figure 8. Transcriptome profiling of nerve-cancer metabolism pathways and cellular compartments, computational network modeling, *in silico* testing, clinical analysis, and trial in GC

Heatmap of the gene expression profile of pathways including WNT/β-catenin signaling, mTOR signaling, synaptogenesis pathway, and TCA cycle in mouse gastric cancer (GC), GC after VT, RC, or BRC (A). See also Figure S5.

Heatmap of the single-cell transcriptome atlas in mouse GC, GC after VT, RC, or BRC (B). The expression levels of marker genes were analyzed in mouse GC versus WT for each representative cell type according to the single-cell atlas (Zhang et al., 2019, PMID: 31067475, GSE134520). EC, endothelial cell; GMC, antral basal gland mucous cell; EEC, enteroendocrine cell; MSC, metaplastic stem-like cell; PC, proliferative cell; PMC, pit mucous cell; NLC, neck-like cell. Percentages of total number of genes in each cell type are displayed under each cell name (smooth muscle cell not included). Gene expression on $\log_2$ fold scale; blue: downregulated; red: upregulated.

Heatmaps in A–B created in RStudio version 3.5.2 using heatmap.2-function. Computational network modeling (IPA) showing interactions within cancer cell gene cluster (C) and T cell gene cluster (D) and connections between the cell type-specific genes and genes involved in WNT/mTOR/glutaminolysis (C,D). See also Figure S6. *In silico* modeling showing WNT/β-catenin signaling (left) and mTOR signaling (right) clusters of mouse GC utilizing the MAP function in IPA (E).

In silico data inhibition to predict effects of inhibition of WNT/β-catenin signaling pathway intermediates on mTOR network cluster (F, black bars) and *vice versa* (F, white bars). Percentages (in F) are calculated based on semi-quantitative reference values derived from predicted downstream effects generated in IPA. Means of n = 7–14 *in silico* tests/group.

See also Figure S7. Kaplan-Meier survival curves of 17 gastric cancer (GC) patients with low GHAI score (0–4, MS: 2420 days) and high GHAI score (5–11, MS: 949.5 days) (G).

Correlation of number of upregulated metabolic genes in patients diagnosed with gastric adenocarcinoma versus GHAI score (H), and correlation of number of upregulated metabolic genes (corresponding to Figure 2) in patients diagnosed with gastric adenocarcinoma versus survival days (I).

Note: metabolic genes are the same as in Figures 2A–2C. Volcano plots of global gene expression profiles in metaplasia (J) and neoplasia (K) in GC patients. Metabolic genes and interactions are highlighted according to regulation status (blue: downregulated; red: upregulated). Note: metabolic genes are the same as presented in Figures 2A–2C and Data S2. Tumor growth was stabilized after 20 weeks post-BoNT-A endoscopic injection in one patient as shown by CT scan (L).

and Locasale, 2016; Schulze and Harris, 2012; Lunt and Vander Heiden, 2011). In line with our recent understanding of tumor heterogeneity, it seems unlikely that there exists a common "metabolic reprogramming" that describes all cancer cell types and/or tumor types (including both cancer cells and TME) (Cluntun et al., 2017). It has been a dogma that GC is associated with the Warburg effect (Vander Heiden et al., 2009). In the present study, we found that the mouse GC model was well representative of human GC, particularly regarding the metabolic reprogramming, which was not associated with the Warburg effect. By comparisons between WT versus GC mice, which also included a comparison of the innervated side versus denervated sides of the same stomach of WT or GC mice, we found that inhibition of glutaminolysis and restoration of OXPHOS/glycolysis after vagotomy were the likely mechanisms underlying vagotomy-induced suppression of GC tumorigenesis. Thus, the lack of glycolytic metabolite elevations, along with a notable increase of glutaminolytic metabolites and inactivated AMPK signaling in the mouse GC model, led us to suggest that GC is glutamine dependent rather than glucose dependent, given the fact that AMPK signaling is considered to be a demand-driven regulator of glucose uptake and glycolysis (Ye and Medzhitov, 2019). This was in line with previous reports in several other cancer types including triple negative breast cancer (Sherwood et al., 2014; Sethi and Vidal-Puig, 2010; Li and Zhang, 2016; Minkler et al., 2005; Berg et al., 2002). This was also in line with reports of fluorine 18-fluorodeoxyglucose positron tomography (FDG-PET) for GC patients showing a limited value in diagnosis and evaluation, as it is designed based on increased glucose metabolism in tumor (Morgagni et al., 2020; Matzinger et al., 2009; Sprinz et al., 2018).

Through a multi-omics approach, we identified common signaling pathways that were shared between transcriptomics and metabolomics analyses. We found that among nerve-related signaling pathways, synaptogenesis signaling pathway was activated in GC and inhibited after vagotomy. This signaling pathway consists of several components involved with the nerve-cancer axis, including WNT signaling-related molecules, neurexins, neuroligins, EphB, and Trk receptors (Biederer and Stagi, 2008; Rosso et al., 2013). By transcriptomics analysis, we found that vagotomy inhibited WNT/β-catenin signaling and mTOR signaling. The WNT/β-catenin signaling pathway has been demonstrated to play prominent roles during embryonic development and adult tissue homeostasis by maintaining somatic stem cell functions (Fu et al., 2013). The mTORC1 signaling pathway has also been implicated in regulating stem cell functions in multiple tissue types (Zoncu et al., 2011). In homeostatic conditions, these pathways show a fine regulation through feedback mechanisms and are connected at multiple levels involving both upstream and downstream common effectors. For instance, activation of mTORC1 signaling could lead to suppression of WNT/β-catenin signaling through downregulating the FZD level in normal mouse intestines (Zeng et al., 2018). However, the interconnection (or feedback loop) between these two signaling pathways could be dysregulated in the case of cancer. The results of the present study suggested that the WNT/β-catenin signaling regulated the mTOR pathway in GC and might be an upstream driver of the mTOR pathway in GC. Both pathways

were suppressed by vagotomy in GC and even more so by RAD001 (inhibition of mTOR) and CPI-613 (inhibition of PDH and α-KGDH). This is in line with the hypothesis that cancer is driven by dysregulated WNT/β-catenin signaling, and the relationship between WNT/β-catenin and mTORC1 pathways is so close that they should be considered as a unique therapeutic target (Prossomariti et al., 2020).

The phenotype of gastric tissue after vagotomy in GC mice appeared to be "normal" in terms of histology (Zhao et al., 2014) and metabolic profile (this study), which was associated with the signaling pathways such as the TCA cycle, protein kinase A signaling, calcium signaling, gap junction signaling, and phospholipases. Thus, these signaling pathways presented in "normalized" tissues would likely not be considered as potential therapeutic targets. Using a network integration approach for drug-target interaction prediction and computational drug repositioning, we predicted that targeting mTOR with RAD001 (everolimus), PDP1/α-KGDH with CPI-613, and SNAP25 with BoNT-A as BRC therapy would inhibit the downstream factors of signaling pathways including proteins, microRNA, and metabolites and lead to therapeutic outcomes. Indeed, the results of the present study showed that the therapeutic effects of either RC or BRC were associated with downregulation of glutaminolysis-WNT-mTOR-c-MYC signaling pathway in the cancer cells as well as the TME. It should be noticed that the metabolic reprogramming took place in the neoplasia but not in the metaplasia in patients, supporting that (1) the metabolic reprogramming is reflected by cancer cells as well as TME; (2) that the metabolic properties evolve during tumor progression, and (3) that the site of neoplasia is ideal location for injection of BoNT-A.

Recent findings in immunometabolism have shown that the effects of cancer cell metabolism on the TME may involve direct modulation of essential T cell metabolic pathways and activities and suggested a "metabolic checkpoint" for tumor immunotherapy, in which effector T cells responded to glutamine antagonism by markedly upregulating oxidative metabolism and adopting a long-lived, highly activated phenotype (Leone et al., 2019). It was also reported that inhibiting glutamine metabolism of myeloid-derived suppressor cells (MDSCs) led to activation-induced cell death and conversion of MDSCs to inflammatory macrophages and suggested that myeloid cells comprised a major component of TME, promoting tumor growth and immune evasion (Oh et al., 2020). The success of immunotherapy in GC has to date been limited in part by the lack of knowledge on gastric-specific TME (Subhash et al., 2015). A recent study showed that a gastric-specific TME atlas consisted of the gene expression pattern in connection with a variety of resident and infiltrating host cells (such as endothelial cells, enterocytes, chief cells, antral basal gland cells, metaplastic stem-like cells, pit mucous cells, enteroendocrine cells, fibroblasts, T cells, B cells, mast cells, and microphages) (Zhang et al., 2019). According to the atlas, the results of the present study further showed that the gene expression of immune/inflammatory cells, such as T cells, B cells, macrophages, and mast cells in TME of GC was reversed together with the metabolic reprogramming after vagotomy or RC or BRC. Presumably, the therapeutic strategy should be to enhance the robustness of GC immunotherapy by the "nerve-cancer metabolism therapy" that was presented in the present study.

GC accounts for the third highest cancer-related disability-adjusted life-years (DALYs) after lung and liver cancers (Collaborators, 2020), in addition to its high incidence and mortality. Although *H. pylori* infection is declining, the trends toward increased obesity and aging of the population will likely result in a continued high incidence of GC. Thus, less invasive and better tolerated therapies need to be developed for the treatment of elderly patients with GC. Based on the successful progress in the treatment of gastric cancer in Japan over the last 50 years, it was suggested that endoscopic submucosal dissection (ESD) combined with "gentler" chemotherapy or immunotherapy could be applied to more than half of the GC patients (Sasako, 2020). The results of the present study indicated that endoscopic submucosal/intratumoral injection of BoNT-A combined with non-cytotoxic chemotherapy could be an ideal therapy for the elderly patients. In the present study, we choose the non-cytotoxic drugs, RAD001 (also known as everolimus) and CPI-613 (also known as devimistat), as they have been well tested in clinical trials for other types of cancer (Kim et al., 2017, 2018; Chung et al., 2016; Pardee et al., 2018; Alistar et al., 2017).

In addition to GC, nerve-cancer crosstalk takes place in other types of cancer, e.g. prostate cancer, colorectal cancer, pancreatic cancer, and breast cancer (Chen and Ayala, 2018; Zahalka et al., 2017; Renz et al., 2018; Dubeykovskaya et al., 2016; Kamiya et al., 2019; Mauffrey et al., 2019). More studies are needed to investigate the underlying mechanisms, along with the metabolic reprogramming and immunometabolism, and to develop the nerve-cancer metabolism therapy.

In conclusion, the nature of the present study was translational in order to develop new treatment that is closely linked with clinical trials. Based on the results of the present study, we suggested that GC (including both the cancer cells and TME) was glutamine dependent with altered neuronal and metabolic signaling pathways; vagotomy and metabolic inhibitors reversed the metabolic reprogramming in GC; WNT-mTOR signaling pathway played an important role in the metabolic switch between oxidative phosphorylation/glycolysis and glutaminolysis in GC; SNAP25, mTOR, PDP1/α-KGDH, and glutaminolysis were potential drug-targets for treatment of GC; and intratumoral injection of BoNT-A with systemic administration of RAD001(everolimus) and CPI-613 (devimistat) can be a potential therapy for GC. The potential therapy was particular for elderly patients with clinical endpoints of increased OS and QoF, which have been established according to the regulation of European Commission. The treatment methods used in the present study were commonly considered having no/little stress and abdominal pain, i.e. injections of BoNT-A (through gastroscopy in patients and laparotomy in mice) and RAD001 and CPI-613 (i.v. in patients and i.p. in mice). In the present study, the long-term follow-up (14 months after starting treatment in mice) showed that OS was 33% without any treatment, 40% with chemotherapy (cytotoxic drugs), but 90% with the new treatment (without cytotoxic drugs).

Limitations of the study

The so-called "metabolic escape" has been suggested as a mechanism by cancer cells to avoid cell death in response to inhibited glutaminolysis. Thus, tumors that suffer from glucose/glutamine starvation frequently activate fatty acid catabolism for survival (Halama et al., 2018; Wise et al., 2008; Li and Zhang, 2016). The results of the present study might suggest that the metabolic escape takes place after vagotomy, leading to an activation of Acetyl-CoA with increased levels of lysolipids and polyunsaturated fatty acids in GC but not in WT mice. Furthermore, acyl carnitine oleoylcarnitine, a long-chain acyl carnitine that accumulates during certain metabolic conditions, such as fasting and nutrient deficiency (Minkler et al., 2005), was increased after vagotomy along with its transporter SLC25A20, probably supporting the notion that acyl carnitines serves to deliver fatty acids to the mitochondria for β-oxidation to produce acetyl-CoA (Berg et al., 2002). Monoacylglycerol 1-stearoylglycerol (1-monostearin) was increased after vagotomy in GC but not in WT mice, probably further suggesting that vagotomy-induced suppression of tumorigenesis was mediated in part through accelerated degradation of diacyl- or triacylglyserols, as well as deoxycarnitine, succinylcarnitine, and 3-dehydrocarnitine. These assumptions need to be further investigated.

Resource availability

Lead contact

Information and requests for resources should be directed to and will be fulfilled by the Lead Contact, Chun-Mei Zhao (chun-mei.zhao@ntnu.no).

Materials availability

This study did not generate new unique reagents.

Data and code availability

All relevant data are available from the Lead Contact upon request. The mouse RNA seq/microarray data (related to Data S1–S3) have been deposited in the NCBI Bioproject database under the accession number PRJNA690520, which can be accessed using the following link: http://www.ncbi.nlm.nih.gov/bioproject/690520, and in the GEO under accession number GSE30295, respectively. The human microarray data (related to Data S1 and S2) are available online via Mendeley Data repository with DOI link at https://doi.org/10.17632/hzmfshy7hp.1.

METHODS

All methods can be found in the accompanying Transparent methods supplemental file.

SUPPLEMENTAL INFORMATION

Supplemental Information can be found online at https://doi.org/10.1016/j.isci.2021.102091.

ACKNOWLEDGMENTS

The authors thank the grant supports by the Liaison Committee between the Central Norway Regional Health Authority (Helse-Midt Norge RHF) and Norwegian University of Science and Technology (NTNU),

Norway (grant numbers 46056636/46056928/90061700/90061701), Joint Program of the Medical Faculty of NTNU and St. Olavs University Hospital, the Cancer Foundation of St. Olavs Hospital (Kreftfondet ved St. Olavs hospital), and the technical support by Genomics Core Facility (GCF), which is funded by the Faculty of Medicine and Health Sciences at NTNU and RHF.

AUTHORS CONTRIBUTION

H-L.R. and G.T.A.: *in vitro*, *in vivo*, and *in silico* experiments, sample/data collection and preparation, data analysis and interpretation, writing manuscript. M.K.O.: *in vivo*, experiments, writing manuscript. A.I. and D.K.: data visualization and drug synergy prediction, writing manuscript. A.Ø.: *in vitro* experiments, writing manuscript. T.C.W.: data acquisitioning, writing manuscript. S.L.: clinical interpretation, writing manuscript. J.E.G.: clinical samples and data collection, writing manuscript. D.C.: project concept, study idea and design, data analysis and interpretation, writing manuscript. C-M.Z.: project concept, study idea and design, lab and clinical experiments, data interpretation, writing manuscript.

DECLARATION OF INTERESTS

The authors declare no competing interests.

Received: September 2, 2020
Revised: November 23, 2020
Accepted: January 18, 2021
Published: February 19, 2021

REFERENCES

Alistar, A., Morris, B.B., Desnoyer, R., Klepin, H.D., Hosseinzadeh, K., Clark, C., Cameron, A., Leyendecker, J., D'agostino, R., Jr., Topaloglu, U., et al. (2017). Safety and tolerability of the first-in-class agent CPI-613 in combination with modified FOLFIRINOX in patients with metastatic pancreatic cancer: a single-centre, open-label, dose-escalation, phase 1 trial. Lancet Oncol. *18*, 770–778.

Berg, J.M., Tymoczko, J.L., and Stryer, L. (2002). Biochemistry: The Utilization of Fatty Acids as Fuel Requires Three Stages of Processing (W.H.Freeman & Co Ltd).

Biederer, T., and Stagi, M. (2008). Signaling by synaptogenic molecules. Curr. Opin. Neurobiol. *18*, 261–269.

Chen, D., and Ayala, G.E. (2018). Innervating prostate cancer. N. Engl. J. Med. *378*, 675–677.

Chung, V., Frankel, P., Lim, D., Yeon, C., Leong, L., Chao, J., Ruel, N., Luevanos, E., Koehler, S., Chung, S., et al. (2016). Phase Ib trial of mFOLFOX6 and everolimus (NSC-733504) in patients with metastatic gastroesophageal adenocarcinoma. Oncology *90*, 307–312.

Cluntun, A.A., Lukey, M.J., Cerione, R.A., and Locasale, J.W. (2017). Glutamine metabolism in cancer: understanding the heterogeneity. Trends Cancer *3*, 169–180.

Collaborators, G.B.D.S.C. (2020). The global, regional, and national burden of stomach cancer in 195 countries, 1990-2017: a systematic analysis for the Global Burden of Disease study 2017. Lancet Gastroenterol. Hepatol. *5*, 42–54.

Coller, H.A. (2014). Is cancer a metabolic disease? Am. J. Pathol. *184*, 4–17.

Correa, P. (1992). Human gastric carcinogenesis: a multistep and multifactorial process–first American cancer society award lecture on cancer epidemiology and prevention. Cancer Res. *52*, 6735–6740.

Deberardinis, R.J., and Chandel, N.S. (2016). Fundamentals of cancer metabolism. Sci. Adv. *2*, e1600200.

Dorsam, B., and Fahrer, J. (2016). The disulfide compound alpha-lipoic acid and its derivatives: a novel class of anticancer agents targeting mitochondria. Cancer Lett. *371*, 12–19.

Dressler, D., Saberi, F.A., and Barbosa, E.R. (2005). Botulinum toxin: mechanisms of action. Arq Neuropsiquiatr *63*, 180–185.

Dubeykovskaya, Z., Si, Y., Chen, X., Worthley, D.L., Renz, B.W., Urbanska, A.M., Hayakawa, Y., Xu, T., Westphalen, C.B., Dubeykovskiy, A., et al. (2016). Neural innervation stimulates splenic TFF2 to arrest myeloid cell expansion and cancer. Nat. Commun. *7*, 10517.

Duran, R.V., Oppliger, W., Robitaille, A.M., Heiserich, L., Skendaj, R., Gottlieb, E., and Hall, M.N. (2012). Glutaminolysis activates Rag-mTORC1 signaling. Mol. Cell *47*, 349–358.

Faivre, S., Kroemer, G., and Raymond, E. (2006). Current development of mTOR inhibitors as anticancer agents. Nat. Rev. Drug Discov. *5*, 671–688.

Fox, J.G., and Wang, T.C. (2007). Inflammation, atrophy, and gastric cancer. J. Clin. Invest. *117*, 60–69.

Fu, Y., Huang, B., Shi, Z., Han, J., Wang, Y., Huangfu, J., and Wu, W. (2013). SRSF1 and SRSF9 RNA binding proteins promote Wnt signalling-mediated tumorigenesis by enhancing beta-catenin biosynthesis. EMBO Mol. Med. *5*, 737–750.

Fung, M.K.L., and Chan, G.C.-F. (2017). Drug-induced amino acid deprivation as strategy for cancer therapy. J. Hematol. Oncol. *10*, 144.

Grigoryan, T., Stein, S., Qi, J., Wende, H., Garratt, A.N., Nave, K.A., Birchmeier, C., and Birchmeier, W. (2013). Wnt/Rspondin/beta-catenin signals control axonal sorting and lineage progression in Schwann cell development. Proc. Natl. Acad. Sci. U S A *110*, 18174–18179.

Halama, A., Kulinski, M., Dib, S.S., Zaghlool, S.B., Siveen, K.S., Iskandarani, A., Zierer, J., Prabhu, K.S., Satheesh, N.J., Bhagwat, A.M., et al. (2018). Accelerated lipid catabolism and autophagy are cancer survival mechanisms under inhibited glutaminolysis. Cancer Lett. *430*, 133–147.

Hanahan, D., and Weinberg, R.A. (2011). Hallmarks of cancer: the next generation. Cell *144*, 646–674.

Hayakawa, Y., Sakitani, K., Konishi, M., Asfaha, S., Niikura, R., Tomita, H., Renz, B.W., Tailor, Y., Macchini, M., Middelhoff, M., et al. (2017). Nerve growth factor promotes gastric tumorigenesis through aberrant cholinergic signaling. Cancer Cell *31*, 21–34.

Hirayama, A., Kami, K., Sugimoto, M., Sugawara, M., Toki, N., Onozuka, H., Kinoshita, T., Saito, N., Ochiai, A., Tomita, M., et al. (2009). Quantitative metabolome profiling of colon and stomach cancer microenvironment by capillary electrophoresis time-of-flight mass spectrometry. Cancer Res. *69*, 4918–4925.

Jobling, P., Pundavela, J., Oliveira, S.M., Roselli, S., Walker, M.M., and Hondermarck, H. (2015). Nerve-cancer cell cross-talk: a novel promoter of tumor progression. Cancer Res. *75*, 1777–1781.

Kahn, M. (2014). Can we safely target the WNT pathway? Nat. Rev. Drug Discov. *13*, 513–532.

Kamiya, A., Hayama, Y., Kato, S., Shimomura, A., Shimomura, T., Irie, K., Kaneko, R., Yanagawa, Y., Kobayashi, K., and Ochiya, T. (2019). Genetic manipulation of autonomic nerve fiber innervation and activity and its effect on breast cancer progression. Nat. Neurosci. *22*, 1289–1305.

Kim, H.S., Shaib, W.L., Zhang, C., Nagaraju, G.P., Wu, C., Alese, O.B., Chen, Z., Brutcher, E., Renfroe, M., and El-Rayes, B.F. (2018). Phase 1b study of pasireotide, everolimus, and selective internal radioembolization therapy for unresectable neuroendocrine tumors with hepatic metastases. Cancer *124*, 1992–2000.

Kim, S.T., Lee, J., Park, S.H., Park, J.O., Park, Y.S., Kang, W.K., and Lim, H.Y. (2017). Prospective phase II trial of everolimus in PIK3CA amplification/mutation and/or PTEN loss patients with advanced solid tumors refractory to standard therapy. BMC Cancer *17*, 211.

Kinoshita, H., Hayakawa, Y., and Koike, K. (2017). Metaplasia in the stomach-precursor of gastric cancer? Int. J. Mol. Sci. *18*, 2063.

Lee, K.C., Maturo, C., Perera, C.N., Luddy, J., Rodriguez, R., and Shorr, R. (2014). Translational assessment of mitochondrial dysfunction of pancreatic cancer from in vitro gene microarray and animal efficacy studies, to early clinical studies, via the novel tumor-specific anti-mitochondrial agent, CPI-613. Ann. Transl Med. *2*, 91.

Leone, R.D., Zhao, L., Englert, J.M., Sun, I.M., Oh, M.H., Sun, I.H., Arwood, M.L., Bettencourt, I.A., Patel, C.H., Wen, J., et al. (2019). Glutamine blockade induces divergent metabolic programs to overcome tumor immune evasion. Science *366*, 1013–1021.

Li, Z., and Zhang, H. (2016). Reprogramming of glucose, fatty acid and amino acid metabolism for cancer progression. Cell Mol. Life Sci. *73*, 377–392.

Liao, G.Y., Lee, M.T., Fan, J.J., Hsiao, P.W., Lee, C.S., Su, S.Y., Hwang, J.J., and Ke, F.C. (2019). Blockage of glutamine-dependent anaplerosis affects mTORC1/2 activity and ultimately leads to cellular senescence-like response. Biol. Open *8*, bio038257.

Liberti, M.V., and Locasale, J.W. (2016). The Warburg effect: how does it benefit cancer cells? Trends Biochem. Sci. *41*, 211–218.

Loponte, S., Lovisa, S., Deem, A.K., Carugo, A., and Viale, A. (2019). The many facets of tumor heterogeneity: is metabolism lagging behind? Cancers (Basel) *11*, 1574.

Lunt, S.Y., and Vander Heiden, M.G. (2011). Aerobic glycolysis: meeting the metabolic requirements of cell proliferation. Annu. Rev. Cell Dev. Biol. *27*, 441–464.

Magnon, C., Hall, S.J., Lin, J., Xue, X., Gerber, L., Freedland, S.J., and Frenette, P.S. (2013). Autonomic nerve development contributes to prostate cancer progression. Science *341*, 1236361.

Matsuda, T., and Saika, K. (2013). The 5-year relative survival rate of stomach cancer in the USA, Europe and Japan. Jpn. J. Clin. Oncol. *43*, 1157–1158.

Matzinger, O., Gerber, E., Bernstein, Z., Maingon, P., Haustermans, K., Bosset, J.F., Gulyban, A., Poortmans, P., Collette, L., and Kuten, A. (2009). EORTC-ROG expert opinion: radiotherapy volume and treatment guidelines for neoadjuvant radiation of adenocarcinomas of the gastroesophageal junction and the stomach. Radiother. Oncol. *92*, 164–175.

Mauffrey, P., Tchitchek, N., Barroca, V., Bemelmans, A., Firlej, V., Allory, Y., Romeo, P.H., and Magnon, C. (2019). Progenitors from the central nervous system drive neurogenesis in cancer. Nature *569*, 672–678.

Minkler, P.E., Kerner, J., North, K.N., and Hoppel, C.L. (2005). Quantitation of long-chain acylcarnitines by HPLC/fluorescence detection: application to plasma and tissue specimens from patients with carnitine palmitoyltransferase-II deficiency. Clin. Chim. Acta *352*, 81–92.

Morgagni, P., Bencivenga, M., Colciago, E., Tringali, D., Giacopuzzi, S., Framarini, M., Saragoni, L., Mura, G., Graziosi, L., Marino, E., et al. (2020). Limited usefulness of 18F-FDG PET/CT in predicting tumor regression after preoperative chemotherapy for noncardia gastric cancer: the Italian research group for gastric cancer (GIRCG) experience. Clin. Nucl. Med. *45*, 177–181.

Naumann, M., and Jankovic, J. (2004). Safety of botulinum toxin type A: a systematic review and meta-analysis. Curr. Med. Res. Opin. *20*, 981–990.

Oh, M.H., Sun, I.H., Zhao, L., Leone, R.D., Sun, I.M., Xu, W., Collins, S.L., Tam, A.J., Blosser, R.L., Patel, C.H., et al. (2020). Targeting glutamine metabolism enhances tumor specific immunity by modulating suppressive myeloid cells. J. Clin. Invest. *130*, 3865–3884.

Pardee, T.S., Anderson, R.G., Pladna, K.M., Isom, S., Ghiraldeli, L.P., Miller, L.D., Chou, J.W., Jin, G., Zhang, W., Ellis, L.R., et al. (2018). A phase I study of CPI-613 in combination with high-dose cytarabine and mitoxantrone for relapsed or refractory acute myeloid leukemia. Clin. Cancer Res. *24*, 2060–2073.

Pardee, T.S., Lee, K., Luddy, J., Maturo, C., Rodriguez, R., Isom, S., Miller, L.D., Stadelman, K.M., Levitan, D., Hurd, D., et al. (2014). A phase I study of the first-in-class antimitochondrial metabolism agent, CPI-613, in patients with advanced hematologic malignancies. Clin. Cancer Res. *20*, 5255–5264.

Parkin, D.M., Bray, F., Ferlay, J., and Pisani, P. (2005). Global cancer statistics, 2002. CA Cancer J. Clin. *55*, 74–108.

Pavlova, N.N., and Thompson, C.B. (2016). The emerging hallmarks of cancer metabolism. Cell Metab. *23*, 27–47.

Prossomariti, A., Piazzi, G., Alquati, C., and Ricciardiello, L. (2020). Are Wnt/beta-catenin and PI3K/AKT/mTORC1 distinct pathways in colorectal cancer? Cell Mol. Gastroenterol. Hepatol. *10*, 491–506.

Rabben, H.L., Zhao, C.M., Hayakawa, Y., Wang, T.C., and Chen, D. (2016). Vagotomy and gastric tumorigenesis. Curr. Neuropharmacol. *14*, 967–972.

Rawla, P., and Barsouk, A. (2019). Epidemiology of gastric cancer: global trends, risk factors and prevention. Prz Gastroenterol. *14*, 26–38.

Renz, B.W., Takahashi, R., Tanaka, T., Macchini, M., Hayakawa, Y., Dantes, Z., Maurer, H.C., Chen, X., Jiang, Z., Westphalen, C.B., et al. (2018). beta2 adrenergic-neurotrophin feedforward loop promotes pancreatic cancer. Cancer Cell *33*, 75–90.e7.

Rosso, S., Inestrosa, N., and Rosso, S. (2013). WNT signaling in neuronal maturation and synaptogenesis. Front. Cell Neurosci. *7*, 103.

Sanderson, S.M., Gao, X., Dai, Z., and Locasale, J.W. (2019). Methionine metabolism in health and cancer: a nexus of diet and precision medicine. Nat. Rev. Cancer *19*, 625–637.

Sasako, M. (2020). Progress in the treatment of gastric cancer in Japan over the last 50 years. Ann. Gastroenterol. Surg. *4*, 21–29.

Schulze, A., and Harris, A.L. (2012). How cancer metabolism is tuned for proliferation and vulnerable to disruption. Nature *491*, 364–373.

Sethi, J.K., and Vidal-Puig, A. (2010). Wnt signalling and the control of cellular metabolism. Biochem. J. *427*, 1–17.

Seyfried, T.N., Flores, R.E., Poff, A.M., and D'agostino, D.P. (2014). Cancer as a metabolic disease: implications for novel therapeutics. Carcinogenesis *35*, 515–527.

Sherwood, V., Chaurasiya, S.K., Ekstrom, E.J., Guilmain, W., Liu, Q., Koeck, T., Brown, K., Hansson, K., Agnarsdottir, M., Bergqvist, M., et al. (2014). WNT5A-mediated beta-catenin-independent signalling is a novel regulator of cancer cell metabolism. Carcinogenesis *35*, 784–794.

Shimobayashi, M., and Hall, M.N. (2014). Making new contacts: the mTOR network in metabolism and signalling crosstalk. Nat. Rev. Mol. Cell Biol. *15*, 155–162.

Smith, R.L., Soeters, M.R., Wüst, R.C.I., and Houtkooper, R.H. (2018). Metabolic flexibility as an adaptation to energy resources and requirements in health and disease. Endocr. Rev. *39*, 489–517.

Sprinz, C., Altmayer, S., Zanon, M., Watte, G., Irion, K., Marchiori, E., and Hochhegger, B. (2018). Effects of blood glucose level on 18F-FDG uptake for PET/CT in normal organs: a systematic review. PLoS One *13*, e0193140.

Stuart, S.D., Schauble, A., Gupta, S., Kennedy, A.D., Keppler, B.R., Bingham, P.M., and Zachar, Z. (2014). A strategically designed small molecule attacks alpha-ketoglutarate dehydrogenase in tumor cells through a redox process. Cancer Metab. *2*, 4.

Subhash, V.V., Yeo, M.S., Tan, W.L., and Yong, W.P. (2015). Strategies and advancements in harnessing the immune system for gastric cancer immunotherapy. J. Immunol. Res. *2015*, 308574.

Uefuji, K., Ichikura, T., and Mochizuki, H. (2000). Cyclooxygenase-2 expression is related to prostaglandin biosynthesis and angiogenesis in human gastric cancer. Clin. Cancer Res. *6*, 135–138.

Vander Heiden, M.G., Cantley, L.C., and Thompson, C.B. (2009). Understanding the Warburg effect: the metabolic requirements of cell proliferation. Science *324*, 1029–1033.

Vander Heiden, M.G., and Deberardinis, R.J. (2017). Understanding the intersections between metabolism and cancer biology. Cell *168*, 657–669.

Wang, D., and Dubois, R.N. (2018). Role of prostanoids in gastrointestinal cancer. J. Clin. Invest. *128*, 2732–2742.

Wang, L., Xu, J., Xia, Y., Yin, K., Li, Z., Li, B., Wang, W., Xu, H., Yang, L., and Xu, Z. (2018). Muscarinic acetylcholine receptor 3 mediates vagus nerve-induced gastric cancer. Oncogenesis *7*, 88.

Wang, T.C., Koh, T.J., Varro, A., Cahill, R.J., Dangler, C.A., Fox, J.G., and Dockray, G.J. (1996). Processing and proliferative effects of human progastrin in transgenic mice. J. Clin. Invest. *98*, 1918–1929.

Whiteside, T.L. (2008). The tumor microenvironment and its role in promoting tumor growth. Oncogene *27*, 5904–5912.

Wise, D.R., Deberardinis, R.J., Mancuso, A., Sayed, N., Zhang, X.Y., Pfeiffer, H.K., Nissim, I., Daikhin, E., Yudkoff, M., Mcmahon, S.B., et al. (2008). Myc regulates a transcriptional program that stimulates mitochondrial glutaminolysis and leads to glutamine addiction. Proc. Natl. Acad. Sci. U S A *105*, 18782–18787.

Wishart, D.S. (2015). Is cancer a genetic disease or a metabolic disease? EBioMedicine *2*, 478–479.

Ye, J., and Medzhitov, R. (2019). Control strategies in systemic metabolism. Nat. Metab. *1*, 947–957.

Yoshida, G.J. (2015). Metabolic reprogramming: the emerging concept and associated therapeutic strategies. J. Exp. Clin. Cancer Res. *34*, 111.

Zachar, Z., Marecek, J., Maturo, C., Gupta, S., Stuart, S.D., Howell, K., Schauble, A., Lem, J., Piramzadian, A., Karnik, S., et al. (2011). Non-redox-active lipoate derivates disrupt cancer cell mitochondrial metabolism and are potent anticancer agents in vivo. J. Mol. Med. (Berl) *89*, 1137–1148.

Zahalka, A.H., Arnal-Estape, A., Maryanovich, M., Nakahara, F., Cruz, C.D., Finley, L.W.S., and Frenette, P.S. (2017). Adrenergic nerves activate an angio-metabolic switch in prostate cancer. Science *358*, 321–326.

Zahalka, A.H., and Frenette, P.S. (2020). Nerves in cancer. Nat. Rev. Cancer *20*, 143–157.

Zeng, H., Lu, B., Zamponi, R., Yang, Z., Wetzel, K., Loureiro, J., Mohammadi, S., Beibel, M., Bergling, S., Reece-Hoyes, J., et al. (2018). mTORC1 signaling suppresses Wnt/beta-catenin signaling through DVL-dependent regulation of Wnt receptor FZD level. Proc. Natl. Acad. Sci. U S A *115*, E10362–E10369.

Zhang, P., Yang, M., Zhang, Y., Xiao, S., Lai, X., Tan, A., Du, S., and Li, S. (2019). Dissecting the single-cell transcriptome network underlying gastric premalignant lesions and early gastric cancer. Cell Rep. *27*, 1934–1947 e5.

Zhang, S., Li, Y., Wu, Y., Shi, K., Bing, L., and Hao, J. (2012). Wnt/beta-catenin signaling pathway upregulates c-Myc expression to promote cell proliferation of P19 teratocarcinoma cells. Anat. Rec. (Hoboken) *295*, 2104–2113.

Zhao, C.M., Hayakawa, Y., Kodama, Y., Muthupalani, S., Westphalen, C.B., Andersen, G.T., Flatberg, A., Johannessen, H., Friedman, R.A., Renz, B.W., et al. (2014). Denervation suppresses gastric tumorigenesis. Sci. Transl. Med. *6*, 250ra115.

Zoncu, R., Efeyan, A., and Sabatini, D.M. (2011). mTOR: from growth signal integration to cancer, diabetes and ageing. Nat. Rev. Mol. Cell Biol. *12*, 21–35.

iScience, Volume *24*

Supplemental Information

Neural signaling modulates metabolism of gastric cancer

Hanne-Line Rabben, Gøran Troseth Andersen, Magnus Kringstad Olsen, Anders Øverby, Aleksandr Ianevski, Denis Kainov, Timothy Cragin Wang, Steinar Lundgren, Jon Erik Grønbech, Duan Chen, and Chun-Mei Zhao

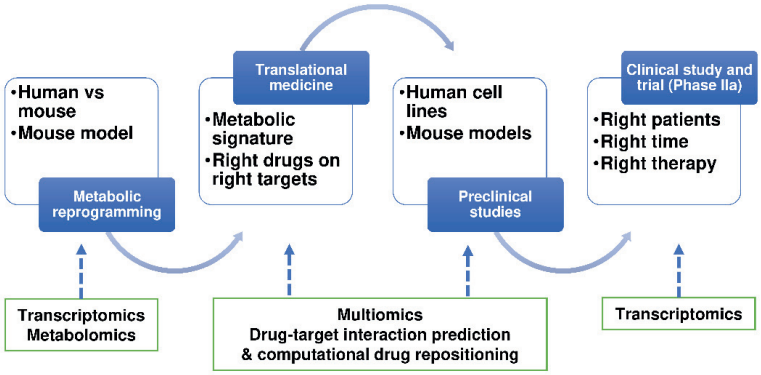

Figure S1, Study design, related to Figure 1: Drawing showing study design of translational research approach and methodology used (indicated in arrows).

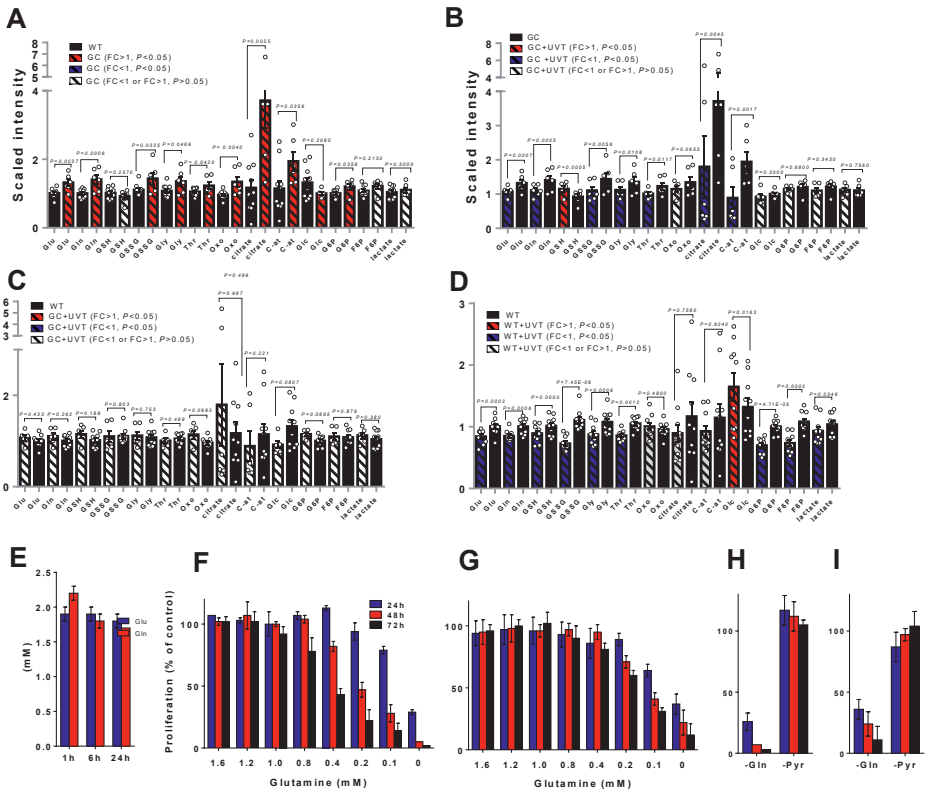

Figure S2, Gastric cancer is glutamine-dependent, related to Figure 4: Levels of metabolites in mouse gastric cancer (GC) (marked in black), wild-type WT (blue), GC after vagotomy (VT) (red) and WT after vagotomy (VT) (purple)(**A-D**) related to **Figure 4.** Glu: L-glutamate; Gln: L-glutamine; GSH: reduced glutathione; GSSG: oxidized glutathione; Gly: glycine; Thr: threonine; Oxo: 5-oxoproline; C-at: cis-aconitate; Glc: glucose; G6P: glucose-6-phosphate; F6P: fructose-6-phosphate. Bars represent relative scaled intensities with SEM and one-way ANOVA p-values. The values were as same as ones in **Figure. 4B-N.** For detailed information, see Table S6. Endogenous levels of L-glutamate and L-glutamine in gastric cancer cells AGS during culture period from 1 to 24 hrs (**E**). Gln reduction (**F,G**) and Gln or Pyr depletion (**H,I**) in the medium in AGS (**F,H**) and MKN45 (**G,I**) cell culture periods of 24, 48 and 72 hrs. Mean of n=3-12 replicates/treatment with SD. Proliferation was assessed using Cell count reagent SF and cell proliferation was calculated relative to controls.

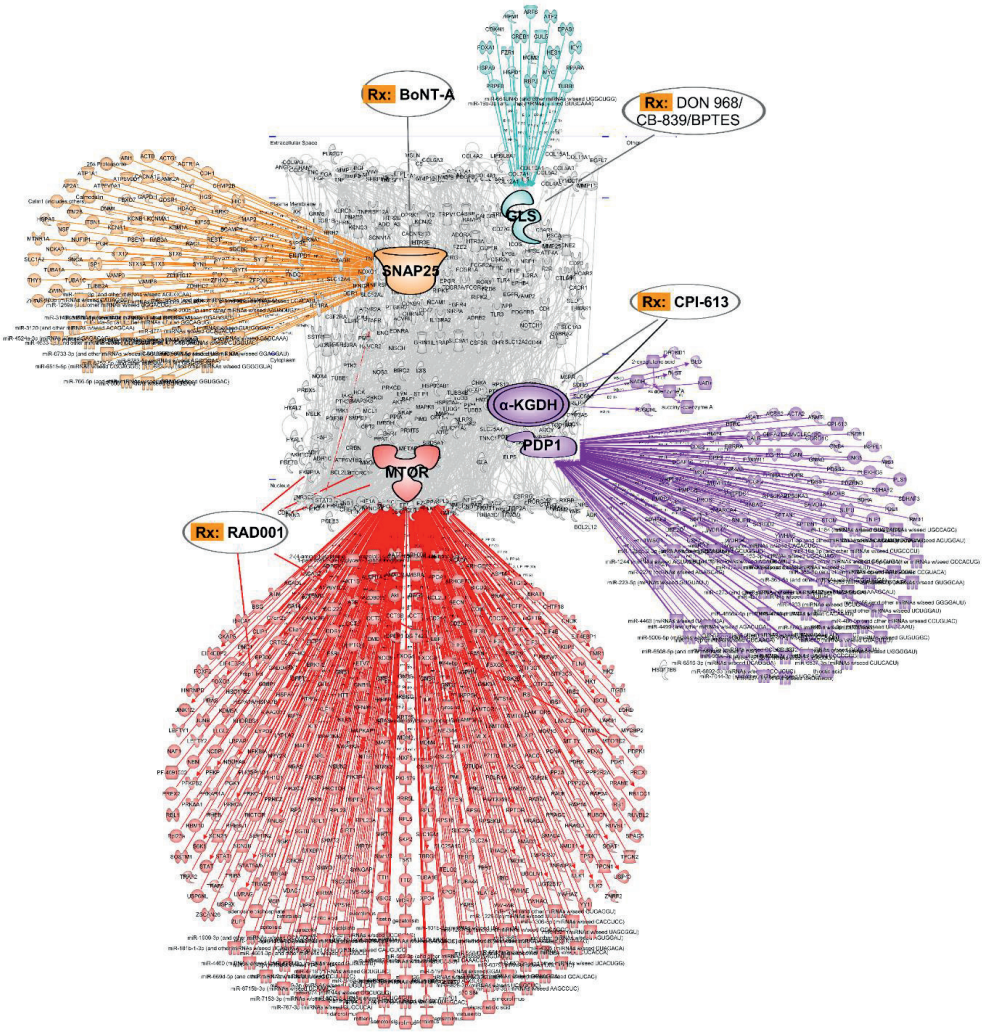

Figure S3, Drug target prediction, related to Figure 6: Waterdrop diagrams showing drug-target interaction prediction and computational drug repositioning in human GC. Note: nodes of RAD001-targeted mTOR (marked in red), CPI-613-targeted PDP1 and α-KGDH (also known as OGDH, purple), BoNT-A-targeted SNAP25 (yellow) and L-DON/968/CB-839/BPTES-targeted GLS (light blue). Lines represent biological interactions between molecules that include proteins, genes, mRNAs, microRNA, lncRNAs and metabolites, generated from differentially expressed drug target genes (only drug targets differentially expressed at $p<0.05$, $q<0.05$ are shown).

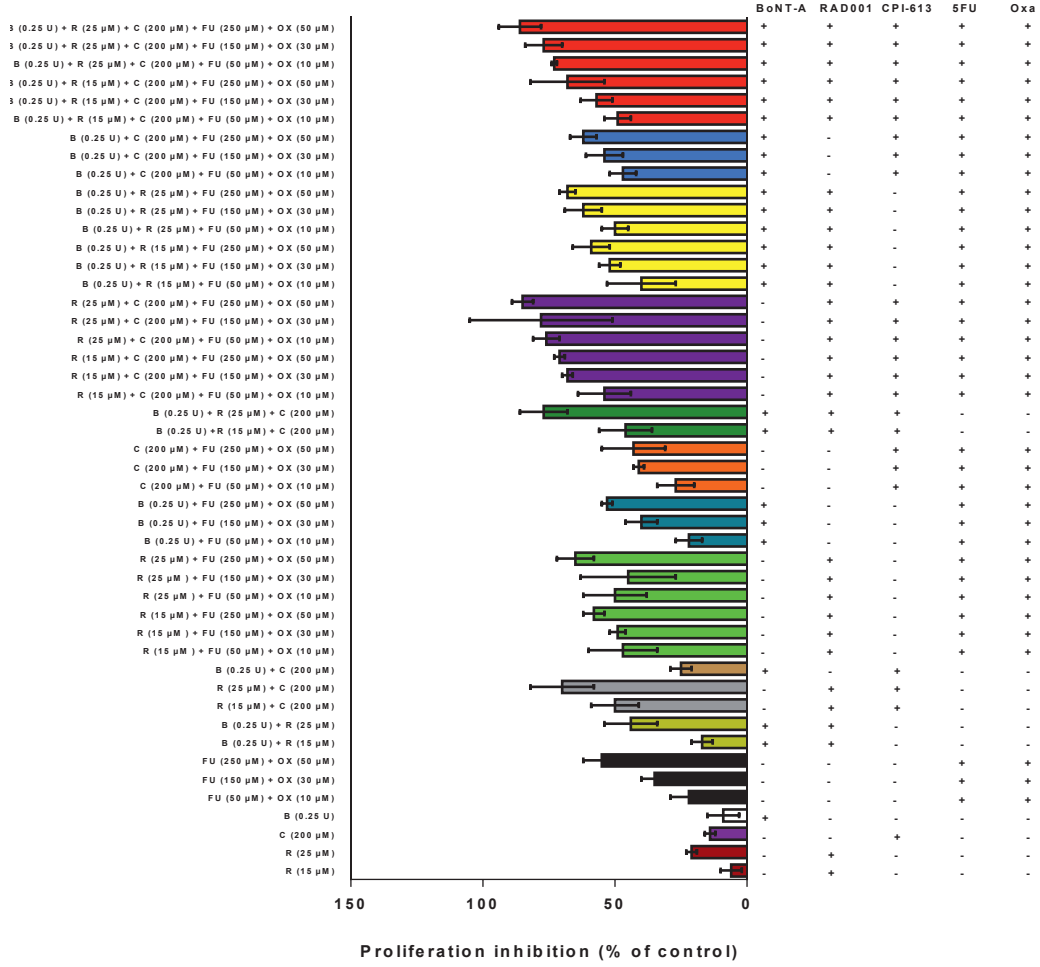

Figure S4, *In vitro* drug screening, related to Figure 7: Proliferation inhibition rates of *in vitro* treatment of BoNT-A, RAD001, CPI-613, 5-FU and oxaliplatin either alone or in different combinations at increasing doses using MKN74 cells. Mean of n=3-12 replicates/treatment with SD. Proliferation was measured using CCK-8 Kit at 450 nm and treatments were normalized to respective vehicle controls.

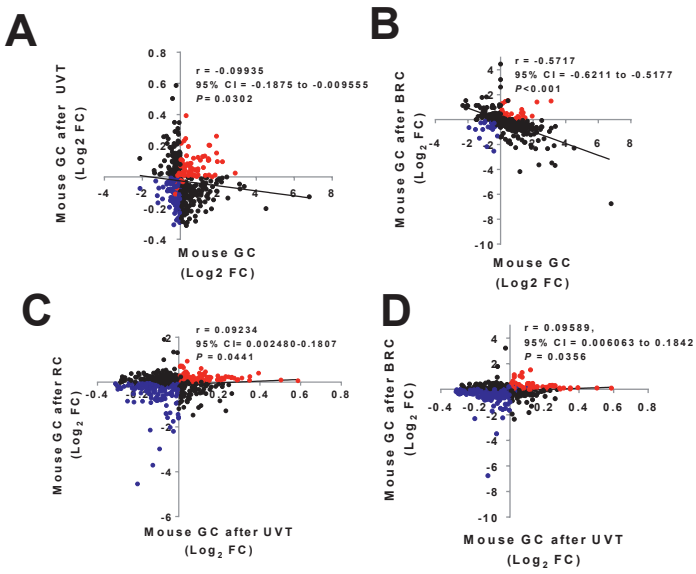

Figure S5, Nerve-cancer metabolism in gastric cancer, related to Figure 8A: Transcriptome profiling of genes involved in the nerve-cancer metabolism pathways of synaptogenesis signaling pathway, WNT/β-catenin signaling, mTOR pathway and energy metabolism. Correlations between mouse GC with *vs.* without unilateral vagotomy (UVT)(**A**), between mouse GC with *vs.* without BRC (**B**), between mouse GC with RC *vs.* UVT (**C**), and between mouse GC with BRC *vs.* UVT (**D**). Linear regression lines were drawn using GraphPad Prism v6. Pearson's test for correlation was used.

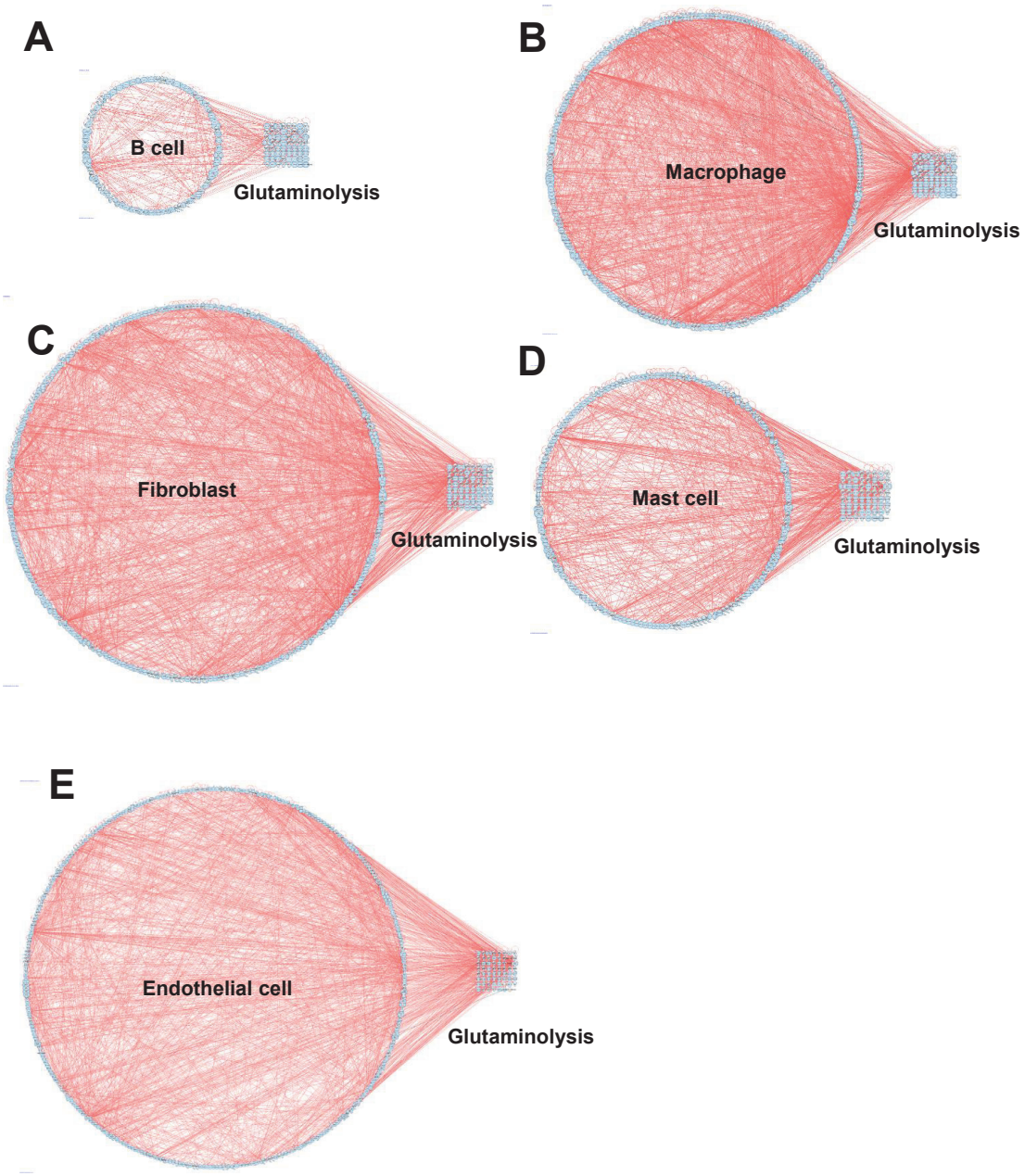

Figure S6, Single-cell atlas and glutamine pathways, related to Figure 8C-D: Computational network modeling showing interactions within B cell gene markers (**A**), macrophage gene markers (**B**), fibroblast gene markers (**C**), mast cell gene markers (**D**) and endothelial cell gene markers (**E**) and connections between the cell types and glutaminolysis (**A-E**) based the single-cell transcriptome atlas (Zhang et al., 2019)(GSE134520).

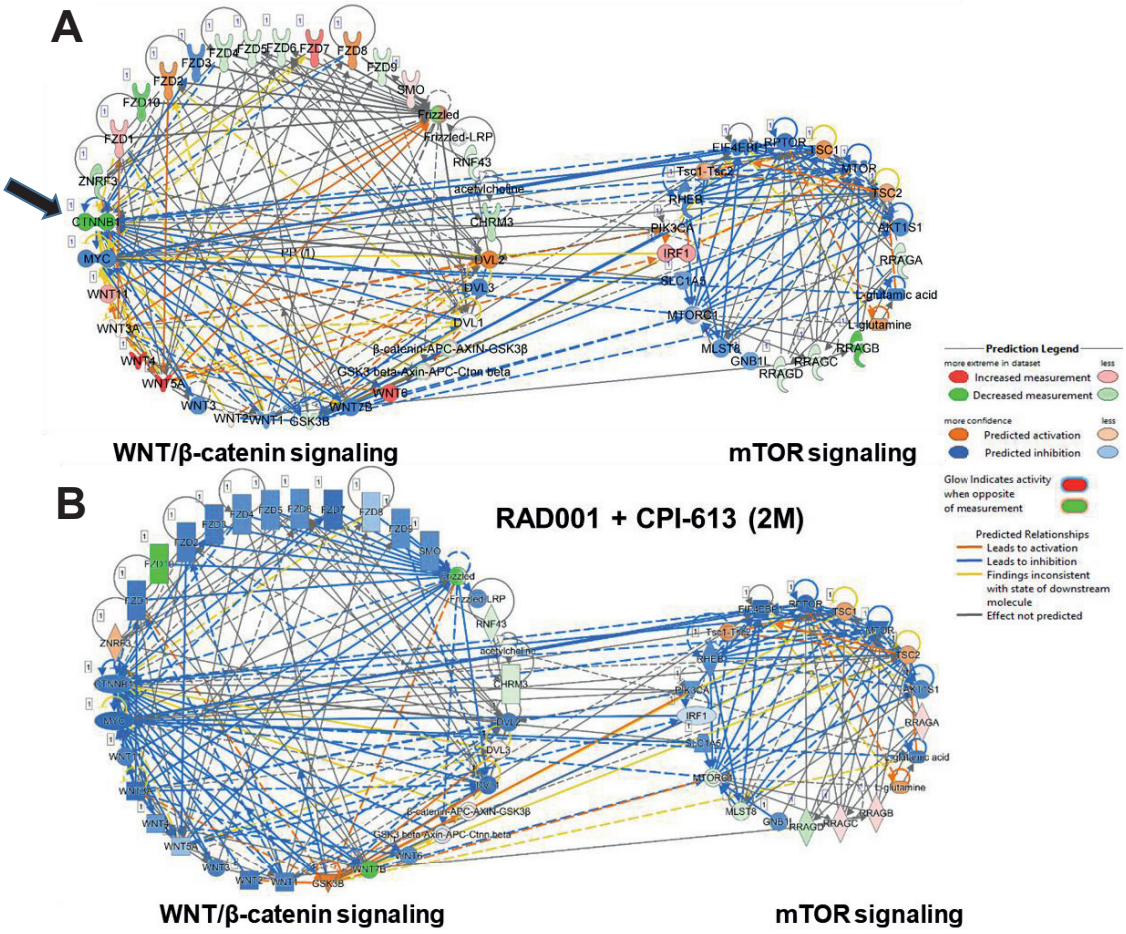

Figure S7, *In silico* modelling, related to Figure 8: Representative prediction of downstream effect of *in silico* inhibition of the CTNNB1 node (marked in green and annotated by black arrow) in the WNT signaling cluster (left) on mTOR signaling (right)(**A**) and effects of treatment of RC for 2 months (2M) on WNT/β-catenin signaling pathway and mTOR signaling clusters (**B**). Overlay gene expression: GC *vs.* WT. MAP (molecular activity prediction) to generate predictions. Semi-quantitative method: dark blue represent -2, light blue represent -1, white represent 0, light orange represent +1 and dark orange represent +2.

Table S1, Genes detected by real-time PCR and RNAseq, related to Figure 1: List of genes detected by both RNAseq and real-time PCR and correlation analysis (figure).

	GenBank	Gene		GenBank	Gene
1	**NM_010347**	Aes	54	**NM_133955**	Rhou
2	**NM_007462**	Apc	55	**NM_029457**	Senp2
3	**NM_009733**	Axin1	56	**NM_013834**	Sfrp1
4	**NM_029933**	Bcl9	57	**NM_009144**	Sfrp2
5	**NM_009771**	Btrc	58	**NM_016687**	Sfrp4
6	**NM_023465**	Ctnnbip1	59	**NM_012030**	Slc9a3r1
7	**NM_007631**	Ccnd1	60	**NM_011441**	Sox17
8	**NM_009829**	Ccnd2	61	**NM_009309**	T
9	**NM_007632**	Ccnd3	62	**NM_009332**	Tcf3
10	**NM_146087**	Csnk1a1	63	**NM_009331**	Tcf7
11	**NM_139059**	Csnk1d	64	**NM_011599**	Tle1
12	**NM_007788**	Csnk2a1	65	**NM_019725**	Tle2
13	**NM_013502**	Ctbp1	66	**NM_011915**	Wif1
14	**NM_009980**	Ctbp2	67	**NM_018865**	Wisp1
15	**NM_007614**	Ctnnb1	68	**NM_021279**	Wnt1
16	**NM_172464**	Daam1	69	**NM_009518**	Wnt10a
17	**NM_178118**	Dixdc1	70	**NM_009519**	Wnt11
18	**NM_010051**	Dkk1	71	**NM_053116**	Wnt16
19	**NM_010091**	Dvl1	72	**NM_023653**	Wnt2
20	**NM_007888**	Dvl2	73	**NM_009520**	Wnt2b
21	**NM_177821**	Ep300	74	**NM_009521**	Wnt3
22	**NM_134015**	Fbxw11	75	**NM_009522**	Wnt3a
23	**NM_013890**	Fbxw2	76	**NM_009523**	Wnt4
24	**NM_013907**	Fbxw4	77	**NM_009524**	Wnt5a
25	**NM_010202**	Fgf4	78	**NM_009525**	Wnt5b
26	**NM_010235**	Fosl1	79	**NM_009526**	Wnt6
27	**NM_008238**	Foxn1	80	**NM_009527**	Wnt7a
28	**NM_008043**	Frat1	81	**NM_009528**	Wnt7b
29	**NM_011356**	Frzb	82	**NM_009290**	Wnt8a
30	**NM_008045**	Fshb	83	**NM_011720**	Wnt8b
31	**NM_021457**	Fzd1	84	**NM_139298**	Wnt9a
32	**NM_020510**	Fzd2	85	**NM_010368**	Gusb
33	**NM_021458**	Fzd3	86	**NM_013556**	Hprt1
34	**NM_008055**	Fzd4	87	**NM_008302**	Hsp90ab1
35	**NM_022721**	Fzd5	88	**NM_008084**	Gapdh
36	**NM_008056**	Fzd6	89	**NM_007393**	Actb
37	**NM_008057**	Fzd7	90	**SA_00106**	MGDC
38	**NM_008058**	Fzd8	91	**SA_00104**	RTC
39	**NM_019827**	Gsk3b	92	**SA_00104**	RTC
40	**NM_010591**	Jun	93	**SA_00104**	RTC
41	**NM_032396**	Kremen1	94	**SA_00103**	PPC
42	**NM_010703**	Lef1	95	**SA_00103**	PPC
43	**NM_008513**	Lrp5	96	**SA_00103**	PPC
44	**NM_008514**	Lrp6			
45	**NM_010849**	Myc			
46	**NM_027280**	Nkd1			
47	**NM_008702**	Nlk			
48	**NM_011098**	Pitx2			
49	**NM_023638**	Porcn			
50	**NM_019411**	Ppp2ca			
51	**NM_016891**	Ppp2r1a			
52	**NM_009358**	Ppp2r5d			
53	**XM_134865**	Pygo1			

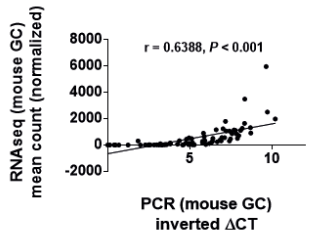

Table S2, Upstream regulators in mouse GC, related to Figure 2F: Upstream analysis of WNT/β-catenin pathway regulators and mTOR targets in mouse GC, related to **Figure 2F.** Predicted Activation State was Activated for z-score>2.000.

Upstream Regulator	Log_2 FC	Predicted Activation State	Activation z-score	p-value of overlap	Target Molecules in Dataset	Target molecules in mTOR pathway	Molecules
Tgf beta		Activated	3.848	2.99E-07	65	0	
WNT1	0.000	Activated	3.138	6.85E-03	34	3	EIF3C,MRAS,PDPK1
CD44	1.156	Activated	3.695	6.05E-08	55	0	
JUN	0.184	Activated	2.219	5.21E-03	55	1	RHOB
TGFB1	0.727	Activated	5.957	2.39E-17	236	3	PPP2CA,PRKCG,RHOA
TGFBR1	-0.536	Activated	2.735	5.98E-04	20	0	
TGFB2	1.573	Activated	3.309	4.55E-11	34	0	
CTNNB1	0.208	Activated	3.741	4.53E-10	165	1	PPP2CA

Table S3, Metabolite signature, related to Figure 4: List of metabolites of gastric cancer (GC) mice and wild-type (WT) mice presented in **Figure 4A.** *GC: gastric cancer; WT: wild-type; FC: Fold change.* Green: p≤0.05, fold change <1.00; Red: p≤ 0.05, fold change ≥1.0. White: p<0.05, 1.0 ≤ fold change >1.0.

Metabolite	Mouse GC *vs.* WT (FC)	Mouse GC after vagotomy *vs.* GC (FC)	Mouse GC after vagotomy *vs.* WT (FC)	Mouse WT after vagotomy *vs.* WT (FC)
prostaglandin B2	4.92	0.54	2.63	0.94
1-arachidonoyl-2-hydroxy-sn-glycero-3-phosphoethanolamine	2.64	0.52	1.36	0.64
inositol 1-phosphate	1.46	0.78	1.14	0.80
docosahexaenoic acid	0.75	1.32	1.00	1.16
gamma-butyrobetaine	0.74	1.22	0.90	1.14
8Z,11Z,14Z-eicosatrienoic acid	0.74	1.45	1.08	0.87
adrenic acid	0.71	1.34	0.95	0.90
13,16-docosadienoic acid	0.65	1.35	0.87	1.06
phosphorylcholine	0.64	1.17	0.75	0.95
propionyl-L-carnitine	0.63	1.71	1.07	1.35
sn-glycero-3-phosphocholine	0.60	1.48	0.89	1.02
arachidonic acid	0.59	1.51	0.88	0.97
icosapent	0.54	1.84	0.99	0.95
1-stearoyl-2-hydroxy-sn-glycero-3-phosphoethanolamine	0.53	1.48	0.79	0.85
cis-4,7,10,13,16-docosapentaenoic acid	0.52	1.64	0.85	1.02
eicosa-11Z, 14Z-dienoic acid	0.51	1.59	0.82	1.01
rac-1-stearoylglycerol	0.47	1.83	0.87	1.09
sn-glycerol-3-phosphate	0.46	1.49	0.69	1.08
3-dehydrocarnitine	0.45	1.11	0.50	0.96
1-palmitoyl-2-hydroxy-sn-glycero-3-phosphoethanolamine	0.44	1.79	0.78	0.91
1-oleoyl-lysophosphatidylethanolamine	0.39	1.82	0.71	0.84
D-sphingosine	0.35	1.87	0.66	0.90
oleoylcarnitine	0.32	2.19	0.71	1.22
citric acid	3.18	0.48	1.54	0.77
cis-aconitic acid	1.70	0.46	0.78	0.81
N-acetyl-L-methionine	2.08	0.59	1.22	0.63
S-glutathionyl-L-cysteine	1.56	0.64	1.00	0.79
L-glutamine	1.40	0.78	1.10	0.85
L-glutamic acid	1.31	0.81	1.06	0.84
glutathione disulfide	1.30	0.77	0.99	0.66
glycine	1.26	0.83	1.04	0.81
L-threonine	1.17	0.82	0.96	0.82
betaine	0.75	1.14	0.86	1.15
5-hydroxytryptamine	0.63	1.36	0.86	1.08
histamine	0.59	1.38	0.81	1.02
gamma-glutamylglutamate	2.15	0.55	1.18	0.83
glycylleucine	1.51	0.82	1.24	0.94
gamma-glutamyl-leucine	1.38	0.76	1.05	1.00
inosine	0.72	1.44	1.03	1.14

deoxyinosine	**0.56**	**1.80**	1.00	**1.63**
guanosine	**0.52**	**1.81**	0.93	**1.55**
deoxyguanosine	**0.46**	**2.36**	1.08	**1.70**
4'-phosphopantetheine	**0.69**	**1.24**	0.86	**0.84**
5-methyltetrahydrofolic acid	**0.68**	**1.73**	1.18	**1.45**
coenzyme A	**0.55**	**1.54**	0.85	0.84
dephospho-coenzyme A	**0.54**	**2.30**	1.25	1.16
beta-glycerophosphoric acid	**0.56**	**1.58**	0.88	1.18
hippuric acid	**0.21**	**1.41**	0.30	**1.25**

Table S4, Energy metabolites, related to Figure 4B-N: Statistic data corresponding to metabolites shown in **Figure 4B-N and Figure S2A-D.**

	WT	*WT (+UVT)*	*GC*	*GC (+UVT)*	*WT v GC*	*GC (+UVT) v GC*	*GC (+)UVT v WT*	*WT (+UVT) v WT*
	Mean ± SEM	**Mean** ± SEM	**Mean** ± SEM	**Mean** ± SEM	***p*-value**	***p*-value**	***p*-value**	***p*-value**
Glu	**1.0058** ±0.041	**0.8414** ±0.0345	**1.3163** ±0.0995	**1.0686** ±0.0582	2.70E-03	7.00E-04	4.33E-01	2.00E-04
Gln	**1.0034**±0.0389	**0.8494** ±0.0263	**1.4036** ±0.1324	**1.1014** ±0.0692	6.00E-04	3.00E-04	2.62E-01	6.00E-04
GSH	**1.0143**±0.0482	**0.8903** ±0.0427	**0.9225** ±0.0757	**1.1482** ±0.0755	2.57E-01	5.00E-04	1.88E-01	5.00E-03
GSSG	**1.1073**±0.0499	**0.7275** ±0.0381	**1.436** ±0.1722	**1.0995** ±0.1168	3.35E-02	5.60E-03	8.03E-01	7.45E-06
Gly	**1.0762**±0.0582	**0.8745** ±0.0509	**1.3519** ±0.1394	**1.1159** ±0.0929	4.69E-02	1.08E-02	7.53E-01	6.00E-04
Thr	**1.0502**±0.0332	**0.8572** ±0.0248	**1.2261** ±0.1052	**1.0057** ±0.0528	4.20E-02	1.17E-02	4.99E-01	1.20E-03
Oxo	**0.9594**±0.0373	**1.0037** ±0.0543	**1.3394** ±0.1572	**1.1404** ±0.0842	4.00E-03	6.55E-02	9.83E-02	0.48E-01
citrate	**1.1665**±0.2424	**0.8943** ±0.1402	**3.7086** ±0.787	**1.7935** ±0.8935	5.50E-03	4.50E-03	9.97E-01	7.58E-01
C-at	**1.1432**±0.2318	**0.9253** ±0.0949	**1.9406** ±0.2825	**0.8868** ±0.3289	3.56E-02	1.70E-03	2.21E-01	8.24E-01
Glc	**1.3181**±0.1462	**1.6463** ±0.2223	**0.9975** ±0.0467	**0.9161** ±0.0768	2.08E-01	3.00E-01	8.07E-02	1.63E-02
G6P	**1.0018**±0.0352	**0.6972** ±0.039	**1.2008** ±0.084	**1.1456** ±0.0344	3.58E-02	6.80E-01	8.95E-02	4.71E-05
F6P	**1.0808**±0.0486	**0.7342** ±0.0466	**1.213** ±0.0772	**1.0979** ±0.0733	2.13E-01	3.43E-01	8.76E-01	2.00E-04
lactate	**1.0359**±0.058	**0.9311** ±0.0669	**1.1007** ±0.0744	**1.1203** ±0.0641	5.00E-01	7.56E-01	3.80E-01	3.46E-02

Mean: scaled intensity of N=10 (WT) or N=6 (GC), *p*-value: One-way ANOVA test between groups, GC: Gastric cancer, WT: wild-type, UVT: Unilateral vagotomy, Glu: L-glutamate, Gln: L-glutamine, GSH: glutathione, reduced, GSSG: glutathione, oxidized, Gly: glycine, Thr: threonine, Oxo: 5-oxoproline, C-at: cis-aconitate, Glc: glucose, G6P: fructose-6-phosphate, F6P: fructose-6-phosphate.

Table S5, Signaling pathways involved in mouse gastric cancer (GC), related to Figure 5A: Multi-omics integrative analysis in IPA revealed 41 signaling pathways that appeared exclusively in Mouse GC *vs*. WT.

Common signaling pathway (IPA)	**Transcriptomics**		**Metabolomics**	
	-log$_{10}$(*P*)	**Z-score**	**-log$_{10}$(*P*)**	**Z-score**
Ethanol Degradation II	1.49E00	-0.632	3.46E-01	N/A
Acyl Carrier Protein Metabolism	7.12E-01	N/A	2.17E00	N/A
β-alanine Degradation I	4.55E-01	N/A	2.29E00	N/A
Glycine Degradation (Creatine Biosynthesis)	4.55E-01	N/A	1.38E00	N/A
Granulocyte Adhesion and Diapedesis	5.38E00	N/A	1.31E00	N/A
Leucine Degradation I	2.00E00	-1.890	7.03E-01	N/A
Synaptogenesis Signaling Pathway	1.79E00	2.887	4.83E-01	N/A
L-cysteine Degradation III	3.21E-01	N/A	1.38E00	N/A
Sphingosine-1-phosphate Signaling	2.20E00	-0.343	7.42E-01	N/A
Role of MAPK Signaling in the Pathogenesis of Influenza	1.35E00	N/A	8.57E-01	N/A
Glutamate Receptor Signaling	2.68E-01	2.000	2.47E00	N/A
Colorectal Cancer Metastasis Signaling	2.71E00	2.689	6.58E-01	N/A
Oleate Biosynthesis II (Animals)	2.00E00	-0.816	1.51E00	N/A
Aspartate Degradation II	3.89E-01	N/A	1.38E00	N/A
UDP-N-acetyl-D-glucosamine Biosynthesis II	1.04E00	N/A	1.86E00	N/A
Isoleucine Degradation I	2.00E00	-1.890	1.48E00	N/A
Glutamate Degradation II	3.21E-01	N/A	1.51E00	N/A
Valine Degradation I	3.92E00	-2.714	1.34E00	N/A
FXR/RXR Activation	9.43E-01	N/A	1.86E00	N/A
Endocannabinoid Neuronal Synapse Pathway	7.12E-01	1.890	1.57E00	N/A
Taurine Biosynthesis	4.55E-01	N/A	1.51E00	N/A

Fatty Acid β-oxidation I	2.37E-01	N/A	3.21E-01	N/A
Serotonin Degradation	1.78E00	-1.886	1.34E00	N/A
Acetyl-CoA Biosynthesis I (Pyruvate Dehydrogenase Complex)	1.82E00	-2.000	6.58E-01	N/A
Neuroinflammation Signaling Pathway	2.49E00	3.250	7.88E-01	N/A
Prostanoid Biosynthesis	1.76E00	0.447	1.51E00	N/A
Human Embryonic Stem Cell Pluripotency	3.32E00	N/A	6.58E-01	N/A
Trna Splicing	2.22E00	0.775	5.30E-01	N/A
Adenine and Adenosine Salvage III	4.80E-01	N/A	1.99E00	N/A
Purine Ribonucleosides Degradation to Ribose-1-phosphate	4.80E-01	N/A	2.72E00	N/A
Glutathione Biosynthesis	3.21E-01	N/A	2.29E00	N/A
Ethanol Degradation IV	2.14E00	0.000	3.75E-01	N/A
Fcγ Receptor-mediated Phagocytosis in Macrophages and Monocytes	2.41E00	1.890	5.88E-01	N/A
Phospholipase C Signaling	3.39E00	0.832	4.83E-01	N/A
Eicosanoid Signaling	2.02E00	0.905	1.27E00	N/A
Branched-chain α-keto acid Dehydrogenase Complex	1.60E00	N/A	6.58E-01	N/A
Purine Nucleotides Degradation II (Aerobic)	3.23E-01	2.000	1.34E00	N/A
Endothelin-1 Signaling	2.14E00	1.820	2.78E-01	N/A
L-cysteine Degradation I	7.64E-01	N/A	1.38E00	N/A
2-oxobutanoate Degradation I	2.22E00	-2.000	3.46E-01	N/A
Flavin Biosynthesis IV (Mammalian)	4.55E-01	N/A	1.51E00	N/A

Table S6, Signaling pathways involved in mouse gastric cancer (GC) after vagotomy, related to Figure 5B: Multi-omics integrative analysis in IPA revealed 24 signaling pathways that appeared exclusively in mouse GC after vagotomy *vs.* sham operation.

Common signaling pathway (IPA)	**Transcriptomics**		**Metabolomics**	
	-log$_{10}$(*P*)	**Z-score**	**-log$_{10}$(*P*)**	**Z-score**
Vitamin-C Transport	2.60E-01	N/A	1.88E00	N/A
Phosphatidylcholine Biosynthesis I	7.01E-01	N/A	1.57E00	N/A
CDP-diacylglycerol Biosynthesis I	2.17E+00	-0.707	1.49E00	N/A
Synaptic Long Term Depression	4.92E-01	-1.706	1.66E00	N/A
Coenzyme A Biosynthesis	4.99E-01	N/A	2.61E00	N/A
Superpathway of Serine and Glycine Biosynthesis I	1.39E00	N/A	1.42E00	N/A
Gαq Signaling	1.89E+00	-1.961	7.14E-01	N/A
Amyotrophic Lateral Sclerosis Signaling	2.25E00	-0.626	1.66E00	N/A
Tetrapyrrole Biosynthesis II	9.55E-01	N/A	1.76E00	N/A
tRNA Charging	7.93E-01	-1.134	1.61E00	2.000
Pyrimidine Ribonucleotides Interconversion	4.13E-01	-2.449	1.49E00	N/A
Purine Nucleotides De Novo Biosynthesis II	2.22E00	0.447	1.37E00	N/A
Phosphatidylglycerol Biosynthesis II (Non-plastidic)	1.95E00	-0.707	1.24E00	N/A
Serine Biosynthesis	1.85E00	N/A	6.7E-01	N/A
5-aminoimidazole Ribonucleotide Biosynthesis I	1.41E00	N/A	2.2E00	N/A
Glutathione Redox Reactions I	3.64E-01	N/A	1.88E00	N/A
Adipogenesis pathway	4.18E-01	N/A	1.58E00	N/A
Stearate Biosynthesis I (Animals)	1.50E00	-1.897	5.04E-01	N/A
Arsenate Detoxification I (Glutaredoxin)	3.99E-01	N/A	1.42E00	N/A
Serotonin and Melatonin Biosynthesis	3.28E-01	N/A	1.49E00	N/A
Triacylglycerol Biosynthesis	1.14E00	-1.000	1.42E00	N/A
Antioxidant Action of Vitamin C	0.00E00	2.530	2.02E00	N/A
Ascorbate Recycling (Cytosolic)	4.99E-01	N/A	1.76E00	N/A

Ceramide Signaling	1.62E00	-1.414	9.96E-01	N/A

Table S7, Signaling pathways involved in mouse gastric cancer (GC) with and without vagotomy, related to Figure 5C: Multi-omics integrative analysis in IPA revealed 13 signaling pathways present in comparison between mouse GC *vs.* WT and in mouse GC after vagotomy *vs.* sham operation.

Common signaling pathway (IPA)	**Mouse GC *vs.* WT**				**Mouse GC after vagotomy**			
	Transcripts		**Metabolites**		**Transcripts**		**Metabolites**	
	-log$_{10}$(*P*)	**Z-score**	**-log$_{10}$(*P*)**	**Z-score**	**-log$_{10}$(*P*)**	**Z-score**	**-log$_{10}$(*P*)**	**Z-score**
Gap Junction Signaling	2.6E00	N/A	8.93E-01	N/A	6.31E-01	N/A	1.36E00	N/A
Phospholipases	1.71E00	1.886	4.06E-01	N/A	0.00E00	-2.449	1.57E00	N/A
Sirtuin Signaling Pathway	3.17E-01	0.949	1.71E00	N/A	2.34E00	-1.029	6.68E-01	N/A
Protein Kinase A Signaling	1.61E00	-0.232	3.46E-01	N/A	2.45E00	-1.089	5.61E-01	N/A
Asparagine Biosynthesis I	7.12E-01	N/A	1.38E00	N/A	9.24E-01	N/A	1.88E00	N/A
TCA Cycle II (Eukaryotic)	5.51E-01	-2.449	2.91E00	N/A	2.77E-01	N/A	1.97E00	N/A
Choline Biosynthesis III	2.71E00	0.378	4.41E-01	N/A	2.03E00	-1.342	1.66E00	N/A
γ-glutamyl Cycle	3.33E00	0.707	2.58E00	N/A	3.68E-01	N/A	2.39E00	N/A
Leukotriene Biosynthesis	1.77E00	2.449	1.02E00	N/A	1.34E00	-1.000	2.61E00	N/A
Agranulocyte Adhesion and Diapedesis	5.38E00	N/A	1.31E00	N/A	4.78E-01	N/A	1.58E00	N/A
Superpathway of Methionine Degradation	9.67E-01	-2.530	2.31E00	2.236	0.00E00	1.000	1.96E00	-2.000
Calcium Signaling	1.52E00	1.826	1.27E00	N/A	7.62E-01	-2.236	1.76E00	N/A
Glutathione-mediated Detoxification	1.02E00	-0.707	1.75E00	N/A	1.16E00	-1.633	3.75E00	-1.000

Table S8, Baseline patient data, related to Figure 8L: Baseline patient data (the first patient was recruited at September 10,

Patient number	Age at inclusion	TNM stage at time of diagnosis	Chemotherapy	TNM stage at inclusion time	Tumor location and size
1	81	T4N1M1	1st line treatment, stopped due toxic side effects	T4N1M1	Greater curvature, lesser curvature and anterior wall. Longest diameter 9 cm
2	70	T3N0M0	Neoadjuvant chemotherapy, inoperabel due to comorbidity	T3N1M0	Cardia and proximal esophagus. Longest diameter 3 cm
3	79	T4aN2M1	Palliativ chemotherapy with EOX	T4aN2M1	Distal part of the stomach. Circular tumor with longest diameter 8 cm
4	49	TxNxM1	1st line treatment, 2nd line treatment.	TxNxM1	Cardia. Extensive liver metastasis
5	83	TxNxMx	No previous chemotherapy due to age and comorbidity	T4aN3M1	Cardia. Extensive liver metastasis
6	84	T4aN3M0	No previous chemotherapy due to age and comorbidity	T4aN3M0	Linitis plastica in whole stomach except the most proximal part

2014).

Note: One additional patient (i.e. patient no. 7) gave his consent for participation in this study, but pretreatment CT scan of the stomach showed no measurable tumor size. According to the study protocol (Supplementary Data Clinical study protocol), this patient was excluded from further participation in the study and did not receive BoNT-A treatment.

Table S9, Primary outcome measures, related to Figure 8L: Primary outcome measure: Tumor evaluation

Patient number	Tumor thickness, diameter or volume density (mean±SD % before BoNT-A injection	Tumor thickness, diameter or volume density (%) 8 weeks after injection	Tumor diameter and volume density (%) 20 weeks after injection
1	14 mm tumor thickness	Not followed (died before the time point)	Not followed (died before the time point)
2	27 x 16 mm, 20x17 mm, 40.8±10.9 %	32x21 mm and 26x20 mm, 34.4±5.3 %	31x21 mm, 28x21 mm, 27.9±10.8 %
3	17-19 mm tumor thickness	Not followed (died before the time point)	Not followed (died before the time point)
4	20x29 mm	Not followed (died before the time point)	Not followed (died before the time point)
5	12 mm tumor thickness	Not followed (died before the time point)	Not followed (died before the time point)

6	22 mm tumor thickness	26 mm tumor thickness	Not followed ((died before the time point)

Table S10, Secondary outcome measure (short term), related to Figure 8L: Secondary outcome measure: Short-time adverse effects and ECOG status after BoNT-A injections

Patient number	Baseline ECOG	Adverse effects during procedure	Adverse effects after observation 24 hours after procedure	Adverse effects at 2 weeks outpatient clinical control	ECOG after 2 weeks
1	1	No	No	No	1
2	2	No	No	No	2
3	1	No	No	No	2
4	1	No	No	No	3
5	1	No	No	No	ECOG status missing from local hospital
6	2	No	No	No	1

Table S11, Secondary outcome measures (long-term), related to Figure 8L. Secondary outcome measure: Long term adverse effects and ECOG status after BoNT-A injections

Patient number	Survival days after BoNT-A injection	8 weeks (56 days) outpatient control performed	Adverse effects /ECOG status	20 weeks control performed	Adverse effects /ECOG status	Any adverse events during the course of the disease until death
1	51	Died before control				Death related to natural progression of disease and no adverse effects recorded until time of death.
2	188	Yes	No/3	Yes	No/3	Death related to natural progression of disease and no adverse effects recorded until time of death.
3	69	Withdrawal from study protocol due to severe progression of disease				Death related to natural progression of disease and no adverse effects recorded until time of death.
4	37	Died before control				Death related to natural progression of disease and no adverse effects recorded until time of death.
5	27	Died before control				Death related to natural progression of disease and no adverse effects recorded until time of death.
6	112	Yes	No/1	No		Death related to natural progression of disease and no adverse effects recorded until time of death.

Table S12, Study groups, related to Figure 7K and Figure 8G-L.

Group	Subjects	Treatment (*N*)(female/male)	Age at intervention	Age at examination
Clinical examination	GC patients	Gastrectomy (16)(6/10)	54-87 years	5 years follow-up
Transcriptomics	**GC mice#**	**UVT (6) (4/2)**	6 months	12 months
Metabolomics	**GC mice**	**UVT (6) (2/4)**	6 months	12 months
		Sham (6)(2/4)	6 months	12 months
	WT mice	**UVT (10)(4/6)**	6 months	12 months
		Sham (10)(4/6)	6 months	12 months
Treatments:	**GC mice**	**UVT + saline (9)(7/2)**	12-14 months	14-16 months
		Sham + saline (9)(7/2)	12-14 months	14-16 months
		UVT + FUOX (16)(10/6)	12-14 months	14-16 months
		Sham + FUOX (16)(10/6)	12-14 months	14-16 months
		Sham + FUOX (16)(10/6)	12-14 months	14-16 months
		Sham + FUOX (16)(10/6)	12-14 months	14-16 months
		BoNT-A + saline (22)(12/10)	12-14 months	14-16 months
		Saline (22)(12/10)	12-14 months	14-16 months
		BoNT-A + FU (12)(7/5)	12-14 months	14-16 months
		FU (12)(7/5)	12-14 months	14-16 months
		BoNT-A + OX (26)(14/12)	12-14 months	14-16 months
		OX (26)(14/12)	12-14 months	14-16 months
		BoNT-A + FUOX (26)(15/11)	12-14 months	14-16 months
		FUOX (26)(15/11)	12-14 months	14-16 months
		BoNT-A (10)(5/5)	9-15 months	12-18 months
		Sham (10)(5/5)	9-15 months	12-18 months
		BoNT-A + RAD001 (15)(5/10)	9-15 months	12-18 months
		RAD001 (15)(5/10)	9-15 months	12-18 months
		BoNT-A + RAD001 + FUOX (48)(24/24)	9-15 months	12-18 months
		RAD001 + FUOX (48)(24/24)	9-15 months	12-18 months
		BoNT-A + CPI-613 (8)(5/3)	9-15 months	12-18 months
		CPI-613 (8)(5/3)	9-15 months	12-18 months
		BoNT-A + CPI-613 + FUOX (12)(6/6)	9-15 months	12-18 months
		CPI-613 + FUOX (12)(6/6)	9-15 months	12-18 months
		BoNT-A + RAD001 + CPI-613 (25)(13/12)	9-15 months	12-18 months
		RAD001 + CPI-613 (25)(13/12)	9-15 months	12-18 months
		BoNT-A + RAD001 + CPI-613 + FUOX (31)(15/16)	9-15 months	12-18 months
		RAD001 + CPI-613 + FUOX (31)(15/16)	9-15 months	12-18 months
		Age-matched controls (32)(15/17)	9-15 months	12-18 months
		Age-matched controls (32)(15/17)	9-15 months	12-18 months
Clinical trial	GC patients	Endoscopic injection of BoNT-A (6)	49-84 years	2 years follow-up

 # group from previous study (Zhao et al., 2014)

Table S13. Metabolites involved with DNA/protein synthesis, related to Figure 4 and Data S3. Effects of vagotomy (unilateral vagotomy, UVT) on gastric tissue levels (scaled intensity) of metabolites that are involved in DNA/protein synthesis in either wild-type (WT) or gastric cancer (GC) mice

	WT	WT (UVT)	*p*-value	GC	GC (UVT)	*p*-value
	Mean ± SEM	**Mean** ± SEM		**Mean** ± SEM	**Mean** ± SEM	
Choline	**1.0382** ±0.0347	**0.9399** ±0.0421	0.0039	**1.1583** ±0.0950	**1.0341** ±0.0902	0.0179
Creatine	**0.9675** ±0.0329	**0.871** ±0.0323	0.0077	**1.1146** ±0.0439	**1.0931** ±0.0385	0.3415
Cytidine	**1.016** ±0.024	**0.769** ±0.0346	0.0001	**1.2553** ±0.0882	**1.1472** ±0.0387	0.1217
Glycine	**1.0762** ±0.0582	**0.8745** ±0.0509	0.0006	**1.3519** ±0.1394	**1.1159** ±0.0929	0.0054
Histidine	**0.9938** ±0.0471	**0.8598** ±0.0725	0.0035	**1.115** ±0.0848	**1.0622** ±0.0791	0.2282
Sarcosine	**1.0912** ±0.0896	**0.8637** ±0.0898	0.0031	**1.1428** ±0.0949	**0.9587** ±0.1357	0.0182
Serine	**1.0827** ±0.0352	**0.914** ±0.0451	0.0022	**1.0947** ±0.0744	**0.9801** ±0.0546	0.0499
Threonine	**1.0502** ±0.0332	**0.8572** ±0.0248	0.0012	**1.2261** ±0.1052	**1.0057** ±0.0528	0.0059
Uracil	**1.0101** ±0.0383	**0.8603** ±0.0359	0.0015	**1.0947** ±0.0694	**1.0704** ±0.0292	0.3945

One-way ANOVA was used for comparisons between WT and WT (UVT) or between GC and GC (UVT).

Table S14, Chemical and reagent list, related to methods. List of reagents and chemicals used.

Name	Cat. no	Supplier	Country
DMSO	D8418	Sigma-Aldrich	Oslo, Norway
Cell Counting Kit-8 (CCK-8)	96992-3000TESTS-F	Sigma-Aldrich	St. Luis, MO, USA
Cell Count Reagent SF	07553-44	Nacalai tesque	Tokyo, Japan
DMEM (no glucose, no glutamine,, no pyruvate, no phenol red)	08456-65/A14430-01-500ML	Nacalai tesque/Gibco by Life Technologies	Tokyo, Japan/Grand Island, NY
DMEM	A14430-01-500ML		
RPMI-1640 with L-Gln (0.3 g/L, 2.0 mM), phenol red	R8758-500ML	Sigma-Aldrich	Norway
D-glucose			
FBS	F7524	Sigma-Aldrich	Norway
Dialyzed FBS	26400-036	Gibco by Life Technologies	USA
L-Gln	G7513-100ML	Sigma Aldrich	Norway
Glutamine/glutamate detection kit	GLN-1	Sigma-Aldrich	Saint Louis, Missouri, USA
Glutamic Dehydrogenase (L-GLDH)	G5900	Sigma-Aldrich	Saint Louis, Missouri, USA
Glutaminase	G8880	Sigma-Aldrich	Saint Louis, Missouri, USA
NAD	N9268	Sigma-Aldrich	Saint Louis, Missouri, USA
Acetate buffer, 0.5 M, pH 5	A4433	Sigma-Aldrich	Saint Louis, Missouri, USA
Adenosine 5'-Diphosphate (ADP), 100 mM, 1 ml	A4558	Sigma-Aldrich	Saint Louis, Missouri, USA
Hydrazine Hydrate, 3ml	H0883	Sigma-Aldrich	Saint Louis, Missouri, USA
L-glutamine	G6275, 2 mM	Sigma-Aldrich	Saint Louis, Missouri, USA
L-glutamate	G6150, 1 mM	Sigma-Aldrich	Saint Louis, Missouri, USA
RNase A	R4875-100MG	Sigma Aldrich	Oslo, Norway
Propidium Iodide	P4170-10MG	Sigma Aldrich,	Oslo, Norway
Triton-X	T9284	Sigma Aldrich	Oslo, Norway
Sodium acetate buffer (10 mM, CH_3COONa, MW: 82.03, pH 5.2)			
Tris-HCl buffer (1M, $NH_2C(CH_2OH)_3$; MW: 121.14, pH 8.0).			

Tris-EDTA Buffer	T3161		
PBS	BR0014G	Oxoid	Hampshire, England
D-PBS	14249-24	Nacalai-Tesque	Tokyo, Japan
Trypsin-EDTA	T4049-500ML	Sigma-Aldrich	Oslo, Norway
Penicillin/Streptomycin cocktail	P4333-100ML	Sigma-Aldrich	Norway
Botox ®	100U	Botox Allergan Inc.	Norway
RAD001 (also known as Everolimus)	Trl-eve	InvivoGen	San Diego, CA, USA
CPI-613 (also known as Devimistat)	SML0404-25MG	Sigma-Aldrich	Oslo, Norway
Fluorouracil (5-FU)	50 MG/ML, vnr. 137864	Hospira	Illinois, USA
Oxaliplatin	5 MG/ML, vnr. 137098	Hospira	Illinois, USA
NucleoSpin® RNA	June 2015, Rev. 17	Macherey-Nagel	
Beta-Mercaptoethanol	M3148-100ML	Sigma-Aldrich	Oslo, Norway
Bulk beads (1.4 mm/2.8mm Zirconium oxide beads)	03961-1-103/03961-1-102	Precellys 24, Bertin Technologies	France
Illumina TruSeq Stranded mRNA Library Prep kit	20020594	Illumina	
Sodium Pyruvate 110.00 mg/L, 1.0 mM		Nacalai tesque/Sigma Aldrich	Tokyo, Japan/Oslo, Norway
Isoflurane	Baxter		
Viscotears ® eye gel		Thèa	Berlin, Germany

Table S15, Description of Metabolon QC samples, related to methods.

Type	Description	Purpose
MTRX	Large pool of human plasma maintained by Metabolon that has been characterized extensively.	Assure that all aspects of Metabolon process are operating within specifications.
CMTRX	Pool created by taking a small aliquot from every customer sample.	Assess the effect of a non-plasma matrix on the Metabolon process and distinguish biological variability from process variability.
PRCS	Aliquot of ultra-pure water	Process Blank used to assess the contribution to compound signals from the process.
SOLV	Aliquot of solvents used in extraction.	Solvent blank used to segregate contamination sources in the extraction.
DS	Derivatization Standard	Assess variability of derivatization for GC/MS samples.
IS	Internal Standard	Assess variability and performance of instrument.
RS	Recovery Standard	Assess variability and verify performance of extraction and instrumentation.

Transparent Methods

GC patients

Twenty-two patients (17 men aged 49-87 years and 5 women aged 51-83 years) were included. 16 of 22 patients underwent total/subtotal or distal gastrectomy because of intestinal or diffuse gastric cancer and were followed-up for 5 years since 2012 at St. Olavs Hospital, Trondheim, Norway. The study was approved by the Regional Committees for Medical and Health Research Ethics Central Norway (REK 2012-1029). 6 of 22 patients were enrolled in a clinical trial (see below) (Table S12). Total, subtotal or distal gastrectomy was performed on 16 patients diagnosed with gastric cancer. Biopsies from 4 pre-determined positions in corpus (major and minor curvature), cardia and antrum were collected, and largest diameter of the tumor was decided. Biopsies from adjacent, normal tissue was taken 5-10 cm from the tumor site. TNM status was defined, and samples were classified according to Lauren's classification, (Intestinal, diffuse or mixed/combined type), WHO classification (tubular, papillary, mucinous and poorly cohesive), WHO grading (well, moderately or poorly differentiated), and were reviewed according to the Japanese pathological classification. Samples were assigned gastric histopathology scoring including inflammation, epithelial defects, oxyntic atrophy, epithelial hyperplasia and dysplasia and an overall GHAI score.

Animals

Three hundred-twenty four mice were used and some of the mice were followed- up for more than one year to measure the overall survival rate. The mouse GC model was the transgenic INS-GAS mice which spontaneously develop GC at our own institute (Wang et al., 1996; Zhao et al., 2014) and its wild-type (WT) mice (FVB strain). Mice were housed ~5 mice per cage on wood chip bedding with a 12-hour light/dark cycle in a specific pathogen free environment with room temperature of 22°C and 40-60% relative humidity. Mice including both INS-GAS and WT mice were age-matched and randomized into different experimental groups (Table S12). All animal experiments were approved by The Norwegian Food Safety Authority (Mattilsynet).

Surgery

Vagotomy and BoNT-A injections were performed under isoflurane anesthesia as described previously(Zhao et al., 2014). The success of UVT was confirmed by reduced thickness of gastric mucosa (Zhao et al., 2014) and reduced tissue-levels of metabolites that are involved in DNA/protein synthesis in the denervated side in comparison with the innervated side of stomach (Table S13).

Chemicals and reagents

For details, see chemical and reagent list in Table S14.

Cells and cell culture

GC cell lines included AGS (female, 54 years, Caucasian), MKN74 (male, 37 years, Asian), MKN45 (female, 54 years, Caucasian) and KATO-III (male, 55 years, Asian). AGS cells were kindly provided by Prof. Sasakawa (Tokyo University, Japan). MKN45 cells were kindly provided by Prof. Kamiya (Kyorin University, Japan). MKN74 cells were provided by Prof. T.C Wang and KATO-III cells were purchased from LGC group.

AGS and MKN45 cells were maintained in Dulbecco's Modified Eagle's Medium (DMEM (1.0 g/l Glucose, 10 mM) with L-Gln (584.00 mg/L, 4.0 mM) and Sodium Pyruvate (110.00 mg/L, 1.0 mM)(Nacalai tesque, Japan) supplemented with 10% fetal bovine serum (FBS; ThermoFisher Scientific, Grand Island, NY) and antibiotic-antimycotic solution (1%) containing penicillin, streptomycin and amphotericin B (Nacalai tesque, Japan). MKN74 and KATO-III cells were maintained in RPMI-1640 medium (Sigma Aldrich, Norway) supplemented with fetal bovine serum (10%, FBS), Sodium pyruvate and penicillin streptomycin solution (1%) in a humidified incubator holding 5% CO_2 and 37°C.

In vitro experiments

Gln/pyr depletion

The cells ($1.0x10^4$) were plated (24h) and treated with 0-2.0 mM L-glutamine and 1.0 mM pyruvate in DMEM supplemented with dialyzed bovine serum (10%) and glucose at 25 mM. In depletion testing, either glutamine or pyruvate were omitted from the medium. Proliferation was assessed using Cell Count Reagent SF or Cell counting Kit-8 reagent at 450 nm and cell proliferation was calculated relative to controls. Determination of endogenous L-glutamine and L-glutamate was performed after 1, 6 and 24 hrs in culture using a detection kit (Glutamine/glutamate determination kit, Sigma, Saint Louis, Missouri).

Drug screen

Cells ($2.5x10^3$) were plated (24 hrs) and subjected to individual dose-response drug screens and sequential combination treatment during 3 days in culture. First, cells were treated with either serum-free medium or BoNT-A- without serum at 0.25 U BoNT-A/well and incubated for 24 hrs. CPI-613 and RAD001 were dissolved in DMSO at highest solubility before diluted in the medium. The cells were treated with RAD001, CPI-613, combination of these or vehicle (DMSO) control and incubated for 24 hrs. A combination of 5-FU and oxaliplatin or medium control was added to the cells for 24 hrs. To assess whether the drug combinations acted synergistically, we calculated Bliss synergy scores for RAD001 + CPI-613 combinations using the SynergyFinder web-application (Ianevski et al., 2017). Synergy scores were quantified as an average excess over expected drug combination effect given by the Bliss reference model (Ianevski et al., 2019). Bliss Independence model was used because the two drugs (i.e. RAD001 and CPI-613) act independently in such a manner that neither of them interferes with the other (different sites of action), but each contributes to a common result, i.e. cell proliferation.

In vivo experiments

GC mice were injected BoNT-A through laparoscopic procedure as described earlier (Zhao et al., 2014), treated with RAD001 (1.5 mg/kg/day for 3 weeks, i.p.), CPI-613 (20 mg/kg/week, once weekly for 3 weeks, i.p.), or combination of RAD001 and CPI-613. Saline injection (i.p.) was used as control. The mice were allowed one-week rest after the first cycle of treatment, and then the treatment cycle was repeated once, yielding a total treatment window of 8 weeks (**Figure 7H**). BoNT-A was dissolved in saline containing methylene blue (1.0 %) to visualize the injection. The achieved

concentration of BoNT-A was 0.25 U of BoNT-A/mL. Injection was performed through laparotomy into the serosa layer in the anterior side of stomach. Thus, for a mouse receiving 0.4 mL BoNT-A (0.25 U/mL) the dose corresponded to 0.10 U. 5-Fluorouracil (5-FU) was given i.p. at dose of 25 mg/kg in a volume of 0.5 mL. Oxaliplatin was given i.p. at dose of 5 mg/kg in volume of 0.5 mL. The two drugs were injected on either left or right side of abdomen at same time once weekly for 3 weeks in 2 cycles, starting one week after BoNT-A injection.

Sample collection and preparation

Mouse tissue samples were taken after the animals were killed under deep isoflurane inhalation anesthesia. The anterior and posterior parts of stomachs were collected for histopathological analysis and cryopreservation for transcriptomics of mouse GC in which mice underwent unilateral vagotomy (UVT) at 6 months of age and the stomachs were collected 6 months afterwards, the data from our previous study was re-analyzed (according to 3R principle)(Zhao et al., 2014). For metabolomics, GC and WT mice at 6 months of age underwent the same UVT or sham operation and the stomachs were collected as described previously. Six months after UVT, animals were terminated for sampling, and tissue samples from the denervated anterior stomach and tissue samples from the posterior stomach with intact innervation were analyzed with liquid chromatography/mass spectrometry and gas chromatography/mass spectrometry. Mouse tissue samples were collected for transcriptomics analysis immediately after completing two months BRC-treatment.

Measurement of survival rate, body weight and tumor size

Animals were followed up by daily inspection with scoring sheet, weighing and euthanized according to primary human endpoints. Scoring parameters included severe body weight loss (>25%), stress behavior, abdominal pain or reduced physical activity and was followed in collaboration with the responsible veterinarian at the animal facility. Body weight was measured daily (during treatment) or weekly (during follow up). Tumor volume density (% of glandular area of the stomach occupied by tumor) was measured using point count method described earlier[14].

Pilot clinical trial (phase II)

Six patients were enrolled according to inclusion criteria and written consent (Supplementary Data: Clinical Trial Protocol). Inclusion criteria included 1) patients who received 1st line and 2nd line chemotherapy but no longer respond to such therapy, 2) patients who, due to toxicity of chemotherapy, could not be offered such treatment, 3) patients who, after meticulous information about chemotherapy, still did not want such treatment and 4) patients with performance status (ECOG) 0-2. Patients were elderly and diagnosed with already advanced gastric cancer which precluded surgical resection (Table S12). Exclusion criteria included 1) known allergy to any of the components in Botox®, 2) known peripheral motor neuropathy disease (for example: Amyotrophic Lateral Sclerosis, ALS), or subclinical or clinical deficiency of neuromuscular transmission (for example: Myasthenia Gravis or Eaton-Lambert`s Syndrome), 3) another cancer disease that is not under control, 4) another concomitant treatment for cancer, 5) serious mental illness and 6) performance status (ECOG) 3-4. One patient with TNM status T3N0M0 was rejected for surgery due to comorbidity following a short period with neoadjuvant chemotherapy. At the time of

enrollment into this study, 4 out of 6 patients had metastatic disease, and 2 of these patients had extensive liver metastasis with short expected life expectancy. Extensive tumor masses in the stomach were present in 3 out of 6 patients. The patients were admitted to the hospital shortly after the baseline CT scan, and endoscopic BoNT-A injection was performed under sedation with midazolam. One hundred units with Botox® were diluted into 14 mL saline by the Department for Clinical Studies at St.Olav Hospital's Pharmacy. This amount was divided into 7 doses of 2 mL (14.3 U/dose) that were injected at 4 sites around the tumor and at 3 sites directly into the tumor. Some of the patients had advanced and extensive tumor masses in the stomach and for those patients, injections were concentrated to the area of the stomach with measurable tumor thickness or diameter, omitting the rest of the tumor masses in the stomach. After the endoscopic procedure, the patients were observed in the surgical ward and discharged from hospital the day after the procedure. Primary outcome measures were assessment of tumor size (volume density and/or thickness) in the stomach using standardized CT protocols after 2, 8 and 20 weeks. Two weeks after the injection, the patients had an outpatient clinical visit with complete physical assessment, specially emphasizing on detecting any adverse or toxic events related to the experimental treatment. At 8 and 20 weeks after the injection, another thoracic and abdominal CT scan was performed, together with a follow-up outpatient clinical examination. Secondary outcomes included toxicity (within 2- and 8-weeks post injection) and performance status (ECOG) after 2, 8 and 20 weeks. The safety evaluation was performed based on the CTC (Common Toxicity Criteria) criteria. The study was conducted in accordance with the guidelines for GCP (Good Clinical Practice) and it was approved by the Regional Committee for Medical and Health Research Ethics (2012/1031) and the Norwegian Medicines Agency (2012-002493-31).

Transcriptomics

Total RNA was extracted from harvested stomachs of mice or surgical biopsies of patients. RNA quality and quantity were obtained using NanoDrop One (Thermo Scientific, Norway) and Agilent Bioanalyser. RNA sequencing of human GC samples was performed using Illumina platform as described earlier[14], whereas RNA sequencing of mouse samples was performed using Illumina HiSeqNS500 instrument (NextSeq 500) at 75 bp with paired end (PE) reads using NS500H flowcells with 25 M reads/sample. Paired end forward read length (R1): 81, reverse read length (R2): 81. Illumina microarray data was analyzed using Lumi on the log2 scale and was analyzed using the empirical Bayesian method implemented in Limma. Gene expression was analyzed using a t-test between cancer and WT mice or between tumor and normal adjacent tissue in patients. Transcripts with a *p*-value of less than 0.05 were considered to be differentially expressed. Benjamini-Hochberg false discovery rates were included.

Metabolomics

Metabolomics was performed using a platform that incorporates two separate ultrahigh-performance liquid chromatography/tandem mass spectrometry (UHPLC/MS/MS2) injections and one gas chromatography/mass spectrometry (GC/MS) injection per sample by Metabolon (USA). Identification, relative quantification, data-reduction and quality-assurance components of the process were

included in the analysis platform. 343 metabolites were identified (Data S3). The informatics system consisted of four major components, the Laboratory Information Management System (LIMS), the data extraction and peak-identification software, data processing tools for QC and compound identification, and a collection of information interpretation and visualization tools for use by data analysts. The hardware and software foundations for these informatics components were the LAN backbone, and a database server running Oracle 10.2.0.1 Enterprise Edition. For more details, see description of Metabolon QC samples in Table S15.

Real-time PCR

Total RNA was isolated and purified using an Ultra-Turrax rotating-knife homogenizer and the mirVana miRNA Isolation Kit (AM1560, Ambion) according to the manufacturer's instructions. Mouse WNT pathway RT2 profiler PCR array was used (StepOnePlusTM, Applied Biosystems), which targeted key genes involved in the canonical and non-canonical WNT pathway and endogenous genes for reaction control (89 genes and 7 controls, see Table S1). The reaction was performed according to the manufacturer's instructions (SABiosciences Corporation, QIAGEN Norway).

Data visualization

R/Bioconductor environment was used to process omics-data before differential expression analysis. Graphical data visualization and data analyses were carried out using GraphPad Prism software 6.0 (GraphPad Software, U.S), Excel 2016 (Microsoft), IPA (Qiagen, Aarhus, Denmark) and RStudio version 3.5.2 (2018-12-20). Diagram plots in Figure 5 were created with JavaScript library D3.js v.4. SPSS v.23-25 was used to perform test statistics including *t*-tests and non-parametric tests, one-way ANOVA, and correlation/linear regression analyses. Heatmaps were encoded in RStudio using the heatmap.2 function. Single-cell data were processed using Seurat v3 (doi.org/10.1016/j.cell.2019.05.031) and visualized in a tSNE plot (Figure 3). IPA was used to cluster cell-specific marker genes to WNT/mTOR-glutamine-dependent gene markers in Figures 8C-D and Figures S6A-E.

Ingenuity Pathway Analysis (IPA)

Transcriptomics and metabolomics datasets were analyzed using IPA (Qiagen, Hilden, Germany) which has sophisticated algorithms and criteria to calculate predicted functional activation/inhibition of canonical pathways, diseases and functions, transcription regulators and regulators based on their downstream molecule expressions (QIAGEN Inc., https://www.qiagenbioinformatics.com/products/ingenuitypathway-analysis). For human GC microarray, Illumina identifiers (ILMN) were uploaded together with log_2-fold change, *p*-values and *q*-values (false discovery rates). A total of 47,323 transcripts was assigned to analysis. A total of 37,489 transcripts were mapped/9,834 transcripts unmapped by IPA. For RNA sequencing, Ensembl identifiers were uploaded together with log_2-fold change, *p*-values and q-values. A total of 54,460 transcripts was assigned to analysis. A total of 53,735 was mapped/725 unmapped by IPA. For mouse GC microarray, ILMN were aligned together with log_2-FC and q-values before

uploaded in IPA. A total of 12,519 transcripts was loaded, a total of 11,773 transcripts was mapped/746 unmapped in IPA. For metabolomics, HMDB and KEGG identities were aligned together with fold changes, expressed *p*-values and *q*-values. A total of 343 metabolites were uploaded for downstream analysis in IPA and 252 metabolites were mapped by IPAThe data was subjected to a metabolomics expression analysis using HMDB or KEGG as identifier type. One-way ANOVA was used between groups. Fold changes were inverted before IPA analyzes. Thus, a molecule with 0.5-fold change was negatively inverted (-1/0.5) to -2.0.

Regulatory z-scores for canonical pathways that overlapped with our experimental data were calculated using the formula described previously (Krämer et al., 2014). To generate the network of up- or down-regulated genes, custom-made molecular networks were developed based on information contained in the IPAs knowledge base. Networks of these genes were then algorithmically generated based on their interrelationships. Filtering of datasets included species, *p*-value cut-off and/or *q*-value cut-offs. Molecular networks and canonical pathways were algorithmically constructed based on known connectivity and relationships among metabolites and genes/proteins using IPAs knowledge base. The significance of the association between the dataset molecules and the canonical pathways was measured by Fischer's exact test that was used to calculate a *p*-value determining the probability that the association between the genes in the dataset and the canonical pathway by chance alone. Z-scores were calculated in IPA based on the dataset's correlation with the activated state. Negative z-scores indicate a decrease in activity, positive z-scores indicate an increase in activity. Canonical pathways were identified using statistical cut-offs at $p<0.05$ and/or $q<0.05$.

***In silico* experiment**

Signaling pathways of WNT/β-catenin and mTOR were constructed based on the transcriptomic data of INS-GAS mice and were then entered into the "Pathway" module of the IPA to obtain the nodes in every corresponding signaling pathway. The expression data from INS-GAS *vs.* FVB mice (Mouse GC *vs.* WT) was compared to all genes in the pathways. Nodes were added as entries into the "My list"-function and all entries in the list were added to the "My pathway" in IPA. My pathway was used to produce a network of nodes/genes from the WNT and mTOR signaling pathways that matched with our experimental data from INS-GAS *vs.* FVB. The build-tool was used to connect nodes using edges, i.e. relationships including both direct and indirect interactions like chemical-protein interactions, ubiquitination, molecular cleavage, translocation, localization, phosphorylation, expression, protein-protein interactions, activation, regulation of binding, inhibition, membership, reaction, protein-DNA interactions, transcription and modification. The Canonical Pathway overlay-tool was used to arrange the entries into two clusters based on pathway. Next, the molecule activity predictor (MAP)-function was used to predict activation/inhibition between the nodes in the network. The *in silico* tool was employed to predict effects on the network after gene inhibition. Categorical values were set to each gene/node using a semi-quantitative method to quantify the color-change resulting from *in silico* inhibition. Dark blue colored nodes were represented by -2, light blue as -1, white as 0, light orange

as +1 and dark orange as +2. Values are represented of n=7-14 experiments per inhibition node/gene.

Upstream regulator analysis

Ingenuity pathway analysis (IPA, QIAGEN) was used to perform upstream analysis of the transcriptomics datasets based on the literature and the Ingenuity Knowledge Base. The analysis examines how many known targets of the upstream regulators are present in the dataset. An overlap *p*-value is computed based on significant overlap between genes in the dataset and known targets regulated by the transcriptional regulator. The activation z-score algorithm is used to make predictions. In mouse GC, 144 regulators were found to be activated (z-score>2, $p<0.05$) based on the expression levels of target molecules in the datasets. The overlay-tool in the "My pathway" module was used to cluster the activated regulators into canonical pathways. Next, upstream regulators of interest were added into custom-made pathways in the Path Designer-tool and relationship-types between upstream regulator and target molecule were added.

tSNE plot of metabolic gene expression according to single-cell atlas

Available data on a single-cell transcriptome network of gastric premalignant and early gastric cancer in patients was utilized (PMID: 31067475), including 13 biopsies from 9 patients: 3 mild superficial gastritis (NAG), 3 chronic atrophic gastritis (CAG), 6 intestinal metaplasia (IM), and 1 early gastric cancer (EGC). Single-cell data were processed using Seurat v3 (doi.org/10.1016/j.cell.2019.05.031) and normalized for each of the 13 samples independently. The functions FindIntegrationAnchors, IntegrateData, ScaleData and RunPCA with default parameters were used. Cells with number of expressed genes lower than 400 or larger than 7000 and 20% or more of UMIs mapped to mitochondrial or ribosomal genes were removed. 50 PCs were utilized to visualize single-cell atlas with a tSNE plot. The expression levels of marker genes in mouse GC *vs.* WT for each representative cell type were analyzed. Marker genes were identified by differential expression analysis with the threshold as fold change > 1.5 and FDR < 0.01.

Statistics

Values are expressed as means ± SEM or SD and statistical methods are shown in the figure legends.

Supplemental references

Ianevski, A., Giri, A. K., Gautam, P., Kononov, A., Potdar, S., Saarela, J., Wennerberg, K. & Aittokallio, T. (2019). Prediction of drug combination effects with a minimal set of experiments. Nature Machine Intelligence *1*, 568-577.

Ianevski, A., He, L., Aittokallio, T. & Tang, J. (2017). SynergyFinder: a web application for analyzing drug combination dose–response matrix data. Bioinformatics *33*, 2413-2415.

Krämer, A., Green, J., Pollard, J., Jr. & Tugendreich, S. (2014). Causal analysis approaches in Ingenuity Pathway Analysis. Bioinformatics (Oxford, England) *30*, 523-530.

Wang, T. C., Koh, T. J., Varro, A., Cahill, R. J., Dangler, C. A., Fox, J. G. & Dockray, G. J. (1996). Processing and proliferative effects of human progastrin in transgenic mice. J Clin Invest *98*, 1918-29.

Zhang, P., Yang, M., Zhang, Y., Xiao, S., Lai, X., Tan, A., Du, S. & Li, S. (2019). Dissecting the Single-Cell Transcriptome Network Underlying Gastric Premalignant Lesions and Early Gastric Cancer. Cell Rep *27*, 1934-1947 e5.

Zhao, C. M., Hayakawa, Y., Kodama, Y., Muthupalani, S., Westphalen, C. B., Andersen, G. T., Flatberg, A., Johannessen, H., Friedman, R. A., Renz, B. W., et al. (2014). Denervation suppresses gastric tumorigenesis. Sci Transl Med *6*, 250ra115.

Paper II

frontiers in Pharmacology

ORIGINAL RESEARCH
published: 31 March 2021
doi: 10.3389/fphar.2021.625991

Computational Drug Repositioning and Experimental Validation of Ivermectin in Treatment of Gastric Cancer

*Hanne-Line Rabben[1,2], Gøran Troseth Andersen[1], Aleksandr Ianevski[1], Magnus Kringstad Olsen[1], Denis Kainov[1], Jon Erik Grønbech[3], Timothy Cragin Wang[4], Duan Chen[1] and Chun-Mei Zhao[1,2]**

[1]Department of Clinical and Molecular Medicine, Norwegian University of Science and Technology (NTNU), Trondheim, Norway, [2]The Central Norway Regional Health Authority (RHA), Stjørdal, Norway, [3]Surgical Clinic, St. Olavs Hospital, Trondheim University Hospital, Trondheim, Norway, [4]Division of Digestive and Liver Diseases, Columbia University College of Physicians and Surgeons, New York, NY, United States

OPEN ACCESS

Edited by:
Klara Gyires, Semmelweis University, Hungary

Reviewed by:
Cedric Coulouarn, INSERM U1242 Laboratoire COSS, France
Pedro Miguel Rodrigues, Biodonostia Health Research Institute (IIS Biodonostia), Spain

***Correspondence:**
Chun-Mei Zhao
chun-mei.zhao@ntnu.no

Specialty section:
This article was submitted to Gastrointestinal and Hepatic Pharmacology, a section of the journal Frontiers in Pharmacology

Received: *04 November 2020*
Accepted: *10 February 2021*
Published: *31 March 2021*

Citation:
Rabben H-L, Andersen GT, Ianevski A, Olsen MK, Kainov D, Grønbech JE, Wang TC, Chen D and Zhao C-M (2021) Computational Drug Repositioning and Experimental Validation of Ivermectin in Treatment of Gastric Cancer. Front. Pharmacol. 12:625991. doi: 10.3389/fphar.2021.625991

Objective: The aim of the present study was repositioning of ivermectin in treatment of gastric cancer (GC) by computational prediction based on gene expression profiles of human and mouse model of GC and validations with *in silico*, *in vitro* and *in vivo* approaches.

Methods: Computational drug repositioning was performed using connectivity map (cMap) and data/pathway mining with the Ingenuity Knowledge Base. Tissue samples of GC were collected from 16 patients and 57 mice for gene expression profiling. Additional seven independent datasets of gene expression of human GC from the TCGA database were used for validation. *In silico* testing was performed by constructing interaction networks of ivermectin and the downstream effects in targeted signaling pathways. *In vitro* testing was carried out in human GC cell lines (MKN74 and KATO-III). *In vivo* testing was performed in a transgenic mouse model of GC (INS-GAS mice).

Results: GC gene expression "signature" and data/pathway mining but not cMAP revealed nine molecular targets of ivermectin in both human and mouse GC associated with WNT/β-catenin signaling as well as cell proliferation pathways. *In silico* inhibition of the targets of ivermectin and concomitant activation of ivermectin led to the inhibition of WNT/β-catenin signaling pathway in "dose-depended" manner. *In vitro*, ivermectin inhibited cell proliferation in time- and concentration-depended manners, and cells were arrested in the G_1 phase at IC_{50} and shifted to S phase arrest at $>IC_{50}$. *In vivo*, ivermectin reduced the tumor size which was associated with inactivation of WNT/β-catenin signaling and cell proliferation pathways and activation of cell death signaling pathways.

Conclusion: Ivermectin could be recognized as a repositioning candidate in treatment of gastric cancer.

Keywords: gastric cancer, ivermectin, drug repositioning, ingenuity pathway analysis, *in silico*

INTRODUCTION

Drug repositioning (also called drug repurposing) is a strategy for identifying new uses for approved or investigational drugs that are outside the scope of the original medical indications. Repositioned drugs may reveal new targets and pathways that can be further exploited (Ashburn and Thor, 2004; Pushpakom et al., 2019). Advantages of drug repositioning are related to the drugs that have known mechanisms of action, pharmacological properties, such as pharmacokinetics, pharmacodynamics, posology (the appropriate doses of drugs) and toxicity (Verbaanderd et al., 2017). Of note is that both the pre-clinical and clinical safety data are available (Verbaanderd et al., 2017; Antoszczak et al., 2020). Thus, compared to traditional methods of drug development, drug repositioning requires drastically shortened development time and reduced costs while providing similar therapeutic benefits. Approaches of drug repositioning include computational methods, such as connectivity map (cMap), data mining, pathway mining, ontology modeling, *in silico* and biological experimental validations (e.g., *in vitro* and *in vivo*). The computational drug repositioning can be conducted as repurposing with a defined purpose, repurposing with a strategy, and repurposing with confidence by utilizing reference datasets which are disease-based, drug-based, or knowledge-based (Liu et al., 2013; Subramanian et al., 2017; Xue et al., 2018).

Ivermectin was identified in late 1960s, first approved as veterinary medicine and then human medicine in 1980s for the control of parasitic infection. The discovery and development of ivermectin by William C. Campbell and Satoshi Ōmura were recognized by Nobel Prize in Physiology or Medicine in 2015 (Callaway and Cyranoski, 2015). Ivermectin acts on γ-aminobutyric acid (GABA)-gated chloride channels in the interneuronic synapses of a parasite, whereas in humans, the nerves that are sensitive to GABA, are protected by the blood/brain barrier (Sutherland and Campbell, 1990; Davis et al., 1999; Ikeda, 2003; Chen and Kubo, 2018). However, ivermectin has been repositioned as a broad-spectrum antiviral and antimicrobial agent (Andersen et al., 2020). Interestingly, it is also known that ivermectin can be widely distributed in humans because of its high lipophilicity and thus might exhibit anti-tumor activity in colorectal cancer, breast cancer, glioma, head and neck cancer, leukemia, melanoma, pancreatic cancer, and prostate cancer (Chiou et al., 1987; Juarez et al., 2018).

Gastric cancer (GC) is the fifth most common malignant disease worldwide with the third highest incidence and mortality rate among all cancers (Rawla and Barsouk, 2019). The 5 years overall survival rate is 10–30% except for Japan (50–70%) (Parkin et al., 2002; Matsuda and Saika, 2013). Gastrectomy combined with platinum-based chemotherapy is the most beneficial approach in patient care, and novel targeted therapy, including PD-1 inhibitor in first and second-line setting for advanced GC, are under development (Sitarz et al., 2018; Selim et al., 2019; GBD 2017 Stomach Cancer Collaborators, 2020). However, new drugs and drug repositioning are needed particularly in consideration of the global burden of this deadly disease.

Previously, we have showed repositioning of botulinum toxin type A (also known as botox), everolimus (RAD001) and devimistat (CPI-613) in treatment of GC (Zhao et al., 2014; Rabben et al., 2016; Rabben et al., 2021). The aim of the present study was to reposition ivermectin in treatment of GC. To this end, we have developed and/or utilized the approaches from computational drug repositioning to *in silico*, *in vitro* and *in vivo* validations (**Figure 1**).

MATERIALS AND METHODS

Patients and Animals

Surgical biopsies were collected from 16 patients who underwent total/subtotal or distal gastrectomy because of GC since 2012 at St. Olav's Hospital, Trondheim, Norway (**Table 1**). Four biopsies per patients were taken from tumor and normal tissue and used for clinical pathological evolution and gene expression profiling. The study was approved by the Regional Committees for Medical and Health Research Ethics Central Norway (REK 2012-1029). Furthermore, seven independent datasets of human GC from the TCGA database were used (**Table 2**).

The mouse model of GC, i.e., the transgenic INS-GAS mice which spontaneously develop gastric cancer, was used (Zhao et al., 2014). Stomachs were collected from 26 mice, i.e., six

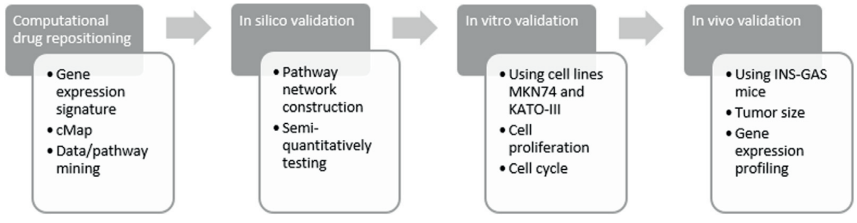

FIGURE 1 | Flow chart of study design. Computational drug repositioning was carried out by using gene expression signatures representing gastric cancer of both patients and mouse model and connectivity map (cMap) and data/pathway mining with the Ingenuity Knowledge Base. Validation included *in silico*, *in vitro* and *in vivo* methods of ivermectin treatment. The rationale of using human samples of GC (without ivermectin treatment) was *i*) to perform computational prediction and data mining and *ii*) to make a comparison with the animal model in order to demonstrate that the animal study could be relevant in the design of clinical trial of ivermectin in the future.

TABLE 1 | Demographic and clinical parameters of gastric cancer patients.

Number of patients		
Age group	49–53	1
	54–58	1
	59–63	2
	64–68	1
	69–73	2
	74–78	5
	79–83	3
	84+	1
Sex	Male	11
	Female	5
Pathologic characteristics		
Lauren classification	Intestinal	3
	Diffuse	4
	Mixed	2
	Not classified	7
Type of gastric resection	Total gastrectomy	7
	Subtotal gastrectomy	5
	Distal gastrectomy	4

females and four males INS-GAS mice at age of 15 months and eight females and eight males wild-type (WT) mice at age of 12 months, for gene expression profiling. In addition, 31 INS-GAS mice, i.e., 12 females and nine males at age of 10 months, and 10 WT mice, i.e., 6 females and four males at age of 10 months, were used for *in vivo* testing.

Animals were housed as four to five mice per cage on wood chip bedding with a 12 h light/dark cycle in a specific pathogen free environment with room temperature of 22°C and 40–60% relative humidity. Animals were inspected daily by investigators and authorized veterinarian using a scoring sheet. Animals should be euthanized at score of 10 if they are emaciated, underconditioned in five consecutive days, or show poor clinical signs (e.g., body weight, appearance, and behavior) before end of the study. This was done according to the Directive 2010/63/EU in which human primary endpoint are defined as "the earliest indicator in an animal experiment of (potential) pain and/or distress that, within the context of moral justification and scientific endpoints to be met, can be used to avoid or limit pain and/or distress by taking actions such as humane killing or terminating or alleviating the pain and distress (Hendriksen and Morton, 1999)" (https://www.humane-endpoints.info/en/council-directive-2010-63-eu). The study was approved by The Norwegian Food Safety Authority (Mattilsynet).

Transcriptomics

Total RNA was extracted from the surgical biopsies of patients and harvested stomachs of mice. RNA quality and quantity were obtained using NanoDrop One (Thermo Scientific, Norway) and Agilent Bioanalyser. For human samples, RNA microarray of GC samples, including 24 tumors of intestinal, diffuse and mixed types from seven patients and 37 normal tissue from six patients, was performed using Illumina platform as described earlier (Zhao et al., 2014). Illumina microarray data was analyzed using Lumi on the $\log_2$ scale and analyzed using the empirical Bayesian method implemented in Limma. The data is accessible via Mendeley Data repository with DOI link at http://dx.doi.org/10.17632/hzmfshy7hp.1. Illumina identifiers (ILMN) were uploaded to Ingenuity Pathway Analysis (IPA, QIAGEN, Hilden, Germany) together with $\log_2$-fold change, *p*-values and *q*-values (false discovery rates). For mouse samples, RNA sequencing was performed using Illumina HiSeqNS500 instrument (NextSeq 500) at 75 bp with paired end (PE) reads using NS500H flow cells with 25M reads/sample. Paired end forward read length (R1): 81, reverse read length (R2): 81. Downstream processing and analysis of the data was performed in the Bioconductor environment in R. For humans, a total of 47,323 transcripts was assigned to analysis in which 37,489 transcripts were mapped and 9,834 transcripts unmapped by Ingenuity Pathway Analysis (IPA) (QIAGEN, Hilden, Germany). For mice, a total of 54,460 transcripts was loaded in which 54,162 were mapped/298 transcripts were unmapped in IPA. For mouse GC after ivermectin treatment, 54,416 transcripts were loaded in which all were mapped in IPA. Filtering of datasets included species (mouse or human) and *p*-value cut-off ($p < 0.05$). Gene expression was analyzed using a *t*-test between tumor and normal tissue in patients, between INS-GAS and WT mice and between INS-GAS mice with and without ivermectin. Genes with a *p*-value of less than 0.05 were considered to be differentially expressed. Transcriptomics datasets were analyzed using IPA. Molecular networks and canonical pathways were algorithmically constructed based on known connectivity and relationships among genes/proteins/metabolites using Ingenuity Knowledge Base. Local and

TABLE 2 | WNT/β-catenin signaling in human gastric cancer (one in the present study and 7 STAD datasets deposited in the TCGA database).

TCGA/Ingenuity Knowledge Base	**WNT/β-catenin signaling**		**N (tumor samples)**	**N (control samples)**
	***Z*-score**	**$-\log_{10}(p)$**		
Human gastric cancer (the present study)	1.604	1.86E00	24	37
GSE48433; 354-stomach cancer [stomach] NA 3485 (PMID: 24885658) Hollingshead et al. (2014)	0.728	N/A	5	5
GSE48433; 171-stomach cancer [stomach] NA 3282 (PMID: 24885658) Hollingshead et al. (2014)	1.155	1.64E00	5	5
GSE118897; 1- stomach cancer [stomach] NA 628 (PMID: 30404039) Yang et al. (2019)	2.121	1.45E00	10	10
1-gastric adenocarcinoma (STAD) [stomach] NA 4052 Ingenuity Knowledge Base	2.138	2.29E00	70	36
10-gastric adenocarcinoma (STAD) [stomach] NA 4053 Ingenuity Knowledge Base	1.342	0	16	71
102-gastric adenocarcinoma (STAD) [stomach] NA 4056 Ingenuity Knowledge Base	1.134	0	20	71
111-gastric adenocarcinoma (STAD) [stomach] NA 4066 Ingenuity Knowledge Base	0.447	0	21	71

FIGURE 2 | Gene expression signature and connectivity map (cMAP). **(A)** Heatmap of human GC gene expression signature that constitutes an activation of cancer disease based on differential expression of >22,000 genes. Size of square is proportional to the number of genes contained in the specific function and color represent activity state (*z*-score; orange: activated, blue: decreased). **(B)** Connectivity map (cMap) showing associations between a large-scale compendium of functional perturbations in cancer cell lines coupled to the human GC gene expression signature based on the L1000 assay (Subramanian et al., 2017). Note: Ivermectin and other known drugs are visualized.

regulatory *z*-scores for canonical pathways and diseases and biofunctions that overlapped with the experimental data of the present study were calculated using the formula described previously (Sitarz et al., 2018). IPA has sophisticated algorithms to calculate predicted functional activation/inhibition of canonical pathways, diseases and functions, transcription regulators and regulators based on their downstream molecule expressions (QIAGEN Inc., https://www.qiagenbioinformatics.com/products/ingenuitypathway-analysis). Fischer's exact test was used to calculate a *p*-value determining the probability that the association between the genes in the datasets from human GC and mouse GC and the canonical pathway or disease/function by chance alone.

Connectivity Map and Data/Pathway Mining

The concept of a Connectivity Map (cMap) was recently developed, whereby genes, drugs, and disease states are connected by virtue of common gene expression signatures (Qu and Rajpal, 2012; Subramanian et al., 2017; Musa et al., 2018). To identify candidate drugs, the gene expression signature of GC was generated based on the gene expression profile of human GC. A positive cMap score indicates there is a positive similarity between a given perturbagen's signature, i.e., genes that are increased by treatment (in reference datasets) are also upregulated in the human GC dataset, while a negative score indicates that the two signatures are opposing. cMap was performed using the gene expression signature of human GC (n = 7 GC vs. n = 6 normal tissue).

Data mining was performed using the gene expression profile data of 61 samples from 16 patients, 26 samples from 26 mice, and 324 samples from seven independent datasets from the TCGA database. Furthermore, knowledge-based pathway mining was used based on previous studies that showed WNT/β-catenin signaling pathway as one of the important pathways in gastric tumorigenesis (Zhao et al., 2014; Rabben et al., 2021). Custom-made molecular networks were generated using the Ingenuity Knowledge Base. Networks were then algorithmically generated based on their interrelationships. WNT/β-catenin signaling pathway was constructed based on the transcriptomic data of INS-GAS mice and were then entered into the "Pathway" module of the IPA to obtain the nodes in every corresponding signaling pathway. Nodes from pathways were added as entries into the "My list"-function and all entries in the list were added to the "My pathway" in IPA. My pathway was used to produce a network of nodes/genes from the WNT/β-catenin signaling pathway that matched with our experimental data from INS-GAS vs. WT mice. The build-tool was used to connect nodes using edges, i.e., relationships including both direct and indirect interactions like chemical-protein interactions, ubiquitination, molecular cleavage, translocation, localization, phosphorylation, expression, protein-protein interactions, activation, regulation of binding, inhibition, membership, reaction, protein-DNA interactions,

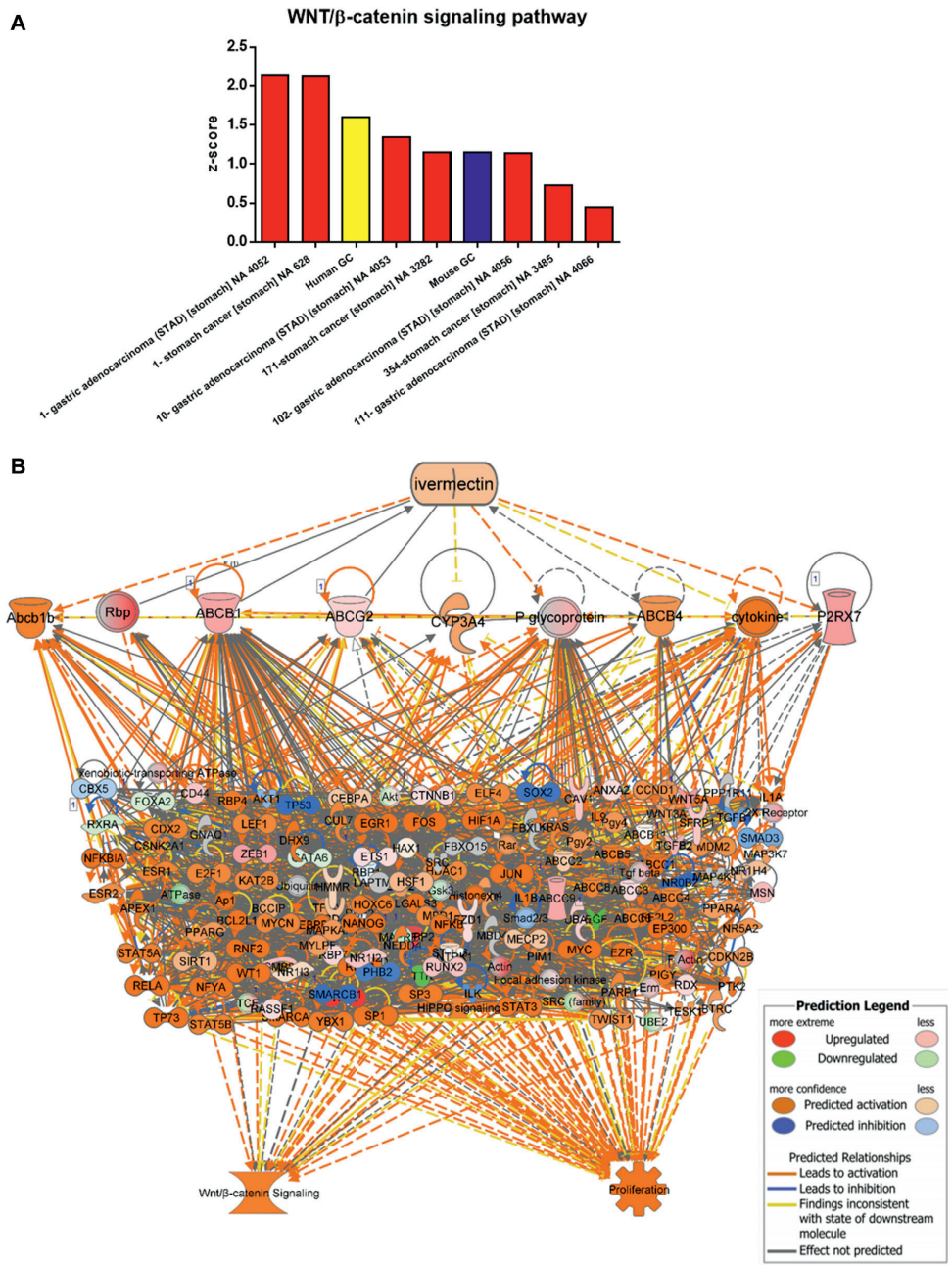

FIGURE 3 | Data/pathway mining of WNT/β-catenin signaling pathway. **(A)** Activation of WNT/β-catenin signaling pathway in eight datasets of human GC (including one used in the present study as indicated in yellow) and one dataset of mouse GC (in blue). **(B)** Hierarchical network representation showing ivermectin and drug targets with downstream signaling pathways of WNT/β-catenin and proliferation. The schema was created in IPA using the grow-tool and the Ingenuity Knowledge Base. The molecular entities (genes and proteins) as well as molecular functions and interactive networks were connected based on interrelationships identified by the Ingenuity Knowledge Base. Expression levels from mouse GC vs. WT. $p < 0.05$. See also **Table 3** *In silico* testing shows ivermectin inhibits WNT/β-catenin signaling.

transcription and modification. The Canonical Pathway overlay-tool was used to arrange the entries into clusters based on pathway. Local *z*-scores were calculated in IPA based on the dataset's correlation with the activated state. Negative *z*-scores indicate a decrease in activity, positive *z*-scores indicate an increase in activity. Canonical pathways were identified using statistical cut-offs at $p < 0.05$.

In Silico Testing

The expression data from mouse GC was compared to all genes in the pathway. The molecule activity predictor (MAP)-function was used to predict activation/inhibition between the nodes in the network. The *in silico* tool integrated with the MAP-function was employed to predict effects on the network after gene inhibition and/or stimulation in the ivermectin cluster. Connections between genes were then algorithmically generated based on their interrelationships including both direct and indirect interactions like chemical-protein interactions, ubiquitination, molecular cleavage, translocation, localization, phosphorylation, expression, protein-protein interactions, activation, regulation of binding, inhibition, membership, reaction, protein-DNA interactions, transcription and modification. Network clusters of WNT/β-catenin pathway was constructed based on the transcriptomic data of INS-GAS mice (i.e., limited to and built on genes from the dataset). The build-tool was used to connect nodes using edges, i.e., relationships. Categorical values were set to each gene/node using a semi-quantitative method to quantify the color-change resulting from *in silico* inhibition. Local *z*-scores were calculated in IPA based on the dataset's correlation with the activated state. Negative *z*-scores indicate a decrease in activity, positive *z*-scores indicate an increase in activity. Canonical pathways were identified using statistical cut-offs at $p < 0.05$.

In Vitro Testing

GC cell lines included human gastric cancer cells MKN74 (intestinal type) and KATO-III (diffuse type) (for detailed information on molecular characteristic, see Yokozaki, 2000). It should be noticed that both cell lines overexpress β-catenin (Asciutti et al., 2011). Cells were maintained in RPMI-1640 medium (Sigma Aldrich, Oslo, Norway) supplemented with fetal bovine serum (10%, FBS), Sodium pyruvate and penicillin streptomycin solution (1%) (Sigma Aldrich, Oslo, Norway) in a humidified incubator holding 5% CO_2 and 37°C. For proliferation assay, MKN74 and KATO-III were seeded in 96-well plates (2,500 cells/well and 3,000 cells/well, respectively) and incubated overnight. Ivermectin (MW: 875.09 g/mol) was dissolved in DMSO (100%) to 50 mM stock solution. Cells were treated with ivermectin (0–50 μM) or vehicle control (0.45% v/v DMSO) for 24, 48, and 72 h. Proliferation was measured using a commercial CCK-8 Kit (Sigma Aldrich, Oslo, Norway) with absorbance read at 450 nm. For cell cycle analysis, KATO-III cells were seeded as 3.0×10^5 cells/well in 6-well plates and incubated for 72 h with medium change after 48 h. Ivermectin was added to the wells as final concentrations of 12, 15 or 18 μM for 24 h. Cells were harvested by trypsin, washed twice in room tempered PBS, resuspended in ice cold ethanol (70%) and kept at −20°C for minimum 15 min. Cells were washed twice in cold PBS and centrifuged (1,500 rpm, 5 min, 4°C), and resuspended in freshly prepared PI staining solution (0.25% Triton- X-100, 50 μg/ml propidium iodide (PI) and 200 μg/ml RNAase) for minimum 30 min. Cell cycle distribution was analyzed using FACS. Single cells were gated to exclude doublets and clustered cells. 2.0×10^4 cells were counted per sample, and percentage cell distribution was derived from obtained histograms in the FACSDiva software. Results are presented as means of $n = 3$ replicates/treatments. Data was analyzed using Microsoft Excel 2010.

In Vivo Testing

Thirty-one INS-GAS mice were randomly divided into two groups: ivermectin treatment (12 females and nine males at age of 10 months) and controls (no treatment, six females and four males at age of 10 months). Ivermectin was reconstituted from lyophilized powder in DMSO to 50 mM solution and then diluted in saline before use. The treatment regimen was designed to let the mice tolerate the procedure easily, i.e., intraperitoneal injection at a dose of 10 mg/kg in a volume of about 0.5 ml/mouse with 27G needle once per day for 5 days, followed by no treatment for 5 days and then injection once per day for 10 days. This regimen was repeated 10 days later. The total duration of treatment was 2 months (2 × 30 days). Vehicle treatment was not performed because neither vehicle *per se* nor procedure would lead to any significant stress response. The mice were euthanized under isoflurane inhalation anesthesia (2–3%), and stomachs were collected as described previously (Zhao et al., 2014). Tumor volume density (% of glandular area of the stomach occupied by tumor) was measured using a point count method (Zhao et al., 2014). The tissue samples were collected for transcriptomics as aforementioned.

Statistical Analysis

Values are expressed as means ± SEM or SD (stated in individual figure legend). For comparison of two independent groups, student independent *t*-test was used. For comparison of multiple groups, one-way ANOVA with Tukey's or Dunnett's post-hoc tests were used (stated in individual figure legend). SPSS version 26.0 for Windows (SPSS Inc., Chicago, IL, United States) was used and a *p*-value < 0.05 was considered to be statistically significant. Other methods are stated in corresponding figure legends.

RESULTS

Computational Drug Repositioning Suggests the WNT/β-Catenin Signaling as Potential Target of Ivermectin

A cMap was created according to the gene expression signature (**Figures 2A,B**). A total of 2,428 drugs were categorized into 47 groups of inhibitors for, e.g., DNA synthesis, murine double minute (MDM) and lactate dehydrogenase, including ivermectin. Additionally, drugs we have demonstrated previously, including

TABLE 3 | Gene expression in networks comprised of ivermectin interactions and WNT/β-catenin signaling pathways in mouse gastric cancer (as presented in **Figure 4A**).

Gene	Ensembl ID	Log_2 FC	*p*-value	Entrez gene ID for patients	Entrez gene ID for mice
ABCB1	ENSMUSG00000040584	1.877	2.04E-04	5243	18671
ABCC3	ENSMUSG00000020865	0.525	1.16E-02	8714	76408
ABCC9	ENSMUSG00000030249	1.835	2.74E-11	10060	20928
ABCG2	ENSMUSG00000029802	0.921	3.97E-03	9429	26357
ANXA2	ENSMUSG00000032231	0.679	3.38E-04	302	12306
CAV1	ENSMUSG00000007655	1.181	8.61E-04	857	12389
CD44	ENSMUSG00000005087	1.156	1.42E-05	960	12505
CRABP2	ENSMUSG00000004885	4.298	2.97E-02	1382	12904
CTNNB1	ENSMUSG00000006932	0.208	4.75E-02	1499	12387
EGF	ENSMUSG00000028017	−1.946	3.86E-03	1950	13645
ETS1	ENSMUSG00000032035	0.621	2.69E-02	2113	23871
FBXL13	ENSMUSG00000048520	3.359	3.15E-02	222235	320118
FOXA2	ENSMUSG00000037025	−0.351	1.45E-02	3170	15376
FZD1	ENSMUSG00000044674	0.670	1.76E-03	8321	14362
GATA6	ENSMUSG00000005836	−0.331	1.95E-02	2627	14465
IL1A	ENSMUSG00000027399	3.560	1.60E-02	3552	16175
MAPRE1	ENSMUSG00000027479	−0.456	5.95E-03	22919	13589
MECP2	ENSMUSG00000031393	−0.374	5.89E-02	4204	17257
MSN	ENSMUSG00000031207	1.383	1.79E-17	4478	17698
NR1I2	ENSMUSG00000022809	1.174	2.29E-08	8856	18171
P2RX7	ENSMUSG00000029468	2.097	3.93E-07	5027	18439
PSMB8	ENSMUSG00000024338	1.376	8.55E-03	5696	16913
RASSF1	ENSMUSG00000010067	0.291	4.88E-02	11186	56289
RBP7	ENSMUSG00000028996	0.851	4.24E-02	116362	63954
RDX	ENSMUSG00000032050	0.749	1.53E-03	5962	19684
RUNX2	ENSMUSG00000039153	1.241	2.32E-04	860	12393
RXRA	ENSMUSG00000015846	−0.404	2.74E-03	6256	20181
SFRP1	ENSMUSG00000031548	1.093	2.91E-03	6422	20377
TGFB2	ENSMUSG00000039239	1.573	3.53E-05	7042	21808
TP63	ENSMUSG00000022510	5.030	2.28E-02	8626	22061
TTR	ENSMUSG00000061808	−1.516	1.78E-04	7276	22139
UBA7	ENSMUSG00000032596	1.008	2.12E-03	7318	74153
WNT5A	ENSMUSG00000021994	2.170	1.90E-14	7474	22418
ZEB1	ENSMUSG00000024238	2.031	8.00E-12	6935	21417

gemcitabine, paclitaxel, everolimus, and scopolamine, were also found (Zhao et al., 2014; Rabben et al., 2021).

Data/pathway mining revealed activation of the WNT/β-catenin signaling in human as well as mouse GC (**Table 2**). In addition to our own human GC and mouse GC data, seven independent datasets of human stomach adenocarcinoma (STAD) were found to have activation of the WNT/β-catenin (**Figure 3A** and **Table 2**). Using the knowledge-based repositioning strategy, nine targets were identified in connection with WNT/β-catenin signaling pathway and proliferation in both human and mouse GC (**Figure 3B**), i.e., ATP-dependent translocase (Abcb1b), retinol-binding proteins (Rbp), ATP binding cassette subfamily B member 1 (ABCB1), ATP Binding cassette subfamily G member 2 (ABCG2), cytochrome P450 family 3 subfamily A member 4 (CYP3A4), P-glycoprotein (also known as multi-drug resistant protein, MDRP), ATP binding cassette subfamily B member 4 (ABCB4), cytokine, and P2X purinoceptor 7 (P2RX7). Each gene/protein connected to a subset of algorithmically chosen genes based on the Ingenuity Knowledge Base. These genes were collectively activating both WNT/β-catenin signaling and proliferation, resulting in locally activated *z*-scores (shown in orange) (**Table 3**).

An *in silico* interaction network of ivermectin with WNT/β-catenin signaling pathway was constructed (**Figure 4A**). Inhibition of the targets of ivermectin led to the inhibition of downstream nodes in a "dose-dependent manner" (**Figure 4B**). It should be noticed that the inhibition of single molecules was not enough to have inhibitory or stimulatory effects on the signaling pathway.

Ivermectin Inhibits Cell Proliferation and Induces Cell Cycle Arrest

Testing of ivermectin in MKN74 and KATO-III cells showed that there were time- and concentration-depended inhibitions of proliferation by the drug with similar IC_{50} values for the periods of 24, 48 and 72 h (**Figures 5A,B**). Furthermore, ivermectin induced cell cycle arrest in a concentration-depended manner (**Figure 5C**). It should be noticed that ivermectin at IC_{50} did not affect the cells in S-phase but increased percentage of cells in G_1 while reducing percentage of cells in G_2/M phases. By contrast, higher concentration of ivermectin increased percentage of cells in S phase while reducing the percentage of cells in G_1 and G_2/M phases, suggesting that

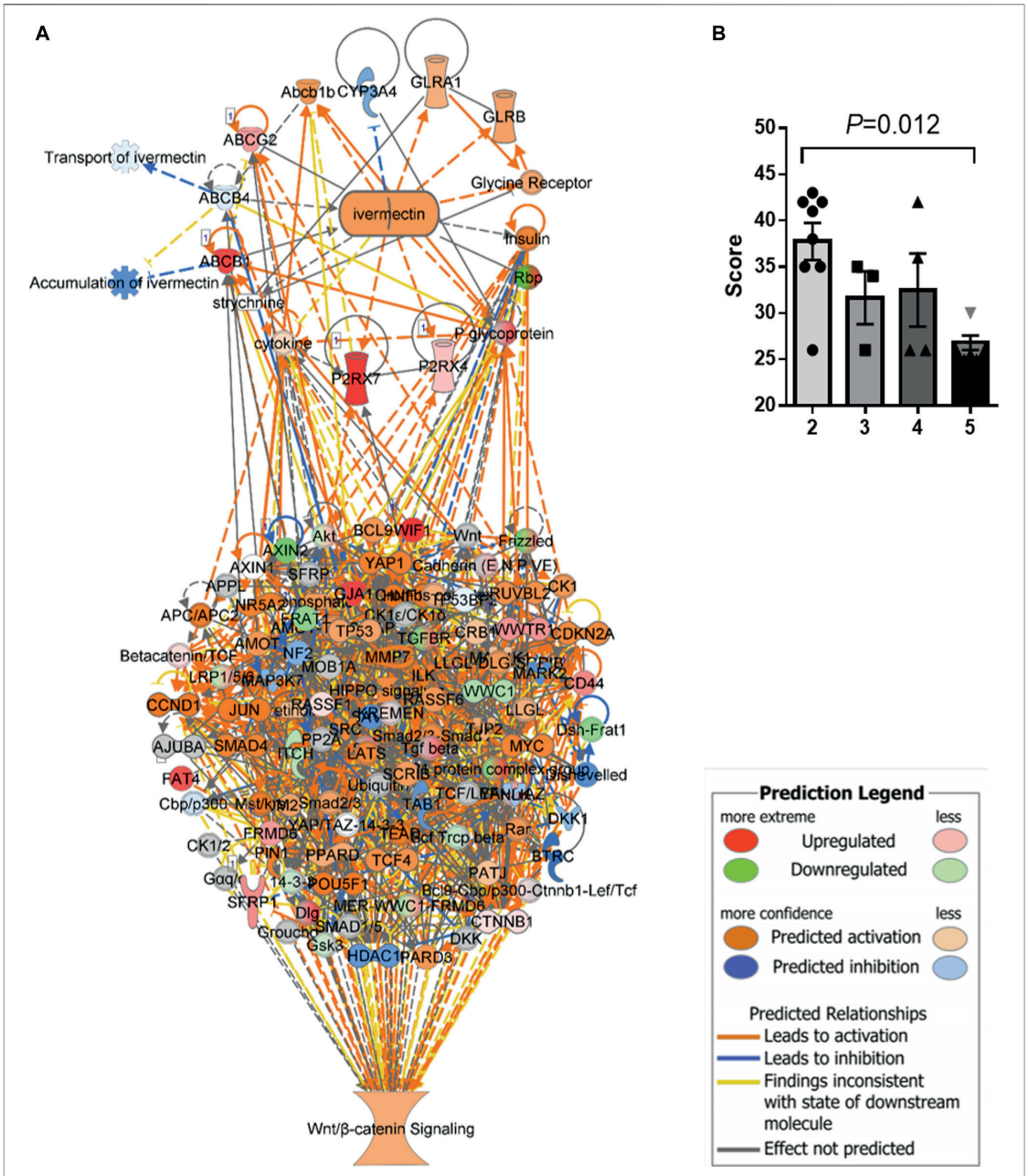

FIGURE 4 | *In silico* interaction network of ivermectin with WNT/β-catenin signaling pathway. **(A)** An interaction network of ivermectin with WNT/β-catenin signaling pathway was made using the Ingenuity Knowledge Base. **(B)** Two-/three-/four-/five combinations of inhibition/stimulation of nodes in the ivermectin cluster (**A**, upper cluster) had "dose-dependent" effect of the sum network scores of WNT/β-catenin (including HIPPO) pathway (**A**, lower cluster). Categorical values were set to each gene/node using a semi-quantitative method to quantify the color-change resulting from *in silico* inhibition. Dark blue colored nodes were represented by – 2, light blue as – 1, white as 0, light orange as +1 and dark orange as +2. Values are represented of means of n = 3–8 experiments per node/gene. Multiple comparison using one-way ANOVA with Tukey post hoc test was used. Created in IPA (QIAGEN).

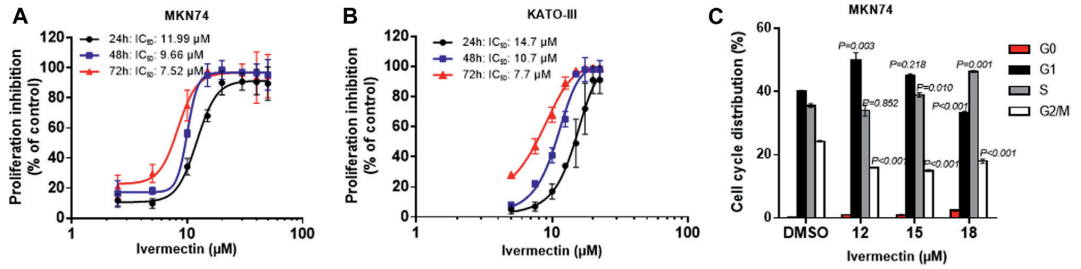

FIGURE 5 | Time- and concentration-dependent effects of ivermectin on proliferation and cell cycle. **(A,B)** Concentration-response curves upon 24–72 h ivermectin-treatment in MKN74 and KATO-III cells. Proliferation was assessed using CCK-8 Kit at 450 nm. IC_{50} values were calculated from sigmoidal regression curve fitting using variable slope on normalized response from log_{10}-transformed x-values (GraphPad Prism v.6). **(C)** Cell cycle analysis of KATO-III cells. Means of $n = 3$ replicates/treatment with SD. One-way ANOVA with Dunnett's post hoc test (2-sided) compared to respective control groups.

ivermectin arrested cells at the G_1 phase at IC_{50} and higher dose of the drug shifted cells to S phase.

Ivermectin Reduces Tumor Size Which Was Associated With Inactivation of WNT/β-Catenin Signaling, Down Regulation of Cell Proliferation and Upregulation of Cell Death Signaling Networks

A treatment regimen using ivermectin at 10 mg/kg for 2 months was established based on the *in silico* and pilot experiments. Mice tolerated the treatment well, although some mice had weight loss during treatment (<15%, $p > 0.05$, two-tailed). The mice had no serious side effects of ivermectin and no mice that were treated with ivermectin were killed according to the human primary endpoints which include stressful behavior, abdominal pain and impaired physical activity. The tumor size was reduced by ivermectin treatment (**Figure 6A**). Comparison analysis between mouse GC with and without ivermectin treatment revealed 4,112 differentially expressed genes (**Figure 6B**). The genes involved in WNT/β-catenin signaling pathway were particularly inhibited by ivermectin treatment, as shown by a change in *z*-scores from 1.151 (mouse GC without treatment) down to −1.789 (mouse GC after ivermectin treatment) (**Figure 6C** and **Table 2**) and log_2 fold-changes (**Figure 6D vs. 6E**).

Expression analysis in IPA revealed that cell proliferation was activated in mouse GC without treatment and inactivated in mouse GC with treatment. On the other hand, cell death including apoptosis was inactivated in mouse GC without treatment but activated in mouse GC with treatment (**Figures 7A–D**).

DISCUSSION

The next generation connectivity map (cMap) has been recently developed and should be acknowledged that the cMap methods and data are available without restriction to the research community (Subramanian et al., 2017). As pointed out in the original paper, a future comprehensive cMap might expand in multiple dimensions, e.g., new cell types, patient-derived induced pluripotent stem cells and genome-edited isogenic cell lines (Subramanian et al., 2017). Using this method, we found that the scores of the known drugs in treatment of GC (including ivermectin) were too low to indicate strong associations between these drugs and human GC gene expression signature, which was most likely due to the fact that the reference profile catalogue of cMap has been built to date on 12,328 genes of various cancer cell lines (including AGS which is a moderately differentiated human gastric adenocarcinoma hyperdiploid cell line) but not tumor tissues (https://clue.io/connectopedia/l1000_gene_space and https://clue.io/connectopedia/core_cmap_cell_panel).

In addition to the hypothesis generation approach by cMap, we further utilized data mining and pathway mining of knowledge-based datasets to identify the potential drugs in connection with a broad concept ranging from molecular entities (such as genes and proteins) to biological phenomena (such as molecular functions, pathways and phenotypes). Based on a better understanding of GC biology and signaling pathways, in the present study we focused on the WNT/β-catenin pathway by utilizing the algorithms of IPA which is built on a comprehensive, manually curated content of the QIAGEN Knowledge Base (over 57,000 publicly available datasets and continuously updated).

The results of the present study showed that the potential molecular targets and the mechanisms of action of ivermectin in GC differed from those in parasites in which ivermectin causes an influx of Cl-ions through the cell membrane of invertebrates by activation of specific ivermectin-sensitive ion channels (Laing et al., 2017; Chen and Kubo, 2018). In the present study, we identified ivermectin in connection with cell proliferation, particularly towards the genes (e.g., members of the adenosine triphosphate (ATP)-binding cassette (ABC) transporters). ABC are a superfamily of membrane proteins which play significant roles in transporting various exogenous and endogenous

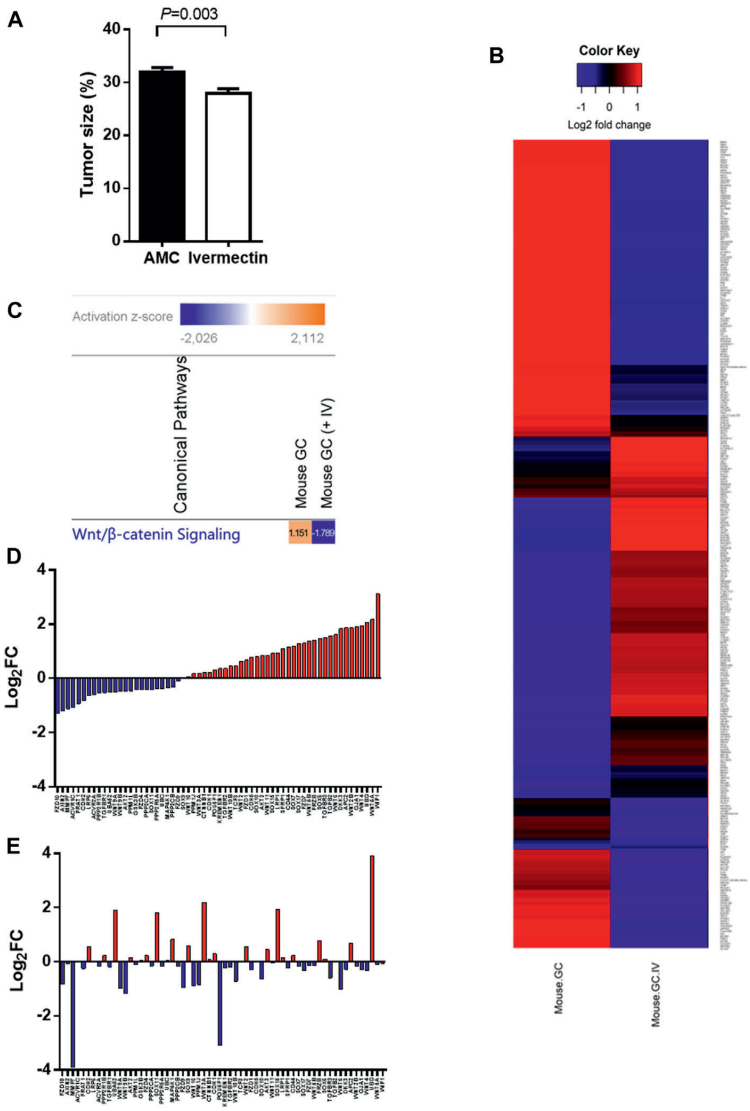

FIGURE 6 | Tumor size and gene expression profiles in response to ivermectin. **(A)** Tumor size (% of glandular area of stomach occupied by tumor) in age-matched controls (AMC, $n = 14$) and ivermectin-treated mice ($n = 17$) (Ivermectin). Independent t-test (2-sided) between group means (normality assumption met). Error bars represent SEM. **(B)** Global gene expression profile of mouse GC with and without ivermectin treatment (created in RStudio using heatmap.2 function). Only differentially expressed genes with $p < 0.05$ are included (4,112 genes). **(C)** WNT/β-catenin pathway was activated (z-score = 1.151) in mouse GC without treatment but inhibited in mouse GC with ivermectin treatment (z-score = −1.789). **(D,E)** WNT/β-catenin gene expressions in mouse GC mice without treatment **(D)** and with ivermectin treatment **(E)**. Note: same orders of individual genes in **(D)** and **(E)**.

substances across membranes against concentration gradients through ATP hydrolysis, and many of these transporters are known as multidrug resistance proteins (MRPs) (Mao et al., 2019). As showed in the present study, ivermectin also acted on the ABC and the signaling pathways, leading to inhibition of cell proliferation by deactivating LXR/RXR signaling (Beltowski, 2011; Saito-Hakoda et al., 2015).

It has been shown that activation of the WNT/β-catenin signaling pathway plays a pivotal role in many types of cancer (Clevers, 2006; Zhan et al., 2017). Previously, we and other

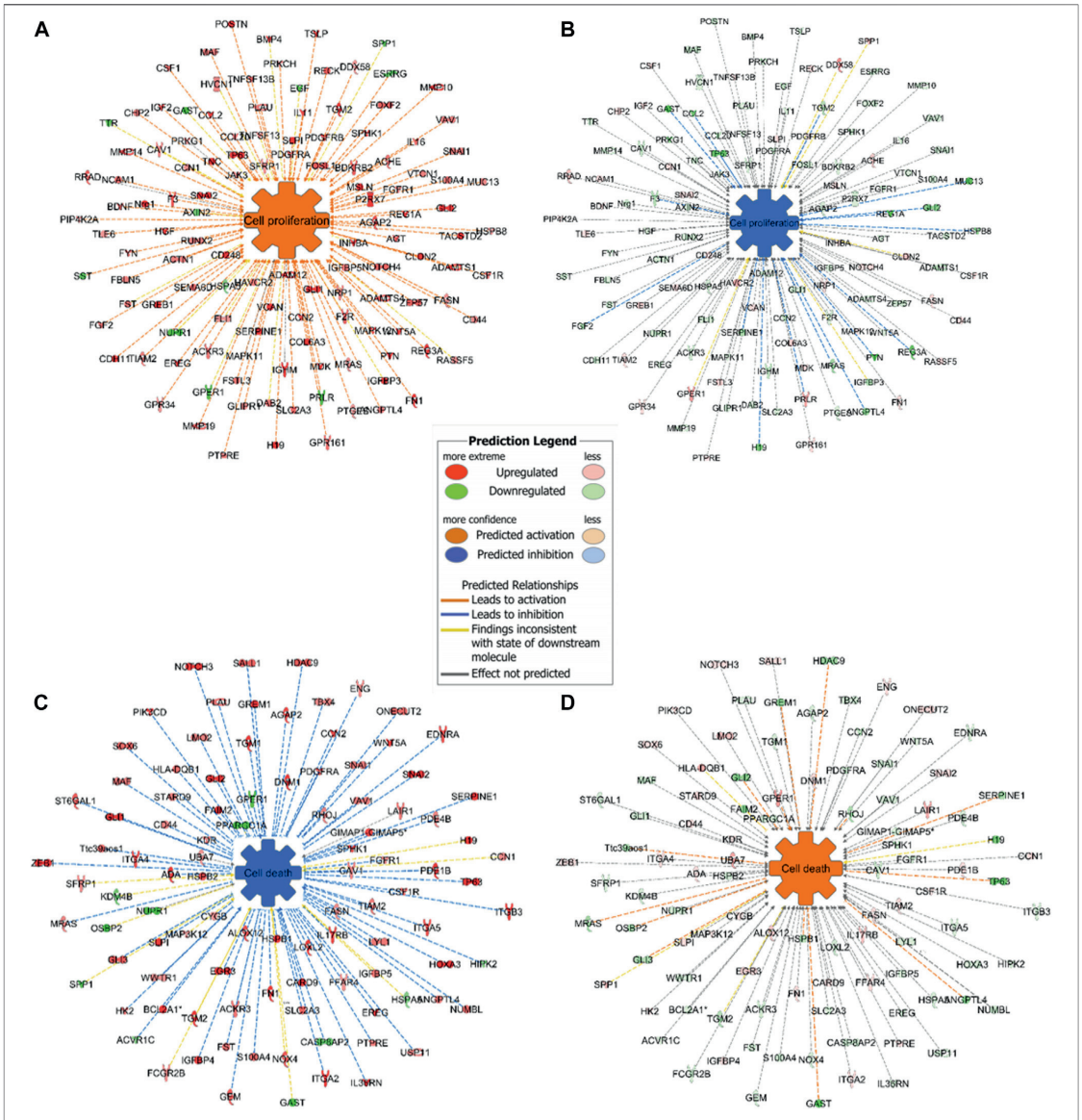

FIGURE 7 | Representative networks of cell proliferation and cell death in mice with or without ivermectin treatment. **(A)** Mouse GC cell proliferation network was created using BioProfiler in IPA. Only genes differentially expressed ($p < 0.05$, $Log_2FC \pm 1.0$) between mouse GC vs. WT were included. Overexpression of genes in the network results in activation of cell proliferation (orange; *z*-score > 0). **(B)** Genes in the cell proliferation network was downregulated in GC mice with ivermectin treatment (blue; *z*-score < 0). **(C)** Mouse GC cell death network including apoptotic markers was created using BioProfiler in IPA. Only genes differentially expressed ($p < 0.05$, $Log_2FC \pm 1.0$) between mouse GC vs. WT were included. Overexpression of genes in the network results in inhibition of cell death (blue; *z*-score < 0). **(D)** Cell death network was aberrantly expressed in GC mice with ivermectin treatment (orange; *z*-score > 0).

research groups have demonstrated that the tumorigenesis of gastric cancer involves the WNT/β-catenin signaling pathway and the inhibition of the signaling pathways by means of denervation can suppress the tumorigenesis (Zhao et al., 2014; Chiurillo, 2015; Koushyar et al., 2020; Rabben et al., 2021). In the present study, we applied *in silico* modelling to

show that ivermectin could inhibit the WNT/β-catenin signaling pathway including HIPPO signaling pathway, which is known to interact each other (Hayakawa et al., 2017; Li et al., 2019). We then employed *in vitro* and *in vivo* approaches to show that ivermectin could inhibit cell proliferation and reduce tumor size, which was associated with the inhibition of the WNT/β-catenin signaling pathway. Thus, we may suggest that ivermectin could target the WNT/β-catenin singling pathway, leading to a reduced tumorigenesis. This was also in line with possible antitumor actions of ivermectin in other types of cancer cells, such as breast, colon, lung, prostate and bladder (Melotti et al., 2014; Diao et al., 2019; Nappi et al., 2020).

Control of cell proliferation generally occurs during the G_1 phase and multiple signals, ranging from growth factors to DNA damage to developmental cues, influence the decision to enter S phase, when DNA is replicated (Duronio and Xiong, 2013). The results of the present study showed that ivermectin altered cell cycle in a concentration-dependent manner, which is consistent with a previous report showing accumulation of cells in the G_1/S phases (Zhang et al., 2019). In the present study, IC_{50}-dose of ivermectin caused cell cycle arrest at G_1 phase, whereas at higher doses, it caused S phase arrest. It has been suggested that WNT/β-catenin activation triggered cells in S phase, and HIPPO signaling might involve in G_1 phase (Benham-Pyle et al., 2016; Kim et al., 2019). The evidence of possible link between the cell cycle arrest and inhibition of WNT/β-catenin and/or HIPPO singling pathways is needed to be further investigated, particularly in the context of ivermectin for GC.

There were several limitations of the present study. The cell proliferation and apoptosis in the *in vitro* experiment were not evaluated further by flow cytometry nor specific assays, e.g., annexin V staining or caspase activity. However, the gene expression profiling confirmed the association between the activities of networks of cell proliferation and cell death in mice, namely increased in cell proliferation and decrease in cell death in GC mice without treatment, and reversed activities in GC mice treated with ivermectin. It should be noticed that the decrease in tumor size 2 months after ivermectin treatment was modest. As a matter of fact, in a separate experiment, we found that chemotherapy with 5-FU and oxaliplatin at the maximal dosage given to GC mice at the same age as ones in this study was without inhibition on the tumor size during 2 months of treatment (as same as in this study) (data not shown). However, the impacts of ivermectin treatment after a longer period of treatment alone and/or in combination with chemotherapy on resistance, migration and invasion could be worthwhile for future investigation. The results of the present study showed evidence of possible involvement of WNT/β-catenin signaling pathway in connection with the anti-cancer effect of ivermectin. For instance, prediction of ivermectin was successfully made by the WNT/β-catenin signaling pathway mining but not cMap. Validation of ivermectin was significant *in silico* model of the WNT/β-catenin signaling pathway. Up-regulation of WNT/β-catenin signaling pathway took place in patients, human cell lines and mouse model of GC. Ivermectin treatment induced downregulation of the WNT/β-catenin signaling pathway in the mouse GC. However, additional evidence is needed to demonstrate that the effect of ivermectin is dependent on WNT/β-catenin signaling pathway. For instance, it would be worthwhile to further investigate how modulation of the WNT/β- catenin signaling pathway with specific inhibitors and activators will affect the response to ivermectin treatment *in vitro* and *in vivo*.

CONCLUSIONS

The results of the present study show that ivermectin is a promising drug candidate for treatment of GC. The results may indicate an alternative mechanism of action of ivermectin, i.e., inhibition of the WNT/β-catenin signaling pathway in mammals rather than it acts on glutamate-gated chloride channels, which are common in nematodes, insects and ticks, thereby paralysing pharyngeal and somatic muscles. As ivermectin is exceptionally safe for mammals because of the blood/brain barrier, further pre-clinical and clinical studies of repositioning ivermectin for GC are warranted.

DATA AVAILABILITY STATEMENT

The original contributions presented in the study are publicly available. This data can be found here: The mouse RNA seq/microarray data have been deposited in the NCBI Bioproject database under the accession number PRJNA690520 which can be accessed using the following link: http://www.ncbi.nlm.nih.gov/bioproject/690520. The human microarray data is available online via Mendeley Data repository with DOI link at http://dx.doi.org/10.17632/hzmfshy7hp.1. The RNAseq data in mouse GC after ivermectin treatment is available from the authors upon request.

ETHICS STATEMENT

The studies involving human participants were reviewed and approved by Regional Committees for Medical and Health Research Ethics Central Norway (REK 2012-1029). The patients/participants provided their written informed consent to participate in this study. The animal study was reviewed and approved by Mattilsynet. Written informed consent was obtained from the individual(s) for the publication of any potentially identifiable images or data included in this article.

AUTHOR CONTRIBUTIONS

H-LR: *In vitro* and *in vivo* experiments, data analysis, manuscript writing; GTA: Patient samples, *in vivo* experiment and manuscript writing; AI and DK: cMap and manuscript writing; MKO: *In vivo* experiments and manuscript writing;

JEG: Patient samples and manuscript writing; TCW: *In vivo* model, manuscript writing; DC: Study idea and design, manuscript writing; C-MZ: Study idea and design, *in vivo* experiment and patient samples; manuscript writing.

FUNDING

We thank the research grants and PhD fellowships supported by the Liaison Committee between the Central Norway Regional Health Authority (Helse-Midt Norge RHF) and Norwegian University of Science and Technology (NTNU) (grant numbers 46056636/46056928/90061700/90061701), Joint Program of the Medical Faculty of NTNU and St. Olavs University Hospital, the Cancer Foundation of St. Olavs Hospital (Kreftfondet ved St. Olavs hospital), and the technical support by Genomics Core Facility (GCF) which is funded by the Faculty of Medicine and Health Sciences at NTNU and RHF.

REFERENCES

Andersen, P. I., Ianevski, A., Lysvand, H., Vitkauskiene, A., Oksenych, V., Bjørås, M., et al. (2020). Discovery and development of safe-in-man broad-spectrum antiviral agents. *Int. J. Infect. Dis.* 93, 268–276. doi:10.1016/j.ijid.2020.02.018

Antoszczak, M., Markowska, A., Markowska, J., and Huczyński, A. (2020). Old wine in new bottles: drug repurposing in oncology. *Eur. J. Pharmacol.* 866, 172784. doi:10.1016/j.ejphar.2019.172784

Asciutti, S., Akiri, G., Grumolato, L., Vijayakumar, S., and Aaronson, S. A. (2011). Diverse mechanisms of Wnt activation and effects of pathway inhibition on proliferation of human gastric carcinoma cells. *Oncogene* 30, 956–966. doi:10.1038/onc.2010.475

Ashburn, T. T., and Thor, K. B. (2004). Drug repositioning: identifying and developing new uses for existing drugs. *Nat. Rev. Drug Discov.* 3, 673–683. doi:10.1038/nrd1468

Beltowski, J. (2011). Inhibition of cell proliferation: a new role of liver X receptors. *Clin. Lipidol.* 6, 137–141. doi:10.2217/clp.11.3

Benham-Pyle, B. W., Sim, J. Y., Hart, K. C., Pruitt, B. L., and Nelson, W. J. (2016). Increasing β-catenin/Wnt3A activity levels drive mechanical strain-induced cell cycle progression through mitosis. *Elife* 5, e19799. doi:10.7554/eLife.19799

Callaway, E., and Cyranoski, D. (2015). Anti-parasite drugs sweep Nobel prize in medicine 2015. *Nature* 526, 174–175. doi:10.1038/nature.2015.18507

Chen, I. S., and Kubo, Y. (2018). Ivermectin and its target molecules: shared and unique modulation mechanisms of ion channels and receptors by ivermectin. *J. Physiol.* 596, 1833–1845. doi:10.1113/JP275236

Chiou, R., Stubbs, R. J., and Bayne, W. F. (1987). Determination of ivermectin in human plasma and milk by high-performance liquid chromatography with fluorescence detection. *J. Chromatogr.* 416, 196–202. doi:10.1016/0378-4347(87)80502-9

Chiurillo, M. A. (2015). Role of the Wnt/β-catenin pathway in gastric cancer: an in-depth literature review. *World J. Exp. Med.* 5, 84–102. doi:10.5493/wjem.v5.i2.84

Clevers, H. (2006). Wnt/beta-catenin signaling in development and disease. *Cell* 127, 469–480. doi:10.1016/j.cell.2006.10.018

GBD 2017 Stomach Cancer Collaborators (2020). The global, regional, and national burden of stomach cancer in 195 countries, 1990-2017: a systematic analysis for the global burden of disease study 2017. *Lancet Gastroenterol. Hepatol.* 5, 42–54. doi:10.1016/S2468-1253(19)30328-0

Davis, J. A., Paylor, R., McDonald, M. P., Libbey, M., Ligler, A., Bryant, K., et al. (1999). Behavioral effects of ivermectin in mice. *Lab. Anim. Sci.* 49, 288–296.

Diao, H., Cheng, N., Zhao, Y., Xu, H., Dong, H., Thamm, D. H., et al. (2019). Ivermectin inhibits canine mammary tumor growth by regulating cell cycle progression and WNT signaling. *BMC Vet. Res.* 15, 276. doi:10.1186/s12917-019-2026-2

Duronio, R. J., and Xiong, Y. (2013). Signaling pathways that control cell proliferation. *Cold Spring Harb. Perspect. Biol.* 5, a008904. doi:10.1101/cshperspect.a008904

Hayakawa, Y., Sakitani, K., Konishi, M., Asfaha, S., Niikura, R., Tomita, H., et al. (2017). Nerve growth factor promotes gastric tumorigenesis through aberrant cholinergic signaling. *Cancer Cell* 31, 21–34. doi:10.1016/j.ccell.2016.11.005

Hendriksen, C. F. M., and Morton, D. B.(Editors) (1999). "Humane endpoints in animal experiments for biomedical research," in Proceedings of the International Conference, Zeist, The Netherlands, November 22–25 (1998), (London: Royal Society of Medicine Press Limited, Laboratory Animals Supplement).

Hollingshead, M. G., Stockwin, L. H., Alcoser, S. Y., Newton, D. L., Orsburn, B. C., Bonomi, C. A., et al. (2014). Gene expression profiling of 49 human tumor xenografts from *in vitro* culture through multiple *in vivo* passages--strategies for data mining in support of therapeutic studies. *BMC Genomics* 15, 393. doi:10.1186/1471-2164-15-393

Ikeda, T. (2003). Pharmacological effects of ivermectin, an antiparasitic agent for intestinal strongyloidiasis: its mode of action and clinical efficacy. *Nippon Yakurigaku Zasshi* 122, 527–(538.) [in Japanese, with English summary]. doi:10.1254/fpj.122.527

Juarez, M., Schcolnik-Cabrera, A., and Dueñas-Gonzalez, A. (2018). The multitargeted drug ivermectin: from an antiparasitic agent to a repositioned cancer drug. *Am. J. Cancer Res.* 8, 317–331.

Kim, W., Cho, Y. S., Wang, X., Park, O., Ma, X., Kim, H., et al. (2019). Hippo signaling is intrinsically regulated during cell cycle progression by APC/CCdh1. *Proc. Natl. Acad. Sci. U.S.A.* 116, 9423–9432. doi:10.1073/pnas.1821370116

Koushyar, S., Powell, A. G., Vincan, E., and Phesse, T. J. (2020). Targeting wnt signaling for the treatment of gastric cancer. *Int. J. Mol. Sci.* 21, 3927. doi:10.3390/ijms21113927

Laing, R., Gillan, V., and Devaney, E. (2017). Ivermectin–old drug, new tricks?. *Trends Parasitol.* 33, 463–472. doi:10.1016/j.pt.2017.02.004

Li, N., Lu, N., and Xie, C. (2019). The Hippo and Wnt signalling pathways: crosstalk during neoplastic progression in gastrointestinal tissue. *FEBS J.* 286, 3745–3756. doi:10.1111/febs.15017

Liu, Z., Fang, H., Reagan, K., Xu, X., Mendrick, D. L., Slikker, W., Jr, et al. (2013). *In silico* drug repositioning: what we need to know. *Drug Discov. Today* 18, 110–115. doi:10.1016/j.drudis.2012.08.005

Mao, X., He, Z., Zhou, F., Huang, Y., and Zhu, G. (2019). Prognostic significance and molecular mechanisms of adenosine triphosphate-binding cassette subfamily C members in gastric cancer. *Medicine* 98, e18347. doi:10.1097/md.0000000000018347

Matsuda, T., and Saika, K. (2013). The 5-year relative survival rate of stomach cancer in the USA, Europe and Japan. *Jpn. J. Clin. Oncol.* 43, 1157–1158. doi:10.1093/jjco/hyt166

Melotti, A., Mas, C., Kuciak, M., Lorente-Trigos, A., Borges, I., and Ruiz i Altaba, A. (2014). The river blindness drug Ivermectin and related macrocyclic lactones inhibit WNT-TCF pathway responses in human cancer. *EMBO Mol. Med.* 6, 1263–1278. doi:10.15252/emmm.201404084

Musa, A., Ghoraie, L. S., Zhang, S. D., Glazko, G., Yli-Harja, O., Dehmer, M., et al. (2018). A review of connectivity map and computational approaches in pharmacogenomics. *Brief. Bioinform.* 19, 506–523. doi:10.1093/bib/bbw112

Nappi, L., Aguda, A. H., Nakouzi, N. A., Lelj-Garolla, B., Beraldi, E., Lallous, N., et al. (2020). Ivermectin inhibits HSP27 and potentiates efficacy of oncogene targeting in tumor models. *J. Clin. Invest.* 130, 699–714. doi:10.1172/JCI130819

Parkin, D. M., Bray, F., Ferlay, J., and Pisani, P. (2002). Global cancer statistics, 2002. *CA Cancer J. Clin.* 55, 74–108. doi:10.3322/canjclin.55.2.74

Pushpakom, S., Iorio, F., Eyers, P. A., Escott, K. J., Hopper, S., Wells, A., et al. (2019). Drug repurposing: progress, challenges and recommendations. *Nat. Rev. Drug Discov.* 18, 41–58. doi:10.1038/nrd.2018.168

Qu, X. A., and Rajpal, D. K. (2012). Applications of connectivity map in drug discovery and development. *Drug Discov. Today* 17, 1289–1298. doi:10.1016/j.drudis.2012.07.017

Rabben, H. L., Zhao, C. M., Hayakawa, Y., Wang, T. C., and Chen, D. (2016). Vagotomy and gastric tumorigenesis. *Curr. Neuropharmacol.* 14, 967–972. doi:10.2174/1570159x14666160121114854

Rabben, H. L., Andersen, G. T., Olsen, M. K., Øverby, A., Ianevski, A., Kainov, A., et al. (2021). Neural signaling modulates metabolism of gastric cancer. *iScience* 24, 102091. doi:10.1016/j.isci.2021.102091

Rawla, P., and Barsouk, A. (2019). Epidemiology of gastric cancer: global trends, risk factors and prevention. *Prz. Gastroenterol.* 14, 26–38. doi:10.5114/pg.2018.80001

Saito-Hakoda, A., Uruno, A., Yokoyama, A., Shimizu, K., Parvin, R., Kudo, M., et al. (2015). Effects of RXR agonists on cell proliferation/apoptosis and ACTH secretion/pomc expression. *PLoS One* 10, e0141960. doi:10.1371/journal.pone.0141960

Selim, J. H., Shaheen, S., Sheu, W. C., and Hsueh, C. T. (2019). Targeted and novel therapy in advanced gastric cancer. *Exp. Hematol. Oncol.* 8, 25. doi:10.1186/s40164-019-0149-6

Sitarz, R., Skierucha, M., Mielko, J., Offerhaus, J., Maciejewski, R., and Polkowski, W. (2018). Gastric cancer: epidemiology, prevention, classification, and treatment. *Cancer Manag. Res.* 10, 239–248. doi:10.2147/cmar.s149619

Subramanian, A., Narayan, R., Corsello, S. M., Peck, D. D., Natoli, T. E., Lu, X., et al. (2017). A next generation connectivity map: L1000 platform and the first 1,000,000 profiles. *Cell* 171, 1437–1452.e17. doi:10.1016/j.cell.2017.10.049

Sutherland, I. H., and Campbell, W. C. (1990). Development, pharmacokinetics and mode of action of ivermectin. *Acta Leiden* 59, 161–168.

Verbaanderd, C., Maes, H., Schaaf, M. B., Sukhatme, V. P., Pantziarka, P., Sukhatme, V., et al. (2017). Repurposing drugs in oncology (ReDO)-chloroquine and hydroxychloroquine as anti-cancer agents. *Ecancermedicalscience* 11, 781. doi:10.3332/ecancer.2017.781

Verbaanderd, C., Meheus, L., Huys, I., and Pantziarka, P. (2017). Repurposing drugs in oncology: next steps. *Trends Cancer* 3, 543–546. doi:10.1016/j.trecan.2017.06.007

Xue, H., Li, J., Xie, H., and Wang, Y. (2018). Review of drug repositioning approaches and resources. *Int. J. Biol. Sci.* 14, 1232–1244. doi:10.7150/ijbs.24612

Yang, Z., Li, C., Yan, C., Li, J., Yan, M., Liu, B., et al. (2019). KIF14 promotes tumor progression and metastasis and is an independent predictor of poor prognosis in human gastric cancer. *Biochim. Biophys. Acta Mol. Basis Dis.* 1865, 181–192. doi:10.1016/j.bbadis.2018.10.039

Yokozaki, H. (2000). Molecular characteristics of eight gastric cancer cell lines established in Japan. *Pathol. Int.* 50, 767–777. doi:10.1046/j.1440-1827.2000.01117.x

Zhan, T., Rindtorff, N., and Boutros, M. (2017). Wnt signaling in cancer. *Oncogene* 36, 1461–1473. doi:10.1038/onc.2016.304

Zhang, P., Zhang, Y., Liu, K., Liu, B., Xu, W., Gao, J., et al. (2019). Ivermectin induces cell cycle arrest and apoptosis of HeLa cells via mitochondrial pathway. *Cell Prolif.* 52, e12543. doi:10.1111/cpr.12543

Zhao, C. M., Hayakawa, Y., Kodama, Y., Muthupalani, S., Westphalen, C. B., Andersen, G. T., et al. (2014). Denervation suppresses gastric tumorigenesis. *Sci. Transl. Med.* 6, 250ra115. doi:10.1126/scitranslmed.3009569

Conflict of Interest: The authors declare that the research was conducted in the absence of any commercial or financial relationships that could be construed as a potential conflict of interest.

Paper III

frontiers in Pharmacology

ORIGINAL RESEARCH
published: 08 April 2021
doi: 10.3389/fphar.2021.613458

Chemopreventive Effects of Dietary Isothiocyanates in Animal Models of Gastric Cancer and Synergistic Anticancer Effects With Cisplatin in Human Gastric Cancer Cells

Hanne-Line Rabben[1,2], Yosuke Kodama[1], Masahiko Nakamura[3], Atle Magnar Bones[4], Timothy Cragin Wang[1,5], Duan Chen[1], Chun-Mei Zhao[1,2] and Anders Øverby[1,3]*

[1]Department of Clinical and Molecular Medicine, Norwegian University of Science and Technology (NTNU), Trondheim, Norway, [2]The Central Norway Regional Health Authority, Stjørdal, Norway, [3]Center for Clinical Pharmacy and Clinical Sciences, School of Pharmacy, Kitasato University, Tokyo, Japan, [4]Cell, Molecular Biology and Genomics Group, Department of Biology, Norwegian University of Science and Technology (NTNU), Trondheim, Norway, [5]Division of Digestive and Liver Diseases, Columbia University College of Physicians and Surgeons, New York, NY, United States

OPEN ACCESS

Edited by:
Ramin Massoumi, Lund University, Sweden

Reviewed by:
Thomas Brzozowski, Jagiellonian University Medical College, Poland
Jianwei Zhou, Nanjing Medical University, China

***Correspondence:**
Hanne-Line Rabben
hanne.l.rabben@ntnu.no

Specialty section:
This article was submitted to Gastrointestinal and Hepatic Pharmacology, a section of the journal Frontiers in Pharmacology

Received: *02 October 2020*
Accepted: *09 February 2021*
Published: *08 April 2021*

Citation:
Rabben H-L, Kodama Y, Nakamura M, Bones AM, Wang TC, Chen D, Zhao C-M and Øverby A (2021) Chemopreventive Effects of Dietary Isothiocyanates in Animal Models of Gastric Cancer and Synergistic Anticancer Effects With Cisplatin in Human Gastric Cancer Cells. Front. Pharmacol. 12:613458. doi: 10.3389/fphar.2021.613458

Naturally occurring isothiocyanates (ITCs) from edible vegetables have shown potential as chemopreventive agents against several types of cancer. The aims of the present study were to study the potential of ITCs in chemoprevention and in potentiating the efficacy of cytotoxic drugs in gastric cancer treatment. The chemoprevention was studied in chemically induced mouse model of gastric cancer, namely N-methyl-N-nitrosourea (MNU) in drinking water, and in a genetically engineered mouse model of gastric cancer (the so-called INS-GAS mice). The pharmacological effects of ITCs with or without cisplatin were studied in human gastric cell lines MKN45, AGS, MKN74 and KATO-III, which were derived from either intestinal or diffused types of gastric carcinoma. The results showed that dietary phenethyl isothiocyanate (PEITC) reduced the tumor size when PEITC was given simultaneously with MNU, but neither when administrated after MNU nor in INS-GAS mice. Treatments of gastric cancer cells with ITCs resulted in a time- and concentration-dependent inhibition on cell proliferation. Pretreatment of gastric cancer cells with ITCs enhanced the inhibitory effects of cisplatin (but not 5-fluorouracil) in time- and concentration-dependent manners. Treatments of gastric cancer cells with PEITC plus cisplatin simultaneously at different concentrations of either PEITC or cisplatin exhibited neither additive nor synergetic inhibitory effect. Furthermore, PEITC depleted glutathione and induced G_2/M cell cycle arrest in gastric cancer cells. In conclusion, the results of the present study showed that PEITC displayed anti-cancer effects, particularly when given before the tumor initiation, suggesting a chemopreventive effect in gastric cancer, and that pretreatment of PEITC potentiated the anti-cancer effects of cisplatin, possibly by reducing the intracellular pool of glutathione, suggesting a possible combination strategy of chemotherapy with pretreatment with PEITC.

Keywords: dietary (or plant) isothiocyanates, gastric cancer, glutathione, glutamine, cisplatin, mice

INTRODUCTION

Gastric cancer is one of the leading causes of cancer in the world with over one million new cases reported in 2018 (GLOBOCAN) (Ferlay et al., 2013; Bray et al., 2018). Despite dramatic decline in gastric cancer incidences in later years, gastric cancer is the fifth most common cancer with a 5-year survival rate below 25%, making gastric cancer the third leading cause of cancer mortality worldwide (Ferlay et al., 2010; Ferlay et al., 2013). Chemoprevention of gastric cancer is to chemically prevent or delay the occurrence of malignancy. Although *Helicobacter pylori (H. pylori)* eradication can be an effective preventive method due to the putative pathogenic mechanisms, the chemoprevention using natural, synthetic or biological agents has enormous potential, given the high incidence together with the healthcare costs of treatment (Steward and Brown, 2013; Tan and Wong, 2013; Dunn et al., 2016). The treatments of gastric cancer include surgery, and chemotherapy regimens with either mono-chemotherapy (using single drug) or combination-chemotherapy (e.g., fluoropyrimidines and platinum-based therapies) for inoperable or metastatic gastric cancer (Van Cutsem et al., 2006; Cunningham et al., 2008; Koizumi et al., 2008; Kang et al., 2009; Orditura et al., 2014). However, patients with unresectable advanced gastric cancer usually have poor outcomes with median survivals of 10–18 months. Nearly half of patients with resectable gastric cancer have a recurrence and median survival is about 6 months (Leiting and Grotz, 2019). Thus, a challenge for improving patient care of gastric cancer in terms of survival and quality of life appears to be ineffective cytotoxic chemotherapy. These facts indicate that there are still great needs for improvement in the prevention and treatment of gastric cancer. Previously, we have showed that denervation (surgically, pharmacologically or genetically) suppressed the tumorigenesis of gastric cancer, which was associated with a decrease in WNT/β-catenin signaling, the suppression of stem cell expansion through M3 receptor-mediated cholinergic signaling and the reversion of metabolic reprogramming, and that the combination of denervation and mono-chemotherapy led to an enhanced effect on tumor growth and survival in an animal model of gastric cancer (Zhao et al., 2014; Rabben et al., 2016). Recently, we have further shown that neural signaling modulated metabolism of gastric cancer, reflected by metabolic switch from glutaminolysis to OXPHOS/glycolysis and normalization of the energy metabolism after denervation (Rabben et al., 2021). In the present study, we wanted to explore the potential of a class of anti-cancer agents, isothiocyanates (ITCs) for chemoprevention and enhancement of chemotherapy as they are also shown to interfere with tumor metabolism (Conaway et al., 2002; Lv et al., 2020).

Naturally occurring isothiocyanates (ITCs) are electrophilic plant phytochemicals derived from glucosinolates of edible vegetables such as broccoli, cauliflower, brussels sprouts, and cabbage. Phenethyl isothiocyanate (PEITC) has been tested in *in vitro*, *in vivo* and in clinical trials to study about the potential effects of prevention and treatment of different types of cancer (Hu and Morris, 2004; Keum et al., 2004; Keum et al., 2005; Clarke et al., 2008; Chu et al., 2009; Wu et al., 2009; Li et al., 2010; Tomczyk and Olejnik, 2010; Zhang, 2010; Chung et al., 2013; Li and Zhang, 2013). The aims of the present study were to study whether ITCs could prevent gastric tumorigenesis and whether ITCs could enhance the inhibitory effect of mono-chemotherapy on gastric cancer; and if so, to investigate the possible underlying mechanisms. To these ends, we utilized chemically induced mouse model of gastric cancer, i.e., N-methyl-N-nitrosourea (MNU) in drinking water, and genetically engineered mouse model of gastric cancer (the so-called INS-GAS mice) for studying chemoprevention, and used human gastric cancer cell lines, i.e., MKN45, AGS, MKN74 and KATO-III derived from either intestinal or diffused types of gastric carcinoma for studying the pharmacological effects of ITCs with or without cisplatin *in vitro*.

The possible mechanisms underlying the anti-cancer effects of ITCs have been suggested to involve inhibition of cytochrome P450 enzymes, induction of phase II detoxification enzymes, such as glutathione S-transferase (GST) and apoptosis, and cell cycle arrest, inhibition of migration, disruption of microtubules, and dysregulation of signaling pathways including major regulators such as WNT/β-catenin signaling pathway, NRF2, ERK, Jun and Akt signaling pathways (Yang et al., 2010; Gupta et al., 2014; Øverby et al., 2014; Lawson et al., 2015; Chen et al., 2018). In addition, glutathione (GSH) is a powerful regulatory tripeptide with antioxidant function that protects cells from oxidative stress by removing free radicals and peroxides. We and others have shown that ITCs conjugate with GSH, leading to depletion of GSH, elevation of oxidative stress and expression of GST-encoding genes, and that there are close relationship between glutathione and the levels of glutamine and glutamate in the cell-pool important for redox homeostasis (Øverby et al., 2015). Thus, we hypothesized that ITCs would enhance the cytotoxicity of cisplatin by depleting cells of GSH, and thus measured the levels of GSH and the ratio between glutamine and glutamate in connection with cell growth inhibition after treatment of ITCs.

MATERIALS AND METHODS

Animals and Experimental Groups

All mice at ages between 1–12 months were housed three to four mice per cage on wood chip bedding with a 12 h light/dark cycle, room temperature of 22°C and 40–60% relative humidity at the standard housing conditions in a specific pathogen-free environment. Ninety mice including 54 wild-type (FVB) mice and 26 INS-GAS mice were divided into the following experimental groups: FVB mice (n = 16, eight male, eight female), FVB mice + MNU (n = 11, five female, six male), FVB mice + MNU + prePEITC (n = 16, eight female, eight male), FVB mice + MNU + postPEITC (n = 11, five female, six male), INS-GAS mice (n = 24, 10 female, 14 male), and INS-GAS mice + PEITC (n = 12, six female, six male). In each experiment, mice were randomly divided into different subgroups with gender-balance.

Treatment of Phenethyl Isothiocyanate in a Chemically Induced Mouse Model of Gastric Cancer

The chemically induced gastric cancer model (FVB + MNU) was established according to our previous report (Zhao et al., 2014). In brief, mice were exposed to N-Methyl-N-nitrosourea (MNU, Sigma Chemicals), which was dissolved in distilled water at a concentration of 240 ppm and freshly prepared twice per week for administration in drinking water in light-shielded bottles ad libitum. MNU was administered in the drinking water starting at 4 weeks of age and continued from the next 10 weeks followed by euthanization at age 12 months. PEITC was administered through an AIN-76A diet (3–5 μmol PEITC/g diet) either during or following administration of MNU. Mice were euthanized at age of 12 months.

Treatment of Phenethyl Isothiocyanate in Genetically Engineered Mouse Model of Gastric Cancer

The transgenic insulin-gastrin mice (INS-GAS mice) that over-express gastrin develop spontaneously gastric cancer were generated as previously described (Zhao et al., 2014). Mice received PEITC through an AIN-76A diet (3–5 μmol PEITC/g diet) for 10 weeks or standard pellet food (RM1801002, Scanbur BK AS). Mice were euthanized at the age of 12 months.

Tissue Sampling

The stomachs were removed, opened along the greater curvature, washed in 0.9% (w/v) NaCl, and pinned flat on a petri-dish-silicone board. Each stomach was photographed digitally; the tumor profiles in both anterior and posterior sides of the stomach were drawn separately and subjected to morphometric analysis of the volume density (expressed as the percentage of glandular volume occupied by the tumor) using point-counting technique with a test grid comprised of a 1.0 cm square lattice. This grid was placed over each photograph (40 cm^2 × 30 cm^2), and the numbers of test points overlying the tumor and gastric glandular area were determined.

Chemicals and Reagents

Phenethyl isothiocyanate (PEITC, Sigma Aldrich, United States, cat. no. 253731-5G), Benzyl isothiocyanate (BITC, Sigma Aldrich, Poland, cat. no. 252492-5G) and Allyl isothiocyanate (AITC, Sigma Aldrich, Germany, cat. no. 377430-100G) were dissolved in 100% dimethylsulfoxide (DMSO) to working concentrations. Cisplatin (Wako Pure Chemical Industries Ltd., Osaka, Japan, cat. no. 033-20091, Lot. SAQ1693 or TOCRIS Bioscience, Abingdon, United Kingdom, cat. no. 2251) was dissolved in PBS (Nacalai Tescue, Japan, cat. no. 14249-24) under gentle warming, and 5-fluorouracil (Sigma Aldrich, China) was dissolved in 100% DMSO. The following cell culture supplements were used: DMEM (Nacalai tesque, Japan, cat. no 08456-65); Fetal Bovine Serum (FBS; ThermoFisher Scientific, United States), antibiotic-antimycotic solution containing penicillin, streptomycin and amphotericin B (Nacalai tesque, Japan, cat. no. 02892-54), Penicillin-streptomycin solution (Sigma Aldrich, Oslo, Norway, cat. no. P4333-100ML), RPMI-1640 medium (Sigma Aldrich, Norway, cat. no. R8758-500ML with 0.3 g/L (2 mM) glutamine), DMEM (Gibco, ThermoFisher Scientific, Oslo, Norway, cat. no. A14430-01 without L-glutamine, D-glucose, phenol red and sodium pyruvate); dialyzed FBS (Life technologies, United States, Cat. no 26400-036); L-glutamine (Sigma Aldrich, Oslo, Norway, cat. no G7513); Sodium pyruvate (Sigma Aldrich, Oslo, Norway, cat. no. S8636). For cell cycle analysis: Propidium iodide (P1, Sigma Aldrich, Oslo, Norway, cat. no P4170-10MG); Triton-X (Sigma Aldrich, Oslo, Norway, cat. no. T9284), RNase A (Sigma Aldrich, Oslo, Norway, cat. no R4875-100MG). For GSH determination: 5-Sulfosalicylic acid (SSA) solution (5.0%); For Western Blot: RIPA cell lysis buffer (Pierce) containing 0.1% MG132 Proteasome Inhibitor (Cayman Chemical), 1.0% Protease inhibitor cocktail (Sigma Aldrich) and 10% PhosStop Phosphatase Inhibitor Cocktail (Roche). Antibodies: Primary antibody mouse monoclonal anti human p53 clone DO-1 (Santa Cruz: sc-126); Mouse monoclonal anti-β-actin clone; Anti-mouse IgG HRP-linked whole Ab sheep (GE Healthcare: NA931)/Anti-Rabbit IgG, HRP-linked whole Ab donkey (GE Healthcare: NA934).

Cell Culture

Human gastric carcinoma cancer cell lines AGS and MKN45 were maintained in Dulbecco's Modified Eagle's Medium (DMEM; Nacalai tesque, Japan) supplemented with 10% fetal bovine serum and 1% antibiotic-antimycotic solution containing penicillin, streptomycin and amphotericin B in a humidified incubator holding 5% CO_2 and 37°C. Human gastric carcinoma cancer cell lines MKN74 and KATO-III were maintained in RPMI-1640 medium supplemented with 10% FBS and 1% penicillin-streptomycin solution. Passages were performed when cultures reached 70–80% confluency. For the studies investigating glutamate and glutamine contents, DMEM containing 4.5 g/L glucose, 2 mM glutamine or 0.2 mM glutamine and 1 mM sodium pyruvate supplemented with dialyzed FBS was used.

Proliferation Assay

For proliferation assay, 1,500 cells of AGS, 2,500 of MKN45 or MKN74 or 3,000 cells of KATO-III were seeded in 96-well plates before incubated overnight allowing cells to confluate. Treatments were always accompanied by vehicle controls (n = 12) on each plate (0.05% DMSO). Cells were treated with AITC (Sigma Aldrich, Germany), BITC (Sigma Aldrich, Poland), PEITC (Sigma Aldrich, United States), cisplatin (Wako Pure Chemical Industries Ltd., Japan) or (Tocris, Norway) and 5-fluorouracil (Sigma Aldrich, China) as indicated in the text. Following treatment, Cell Count Reagent SF (Nacalai tesque, Japan) was added according to providers' instructions to each well before mixing and incubating for 1.0–1.5 h. Proliferation was determined by measuring absorbance at 450 nm using a well plate reader. Defined DMEM was used to perform experiments with controlled levels of glutamine and glucose.

Cell Cycle Analysis

Human gastric cancer cells KATO-III were seeded as 2.5 × 10^5 cells in 6-well plates and incubated over two nights before treated with 0, 5 or 10 μM PEITC for 12 and 24 h or PEITC (0, 5, 10 μM)

together with cisplatin (25 or 50 μM) for 24 h. Cells were harvested, resuspended in PBS and fixated in chilled ethanol (−20°C, 70%, Kemetyl Norway) for minimum 15 min. Cells were then pelleted and resuspended in freshly prepared propidium iodide (PI) staining solution (0.25% Triton- X-100, 50 μg/ml PI and 200 μg/ml RNase A) for 30 min. Cell cycle distribution was analyzed using a FACS Canto flow cytometer counting 2×10^4 cells per sample in triplicates. Cell cycle distribution was acquired from the obtained histograms using FACS Diva software.

Morphology

To study the effect of PEITC on cells, AGS and MKN74 cells were seeded in T_{25} flasks (1.5×10^5 cells per flask) and left for overnight incubation before treating with 5–20 μM PEITC or vehicle control (0.1% DMSO) for 24 h. The cultures were then observed and pictures captured through an inverted microscope in phase contrast mode.

Total GSH Determination

Total cellular glutathione level was determined in PEITC, AITC or BSO-treated AGS cells. Cells were seeded in T_{25} flasks (1.5×10^5 cells per flask) and incubated overnight prior to treatment. The cultures were treated with either 10–20 μM PEITC, 50–100 μM AITC, or 0–100 μM BSO or vehicle control (0.1% DMSO) for 3 or 6 h. The doses were based on IC_{50}-range and previous literature. Each treatment was performed in quadruples. Cells were harvested and centrifuged (1,500 rpm, 5 min) before determination of total cellular glutathione using a commercial glutathione assay kit (Sigma, United States) according to manufacturers' instructions. Briefly, cell pellets were deproteinized in 5-sulfosalicylic acid (SSA) solution (5%), vortexed and snap-freezed (3 times in total) before centrifugation (1,500 rpm, 5 min). Supernatants were transferred to clean tubes and stored on ice until analysis. 10 μl from each sample was applied to a 96—well plate in separate wells in duplicates and mixed together with 150 μl reaction mixture containing 95 mM potassium phosphate buffer (pH 7), 0.95 mM EDTA, 0.031 mg/ml DTNB, 0.115 units/ml glutathione reductase and 0.24% 5-sulfosalicylic acid. Finally, 50 μl of NADPH solution (0.16 mg/ml, resulting in final concentration of 0.038 mg/ml (48 μM) NADPH) was added to each well and mixed. Immediately after mixing, a kinetic read was performed in 1 min intervals for 5 min at 412 nm using a spectrophotometric plate reader in order to detect the formation of the yellow product 5-thio-2-nitrobenzoic acid (TNB).

Glutamate/Glutamine Determination

For glutamate/glutamine detection, AGS cells were seeded in 24-well plates (1.0×10^4 cells per well) and incubated over night to attain confluency. The cultures were then treated with PEITC (10–30 μM) and AITC (50–200 μM) for 2–24 h in defined DMEM containing dialyzed FBS before samples were collected and analyzed for glutamate and glutamine content. Determination of glutamate/glutamine was performed using a detection kit (Sigma, United States) following the manufacturers' instructions. Briefly, from each sample to be analyzed, one sample was prepared for estimating endogenous glutamate, and one sample was prepared for estimating endogenous glutamate and glutamate converted from glutamine based on an initial deamination reaction catalyzed by glutaminase of the samples. All samples were then mixed with glutamic dehydrogenase which generates α-ketoglutarate and converts NAD^+ to NADH which was detected spectrophotometrically at 340 nm. Glutamate content was then calculated using a standard curve, whereas glutamine content was calculated by subtracting the endogenous glutamate concentration from the total concentration of endogenous glutamate and glutamine-derived glutamate.

Spheroid 3D Culture

AGS cells were seeded in 96-well plates (1,500 cells per well) with U-shaped bottoms with surface that prevents cells from attaching to the surface (Sumitomo Bakelite Co. Ltd., Japan). The cells were then incubated for 1 day to allow the cells to generate a spheroid-like structure before these spheroids were treated with PEITC (0–50 μM) for 48 h. After treatment, proliferation was assayed as described above.

Western Blot

Western Blot from whole cell extract was performed in order to investigate the presence of protein p53. Cell extracts were prepared using ice-cold RIPA cell lysis buffer (Pierce) containing 0.1% MG132 Proteasome inhibitor (Cayman Chemical), 1% Protease inhibitor cocktail (Sigma Aldrich) and 10% PhosStop phosphatase inhibitor Cocktail (Roche). Bicinchoninate protein quantification (BCA) assay (Nacalai Tesque) was performed in order to determine protein concentrations in the cell lysates prior to SDS PAGE. Samples were denatured in sample buffer (4x) (NuPAGE LDS, Novex, Life Technologies, pH 8.4) with 5% 2-mercaptoethanol at 100°C for 10 min. Five microgram of protein or molecular weights marker were loaded into the lanes on the SDS PAGE gel and run in MOPS running buffer (NuPAGE, Life Technologies, pH 7.7) for 5 min at 150 V followed by 40 min at 200 V. After electrophoresis, gels were blotted onto polyvinylidene difluoride (PVDF) membranes in NuPAGE transfer buffer (Life Technologies). Block ACE solution (DS Pharma Biomedical) was used to block the membrane for 1 h at room temperature. Primary antibody mouse monoclonal anti human p53 clone DO-1 (1:200, Santacruz: sc-126) was added to the membrane and incubated overnight at 4°C. Mouse monoclonal anti-β-actin clone, which recognize β-actin, was used as internal standard. The membrane was washed in tris-buffered saline with 0.5% Tween 20 (TBST) followed by incubation with secondary antibody anti-mouse IgG HRP-linked whole Ab sheep (1:500) (GE Healthcare: NA931)/Anti-Rabbit IgG, HRP-linked whole Ab donkey (1:500) (GE Healthcare: NA934) for 1 h at room temperature. Finally, chemiluminescence capturing using Clarity Western ECL substrate (Bio-RAD) was applied, and images were acquired using a ImageQuant LAS 500 system (GE Healthcare). Quantification of p53 band area was performed in Image studio Lite (LI-COR Biosciences).

Statistical Analysis

Values are expressed as means ± SEM in *in vivo* experiments. Pairwise comparisons between experimental groups were done using one-way ANOVA with Dunnett's test (1-sided) or student's

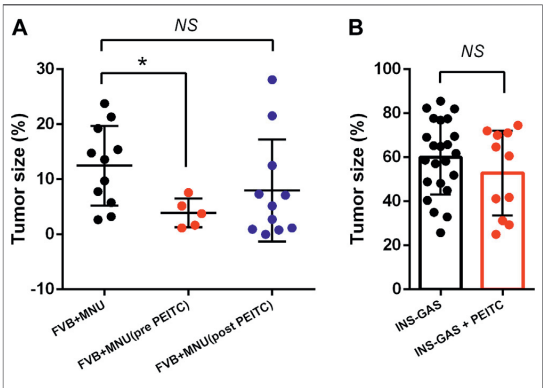

FIGURE 1 | Tumor size of gastric cancer in mice that completed the study period of 45–50 weeks. FVB mice received MNU for 10 weeks (n = 11) or MNU together with PEITC (3–5 μmol PEITC/g diet) for 10 weeks (n = 5) or post MNU treatment (n = 11) **(A)** and in INS-GAS mice with or without PEITC (3–5 μmol PEITC/g diet) for 10 weeks **(B)**. Mean ± SEM. Tumor size expressed as volume density (% of glandular area occupied by tumor). ANOVA + Dunnett's test (1-tailed) in **(A)**, student t-test in **(B)**. *$p < 0.05$; NS, not significant; PEITC, phenethyl isothiocyanate; MNU, N-methyl-N-nitrosourea.

t-test between INS-GAS mouse GC tumors with *vs.* without PEITC. In *in vitro* experiments, cell proliferation is represented by means of n = 3-6 replicates/treatment ± SD. IC_{50} values were calculated from sigmoidal regression curve fitting using variable slope on normalized response from log (10)-transformed x-values (GraphPad Prism v.6). Standard deviation (SD) values (%) were omitted from cultures with 98% or higher inhibited growth as these yielded non-representatively high SD values. Cell cycle distribution was analyzed using one-way ANOVA on normally distributed data with Dunnett's 2-sided post hoc test *vs.* control groups. All tests were with a significance cutoff of $p < 0.05$.

RESULTS

Two mouse models of gastric cancer were used, i.e., MNU-induced gastric cancer (MNU mice) and genetically engineered spontaneously gastric cancer (INS-GAS mice). Body weight of mice with or without PEITC increased due to aging of the mice but was not affected by PEITC treatment during the period of experiment (10 weeks). Tumour size of gastric cancer was significantly reduced by PEITC when given during MNU but neither after MNU, nor in INS-GAS mice (**Figures 1A,B**).

To demonstrate the cytotoxicity of ITCs in gastric cancer, four human gastric carcinoma cell lines were used; MKN45, AGS, MKN74 and KATO-III. Aromatic PEITC, BITC or aliphatic AITC resulted in a time and dose-dependent inhibition of cell proliferation (**Figures 2A–E**). The aromatic ITCs displayed a higher potential in inhibiting cell proliferation in both MKN45 and AGS compared to AITC. The MKN74, MKN45 and KATO-III cells proved to be more tolerant to ITC-treatment than the AGS cells in terms of IC_{50}-values. All cell lines showed alterations in cell morphology by ITC-treatments with a gradual increase in non-confluent cells with increasing ITC-doses as demonstrated by PEITC-treated AGS cells (**Figure 2F**). A spheroid 3D culture of AGS cells treated with PEITC for 24 and 48 h showed decreased growth upon increasing doses (**Figure 2G**).

Due to the electrophilic central C-atom in the reactive –N=C=S group, ITCs are able to antagonize multiple targets including glutathione. We therefore next examined the GSH concentration upon PEITC and AITC treatment. GSH depletion was both time- and dose-dependent in AGS cells (**Figures 3A,B**). Additionally, the synthetic amino acid Buthionine sulfoximine (BSO) depleted GSH in time- and dose-dependent manner (**Figure 3C**).

Reflected by the glutathione cycle, there are close relationships between glutathione and the levels of glutamine and glutamate in the cell-pool important for redox homeostasis. We next investigated the ratio between glutamine and glutamate after PEITC. PEITC increased the ratio of glutamine/glutamate in a dose-dependent manner, and furthermore inhibited cell proliferation in glutamine-reduced medium in a concentration-depended manner (**Figures 4A,B**).

The GSH-pool is an important factor for the cancer cells to maintain redox homeostasis. By depleting cells of glutathione, we hypothesized that ITCs would enhance the *in vitro* cytotoxicity of cisplatin. To investigate the potential effects of ITCs, AGS and MKN45 cells were pretreated with PEITC, BITC or AITC for 1, 3 or 24 h followed by cisplatin or 5-FU treatment for 48 h (**Figures 5A–E**). Pretreatment with 20 μM PEITC in MKN45 cells for 1 h lowered the IC_{50} of cisplatin by 2.7-fold, while pretreatment for 3 h lowered the IC_{50} of cisplatin 7-fold. After 24 h, the reduction in IC_{50} was 8.5-fold (**Figure 5A**, third panel). Pre-treatment with 20 μM PEITC in AGS cells showed 10-fold reduction after 1 h (**Figure 5B**). A similar observation was made for the BITC compound, where 20 μM BITC showed 4.6 and 5.7-folds reductions in IC_{50} after 1 and 24 h, respectively (**Figure 5C**). The aliphatic AITC failed to induce the synergistic effects with cisplatin, only lowering the IC_{50} by 1.3-fold after 3 h or even showing increased IC_{50} upon pretreatment (1 and 24 h, **Figure 5D**). Substituting cisplatin by 5-FU did not achieve the same inhibition using PEITC (**Figure 5E**).

Simultaneous treatments with PEITC (2.5 μM) and cisplatin at increasing doses showed no additional inhibitory effect or even had antagonistic effect as reflected in increased IC_{50} values when PEITC was added (**Figures 6A,B**).

Cell cycle distribution of KATO-III cells upon 12 and 24 h treatments with PEITC resulted in G_2/M phase arrest (**Figure 7A**). However, when treated with 0, 5 or 10 μM PEITC together with 0, 25 or 50 μM cisplatin, a decrease in G_1 phase was accompanied by increase in G_2/M phase and slight increase in apoptotic cells (reflected by sub G_1/G_0 phase increase) (**Figure 7B**). Treatment of AGS cells with 0 or 5 μM PEITC for 24 h showed increased level of protein p53 as determined by Western Blot (**Figures 7C,D**).

DISCUSSION

Long-term exposure to *H. pylori* is associated with progression of precancerous lesions in the stomach and infected individuals may

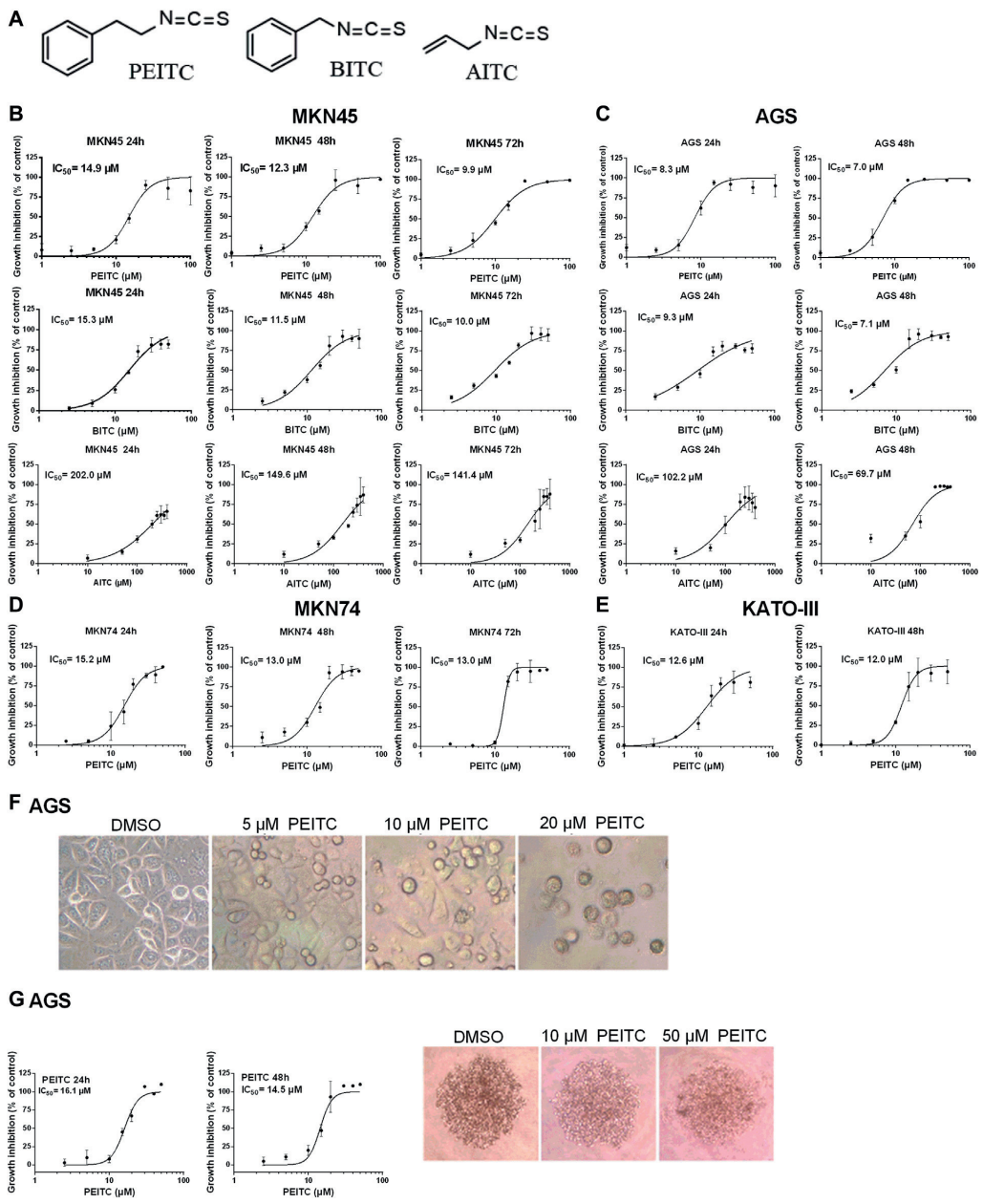

FIGURE 2 | Chemical structures of ITCs **(A)** and proliferation dose-response curves of gastric cancer cell lines MKN45 **(B)** and AGS **(C)** when treated with PEITC (1–100 μM), BITC (2.5–50 μM) and AITC (10–400 μM) for 24, 48 and 72 h in medium containing 1.0 g/L (5.6 mM) glucose and 0.584 g/L (4 mM) glutamine. Values represent means of n = 3–6 replicates relative to vehicle control (0.1% DMSO), and IC_{50} values were calculated from the logistic sigmoidal regression curves shown. Standard deviation (SD) values were omitted from cultures with 98% or higher inhibited growth as these yielded non-representatively high SD values. Proliferation dose-response curves of gastric cancer cell lines MKN74 and KATO-III when treated with PEITC (1–50 μM) **(D, E)**. Morphology of AGS cells affected by ITC-treatments **(F)**. Proliferation and morphology of spheroid 3D cultures of AGS cells treated with PEITC for 24–48 h **(G)**. PEITC, phenethyl isothiocyanate; BITC, benzyl isothiocyanate; AITC, allyl isothiocyanate; DMSO, dimethylsulfoxide.

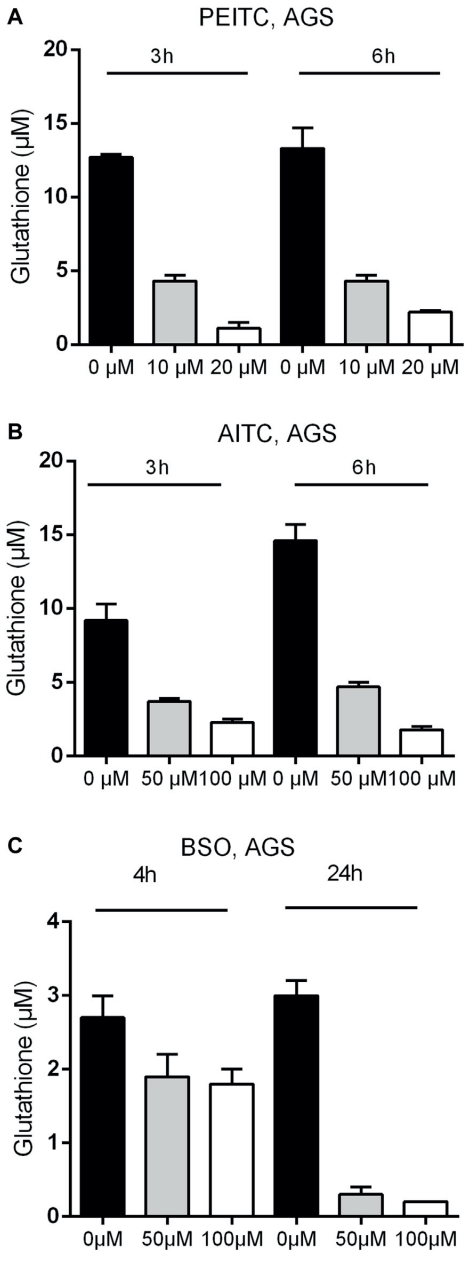

FIGURE 3 | Glutathione concentration upon 3 and 6 h treatments with PEITC **(A)** or AITC **(B)** on AGS cells and upon 4 and 24 h of treatment with BSO **(C)** on AGS cells. Mean + SD of $n = 4$ replicates/treatment. PEITC, phenethyl isothiocyanate; AITC, allyl isothiocyanate; BSO, Buthionine sulfoximine.

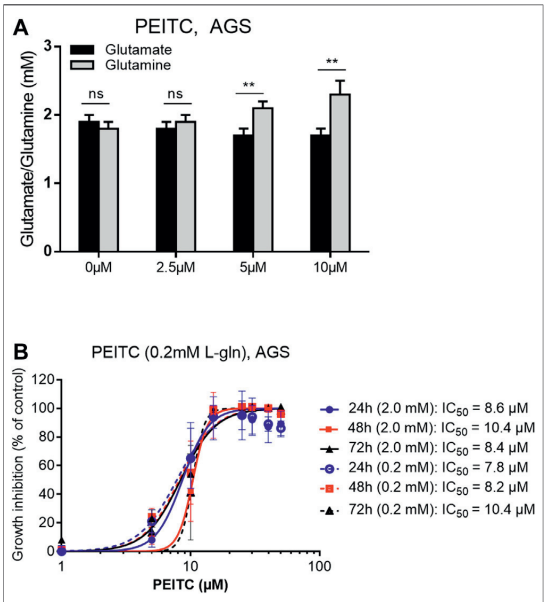

FIGURE 4 | Glutamate/glutamine determination upon 6 h treatments with 0, 2.5, 5 or 10 μM PEITC on AGS cells **(A)**. PEITC treatment in L-glutamine-reduced (×10) DMEM medium **(B)**. Mean ± SD. Paired *t*-test in **(A)**. $^{**}p < 0.01$; ns, not significant; PEITC, phenethyl isothiocyanate; L-gln, L-glutamine.

benefit from successful *H. pylori* eradication, and population-based chemopreventive strategy of *H. pylori* eradication is still under the development (Tan and Wong, 2013; Mera et al., 2018). Other strategies using drugs, such as non-steroidal anti-inflammatory drugs and statins, have also been suggested (Ford, 2011). In the present study, we found the chemopreventive effects by PEITC in chemically induced (MNU) animal model of gastric cancer. Interestingly, the chemopreventive effects were neither seen when PEITC was given after the tumor initiation by MNU nor in genetically induced (INS-GAS) gastric cancer. Thus, it is unlikely that PEITC interacts directly with MNU on one hand, but on the other hand, PEITC may act on gastric epithelial cells to prevent the initiation of tumorigenesis as it has been suggested that PEITC induce apoptosis, inhibits cell cycle progression and inhibits angiogenesis (Mitsiogianni et al., 2019). It is known that the regulation of apoptosis by ITC is achieved primarily through mitochondrial cytochrome c release, regulation of the Bcl-2 family, MAPK signaling and subsequent activation of caspases, responsible for the initiation and execution of apoptosis. Specifically, AITC and phenyl-ITC (PITC) inhibit TNF (extrinsic apoptosis), generating a mycelial inhibition for several months, while BITC and PEITC induce a cytochrome c release-dependent type of apoptosis from mitochondria (intrinsic apoptosis) that generates a mycelial inhibition that lasts only for a

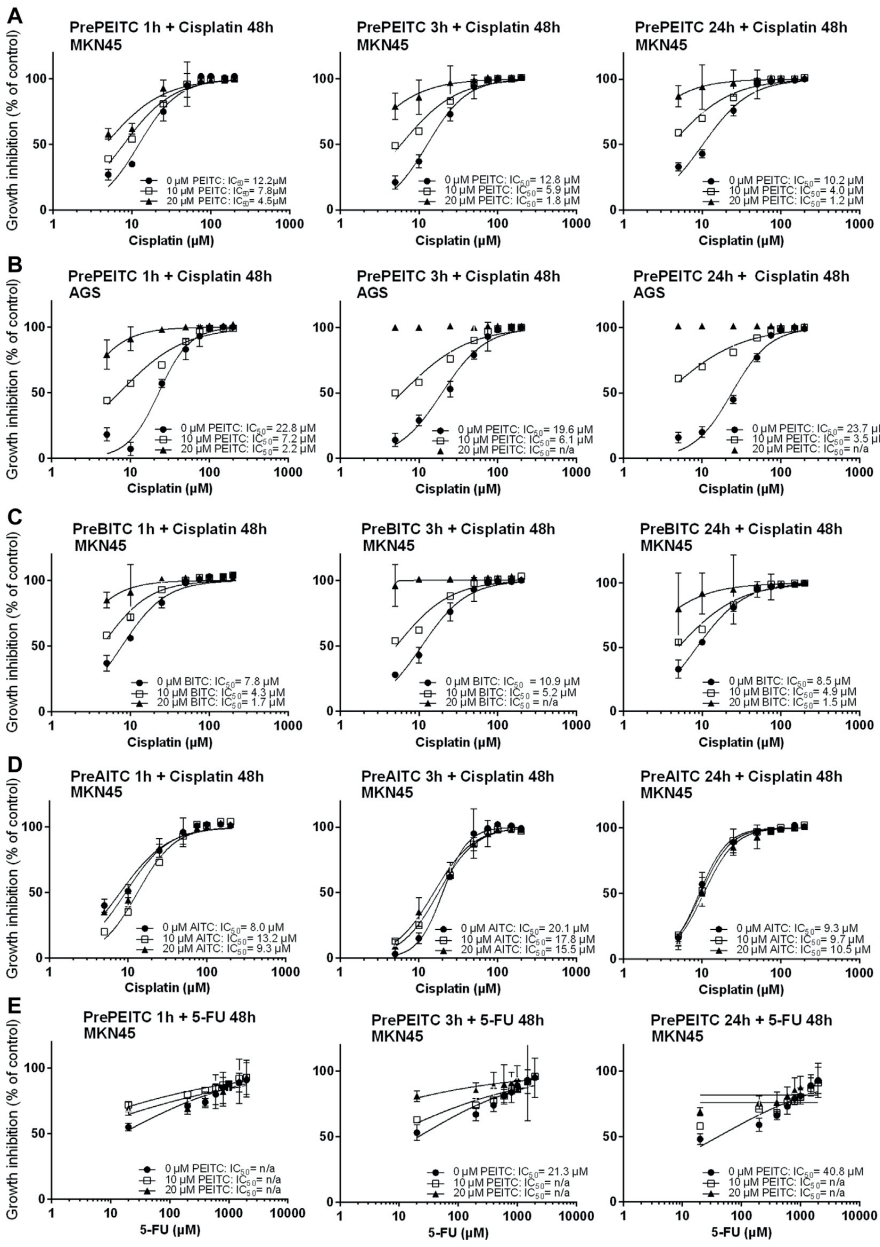

FIGURE 5 | Inhibition of proliferation (relative to vehicle control, 3% PBS) in cell cultures of MKN45 pre-treated with 10 and 20 μM PEITC for 1, 3 and 24 h before treated with 5–200 μM Cisplatin for 48 h **(A–E)**. (**B, C)** same as **(A)** but with pre-treatment with BITC or AITC instead of PEITC, respectively. **(D)** same as in **(A)** using AGS cells instead of MKN45. **(E)** same as in **(A)** but treating cells with 5-fluorouracil for 48 h instead of cisplatin following pre-treatment with PEITC. Values represent mean of n = 3–6 replicates. SD values were omitted from cultures with 98% or higher inhibited growth as these yielded non-representatively high SD values. PEITC: phenethyl isothiocyanate; BITC, benzyl isothiocyanate; AITC, allyl isothiocyanate.

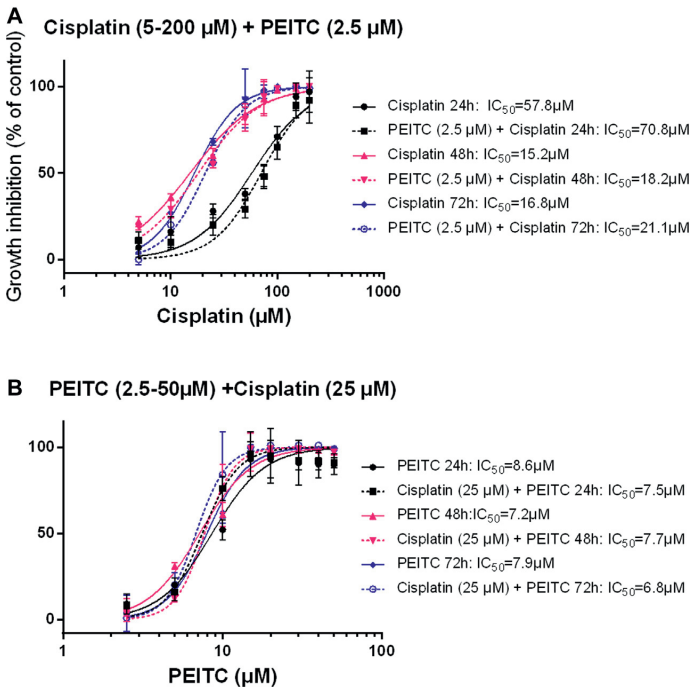

FIGURE 6 | Simultaneous treatment with PEITC and Cisplatin as different concentrations of cisplatin **(A)** and different concentrations of PEITC **(B)**. Mean ± SD. PEITC, phenethyl isothiocyanate.

few days. The differences in the fungistatic effect of ITC are possibly due to the type of apoptosis induced. It appears that significant portion of the chemopreventive effects of ITCs might be associated with the inhibition of the metabolic activation of carcinogens by cytochrome P450s (Phase I), coupled with strong induction of Phase II detoxifying and cellular defensive enzymes. Inductions of Phase II cellular enzymes are largely mediated by the antioxidant responsive element (ARE), which is regulated by the transcriptional factor (Nrf2). Additional potent regulatory mechanisms of Nrf2 include the different signaling kinase pathways (MAPK, PI3K, PKC and PERK) as well as other non-kinase dependent mechanisms. Moreover, apoptosis and cell cycle perturbations appear to be yet another potential chemopreventive mechanisms elicited by ITCs, especially with respect to the effects on pre-initiated or initiated tumor cells. Finally, modulation of other critical signaling mediators, including the NF-κB and AP-1 by a wide array of chemopreventive agents including ITCs might also contribute to the overall chemopreventive mechanisms (Keum et al., 2004).

Although surgery-related outcomes for treatment of gastric cancer, e.g., minimally invasive surgery techniques, continue to improve, the best regimen of either mono- or combination chemotherapy treatments still needs to be improved (Leiting and Grotz, 2019). In fact, the survival benefit of combinations of 5-fluorouracil (5-FU) with leucovorin, etoposide, methotrexate, doxorubicin, epidoxorubicin, cisplatin or oxaliplatin has been demonstrated (Sjoquist and Zalcberg, 2015). The results of the present study showed that there were time- and dose-dependent proliferative inhibitions by PEITC, BITC or AITC *in vitro* using the human cancer cell lines MKN45, AGS, MKN74 and KATO-III which were derived from intestinal and diffuse types of gastric carcinoma. Furthermore, the results of the present study showed that PEITC depleted intracellular levels of GSH and induced G_2/M arrest. It is well established that ITCs conjugate with GSH which is a linear tripeptide of L-glutamine, L-cysteine, and glycine. GSH is the main antioxidant metabolite in the cell and provides electrons for enzymes such as glutathione peroxidase, which reduce H_2O_2 to H_2O. GSH is crucial for cell proliferation, cell cycle progression and apoptosis and to protect cells from toxic insult by detoxifying toxic metabolites of drugs and ROS (Aquilano et al., 2014; Diaz-Vivancos et al., 2015). The results of the present study showed that intracellular GSH depletion upon PEITC and AITC treatment was both time- and dose-dependent, suggesting gastric cancer are susceptible to glutathione depletion. In fact, it was also reported that combined targeting of the epidermal growth factor receptor effector AKT and the glutathione antioxidant pathway mimicked Nrf2 ablation to potently inhibit pancreatic cancer, representing a promising synthetic lethal strategy for treating pancreatic cancer (Chio et al., 2016). This was in line with the

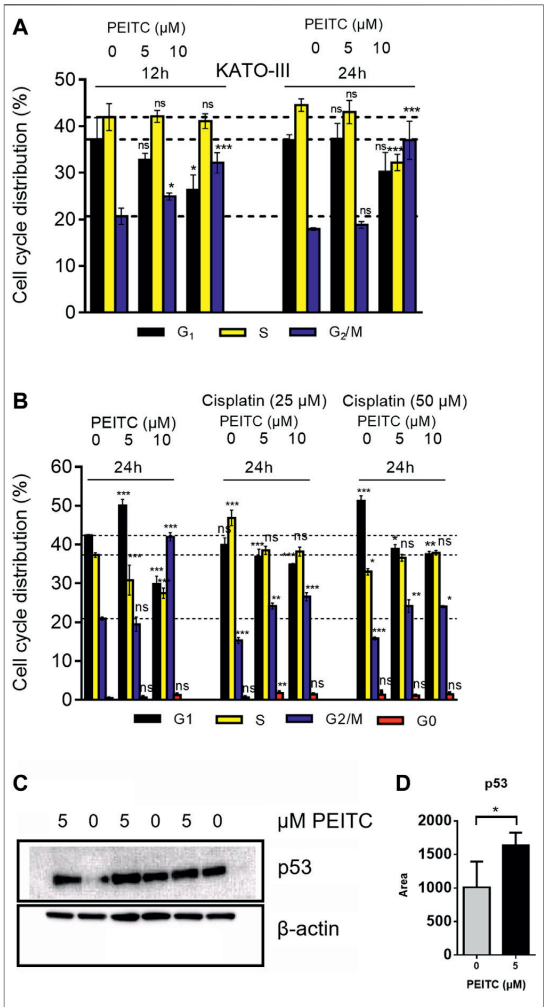

FIGURE 7 | Cell cycle analysis of PEITC **(A)** and PEITC + cisplatin **(B)** in KATO-III cells. Analyzed using FACS Canto cell cycle sorter with 20,000 cell reads/sample. Distribution is derived from histograms in FACS Diva software. Mean ± SD of $n = 3$ replicates/treatment. ANOVA with Dunnett's test (2-sided) vs. control groups was used. Western blot assessment of proteins p53 and β-actin (control) in response to PEITC were included in triplicates **(C)**. p53 band area were quantified in Image Studio Lite **(D)**. Bars represent means ± SD. Independent samples *t*-test (one-tailed) between 0 and 5 μM *: $p < 0.05$.

results of the present study showing that the synergistic effect of PEITC took place when it was given prior to cisplatin but not simultaneously with cisplatin, as it needs to deplete the intracellular pool of glutathione in order to achieve cell cycle arrest in response to cisplatin. Of note, the results of the present study also showed that pretreatment with PEITC could enhance the cytotoxicity of cisplatin but not of 5-FU. This effect should be explained by the different mechanisms of action between cisplatin (forming DNA crosslinks) and 5-FU (inhibiting thymidylate synthase) (Larionova et al., 2019). It would be of interest to investigate further the effects of PEITC in combination with different chemotherapeutic agents (including cisplatin, 5-FU, paclitaxel, gemcitabine, and trabectedin) that have different mechanisms of action in order to explore the mechanism of PEITC and to find the best combination therapy.

Interference of ITC with microtubules have also been established as a contributor to cells stagnating in the G_2/M-phase (Mi et al., 2009; Øverby et al., 2014). Buthionine sulfoximine (BSO), a synthetic amino acid, is an inhibitor of GSH synthesis on intracellular GSH levels (Griffith and Meister, 1979; Aldini et al., 2018). The results of the present study showed that BSO depleted GSH in a time- and dose-dependent manner and that PEITC-treatment altered the intracellular glutamine/glutamate ratio, providing a possible link between ITCs and amino acid metabolism. We suggested that the increase in glutamine but not glutamate levels shown in the present study could be attributed to compensatory mechanisms towards GSH replenishment in the cell when GSH level decreases. Indeed, a previous report has found that glutamine consumption correlated with glutathione excretion (Sappington et al., 2016).

It is known that elevated GSH levels are associated with tumor cell resistance to alkylating agents and platinum compounds (Estrela et al., 2006; Ortega et al., 2011; Bansal and Simon, 2018). Elevated GSH levels are observed in various types of tumors (Calvert et al., 1998). It has been suggested that high intracellular GSH level increases the antioxidant capacity and is thus conferring therapeutic resistance to cancer cells through the ability to resist oxidative stress which is a critical component of cisplatin cytotoxicity (Yu et al., 2018). We hypothesized that ITCs would enhance the cytotoxicity of cisplatin by depleting cells of glutathione, and indeed we found that PEITC and BITC but not AITC sensitized the gastric cancer cells to cisplatin. Conceivably, when the cell is depleted of GSH and oxidative stress is introduced using cytotoxic agents, a collapse in the antioxidant system eventually leads to cell death. Although reduction in GSH is proposed as a possible mechanism in the present study, it should be noticed that ITCs at sufficiently low doses might actually increase GSH levels as a consequence of ROS induction. Di Pasqua and colleagues described reduction of GSH as a less likely explanation to potentiating lung cancer cells by ITC but accredited the binding to tubulin as a more plausible explanation (Di Pasqua et al., 2010). In fact, PEITC and cisplatin have been co-administered using liposomal nanoparticles for treatment of non-small cell lung cancer (Sun et al., 2019). The efficacy potentiating of ITCs on existing chemotherapy has also been studied in cancers such as Barrett esophageal adenocarcinoma (Qazi et al., 2010), ovarian carcinoma (Stehlik et al., 2010), non-small cell lung carcinoma (Di Pasqua et al., 2010), prostate cancer (Xiao and Singh, 2010) and cervical cancer cells (Wang et al., 2011) in combination with drugs such as paclitaxel, MST-312, GRN163L, cisplatin and docetaxel. Thus, the results of the present study provide additional evidence in gastric cancer. The results of the present study also showed that PEITC induced cell cycle arrest in G_2/M phase which was associated with increased p53 protein

levels. p53 is one of the classical tumor suppressor genes that interferes with cell transformation events and plays a critical role in cell cycle control and induction of apoptosis (Ozaki and Nakagawara, 2011; Bykov et al., 2016; Bykov et al., 2018). It can be elevated in response to genotoxic agents, such as ionizing radiation, UV light, or chemicals. It has been shown that p53 elevation was required for PEITC-induced apoptosis (Huang et al., 1998).

However, some limitations of the present study should be noticed. First, we did not include additional animal groups, e.g., normal mice, MNU and INS-GAS mice that should be treated with PEITC or cisplatin alone and combination of PEITC plus cisplatin to explore the possibilities that PEITC may have differential effects on gastric cancer cells compared to normal gastric epithelial cells and that there is likely a synergistic anticancer effect *in vivo*. In fact, it has been showed that combining AITC with cisplatin reduced tumor volume in a mouse model of human lung cancer (Ling et al., 2015), thus this could also be a promising strategy in gastric cancer. Secondly, we did not investigate the molecular mechanism of action including signaling pathways of ITCs in combination with cisplatin, in gastric cancer cells. Third, we did not perform the combination of denervation and PEITC with or without chemotherapy, as initially planned. Forth, we did not further investigate the possible mechanism by which the only pretreatment with PEITC was effective against NMU-induced gastric cancer, and neither concomitant treatment nor administration of this agent after cancer development (either in NMU or INS-GAS mice) was successful. In addition to pre-initiated or initiated tumor cells as a possible target of PEITC (aforementioned), there are other possible hypotheses/explanations. It has been known that there are different windows for chemoprevention and therapeutic effects during the tumorigenesis from initiation, promotion and progression (Hanahan and Weinberg, 2011; Liu et al., 2015). It is also possible that the anti-cancer agents (e.g., ITCs) exhibit the effect on the initiation phase when given at a low dose and on the progression phase at a high dose. In the present study, PEITC (MW 163.24 g/mol) was given at 3–5 μmol/g diet in mice. Based on the pharmacokinetics of PEITC, the oral administration of PEITC at this dose level would reach a circulation level that is in a similar order of magnitude of IC_{50} (15 μM) *in vitro* but be a lower order of magnitude in gastric tissue (pmol/mg) (Reimer, 1972; Conaway et al., 1999). Fifth, it is still unclear why the synergistic effect was not obtained when PEITC and cisplatin were given simultaneously in the cell culture model. In fact, we failed to measure GSH levels because of heavily fluctuating potentiating effect. Fluctuating levels of GSH was found across our experiments measuring GSH concentration, where the intracellular GSH levels ranged between 3 and 10 μM GSH between experiments, adding to the complexity of GSH's role in the observations. Finally, it should also be noticed that this study was carried out in the mouse models of gastric cancer and in the cell lines derived from human gastric cancer. It would be of interest to study the possible cytotoxic effects of ITCs in normal tissue and/or cell lines derived from normal healthy human stomach, e.g., cell line of HGaEpC, in the future. Taken together, it is still a challenge for future development of food products that contains high levels of edible ITCs for chemo-prevention and for being used during chemotherapy in patients with gastric cancer.

It would also be of interest to explore the possible efficacy's potentiating role of ITCs on other therapies, such as targeted therapy and immunotherapy. In fact, combination of ERBB2 antagonist or RARA agonist was reported to be effective synergistic regimens for ERBB2 positive gastric cancer (Xiang et al., 2018). In clinical setting, the treatment options for advanced-stage gastric cancer are limited, despite an approval of two targeted agents, trastuzumab and ramucirumab. Consequently, the overall clinical outcomes for patients with advanced-stage gastric cancer remain poor. Numerous agents that are active against novel targets have been evaluated in the course of randomized trials; however, most have produced disappointing results because of the heterogeneity of gastric cancer (Kumar et al., 2018). Immunotherapy, e.g., immune checkpoint inhibitors (ICIs), has been tested in gastric cancer. Despite having good efficacy and safety profile, ICIs are clinically active only in small subset of patients and therefore, there is a huge unmet need to enhance their efficacy. Indeed, there are several ongoing clinical trials that are exploring the role of ICIs in various gastrointestinal cancers either as single agent or in combination with chemotherapy, radiation therapy, targeted agents or other immunotherapeutic agents, but not yet ITC (Mazloom et al., 2020).

CONCLUSION

PEITC displayed anti-cancer effects, particularly when given before the tumor initiation, suggesting a chemopreventive effect in gastric cancer, and that aromatic ITCs potentiated the anti-cancer effects of cisplatin, particularly when given before cisplatin, suggesting a possible combination strategy in treatment of gastric cancer.

DATA AVAILABILITY STATEMENT

The raw data supporting the conclusions of this article will be made available by the authors, without undue reservation.

ETHICS STATEMENT

The animal study was reviewed and approved by The Norwegian Food Safety Authority (Mattilsynet).

AUTHOR CONTRIBUTIONS

H-LR: *in vitro* experiments, all sample/data collection and preparation, data analysis and interpretation, writing manuscript. YK: *in vivo* Experiments, sample/data collection and preparation, writing manuscript. MN, AMB, and TCW: Project discussion, data interpretation, writing manuscript. DC: Project concept, study idea

and design, data analysis and interpretation, writing manuscript. C-MZ: Project concept, study idea and design, *in vivo* experiments, sample collection and preparation, data interpretation, writing manuscript. AØ: project design, *in vivo* and *in vitro* experiments, sample/data collection and preparation, data analysis and interpretation, writing manuscript.

FUNDING

The research was supported by the Liaison Committee between the Central Norway Regional Health Authority (Helse-Midt Norge RHF), Norwegian University of Science and Technology (NTNU grant no. 46056636/46056928/90061700/90061701), Joint Program of the Medical Faculty of NTNU, the Research Council of Norway, and the Cancer Foundation of St. Olavs Hospital (Kreftfondet ved St. Olavs hospital), the Japan Society for the Promotion of Science (JSPS grant no. 15F14741) and the Scandinavia-Japan Sasakawa Foundation (SJSF).

ACKNOWLEDGMENTS

We thank Dr. Signe E. Åsberg and Ragni A. Stokland (NTNU) for participating in animal experiments and Dr. Tetsufumi Takahashi (Kitasato University) for assisting on *in vitro* experiments.

REFERENCES

Aldini, G., Altomare, A., Baron, G., Vistoli, G., Carini, M., Borsani, L., et al. (2018). N-Acetylcysteine as an antioxidant and disulphide breaking agent: the reasons why. *Free Radic. Res.* 52, 751–762. doi:10.1080/10715762.2018.1468564

Aquilano, K., Baldelli, S., and Ciriolo, M. R. (2014). Glutathione: new roles in redox signaling for an old antioxidant. *Front. Pharmacol.* 5, 196. doi:10.3389/fphar.2014.00196

Bansal, A., and Simon, M. C. (2018). Glutathione metabolism in cancer progression and treatment resistance. *J. Cell Biol.* 217, 2291–2298. doi:10.1083/jcb.201804161

Bray, F., Ferlay, J., Soerjomataram, I., Siegel, R. L., Torre, L. A., and Jemal, A. (2018). Global cancer statistics 2018: GLOBOCAN estimates of incidence and mortality worldwide for 36 cancers in 185 countries. *CA Cancer J. Clin.* 68, 394–424. doi:10.3322/caac.21492

Bykov, V. J., Zhang, Q., Zhang, M., Ceder, S., Abrahmsen, L., and Wiman, K. G. (2016). Targeting of mutant p53 and the cellular redox balance by APR-246 as a strategy for efficient cancer therapy. *Front. Oncol.* 6, 21. doi:10.3389/fonc.2016.00021

Bykov, V. J. N., Eriksson, S. E., Bianchi, J., and Wiman, K. G. (2018). Targeting mutant p53 for efficient cancer therapy. *Nat. Rev. Cancer* 18, 89–102. doi:10.1038/nrc.2017.109

Calvert, P., Yao, K. S., Hamilton, T. C., and O'Dwyer, P. J. (1998). Clinical studies of reversal of drug resistance based on glutathione. *Chem. Biol. Interact.* 111–112, 213–224. doi:10.1016/s0009-2797(98)00008-8

Chen, Y., Li, Y., Wang, X. Q., Meng, Y., Zhang, Q., Zhu, J. Y., et al. (2018). Phenethyl isothiocyanate inhibits colorectal cancer stem cells by suppressing Wnt/β-catenin pathway. *Phytother. Res.* 32, 2447–2455. doi:10.1002/ptr.6183

Chio, I. I. C., Jafarnejad, S. M., Ponz-Sarvise, M., Park, Y., Rivera, K., Palm, W., et al. (2016). NRF2 promotes tumor maintenance by modulating mRNA translation in pancreatic cancer. *Cell* 166, 963–976. doi:10.1016/j.cell.2016.06.056

Chu, W. F., Wu, D. M., Liu, W., Wu, L. J., Li, D. Z., Xu, D. Y., et al. (2009). Sulforaphane induces G2-M arrest and apoptosis in high metastasis cell line of salivary gland adenoid cystic carcinoma. *Oral Oncol.* 45, 998–1004. doi:10.1016/j.oraloncology.2009.05.641

Chung, M. Y., Lim, T. G., and Lee, K. W. (2013). Molecular mechanisms of chemopreventive phytochemicals against gastroenterological cancer development. *World J. Gastroenterol.* 19, 984–993. doi:10.3748/wjg.v19.i7.984

Clarke, J. D., Dashwood, R. H., and Ho, E. (2008). Multi-targeted prevention of cancer by sulforaphane. *Cancer Lett.* 269, 291–304. doi:10.1016/j.canlet.2008.04.018

Conaway, C. C., Jiao, D., Kohri, T., Liebes, L., and Chung, F. L. (1999). Disposition and pharmacokinetics of phenethyl isothiocyanate and 6-phenylhexyl isothiocyanate in F344 rats. *Drug Metab. Dispos.* 27, 13–20.

Conaway, C. C., Yang, Y. M., and Chung, F. L. (2002). Isothiocyanates as cancer chemopreventive agents: their biological activities and metabolism in rodents and humans. *Curr. Drug Metab.* 3, 233–255. doi:10.2174/1389200023337496

Cunningham, D., Starling, N., Rao, S., Iveson, T., Nicolson, M., Coxon, F., et al. (2008). Capecitabine and oxaliplatin for advanced esophagogastric cancer. *N. Engl. J. Med.* 358, 36–46. doi:10.1056/NEJMoa073149

Di Pasqua, A. J., Hong, C., Wu, M. Y., McCracken, E., Wang, X., Mi, L., et al. (2010). Sensitization of non-small cell lung cancer cells to cisplatin by naturally occurring isothiocyanates. *Chem. Res. Toxicol.* 23, 1307–1309. doi:10.1021/tx100187f

Diaz-Vivancos, P., de Simone, A., Kiddle, G., and Foyer, C. H. (2015). Glutathione--linking cell proliferation to oxidative stress. *Free Radic. Biol. Med.* 89, 1154–1164. doi:10.1016/j.freeradbiomed.2015.09.023

Dunn, B. K., Umar, A., and Richmond, E. (2016). Introduction: cancer chemoprevention and its context. *Semin. Oncol.* 43, 19–21. doi:10.1053/j.seminoncol.2015.11.002

Estrela, J. M., Ortega, A., and Obrador, E. (2006). Glutathione in cancer biology and therapy. *Crit. Rev. Clin. Lab Sci.* 43, 143–181. doi:10.1080/10408360500523878

Ferlay, J., Shin, H. R., Bray, F., Forman, D., Mathers, C., and Parkin, D. M. (2010). Estimates of worldwide burden of cancer in 2008: GLOBOCAN 2008. *Int. J. Cancer* 127, 2893–2917. doi:10.1002/ijc.25516

Ferlay, J. S. I., Ervik, M., Dikshit, R., Eser, S., Mathers, C., et al. (2013). *GLOBOCAN 2012 v1.0, cancer incidence and mortality worldwide: IARC CancerBase No. 11*. Lyon, France: International Agency for Research on Cancer.

Ford, A. C. (2011). Chemoprevention for gastric cancer. *Best Pract. Res. Clin. Gastroenterol.* 25, 581–592. doi:10.1016/j.bpg.2011.09.002

Griffith, O. W., and Meister, A. (1979). Potent and specific inhibition of glutathione synthesis by buthionine sulfoximine (S-n-butyl homocysteine sulfoximine). *J. Biol. Chem.* 254, 7558–7560. doi:10.1016/s0021-9258(18)35980-5

Gupta, P., Wright, S. E., Kim, S. H., and Srivastava, S. K. (2014). Phenethyl isothiocyanate: a comprehensive review of anti-cancer mechanisms. *Biochim. Biophys. Acta* 1846, 405–424. doi:10.1016/j.bbcan.2014.08.003

Hanahan, D., and Weinberg, R. A. (2011). Hallmarks of cancer: the next generation. *Cell* 144, 646–674. doi:10.1016/j.cell.2011.02.013

Hu, K., and Morris, M. E. (2004). Effects of benzyl-, phenethyl-, and alpha-naphthyl isothiocyanates on P-glycoprotein- and MRP1-mediated transport. *J. Pharm. Sci.* 93, 1901–1911. doi:10.1002/jps.20101

Huang, C., Ma, W. Y., Li, J., Hecht, S. S., and Dong, Z. (1998). Essential role of p53 in phenethyl isothiocyanate-induced apoptosis. *Cancer Res.* 58, 4102–4106.

Kang, Y. K., Kang, W. K., Shin, D. B., Chen, J., Xiong, J., Wang, J., et al. (2009). Capecitabine/cisplatin versus 5-fluorouracil/cisplatin as first-line therapy in patients with advanced gastric cancer: a randomised phase III noninferiority trial. *Ann. Oncol.* 20, 666–673. doi:10.1093/annonc/mdn717

Keum, Y. S., Jeong, W. S., and Kong, A. N. (2004). Chemoprevention by isothiocyanates and their underlying molecular signaling mechanisms. *Mutat. Res.* 555, 191–202. doi:10.1016/j.mrfmmm.2004.05.024

Keum, Y. S., Jeong, W. S., and Kong, A. N. (2005). Chemopreventive functions of isothiocyanates. *Drug News Perspect.* 18, 445–451. doi:10.1358/dnp.2005.18.7.939350

Koizumi, W., Narahara, H., Hara, T., Takagane, A., Akiya, T., Takagi, M., et al. (2008). S-1 plus cisplatin versus S-1 alone for first-line treatment of advanced gastric cancer (SPIRITS trial): a phase III trial. *Lancet Oncol.* 9, 215–221. doi:10.1016/S1470-2045(08)70035-4

Kumar, V., Soni, P., Garg, M., Kamholz, S., and Chandra, A. B. (2018). Emerging therapies in the management of advanced-stage gastric cancer. *Front. Pharmacol.* 9, 404. doi:10.3389/fphar.2018.00404

Larionova, I., Cherdyntseva, N., Liu, T., Patysheva, M., Rakina, M., and Kzhyshkowska, J. (2019). Interaction of tumor-associated macrophages and cancer chemotherapy. *Oncoimmunology* 8, e1596004. doi:10.1080/2162402X.2019.1596004

Lawson, A. P., Long, M. J. C., Coffey, R. T., Qian, Y., Weerapana, E., El Oualid, F., et al. (2015). Naturally occurring isothiocyanates exert anticancer effects by inhibiting deubiquitinating enzymes. *Cancer Res.* 75, 5130–5142. doi:10.1158/0008-5472.CAN-15-1544

Leiting, J. L., and Grotz, T. E. (2019). Advancements and challenges in treating advanced gastric cancer in the West. *World J. Gastrointest. Oncol.* 11, 652–664. doi:10.4251/wjgo.v11.i9.652

Li, Y., Zhang, T., Korkaya, H., Liu, S., Lee, H. F., Newman, B., et al. (2010). Sulforaphane, a dietary component of broccoli/broccoli sprouts, inhibits breast cancer stem cells. *Clin. Cancer Res.* 16, 2580–2590. doi:10.1158/1078-0432.CCR-09-2937

Li, Y., and Zhang, T. (2013). Targeting cancer stem cells with sulforaphane, a dietary component from broccoli and broccoli sprouts. *Future Oncol.* 9, 1097–1103. doi:10.2217/fon.13.108

Ling, X., Westover, D., Cao, F., Cao, S., He, X., Kim, H. R., et al. (2015). Synergistic effect of allyl isothiocyanate (AITC) on cisplatin efficacy *in vitro* and *in vivo*. *Am. J. Cancer Res.* 5, 2516–2530.

Liu, Y., Yin, T., Feng, Y., Cona, M. M., Huang, G., Liu, J., et al. (2015). Mammalian models of chemically induced primary malignancies exploitable for imaging-based preclinical theragnostic research. *Quant Imaging Med. Surg.* 5, 708–729. doi:10.3978/j.issn.2223-4292.2015.06.01

Lv, H., Zhen, C., Liu, J., and Shang, P. (2020). β-Phenethyl isothiocyanate induces cell death in human osteosarcoma through altering iron metabolism, disturbing the redox balance, and activating the MAPK signaling pathway. *Oxid Med. Cell Longev.* 2020, 5021983. doi:10.1155/2020/5021983

Mazloom, A., Ghalehsari, N., Gazivoda, V., Nimkar, N., Paul, S., Gregos, P., et al. (2020). Role of immune checkpoint inhibitors in gastrointestinal malignancies. *J. Clin. Med.* 9, 2533. doi:10.3390/jcm9082533

Mera, R. M., Bravo, L. E., Camargo, M. C., Bravo, J. C., Delgado, A. G., Romero-Gallo, J., et al. (2018). Dynamics of *Helicobacter pylori* infection as a determinant of progression of gastric precancerous lesions: 16-year follow-up of an eradication trial. *Gut* 67, 1239–1246. doi:10.1136/gutjnl-2016-311685

Mi, L., Gan, N., and Chung, F. L. (2009). Aggresome-like structure induced by isothiocyanates is novel proteasome-dependent degradation machinery. *Biochem. Biophys. Res. Commun.* 388, 456–462. doi:10.1016/j.bbrc.2009.08.047

Mitsiogianni, M., Koutsidis, G., Mavroudis, N., Trafalis, D. T., Botaitis, S., Franco, R., et al. (2019). The role of isothiocyanates as cancer chemo-preventive, chemo-therapeutic and anti-melanoma agents. *Antioxidants (Basel)* 8, 106. doi:10.3390/antiox8040106

Orditura, M., Galizia, G., Sforza, V., Gambardella, V., Fabozzi, A., Laterza, M. M., et al. (2014). Treatment of gastric cancer. *World J. Gastroenterol.* 20, 1635–1649. doi:10.3748/wjg.v20.i7.1635

Ortega, A. L., Mena, S., and Estrela, J. M. (2011). Glutathione in cancer cell death. *Cancers (Basel)* 3, 1285–1310. doi:10.3390/cancers3011285

Øverby, A., Stokland, R. A., Åsberg, S. E., Sporsheim, B., and Bones, A. M. (2015). Allyl isothiocyanate depletes glutathione and upregulates expression of glutathione S-transferases in *Arabidopsis thaliana*. *Front. Plant Sci.* 6, 277. doi:10.3389/fpls.2015.00277

Øverby, A., Zhao, C. M., Bones, A. M., and Chen, D. (2014). Naturally occurring phenethyl isothiocyanate-induced inhibition of gastric cancer cell growth by disruption of microtubules. *J. Gastroenterol. Hepatol.* 29 (Suppl. 4), 99–106. doi:10.1111/jgh.12732

Ozaki, T., and Nakagawara, A. (2011). Role of p53 in cell death and human cancers. *Cancers (Basel)* 3, 994–1013. doi:10.3390/cancers3010994

Qazi, A., Pal, J., Maitah, M., Fulciniti, M., Pelluru, D., Nanjappa, P., et al. (2010). Anticancer activity of a broccoli derivative, sulforaphane, in barrett adenocarcinoma: potential use in chemoprevention and as adjuvant in chemotherapy. *Transl. Oncol.* 3, 389–399. doi:10.1593/tlo.10235

Rabben, H.-L., Andersen, G. T., Olsen, M. K., Øverby, A., Ianevski, A., et al. (2021). Neural signaling modulates metabolism of gastric cancer. *iScience* 24, 102091. doi:10.1016/j.isci.2021.102091

Rabben, H. L., Zhao, C. M., Hayakawa, Y., Wang, T. C., and Chen, D. (2016). Vagotomy and gastric tumorigenesis. *Curr. Neuropharmacol.* 14, 967–972. doi:10.2174/1570159x14666160121114854

Reimer, F. (1972). Developmental trends in psychiatric hospitals. *Offentl. Gesundheitswes.* 34 (Suppl. 1), 26–33.

Sappington, D. R., Siegel, E. R., Hiatt, G., Desai, A., Penney, R. B., Jamshidi-Parsian, A., et al. (2016). Glutamine drives glutathione synthesis and contributes to radiation sensitivity of A549 and H460 lung cancer cell lines. *Biochim. Biophys. Acta* 1860, 836–843. doi:10.1016/j.bbagen.2016.01.021

Sjoquist, K. M., and Zalcberg, J. R. (2015). Gastric cancer: past progress and present challenges. *Gastric Cancer* 18, 205–209. doi:10.1007/s10120-014-0437-0

Stehlik, P., Paulikova, H., and Hunakova, L. (2010). Synthetic isothiocyanate indole-3-ethyl isothiocyanate (homoITC) enhances sensitivity of human ovarian carcinoma cell lines A2780 and A2780/CP to cisplatin. *Neoplasma* 57, 473–481. doi:10.4149/neo_2010_05_473

Steward, W. P., and Brown, K. (2013). Cancer chemoprevention: a rapidly evolving field. *Br. J. Cancer* 109, 1–7. doi:10.1038/bjc.2013.280

Sun, M., Shi, Y., Dang, U. J., and Di Pasqua, A. J. (2019). Phenethyl isothiocyanate and cisplatin Co-encapsulated in a liposomal nanoparticle for treatment of non-small cell lung cancer. *Molecules* 24, 801. doi:10.3390/molecules24040801

Tan, V. P., and Wong, B. C. (2013). Gastric cancer chemoprevention: the current evidence. *Gastroenterol. Clin. N. Am.* 42, 299–316. doi:10.1016/j.gtc.2013.02.001

Tomczyk, J., and Olejnik, A. (2010). Sulforaphane–a possible agent in prevention and therapy of cancer. *Postepy Hig Med Dosw (Online)* 64, 590–603.

Van Cutsem, E., Moiseyenko, V. M., Tjulandin, S., Majlis, A., Constenla, M., Boni, C., et al. (2006). Phase III study of docetaxel and cisplatin plus fluorouracil compared with cisplatin and fluorouracil as first-line therapy for advanced gastric cancer: a report of the V325 Study Group. *J. Clin. Oncol.* 24, 4991–4997. doi:10.1200/JCO.2006.06.8429

Wang, X., Govind, S., Sajankila, S. P., Mi, L., Roy, R., and Chung, F. L. (2011). Phenethyl isothiocyanate sensitizes human cervical cancer cells to apoptosis induced by cisplatin. *Mol. Nutr. Food Res.* 55, 1572–1581. doi:10.1002/mnfr.201000560

Wu, X., Zhou, Q. H., and Xu, K. (2009). Are isothiocyanates potential anti-cancer drugs?. *Acta Pharmacol. Sin* 30, 501–512. doi:10.1038/aps.2009.50

Xiang, Z., Huang, X., Wang, J., Zhang, J., Ji, J., Yan, R., et al. (2018). Cross-database analysis reveals sensitive biomarkers for combined therapy for ERBB2+ gastric cancer. *Front. Pharmacol.* 9, 861. doi:10.3389/fphar.2018.00861

Xiao, D., and Singh, S. V. (2010). Phenethyl isothiocyanate sensitizes androgen-independent human prostate cancer cells to docetaxel-induced apoptosis *in vitro* and *in vivo*. *Pharm. Res.* 27, 722–731. doi:10.1007/s11095-010-0079-9

Yang, M. D., Lai, K. C., Lai, T. Y., Hsu, S. C., Kuo, C. L., Yu, C. S., et al. (2010). Phenethyl isothiocyanate inhibits migration and invasion of human gastric cancer AGS cells through suppressing MAPK and NF-kappaB signal pathways. *Anticancer Res.* 30, 2135–2143.

Yu, W., Chen, Y., Dubrulle, J., Stossi, F., Putluri, V., Sreekumar, A., et al. (2018). Cisplatin generates oxidative stress which is accompanied by rapid shifts in central carbon metabolism. *Sci. Rep.* 8, 4306. doi:10.1038/s41598-018-22640-y

Zhang, Y. (2010). Allyl isothiocyanate as a cancer chemopreventive phytochemical. *Mol. Nutr. Food Res.* 54, 127–135. doi:10.1002/mnfr.200900323

Zhao, C. M., Hayakawa, Y., Kodama, Y., Muthupalani, S., Westphalen, C. B., Andersen, G. T., et al. (2014). Denervation suppresses gastric tumorigenesis. *Sci. Transl. Med.* 6, 250ra115. doi:10.1126/scitranslmed.3009569

Conflict of Interest: The authors declare that the research was conducted in the absence of any commercial or financial relationships that could be construed as a potential conflict of interest.

ISBN 978-82-326-6859-5 (printed ver.)
ISBN 978-82-326-6537-2 (electronic ver.)
ISSN 1503-8181 (printed ver.)
ISSN 2703-8084 (online ver.)

NTNU

Norwegian University of
Science and Technology